INVESTIGATING A MITOCHONDRIAL ROLE FOR KYNURENINE 3-MONOOXYGENASE

Thesis submitted for the degree of
Doctor of Philosophy
at the University of Leicester

by

Daniel Christopher Maddison
Department of Genetics & Genome Biology
University of Leicester

September 2018

INVESTIGATING A MITOCHONDRIAL ROLE FOR KYNURENINE 3-MONOOXYGENASE

Daniel Maddison

Abstract

Kynurenine 3-monooxygenase (KMO) is an enzyme which operates within the kynurenine pathway (KP), catalysing the hydroxylation of kynurenine to produce 3-hydroxykynurenine (3-HK). KMO is a mitochondrial protein, localising at the outer membrane (MOM) due to a C-terminal domain, yet a mitochondrial role for KMO has not been described. However, the KMO encoding gene in *Drosophila*, *cinnabar* (*cn*), was identified in an RNAi screen as a modulator of both mitochondrial morphology and the recruitment of an autosomal recessive juvenile parkinsonism related protein, Parkin, to the MOM. Given the prospective use of KMO inhibition in the treatment of neurodegenerative disorders, of which mitochondrial dysfunction is a well-established aspect of pathology, mitochondrial functions of KMO warrant thorough investigation. This thesis interrogates the mitochondrial role of KMO in *Drosophila* and mammalian-cell models.

A range of mitochondrial-related phenotypes were identified in *cinnabar* deficient *Drosophila,* including elongated mitochondria and an increase in mitochondrial mass, yet a decrease in capacity of the mitochondrial electron transfer system (ETS) complex I. Supplementation of flies with 3-HK was not sufficient to reverse these phenotypes, indicating a novel role of KMO in mitochondrial quality control, independent from its enzymatic function in the KP. This implicates KMO in two mechanisms which maintain a healthy mitochondrial network - mitochondrial dynamics and mitophagy.

The interplay between KMO and components of these pathways was explored by means of genetic epistasis experiments in *Drosophila*, accompanied by functional assays in *Drosophila* and human immortalised cells. Deletion of *cinnabar* in flies lacking Parkin or another juvenile parkinsonism related protein, PTEN-induced kinase 1 (PINK1), caused partial lethality, indicating a functional overlap between these mitophagy-related proteins and KMO. Furthermore, overexpression of *cinnabar* or human *KMO* was sufficient to rescue locomoter defects in PINK1, but not Parkin deficient flies. Parkin interaction and localisation experiments implied a transient interaction between KMO and Parkin at the MOM, however a downstream function of Parkin MOM recruitment, the ubiquitation and degradation of *Drosophila* Mitofusin (MARF) was unaffected by *cinnabar* modulation. Overexpression of *dynamin related protein 1* (*Drp1*) reversed locomoter defects in *cinnabar* deficient flies, indicating that a decrease in mitochondrial fission could be responsible for this phenotype. Furthermore, overexpression of KMO influenced post-translational modification of DRP1. These findings implicate KMO in regulation of mitochondrial dynamics and mitochondrial quality control.

Acknowledgements

I would first of all like to thank Prof. Flaviano Giorgini for being the best supervisor imaginable. For the fact that your door is always open and for your eternal optimism, particularly at the more desperate periods of my project, I couldn't have hoped for a better mentor. For the numerous projects you involved me in and the conferences you encouraged me to attend, which have made me feel like a real part of the scientific community, I am forever grateful.

To the rest of "The Giorginis", past and present, I was privileged to work amongst and learn from such a talented and diverse group of people. Carlo - from flies, to buying fridges, to fatherhood, I learned a huge amount from you during these years. Thank you for sharing "your" bay with me! Susy, you have always been incredibly approachable and thoughtful, particularly at the beginning of my project when I was finding my feet. Mariaelena - your dedication and attention to detail have been hugely inspiring for me. It was a privilege to work with you and I really appreciate the support you gave me. Rob - thanks for always being there to discuss things science and miscellaneous(!), and for helping me get set up with tissue culture work. Thanks to Aisha and Mahdieh for the resources and advice that you provided me with at the beginning of my project and to Charlotte and Monica for taking the mantle as most junior lab members!

Thanks also to my second supervisor, Prof. Charalambos (Bambos) Kyriacou, for your continuous support, from my BSc project through to this day. I will never forget our first meeting, in which you serenely destroyed my attempt to summarise one of your papers. It was in that moment I released that I needed to up my game. To Dr. Fred Tata, for being an incredible teacher throughout my BSc and MSc studies, as well as for your support and advice during my PhD. Thanks also to Dr. Miguel Martins and Dr. Alex Whitworth for your generosity with both time and resources, which helped me a lot throughout my project. Special thanks to Giorgio, you are another person that really inspired me to pursue a career in research and have always been available to provide discussion and advice. Many thanks to Natalie Allcock, Dr. Anna Iwanowska-Straatman and Dr. Kees Straatman for sharing your expertise in microscopy, and more to the point, for being lovely people to spend time with.

To the "lunch group" members 2013-2018; Mirko, Ben, Kam, Nathaniel, Marta, Joana, Usha, Ane, Marcela, Alex, Abi, Thom, Yue, Charlotte, Letizia, Joe, Liam, Monica, Emily, Liliane, Nikola –escaping the lab and enjoying time with you guys is something I really valued. Bili, Entoni and James - my brothers - life in Leicester would have been unimaginably different had we not met and you truly changed my perspective on many things. To my parents - Mum, Dad, Ruth & Eric, my grandparents, my sister Kate and wider family, making you proud is still what gets me out of bed in the morning. Thank you so much for the support you have and will always give me. Marcela – I am so proud of what we have made over the past four years. Thank you for suffering me and for demanding the best of me. I owe it all to you.

"No book can ever be finished. While working on it we learn just enough to find it immature the moment we turn away from it." Karl R. Popper.

Tables

Figures

Abbreviations

3-HANA	3-hydroxyanthranilic acid
3-HAO	3-hydroxyanthranilate 3,4-dioxygenase
3-HK	3-hydroxykynurenine
α7nACh	α7-nicotinic acetylcholine
aß	amyloid ß peptide
$\Delta\Psi_m$	mitochondrial membrane potential
ACMS	2-amino-3-carboxymuconic 6-semialdehyde
ACMSD	2-amino-3-carboxymuconic 6-semialdehyde decarboxylase
AD	Alzheimer's disease
AKAP1	A-kinase anchoring protein 1
ALS	amyloid lateral sclerosis
AMPAR	α-amino-3-hydroxy-5-methyl-4-isoxazolepropionic acid receptor
APP	amyloid precursor protein
ARJP	autosomal recessive juvenile parkinsonism
ATP	adenosine triphosphate
aSyn	α-synuclein
BNA4	*biosynthesis of nicotinic acid 4*
BSA	bovine serum albumin
CCCP	carbonyl cynanide *m*-chlorophenoyl hydrazone
CDK1	cyclin dependant kinase 1
cDNA	copy deoxyribonucleic acid
cn	*cinnabar*
CNS	central nervous system
CoIP	co-immunoprecipitation
Cp	crossing points
CS	citrate synthase
CSF	cerebrospinal fluid
CyO	Curly of Oster
DA	dopaminergic
DAM	*Drosophila* activity monitoring
DD	constant darkness
DMEM	Dulbecco's modified Eagle medium
DMSO	dimethyl sulfoxide
DNA	deoxyribonucleic acid
DRP1	dynamin related protein 1
dsRNA	double-stranded ribonucleic acid
ETS	electron transfer system
GAS	gamma interferon activated site
GFP	green fluorescent protein

GPR35	G-protein coupled receptor 35
GWAS	genome-wide association study
ER	endoplasmic reticulum
FAD	flavin adenine dinucleotide
FBS	fetal bovine serum
fzo	*fuzzy onions*
HD	Huntington's disease
HEK	human embryonic kidney
IDO	indolamine 2,3-dioxygenase
IFM	indirect flight muscle
IL-1ß	interleukin-1ß
INF-γ	interferon-γ
KAT	kynurenine aminotransferase
KMO	kynurenine 3-monooxygenase
KP	kynurenine pathway
KYN	kynurenine
KYNA	kynurenic acid
KYNU	kynureninase
LB	luria broth
LD	light:dark
LOF	loss of function
LPS	lipopolysaccharide
f.luc	firefly *luciferase*
MAPL	mitochondrial-anchored ubiquitin ligase
MAO-B	monoamine oxidase B
Marf	*mitochondrial assembly regulatory factor*
MCP1	Mdm10-complementing protein 1
MCU	mitochondrial calcium transporter
M-G	malate and glutamate
MFF	mitochondrial fission factor
Mfn	mitofusin
mHTT	mutant huntingtin protein
MIA	mitochondrial import and assembly machinery
miAAT	mitochondrial aspartate aminotransferase
MiD	mitochondrial dynamics proteins
MIM	mitochondrial inner membrane
MIRO	mitochondrial Rho GTPase
MOM	mitochondrial outer membrane
M-P	malate and pyruvate
MPP	mitochondrial processing peptidase
MPPP	1-methyl-4-phenyl-4-propionoxy-piperidine
MPTP	methyl-4-phenyl-1,2,3,6-tetrahydropyridine
mRNA	messenger ribonucleic acid

mtDNA	mitochondrial deoxyribonucleic acid
MUL1	mitochondrial ubiquitin ligase
mw	*mini-white*
tRNA	transfer ribonucleic acid
NAD	nicotinamide adenosine dinucleotide
N/D	nocturnal/diurnal ratio
NAD(P)H	nicotinamide adenosine dinucleotide phosphate
NDUFA10	NADH:ubiquinone oxidoreductase subunit A10
NMDA	N-methyl-d-aspartate
NOS	nitric acid synthase
iNOS	inducible nitric acid synthase
nNOS	neuronal nitric acid synthase
OPA1	optic atrophy 1
ORF	open reading frame
OXPHOS	oxidative phosphorylation
p-38 MAPK	p-38 mitogen-activated protein kinase
PAM	presequence translocase associated motor
PARL	presenilin-associated rhomboid-like protein (PARL)
PERK	protein kinase R-like endoplasmic reticulum kinase
PINK1	PTEN-induced putative kinase 1
PARP-1	poly[ADP-ribose] polymerase 1
PBS	phosphate buffered saline
PD	Parkinson's disease
PFA	paraformaldehyde
PGC1α	proliferator activated γ coactivator 1α
PKA	protein kinase A
qPCR	quantitative polymerase chain reaction
QPRT	quinolinate phosphoribosyltransferase
QUIN	quinolinic acid
RFP	red fluorescent protein
RING	rapid iterative negative geotaxis
RNA	ribonucleic acid
RNAi	ribonucleic acid interference
ROS	reactive oxygen species
RT	room temperature
SAM	sorting assembly machinery
SDS	sodium dodecyl sulphate
SDS-PAGE	SDS-polyacrylamide gel electrophoresis
SFM	serum-free medium
SNP	single nucleotide polymorphism
SUMO	small ubiquitin modifier
TBS	tris buffered saline
TCA	tricarboxylic acid

TDO	tryptophan 2,3-dioxygenase
TEM	transmission electron microscopy
TFAM	transcription factor A, mitochondrial
TIM	translocase of the inner mitochondrial membrane
TOM	translocate of the outer mitochondrial membrane
TPM	transcripts per kilobase million
TRP	tryptophan
UAS	upstream activation sequence
UCP1	uncoupling protein 1
UQ	ubiquinone
v	*vermillion*
VDAC	voltage dependant ion channel
VSP13	variable small protein 13 precursor
YFP	yellow fluorescent protein

1 Introduction

1.1 Kynurenine 3-monooxygenase and the kynurenine pathway

Kynurenine 3-monooxygenase (KMO) is an enzyme which operates within the kynurenine pathway (KP), the major route of tryptophan metabolism (Figure 1.1). Tryptophan is an essential amino acid required for protein synthesis, and in higher eukaryotes is also converted into the key neurotransmitters serotonin and tryptamine. However, >95% of tryptophan is metabolised through the KP - a series of enzymatic reactions producing several metabolites - which ultimately leads to the production of nicotinamide adenosine dinucleotide (NAD^+) (Beadle *et al.*, 1947; Stone *et al.*, 2003). In mammals, the kynurenine pathway (KP) is initiated by the oxidative cleavage of the indole-ring of L-tryptophan (L-TRP) to produce *N*-formylkynurenine, facilitated by one of two indoleamine 2,3-dioxygenases (IDO1) (Thomas & Stocker, 1999) and IDO2 (Ball *et al.*, 2009), or by tryptophan-2,3-dioxygenase (TDO2) (Ren & Correia, 2000). *N*-formyl L-kynurenine is degraded by formamidase to produce L-kynurenine (L-KYN) (Mehler & Knox, 1950). L-KYN can then be deaminated by the kynurenine aminotransferase (KAT) family of enzymes (Han *et al.*, 2010), resulting in the production of kynurenic acid (KYNA), the first KP metabolite discovered over 160 years ago (Liebig; 1853). Cleavage of L-KYN by kynureninase, on the other hand, results in the production of anthranilic acid (Bender & McCreanor; 1982), whereas hydroxylation *via* KMO produces 3-hydroxykynurenine (3-HK) (De Castro *et al.*, 1956).

Some evidence suggests an alternative route for KYNA and 3-HK synthesis under physiological conditions which involves D-kynurenine (D-KYN) as a precursor. Indeed, systemic administration of D-KYN, thought to be synthesised from bacterial D-tryptophan (D-TRP) (Lam *et al.*, 2009), leads to increased KYNA levels in both the brain (Ogaya *et al.*, 2010; Pérez-De la Cruz *et al.*, 2012a) and periphery in rats (Loh & Berg, 1971; Fukushima *et al.*, 2009) and in human brain tissue homogenates (Pérez-De la Cruz *et al.*, 2012a). Administration of inhibitors of D-amino acid oxidase 1 (DAO1) suppressed KYNA synthesis from D-KYN (Fukushima *et al.*, 2009; Ishii *et*

al., 2010; Pérez-De la Cruz *et al*., 2012a; Blanco *et al*., 2015) indicating deamination of D-KYN by DAO1 as a mechanism of KYNA synthesis. Both L-KYN and D-KYN can also be converted into KYNA by the reactive oxygen species (ROS) peroxynitrite ($OONO^-$) and hydroxyl radicals (OH^-) (Blanco *et al*., 2015). D-KYN administration in mice results in the synthesis of 3-HK in both peripheral and brain tissues (Wang *et al*., 2012).

Anthranilic acid and 3-HK are subsequently converted into 3-hydroxyanthranilic acid (3-HANA) by kynureninase (KYNU) (Kawai *et al*., 1988; Baran & Schwarcz; 1990), which is then oxidised by 3-hydroxyanthranilate 3,4- dioxygenase (3-HAO) into 2-amino-3-carboxymuconic 6-semialdehyde (ACMS) (Decker *et al*., 1961). Under physiological conditions, this intermediate spontaneously reassembles to form quinolinic acid (QUIN), which is then transaminated by quinolinate phosphoribosyltransferase (QPRT) to generate nicotinic acid, and ultimately NAD^+. The rate of NAD^+ production in the brain is limited by relatively low QPRT levels (Foster *et al*., 1985), which also results in higher QUIN concentrations in the central nervous system (CNS). ACMS can also be metabolised to produce picolinic acid via the activity of 2-amino-3-carboxymuconic-6-semialdehyde decarboxylase (ACMSD). However, ACMSD levels in the brain are also low (Pucci *et al*., 2007), thus favouring the production of QUIN.

In the genetic model organism used extensively in this study, the fruit fly *Drosophila melanogaster,* the KP is believed to be uncoupled from the production of NAD+ (Rongvaux *et al*., 2003) (Figure 1.1). L-TRP is metabolised by the TDO orthologue, encoded by the gene *vermillion* (*v*), to produce *N*-formylkynurenine (Searles and Voelker, 1986), followed by the synthesis of L-KYN by KFase. L-KYN is metabolised either by KATs to produce KYNA, or by the KMO homologue encoded by *cinnabar* (*cn*) to produce 3-HK (Warren *et al*., 1996). 3-HAO and QPRT are not present in *Drosophila*, therefore no QUIN is produced by the fly KP (Greene *et al*., 2012). Instead, 3-HK is metabolised by the phenoxazinone synthetase homologue cardinal to produce the brown ommochrome xanthommatin, which is responsible for pigmentation in the compound eye (Tearle, 1991).

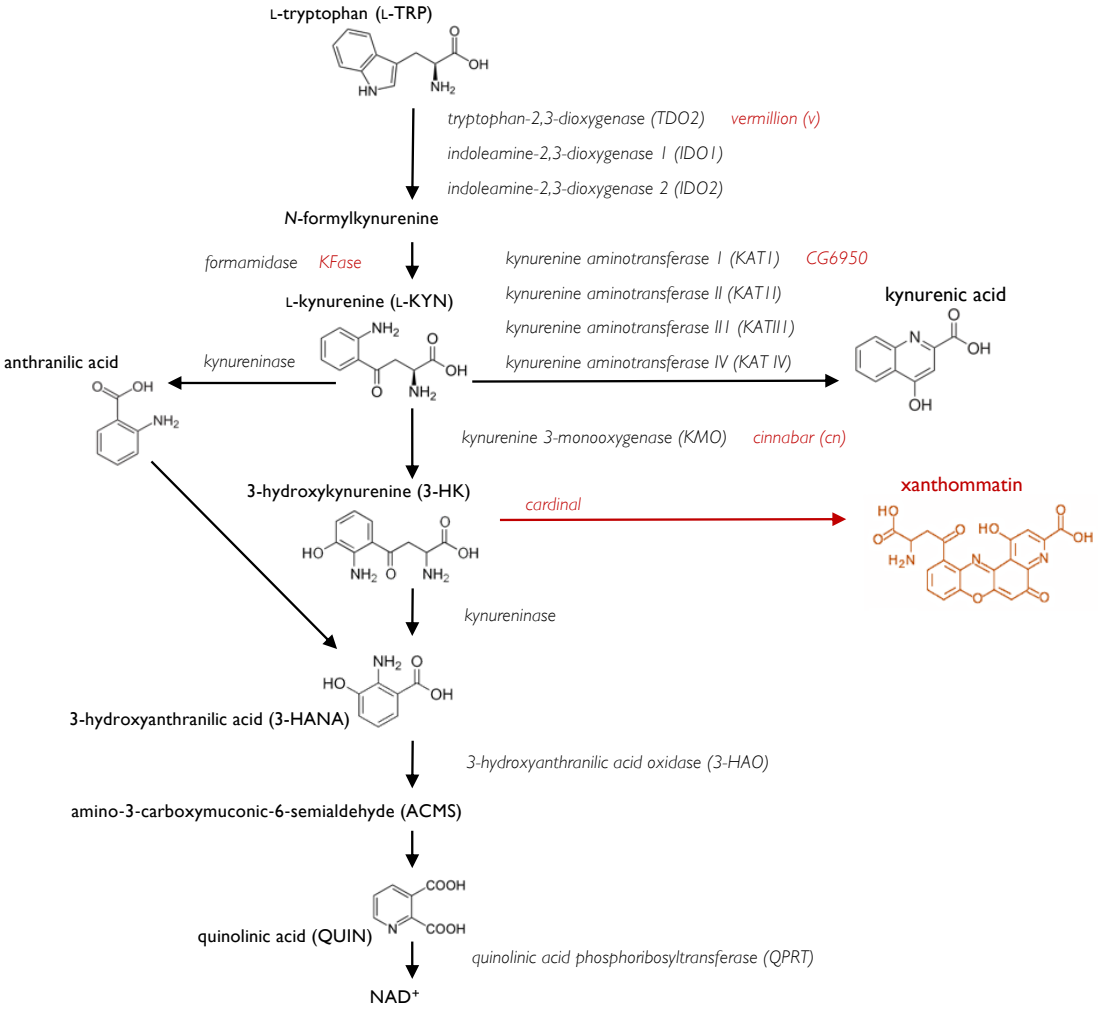

Figure 1.1. The kynurenine pathway (KP) in mammals and *Drosophila.*
The KP is the major route of tryptophan (TRP) degradation, with >95% of the essential amino acid degraded through the pathway. TRP is metabolised by IDO1/2 or TDO2 to produce L-kynurenine (L-KYN). L-KYN is metabolised through two distinct branches of the pathway; by kynurenine aminotransferases (KATs) to produce kynurenine acid (KYNA) or by KMO to produce 3-hydroxykynurenine (3-HK), 3-hydroxyanthranillic acid (3-HANA), quinolinic acid (QUIN) and ultimately NAD^+. Genes encoding enzymes in *Drosophila* are in red text. Flies lack homologues for 3-hydroxyanthranilic acid (3-HAO) and quinolinic acid phosphoribosyltransferase (QPRT), so the pathway is uncoupled from NAD^+ synthesis in flies. 3-HK is converted into the brown ommochrome pigment xanthommatin by phenoxazinone synthetase (*cardinal*) (adapted from Campesan *et al.*, 2011 & van der Goot & Nollen, 2013).

1.1.1 Regulation of the KP

Metabolic flux through the KP is primarily regulated by the activity of IDO1, IDO2 and TDO2, which control the production of KYN from TRP. The balance in flux through the two main branches of KYN metabolism are regulated through the activities of KATs and KMO.

1.1.1.1 TDO2, IDO1 and IDO2

TDO2 and IDO1/2 show low sequence identity and are regulated by distinct mechanisms (Rafice *et al.*, 2014; Meng *et al.*, 2014). TDO2 is a heme-containing dioxygenase and reduction of its heme group facilitates the oxidation of L-TRP, and is therefore influenced by reducing agents and reactive oxygen species (ROS) (Ren & Correia, 2000). TDO2 can also be activated by corticosteroids (Ren & Correia, 2000) and proinflammatory cytokines, although this is thought to occur indirectly through the activation of glucocorticoid receptors (Walker *et al.*, 2013). The proinflammatory cytokine interferon-γ (INF-γ) directly promotes IDO1 expression, binding to one of two INF-γ activated sites (GAS) in the 5' region of the gene encoding IDO1. Activation of IDO1 can also be promoted by other cytokines such as interleukin-1ß (IL-1ß) and toll-like receptor agonists such as lipopolysaccharide (LPS) (Alberati-Giani *et al.*, 1997a; Fujigaki *et al.*, 2006; Connor *et al.*, 2008). IDO2 is also induced by proinflammatory cytokines, but is more narrowly expressed and less active than IDO1 (Prendergast *et al.*, 2014).

1.1.1.2 KATs

There have been 4 distinct KATs identified in the mammalian brain (KATI, KATII, KATIII, KATIV). The expression of KATI (glutamine transaminiase K) and KATII (L-α-aminoadipate aminotransferase) in the CNS is limited to astrocytes (Okuno *et al.*, 1991; Du *et al.*, 1992; Roberts *et al.*, 1992; Guidetti *et al.*, 2007a). KATI is considered to function optimally at high pH, (Baran *et al.*, 1994; Guidetti *et al.*, 1997), whereas KATII functions at neutral pH (Guidetti *et al*; 1997; Han *et al.*, 2008), and thus KATII is thought be more important in the production of KYNA in the brain under physiological conditions (Guidetti *et al.*, 1997). Two additional KATs, KATIII - which

has high sequence similarity to KATI (Yu *et al.*, 2006) - and KATIV (mitochondrial aspartate transaminase) (Guidetti *et al.*, 2007b) have also been identified in the mammalian brain. The relevance of KATIV localisation to mitochondrial function is discussed in further detail in section 1.3 of this chapter.

1.1.1.3 KMO

KMO was first found to be responsible for the conversion of L-KYN to 3-HK in cat and rat livers (De Castro *et al.*, 1956) and was subsequently characterised as a flavin adenine dinucleotide (FAD)-dependent monooxygenase, dependent upon NAD(P)H as an electron donor (Saito *et al.*, 1957; Okamoto & Hayaishi, 1967; Nisimoto *et al.*, 1977). The human *KMO* gene was originally cloned using a cDNA probe of exon 2 from *Drosophila* KMO (Alberati-Giani *et al.*, 1997b). The amino acid sequence is well conserved between prokaryotic and mammalian KMO in domains important for the binding of L-KYN and FAD (Figure 1.2). Two transmembrane domains that embed KMO in the mitochondrial outer membrane (MOM) are also well conserved between mammals and *Drosophila*. The first crystal structure of KMO was obtained of the *S. cerevisiae* orthologue (Amaral *et al.*, 2013), revealing its similarity to members of the flavin-dependent hydroxylase family such as 2-methyl-3-hydroxypyridine-5-carboxylic acid oxygenase (McCulloch *et al.*, 2009). The protein features a Rossman fold with five ß-sheets and four α-helices as part of the domain that interacts with FAD. An R83M mutation at a highly conserved residue in *S. cerevisiae* KMO results in a catalytically inactive protein, due to inability to bind L-KYN (Amaral *et al.*, 2013). KMO has also been identified in a number of prokaryotic species (Kurnasov *et al.*, 2003; Crozier-Reabe *et al.*, 2008) and the crystal structures of prokaryotic *Pseudomonas fluorescens* KMO and human KMO have recently been solved (Kim *et al.*, 2018).

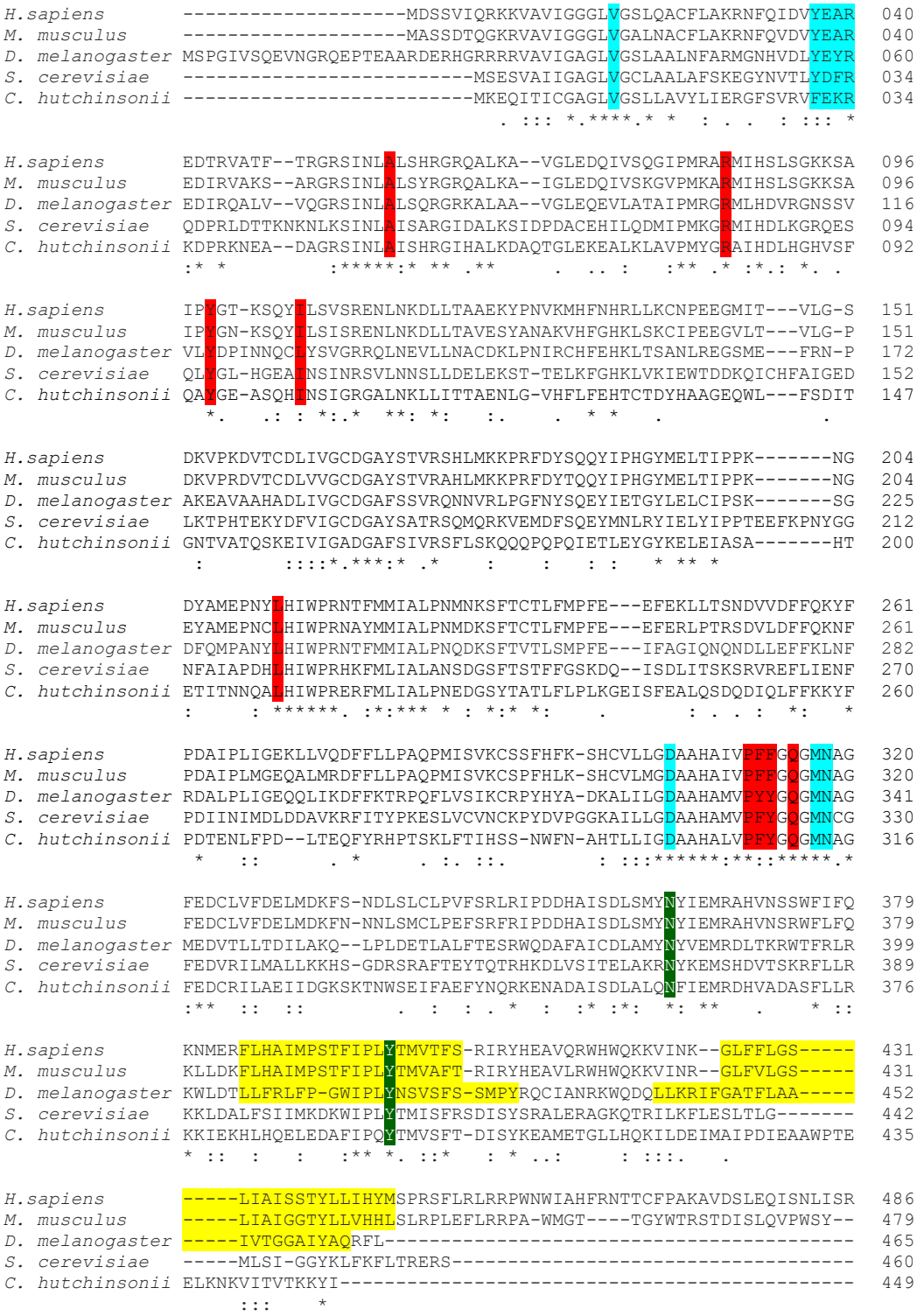

Figure 1.2. Multiple sequence alignment of KMO from diverse species.

Amino acid sequences of KMO from humans, mice, flies, yeast and bacteria were aligned using Clustal X software.

Proposed residues involved in L-KYN binding (Amaral *et al.*, 2013)

Proposed residues involved in L-KYN binding (Mole *et al.*, 2016)

Proposed residues involved in FAD binding (Kim *et al.*, 2018)

UniProt predicted transmembrane domains

KMO is tissue specific in its expression pattern in mammals (Figure 1.3A), with high expression in the liver, kidney, placenta (Erickson *et al.*, 1992; Alberati-Giani *et al.*, 1997b), blood monocytes (Jones *et al.*, 2015) and monocyte-derived macrophages (Heyes *et al.*, 1997; Chiarugi *et al.*, 2001; Guillemin *et al.*, 2003a). In the CNS, KMO expression is limited to microglia (Guillemin *et al.*, 2001; Guillemin *et al.*, 2003a; Giorgini *et al.*, 2008). Like TDO2 and IDO1/2, KMO expression is upregulated in the CNS by inflammatory challenge *in vivo* (Connor *et al.*, 2008; Molteni *et al.*, 2013) and in primary and immortalised microglial cells *in vitro* (Alberati-Giani *et al.*, 1996; Giorgini *et al.*, 2008; Wang *et al.*, 2010). KMO is highly expressed in the iris/ciliary body of the human eye, leading to the production of 3-HK which is taken up by the lens, protecting the eye from UV radiation (Roberts *et al.*, 1991; Chiarugi *et al.*, 1999). In *Drosophila*, *cn* is tissue specific in its expression and expressed at low levels in most adult tissues (Chintapalli *et al.*, 2007; Figure 1.3B). In the adult, *cn* is expressed most highly in the salivary gland and the eye and is best described for its role in the eye pigmentation process (Tearle *et al.*, 1991).

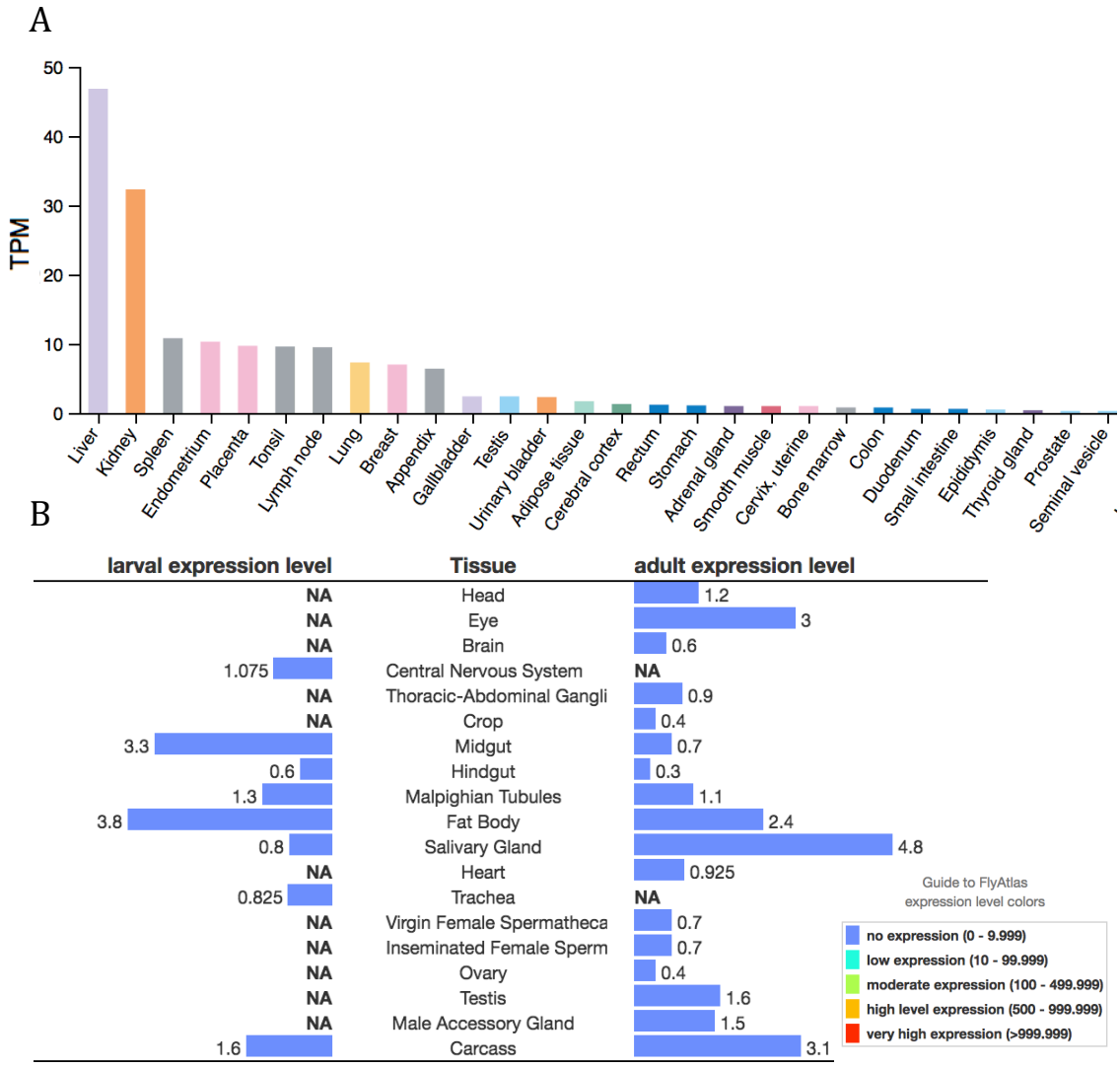

Figure 1.3 *KMO* mRNA expression data in human and *Drosophila*.
A) Human Protein Atlas overview of *KMO* mRNA expression in human tissues. *KMO* is expressed highly in the liver, kidney and organs containing lymphoid tissue, such as lymph node, spleen and lung (TPM = transcripts per kilobase million) (Uhlén *et al.*, 2015). **B)** FlyAtlas microarray-based anatomical expression data for *cn* in larval and adult *Drosophila*. *cn* is expressed at low levels in all tissues, with highest adult expression in salivary glands and the eye (arbitrary units) (Chintapalli *et al.*, 2007).

1.1.2 Neuromodulatory properties of KP metabolites

Metabolites of the KP possess diverse functions in neurons which can be either neurotoxic or neuroprotective. Through the KMO-operating arm of KYN metabolism, 3-HK (Vazquez *et al.*, 2000; Giles *et al.*, 2003), 3-HANA (Iwahashi *et al.*, 1988; Golstein *et al.*, 2000) and QUIN (Platenik *et al.*, 2001) act as oxidising agents at physiological levels, causing the generation of ROS. 3-HK and 3-HANA treatment of cultured rat neurons results in the production of hydrogen peroxide and hydroxyl radical, p38-mitogen-activated protein kinase (p38-MAPK) activation (Okuda *et al.*, 1996) and neurotoxicity, all of which can be attenuated by the hydroxyl scavenger catalase (Okuda *et al.*, 1996; and Smith *et al.*, 2009, Iwahashi *et al.*, 1988).

QUIN was first identified as a potential neurotoxin by the strong convulsions it caused when injected into the cerebellum of mice (Lapin *et al.*, 1978). Striatal injection of QUIN into rodent brains is excitotoxic, causing axon-sparing lesions of dose-dependent size, proximal to the site of injection (Schwarcz *et al.*, 1983). This effect is rescued by co-administration of a selective N-methyl-d-aspartate (NMDA) receptor antagonist (Foster *et al.*, 1983), due to the role of QUIN as a selective NMDA receptor agonist (Stone *et al.*, 1981) (Figure 1.4). A marginal increase in QUIN above physiological levels is sufficient to cause rapid neurodegeneration in rat corticostriatal cell culture (Whetsell & Schwarcz, 1989). The potency of QUIN-induced neurotoxicity is likely due to the multiple mechanisms through which it is able to cause neuronal insult. Indeed, as well as stimulating neuronal release of glutamate at presynaptic NMDA receptors, QUIN inhibits reuptake of the neurotransmitter by astrocytes (Tavares *et al.*, 2002) and also inhibits the production of glutamine from glutamate and ammonia, by glutamine synthetase (Ting *et al.*, 2009). High concentrations of extracellular glutamate and persistent activation of excitatory neurons causes excitotoxicity due to augmented Ca^{2+} influx through the ion-channel complex, leading to mitochondrial dysfunction, cytochrome C release, the activation of proteases and caspases, as well as nitric oxide synthase (NOS) activation (Pérez-De La Cruz *et al.*, 2012b).

QUIN promotes lipid peroxidation (Rios & Santamaria, 1991) in an NMDA receptor (Santamaria & Rios, 1993) and iron (II) (Stipek *et al.*, 1997) dependent manner. In cultured human neurons and astrocytes, treatment with QUIN results in a dose-dependent increase in the activity of inducible and neuronal NOS (iNOS and nNOS respectively), leading to increased cellular toxicity, depletion of NAD^+ and activation of the NAD^+ dependent nuclear DNA repair enzyme poly[ADP-ribose] polymerase 1 (PARP-1) (Brady *et al.*, 2009). In the rat brain, QUIN-induced increases in both iNOS and nNOS are accompanied by lipid peroxidation and neuronal toxicity (Pérez-De La Cruz *et al.*, 2012b). Inhibition of both forms of NOS is sufficient to rescue QUIN toxicity (Perez-Severiano *et al.*, 1998; Braidy *et al.*, 2009) and the antioxidants melatonin (Behan *et al.*, 1999), alpha-phenyl-t-butyl nitrone and U-83826E (Nakao *et al.*, 1996) are also able to reduce QUIN-induced cell death in rat striatal neurons *in vivo* and *in vitro*, indicating that NO production plays a causative role.

In the other branch of KYN metabolism, KYNA at physiological levels acts as a non-competitive antagonist of α7-nicotinic acetylcholine (α7nACh) receptors and at high micromolar concentrations is a non-selective NMDA receptor antagonist (Perkins & Stone; 1982) (Figure 1.4). KYNA activity therefore inhibits cholinergic, glutamatergic and downstream dopaminergic signalling (Hilmas *et al.*, 2001) counteracting potential excitotoxicity caused by QUIN. At high concentrations KYNA possesses antioxidant properties due to its ability to scavenge free radicals such as hydroxyls and superoxide anions (Lugo-Huitron *et al.*, 2011), which are produced by 3-HK, 3-HANA and QUIN. It also acts as a ligand for G-protein coupled receptor 35 (GPR35), which inhibits the LPS-induced secretion of tumor necrosis factor-α from macrophages (Wang *et al.*, 2006) and LPS-induced death in mice (Moroni *et al.*, 2012).

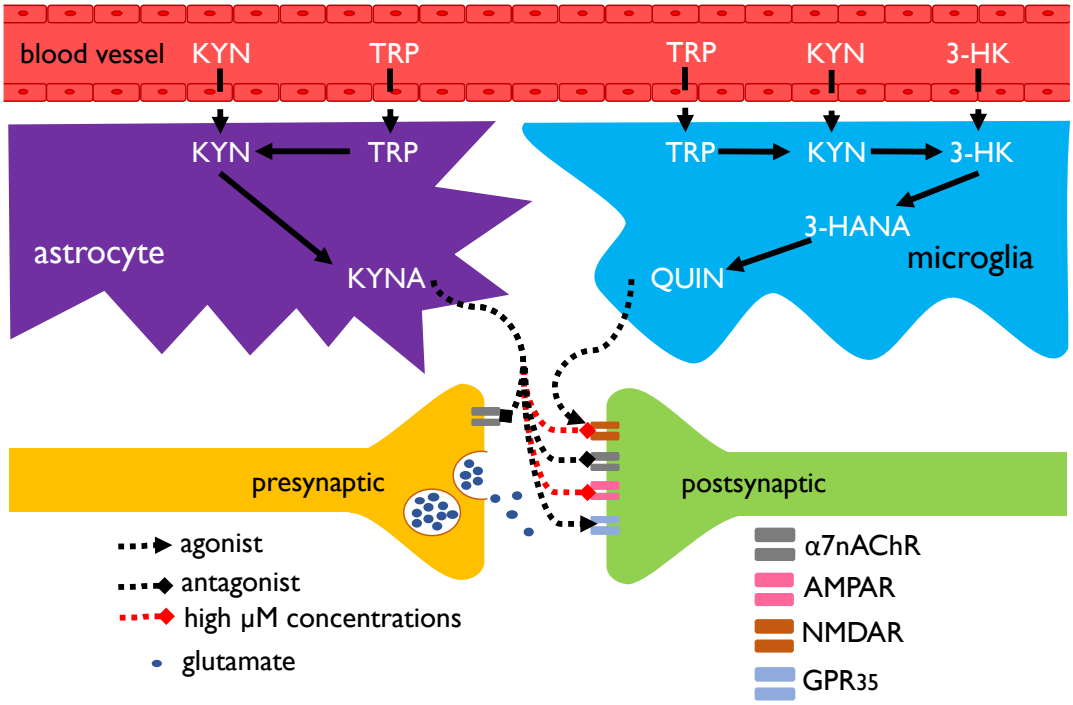

Figure 1.4. The kynurenine pathway (KP) in the central nervous system.
Tryptophan (TRP), kynurenine (KYN) and 3-hydroxykynurenine (3-HK) readily cross the blood brain barrier, entering the brain from the periphery through the bloodstream. The kynurenic acid (KYNA) and quinolinic acid (QUIN) producing branches of the KP are spatially separate in the brain. Kynurenine amino transferase (KAT) expression and thus KYNA synthesis occurs in astrocytes, whereas kynurenine 3-monooxygenase (KMO) expression and thus 3-HK and QUIN production is limited to microglia. QUIN acts as an N-methyl-d-aspartate receptor (NMDAR) agonist, therefore increases in QUIN levels can lead to excitotoxicity due to excessive glutamatergic signalling. KYNA acts as an α7-nicotinic acetylcholine receptor (α7nAChR) antagonist and at high mM concentrations as an NMDAR and α-amino-3-hydroxy-5-methyl-4-isoxazolepropionic acid receptor (AMPAR) antagonist. KYNA is also a G-protein coupled receptor 35 (GPR35) agonist (adapted from Maddison & Giorgini; 2015).

1.1.3 The KP and human disease

Disruption of the KP has been reported in a whole host of human diseases, including cancers, HIV, psychiatric disorders such as schizophrenia and bipolar and neurodegenerative diseases including Alzheimer's (AD), Huntington's (HD), Parkinson's disease (PD) and amyloid lateral sclerosis (ALS) (Chen & Guillemin, 2009). The most comprehensive research into the role of KP in pathology and its potential as a therapeutic target has been in neurological diseases such as schizophrenia and neurodegeneration, therefore these are discussed in more detail below.

1.1.3.1 Psychiatric disorders

KYNA levels are elevated in the plasma (Ravikumar *et al.*, 2000) and cerebrospinal fluid (CSF) (Erhardt *et al.*, 2001) of schizophrenia patients and in the post-mortem prefrontal cortex (Schwarcz *et al.*, 2001; Nilsson *et al.*, 2005; Sathyasaikumar *et al.*, 2011; Linderholm *et al.*, 2012). Similarly in bipolar disorder, CSF KYNA levels are raised (Olsson *et al.*, 2010) and correlate with psychosis (Olsson *et al.*, 2012; Lavebratt *et al.*, 2014; Sellgren *et al.*, 2015). A decrease in KMO activity is a possible cause of raised KYNA in these disorders, as a decrease in KMO expression and activity are observed in schizophrenia patients (Sathyasaikumar *et al.*, 2011; Wonodi *et al.*, 2011a). Single nucleotide polymorphisms (SNPs) within the *KMO* gene have also been associated with patients with schizophrenia and bipolar disorder (Wonodi *et al.*, 2011b; Holtze *et al.*, 2012; Lavebratt *et al.*, 2014). Notably, in a KMO knockout mouse model, an enrichment of schizophrenia-associated genes was found to be differentially expressed in the cerebellum and cerebral hemisphere (Erhardt *et al.*, 2015). This was accompanied by a range of schizophrenia-like traits such as contextual memory deficits and increased anxiety – providing the first evidence for a functional link between KMO deficit and these impairments.

1.1.3.2 Neurodegenerative disease

Neuroinflammation is a common feature across many neurodegenerative diseases (McManus & Heneka, 2017). Given the role of inflammatory molecules in the

upregulation of KP enzymes TDO2, IDO1/2 and KMO, neuroinflammation is the most probable cause of KP dysregulation in neurodegenerative disease (Campbell, 2014). An increase in L-KYN/L-TRP ratio has been reported in the blood of Huntington's disease (HD) patients, signifying an increase in flux through the KP (Stoy *et al.*, 2005; Forrest *et al.*, 2010). Levels of 3-HK and QUIN are raised in the neostriatum and cortex of post-mortem HD patient brains at the early stages of symptom onset (Guidetti *et al.*, 2004; Sathyasaikumar *et al.,* 2018), whereas KYNA levels are reduced in the brain (Jauch *et al.*, 1995) and CSF (Heyes *et al.*, 1992). An increase in KP flux, as well as an imbalance between the KMO and KAT-operating branches of the KP has been observed in mouse models of HD. Increased expression of *IDO1* has been demonstrated in the striatum of YAC128 mice (Mazarei *et al.*, 2010). Levels of 3-HK and QUIN are increased in the striatum and cerebellum of YAC128 and R6/2 mice and correlate with the onset of HD-relevant phenotypes, whereas KYNA remains unaffected (Guidetti *et al.*, 2006). Notably, intrastriatal QUIN injection causes axon-sparing neuronal lesions in rats which resemble pathology found in HD patients, along with progressive motor and behavioural deficits (Schwarcz *et al.*, 1983), suggesting a significant role for elevated QUIN in the progression of HD.

An increased L-KYN/ L-TRP ratio has also been reported in the blood and CSF of AD patients (Gulaj *et al*; 2010), with raised TDO, IDO1, 3-HK & QUIN levels also found in post-mortem patient brains (Guillemin *et al.*, 2005; Bonda *et al.*, 2010; Wu *et al.*, 2013). Expression of an aggregate-prone 42 amino acid amyloid ß peptide ($aß_{42}$), the main component of amyloid plaques in the brain of AD patients, induces IDO1 expression and QUIN production in human macrophages and microglia (Guillemin *et al.*, 2003b). Furthermore, TDO and QUIN immunoreactivity has been detected in Aß deposits and Tau-positive neurofibrillary tangles (Wu *et al.*, 2013). Treatment of human neurons with QUIN results in the upregulation of genes involved in Tau phosphorylation (Rahman *et al.*, 2009), a marker for AD (Hampel *et al.*, 2010), indicating a causal link between upregulation of the KP and AD pathogenesis.

An increased L-KYN/ L-TRP ratio has also been observed in the serum and CSF of PD patients compared to controls, indicating an upregulation of IDO/TDO2 activity and

thus KP flux (Widner *et al*., 2002). Increased 3-HK levels and decreased KYNA have also been reported in the putamen, prefrontal cortex and *pars compacta* of the *substantia nigra* in PD patients (Ogawa *et al*., 1992). A study investigating genetic links between KMO and PD found no association between the frequency of four KMO SNPs and PD patients (Török *et al*., 2015). The study investigated SNPs that have previously linked KMO to schizophrenia and bipolar disorders, which are associated with a decrease in KMO enzymatic activity. The authors concluded that these SNPs do not influence the potential binding of PD relevant proteins and that there is likely no association between KMO activity and PD. However, the sample size of the study was small, enrolling just 105 PD patients and 131 controls. Furthermore, the study did not investigate other KMO SNPs which might have different effects on protein form and function. A genetic link between KMO and PD is therefore yet to be elucidated, but cannot necessarily be ruled out. Downstream of KMO in the KP, four SNPs proximal to *ACMSD* have been associated with PD (Lill *et al*. 2012; Sharma *et al*., 2012; Pihlstrom *et al*., 2013; Bandrés-Ciga *et al*., 2016). Two larger GWAS studies also found a SNP proximal to *ACMSD* to be associated with PD (Nalls *et al*., 2014; Chang *et al*., 2017). Mutations in the coding sequence of *ACMSD* have been identified in both familial (Marti-Masso *et al*., 2013) and sporadic cases (Vilas *et al*., 2017), again implicating the KMO operating branch of the KP in PD.

1.1.3.3 The KP as a therapeutic target

The imbalance in KP flux observed across neurodegenerative diseases have stimulated the interest in the therapeutic targeting of KP enzymes. Deletion of the KMO encoding gene *biosynthesis of nicotinic acid 4* (*BNA4)* in *Saccharomyces cerevisiae* leads to reduced ROS generation and cell toxicity in a mutant huntingtin protein (mHTT) model, corresponding to a decrease in 3-HK and QUIN levels (Giorgini *et al*., 2005). Genetic inhibition of *vermillion* (encoding TDO) or *cinnabar* (encoding KMO) in *Drosophila,* through RNAi or amorphic alleles, is protective in mHTT, Aß$_{42}$ and α-synuclein (aSyn) models of neurodegeneneration (Campesan *et al*., 2011; Breda *et al*., 2016). Pharmacological inhibition of TDO and KMO enzymatic activity, overexpression of hKATII, and L-TRP supplementation all convey protection against mHTT induced neurodegeneration in flies, which is associated

with a shift in L-KYN metabolism towards the production of KYNA and away from KMO-mediated production of 3-HK. Furthermore, protection is abolished by 3-HK supplementation, supporting the notion that changes in KP metabolites are the underlying cause of neuroprotection (Campesan *et al.*, 2011; Breda *et al.*, 2016). In the nematode *Caenorhabditis elegans,* genetic inhibition of *tdo-2* suppressed pathogenesis of aSyn, Aß$_{42}$ and a polyglutamine (128Q) protein (van der Goot *et al.*, 2012). Interestingly, in the aSyn model, deletion of *kmo-1* does not convey protection, whereas *tdo-2* knockdown in a *kmo-1* null background does, indicating that this protection is independent of KP metabolites downstream of KMO. KYNA levels were unaffected by *tdo-2* knockdown, however TRP was significantly elevated. L-TRP supplementation was also protective against aSyn toxicity, indicating that in *C. elegans*, L-TRP influences toxicity independent from the KP.

The therapeutic targeting of the KP has also been extended to mammalian models of neurodegenerative disease. Peripheral administration of JM6, a small-molecule prodrug inhibitor of KMO, ameliorated synaptic loss and spatial memory deficits in a human amyloid precursor protein (hAPP) expressing mouse model of AD (Zwilling *et al.*, 2011). In the same study, synaptic loss, neuroinflammation and neurodegeneration were all reduced in the R6/2 HD model mice administered with JM6, which also caused a significant increase in lifespan. However, the mechanism of action of JM6 is unclear. It was proposed to act as a precursor for the small molecule KMO inhibitor Ro 61-8048 (Muchowski *et al.*, 2008; Zwilling *et al.*, 2011), although a later study found that KMO inhibition achieved by JM6 is characteristically weak and likely caused by Ro 61-8048 impurity in JM6 synthesis (Beconi *et al.*, 2012). Oral administration of another KMO inhibitor, CHDI-340246, rescued synaptic plasticity in the hippocampus of R6/2 mice and increased survival of male but not female mice (Beaumont *et al.*, 2016). However, the drug had no significant effect on other clinically relevant phenotypes such as motor function and brain volume. Nevertheless, KMO continues to be a promising therapeutic target in the treatment of neurodegenerative disease.

Interestingly, KMO deletion or inhibition has been demonstrated to reduce proinflammatory response to LPS and microglial activation in mice and this was

attributed to increased L-KYN levels by the authors (Garrison *et al.*, 2018). This could account for the reduced neuroinflammation caused by KMO inhibition in mouse models of trypanosomiasis (Rodgers *et al.*, 2009) and chronic nerve pain (Rojewska *et al.*, 2016). KMO knockout or inhibition *via* the novel inhibitor GSK180, markedly protected against a mouse model of acute pancreatitis-induced multiple organ dysfunction syndrome (AP-MODS), which features profound inflammation (Mole *et al.*, 2016). Together these findings indicate the potential of KMO inhibition in the treatment of disorders featuring systemic inflammation. Given the role of KYNA as a GPR35 agonist which leads to protection against inflammatory challenge (Wang *et al.*, 2006; Moroni *et al.*, 2012), it is hypothesised that increased KYNA as a result of KMO deletion or inhibition (Giorgini *et al.*, 2013; Mole *et al.*, 2016) could be responsible for this effect.

1.2 Mitochondria – evolution, function, maintenance and disease relevance

Mitochondria are double-membrane bound organelles that act as essential "power stations" in eukaryotic cells, providing the adenosine triphosphate (ATP) required to drive diverse active cellular processes. Mitochondria evolved from endosymbiotic bacteria, a hypothesis first postulated by Ivan Wallin (Wallin, 1925), as an expansion of Andreas Schimper and Kobstantin Mereschkowski's theories that chloroplasts evolved from cyanobacteria. The idea was largely ignored until the 1960's, when it was again proposed by Lynn Sagan (Sagan, 1967). Although initially derided, phylogenetic analyses of mitochondrial encoded genes supported the concept (Bonen *et al.*, 1977; Schwartz & Dayhoff., 1978; Yang *et al.*, 1985), resulting in its wide acceptance. It is now believed that all known eukaryotic lifeforms descend from a common, mitochondria-containing ancestor (Dacks *et al.*, 2016).

The sequencing of the human mitochondrial genome (mtDNA), a 16,569 bp circular molecule (Anderson *et al.*, 1981), revealed that it contains 37 genes, encoding 13 proteins, 22 transfer RNAs (tRNAs) and two (small and large) ribosomal subunits. All 13 proteins are components of the electron transfer system (ETS), the mechanism which generates most of the ATP in the majority of eukaryotic organisms, via oxidative phosphorylation (OXPHOS). There are ~77 nuclear encoded additional components of the ETS and furthermore, the proteins required for the transcription, translation, post-translational modification and assembly of the 13 mtDNA encoded proteins are all nuclear encoded (DiMauro & Schon, 2003). The mammalian mitochondrial proteome consists of proteins which are primarily associated with this cellular compartment and contains ~1000 – 1500 distinct proteins (Calvo & Mootha., 2010). Interestingly, this is approximately the same as the number of proteins encoded by alpha-proteobacteria, which are the closest living relatives of human mitochondria (Andersson *et al.*, 1998). The transfer of mitochondrial genes to the nucleus, along with the loss of redundant genes, are two of many evolutionary changes that have occurred in mitochondria since its origins as an endosymbiotic alpha-proteobacterium.

Mitochondria have developed mechanisms which facilitate the import of lipids and nuclear encoded proteins across the mitochondrial outer membrane (MOM) into the intermembrane space. Most proteins are imported through the translocase of the outer mitochondrial membrane (TOM) complex (Kiebler *et al.*, 1990) and are subsequently incorporated into the MOM by sorting and assembly machinery (SAM) (Wiedemann *et al.*, 2003), into the mitochondrial inner membrane (MIM) via translocase of the inner mitochondrial membrane (TIM22) (Sirrenberg *et al.*, 1996), or reside in the inter-membrane space, where they are sorted and assembled by mitochondrial import and assembly machinery (MIA) (Chacinska *et al.*, 2004; Naoé *et al.*, 2004). Alternatively, proteins can be transported through TIM23 into the matrix, an active process which requires the ATP-driven presequence translocase-associated motor (PAM) and the chaperone mitochondrial heat-shock protein 70 (mtHsp70) (Kang *et al.*, 1990).

Invaginations of the MIM (cristae) also emerged during the evolution of mitochondria. Cristae maximise the surface area of the MIM, where the ETS components are housed and thus leads to increased efficiency of OXPHOS. One of the causes of MIM invaginations is the presence of ETS subunit ATP synthase multimers, which cause the MIM to bend (Kühlbrandt, 2015). The ETS consists of five multi-subunit complexes; complex I (NADH:ubiquinone oxidoreductase) is the largest with a mass of ~1 MDa and comprises 45 subunits in mammals, 7 of which are encoded by mtDNA (Carroll *et al.*, 2006). Complex II (succinate dehydrogenase) is made up of just four nuclear encoded subunits. Complex III (coenzyme Q cytochrome c - oxidoreductase / cytochrome b) contains 11 subunits, one of which is mtDNA encoded, whereas complex IV (cytochrome C oxidase) contains 11 nuclear encoded and 3 mtDNA encoded protein subunits. The final ETS complex, ATP synthase comprises of two main subunits, F_0 and F_1. F_0 consists of 6 protein subunits, 2 of which are mtDNA encoded and F_1 consists of 8 nuclear encoded subunits (Jonckheere *et al.*, 2012).

OXPHOS occurs in mitochondria through the function of the ETS in tandem with the tricarboxylic acid (TCA) cycle, which occurs in the matrix (Figure 1.5). Acetyl-CoA produced from the catabolism of fats, proteins and sugars enters the TCA cycle, the

reactions of which are catalysed by eight enzymes. The cycle results in the reduction of three NAD+ molecules to NADH and one FAD molecule into $FADH_2$. NADH and $FADH_2$ are then re-oxidised by the ETS, driving the process of OXPHOS. Complex I removes two electrons from NADH, which are transferred to ubiquinone (UQ) in the quinone pool (Q), reducing it to ubiquinol (UQH2). The continuous redox reactions that occur within complex I create an electron current, which is used to actively translocate protons (H^+) from the matrix into the intermembrane space, initiating an electrochemical proton gradient ($\Delta\Psi_m$). $FADH_2$ produced from succinate in the TCA cycle, is re-oxidised to FAD by complex II, transferring additional electrons to Q. UQH2 is able to freely diffuse within the MIM and translocates to complex III. Here, electrons are transferred from Q to cytochrome c which is located within the intermembrane space. In the process, complex III translocates more protons into the intermembrane space, contributing to the proton gradient. Complex IV transfers electrons from cytochrome c to O_2 along with protons in the matrix, producing H_2O. Complex IV also translocates more protons into the intermembrane space. Protons flow back along the electrochemical gradient into the matrix through the F_O subunit ion channel of ATP synthase, causing it to rotate. This energy is used by the F_1 subunit to add an additional phosphate group to ADP, producing ATP (Gnaiger *et al.*, 2014).

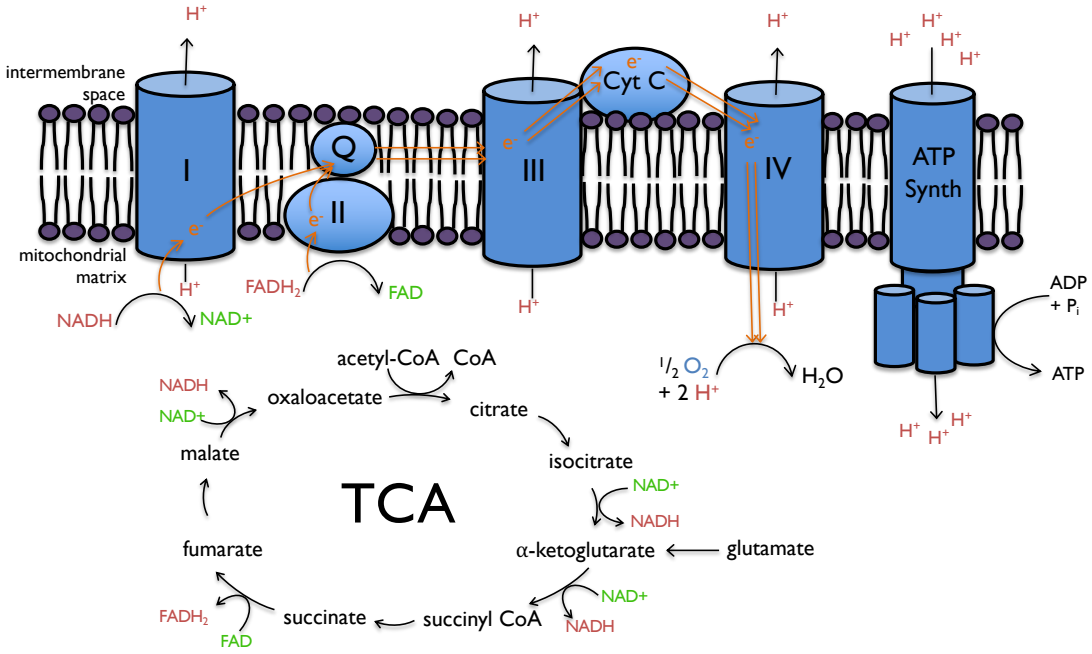

Figure 1.5. Oxidative phosphorylation (OXPHOS) through the tricarboxylic acid (TCA) cycle and electron transfer system (ETS).
The TCA cycle takes place in the mitochondrial matrix, reducing NAD^+ and FAD to NADH and $FADH_2$. NADH and $FADH_2$ act as donors for the ETS, which generates an electron current and an electrochemical proton gradient ($\Delta\Psi_m$). This drives the conversion of ADP to ATP by ATP synthase and the reduction of oxygen to H_2O.

1.2.1 Maintaining a healthy mitochondrial network – biogenesis, mitophagy and mitochondrial dynamics

1.2.1.1 Mitochondrial biogenesis

Mitochondrial proliferation, or biogenesis, is controlled by the master regulator proliferator activated γ coactivator 1α (PGC1α) (Puigserver *et al.*, 1998). PGC1α both upregulates expression of and acts as a coactivator for nuclear respiratory factors (NRFs), which in turn activate transcription factors such as transcription factor A, mitochondrial (TFAM), regulating the expression of nuclear encoded mitochondrial genes (Wu *et al.*, 1999). PGC1α also regulates the uncoupling of the ETS from ATP production, through induction of expression of mitochondrial uncoupling protein 1 (UCP1). Uncoupled respiration generates heat through dissipation of the proton gradient and is important for thermoregulation, occurring

predominantly in brown adipocytes (Puigserver *et al.*, 1998). PGC1α is regulated by a number of stimuli, including cold, exercise, oxidative stress and fasting (Austin & St -Pierre, 2012).

1.2.1.2 Mitophagy

As well as maintaining efficient respiration through mitochondrial biogenesis, mitochondria that are damaged and no longer functional must be cleared from the cell. This is achieved through engulfment of mitochondria into autophagosomes and clearance via autophagy machinery, in a process referred to as mitophagy. In healthy mitochondria, the serine/threonine kinase PTEN-induced putative kinase 1 (PINK1) is imported into the organelle through association with the TOM core complex (Lazarou *et al.*, 2012) and into the TIM complex, where it is initially cleaved by the mitochondrial processing peptidase (MPP) (Greene *et al.*, 2012). The MIM rhomboid protease presenilin-associated rhomboid-like protein (PARL) mediates N-terminal cleavage between Ala103 and Phe104, generating a 52 kDa ($PINK1_{52}$) protein (Jin *et al.*, 2010; Meissner *et al.*, 2011; Deas *et al.*, 2011). $PINK1_{52}$ is released into the cytosol and degraded by the ubiquitin proteasome system (Yamano & Youle, 2013). When mitochondria become damaged and lose $\Delta\Psi_m$ due to depolarizing agents or ETS dysfunction, the import of PINK1 through the TOM complex and inter the TIM complex is inhibited, resulting in an accumulation of $PINK1_{63}$ on the MOM. Unfolded protein accumulation in the matrix also leads to PINK1 accumulation on the MOM without dissipation of $\Delta\Psi_m$, in mammals (Jin & Youle, 2013) and *Drosophila* (Thomas *et al.*, 2014).

The E3 ubiquitin ligase Parkin is recruited from the cytosol to dysfunctional mitochondria in a PINK1 kinase activity dependent manner (Narendra *et al.*, 2008; Narendra *et al.*, 2010a), through phosphorylation of Ser65 of Parkin ubiquitin-like (Ubl) domain (Kondapalli *et al.*, 2012; Shiba-Fukushima *et al.*, 2012). PINK1 immunoprecipitated from cells treated with the mitochondrial depolarising agent carbonyl cyanide *m*-chlorophenoyl hydrazone (CCCP) but not untreated cells, is able to phosphorylate Parkin *in vitro*, indicating that PINK1 localisation is not the only factor which determines phosphorylation of Parkin (Kondapalli *et al.*, 2012). PINK1

also phosphorylates Ser65 of ubiquitin, and phospho-ubiquitin both recruits Parkin to mitochondria and promotes its E3 ligase activity (Kane *et al.*, 2014; Kazlauskaite *et al.*, 2014; Koyano *et al.*, 2014). Immunoprecipitation of ubiquitin chains found that PINK1 increases the abundance of mitochondrial pSer65-ubiquitin chains and that phosphorylated Parkin has a much higher affinity for binding these chains than unphosphorylated Parkin, suggesting that PINK1 kinase activity triggers a self-amplifying mechanism of Parkin recruitment and ubiquitination of MOM proteins.

It is thought that the Parkin Ubl domain inhibits its own E3 ligase activity (Chaugule *et al.*, 2011) until Ser65 phosphorylation, upon which inhibition is relieved (Kondapalli *et al.*, 2012) (Figure 1.6). Although phosphorylation is necessary for Parkin translocation to mitochondria, it is not sufficient, as characterised in pathogenic *parkin* mutants with translocation impairments, which display comparable phosphorylation levels to wild-type Parkin (Shiba-Fukushima *et al.*, 2012). The kinase domain of PINK1 binds to only Parkin fragments containing the RING1 domain and that cleaved $PINK1_{52}$ binds to Parkin in the cytosol, inhibiting Parkin recruitment to depolarised mitochondria and mitophagy (Fedorowicz *et al.,* 2014). In *Drosophila*, overexpression of Parkin is sufficient to rescue a number of PINK1-null phenotypes but not vice versa, indicating that PINK1 phosphorylation of Parkin is not essential for Parkin activation in this model (Clark *et al.*, 2006; Park *et al.*, 2006, Yang *et al.*, 2006).

PINK-1 dependent phosphorylation of Parkin after ($\Delta\psi_m$) dissipation results in a marked increase in Parkin E3-ubiquitin ligase activity leading to the ubiquitination of a number or targets, including auto-ubiquitination. The ubiquitination of the MOM recruits optineurin and p62 (ref(2)P in *Drosophila*), leading to the perinuclear clustering of mitochondria and the recruitment of autophagy proteins such as LC3 (Geisler *et al.*, 2010; Okatsu *et al.*, 2010; Narendra *et al.*, 2010b; Wong & Holzbaur, 2014; Lazarou *et al.*, 2015). PINK1 has also been shown to induce mitophagy independently of Parkin through the recruitment of autophagy adapters optinuerin and NDP52 (Lazarou *et al.*, 2015). However, loss of function (LOF) ref(2)P mutations abolish Parkin mediated rescue of *Pink1* mutants (De Castro *et al.*, 2013), indicating that Parkin recruitment of p62 is important in *Drosophila* and not

compensated by Parkin-independent alternative autophagy adapters. *Pink1*, *parkin and Atg7* mutant flies show a decrease in turnover of mitochondrial proteins *in vivo* (Vincow *et al.*, 2013). Protein turnover appears to be more selective for ETS components in both *Pink1* and *parkin* mutants than *Atg7* mutants, reinforcing the importance of PINK1/Parkin-mediated mitophagy in mitochondrial quality control and maintained efficiency of the ETS (Vincow *et al.*, 2013).

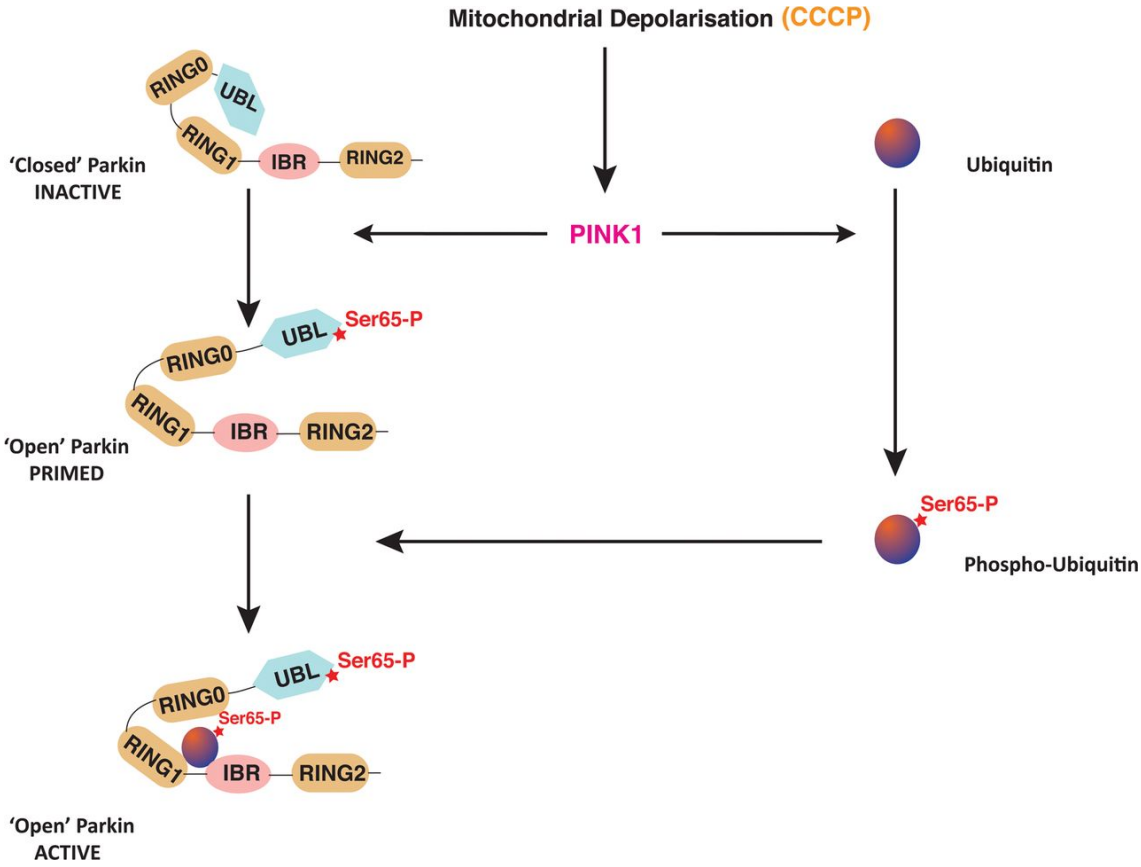

Figure 1.6. Parkin protein domains, phosphorylation by PINK1 and activation of Parkin E3 ubiquitin ligase activity.

When the mitochondrial network is polarised, Parkin exists in an inactive state. Upon mitochondrial depolarisation, PINK1 accumulates on the MOM, where it phosphorylates Ser65 of ubiquitin and Parkin ubiquitin like domain (UBL), priming Parkin for activation. Subsequent phosphorylation of Parkin RING1 domain Ser65 by PINK1 activates Parkin E3 ubqituiin ligase activity (Kazlauskaite et al., 2014).

1.2.1.3 Mitochondrial dynamics

Mitochondria are dynamic organelles which undergo continuous fusion and fission events to maintain morphology and functionality. Mitochondrial fusion facilitates functional complementation, compensating for inherited or *de novo* mutations within mtDNA, of which there are multiple copies per cell and are heteroplasmic in nature. Fusion between individual mitochondria harbouring two different mtDNA mutations can thus maintain functionality by cross-complementation, sharing RNA or proteins required for OXPHOS to continue efficiently (Yoneda *et al.*, 1994; Nakada *et al.*, 2001; Schon & Gilkerson, 2010). Fusion of the MOM is regulated by Mitofusins 1 and 2 (Mfn1 and Mfn2) (Santel & Fuller, 2001; Rojo *et al.*, 2002; Chen *et al.*, 2003). Mfn1 and Mfn2 are also thought to play a role in mitochondrial transport through interaction with the microtubule-based transport system, specifically a MIRO-Milton-Kinesin complex (Misko *et al.*, 2012). Mfn2 also tethers mitochondria to the endoplasmic reticulum (ER) through interaction with MIRO (de Britto & Scorrano, 2008; Naon *et al.*, 2016), controlling mitochondrial Ca^{2+} uptake (Rizzuto *et al.*, 1998), lipid exchange (Voss *et al.*, 2012) autophagasome formation (Hamasaki *et al.*, 2013) and apoptosis (Szalai *et al.*, 1999). Mitofusin homologues in *Drosophila* are encoded by *fuzzy onions* (*fzo*) and *mitochondrial assembly regulatory factor (Marf)*, which have distinctly different patterns of expression. *Marf* has a broad pattern of expression with mRNA identified in S2 cells, embryos, testes, ovaries and in adult males and female whole bodies, whereas *fzo* expression is restricted to male germline cells (Hwa *et al.*, 2002). Fusion of the MIM is regulated by optic atrophy 1 (OPA1), which is also involved in cristae remodelling (Frezza *et al.*, 2006) and mitochondrial Ca^{2+} uptake (Fülöp *et al.*, 2011).

The segmentation of mitochondria via fission is essential in dividing cells, in order to ensure enough organelles populate each daughter cell. However, mitochondrial fission is also important in nonproliferating cells and this is likely due to the facilitation of segregation and autophagic clearance of segments of mitochondria that are beyond repair, a point which is discussed in more detail below. Mitochondrial fission is mediated by the dynamin-related GTPase, dynamin related protein 1 (DRP1), a cytosolic protein which is recruited to the MOM, where it assembles into oligomers (Smirnova *et al.*, 2001). These helical structures cause mitochondrial fission by constricting the mitochondrial outer and inner membranes (Mears *et al.*, 2011). DRP1 activity is governed by a number of post-translational modifications, including phosphorylation, ubiquitination, small ubiquitin-like modifier (SUMO)ylation, S-nitrosylation and O-GlcNAcylation (Chang & Blackstone, 2010). Phosphorylation occurs at two serine residues, which correspond to Ser616 and Ser637 in human DRP1 isoform 1. Phosphorylation at the Ser616 residue by the mitosis promoting factor Cyclin dependant kinase 1(CDK1)/cyclin B promotes DRP1 GTPase activity and thus mitochondrial fission during mitosis, tightly linking mitochondrial fission to the cell cycle and thus facilitating the distribution of organelles between daughter cells (Taguchi *et al.,* 2007). Conversely, Ser637 phosphorylation by protein kinase A (PKA) inhibits DRP1 GTPase activity and mitochondrial fission (Chang & Blackstone, 2007; Cribbs & Strack, 2007). On the mitochondrial outer membrane, tetrameric PKA is tethered by OMM-bound A-kinase anchoring protein 1 (AKAP1), which also orientates PKA substrates into phosphorylatable configurations (Smith *et al.*, 2013). The Ser637 residue can also be phosphorylated by calcium/calmodulin-dependant kinase 1α (CaMKIα), although this was shown to have a positive effect on mitochondrial fission (Han *et al.*, 2008).

Four proteins have been shown to play a role in DRP1 recruitment to the MOM in mammals; mitochondrial fission factor (MFF) appears to have the most dominant role, with very elongated and interconnected mitochondria correlating with a reduction in DRP1 puncta at the MOM when *Mff*is silenced (Otera *et al.,* 2010; Losón *et al.*, 2013). Mitochondrial fission protein 1 (FIS1) is believed to play a less prominent role in DRP1 recruitment than MFF, with a small but significant

reduction in DRP1 puncta and moderately elongated and interconnected mitochondria in *Fis1*-null cells. Mitochondrial dynamics proteins of 49 and 51 kDa (MiD49 and MiD51) are both capable of recruiting DRP1 in the absence of MFF or FIS1. Overexpression of both MiD49 and MiD51 enhances DRP1 recruitment to mitochondria, but also causes an increase in the proportion of mitochondrial DRP1 phosphorylated at Ser637 (Losón *et al.*, 2013). Cells overexpressing MiD49 or MiD51 thus demonstrate an elongated mitochondrial network (Palmer *et al.*, 2013; Losón *et al.*, 2013); however upon CCCP treatment these cells undergo more rapid mitochondrial fragmentation than untransfected cells, which coincides with a decrease in DRP1 pSer637 (Losón *et al.*, 2013). These findings indicate that MiD49 and MiD51 "prime" mitochondria for more rapid fragmentation, by recruiting DRP1 but maintaining it in its inactive state.

PINK1/Parkin-mediated mitophagy has been repeatedly linked to mitochondrial dynamics (Figure 1.7) although our understanding of the relationship between mitophagy and fission/fusion is incomplete. Phosphorylation of the complex I subunit NADH:ubiquinone oxioreductase subunit A10 (NDUFA10) at Ser250, which is required for reduction of ubiquinone, is decreased in the liver and brain of *Pink1* knockout mice and phosphomimetic NDUFA10 expression rescued complex I deficits in these mice, as well as loss of $\Delta\Psi_m$ and synaptic transmission in *Pink1* mutant flies (Morais *et al.*, 2014). Knockdown of *NDUFA10 (ND42)* in *Drosophila* S2R+ cells results in elongated mitochondria similar to *Pink1* and *parkin* knockdown, whereas knockdown of other complex I subunits did not produce the same effect (Pogson *et al.*, 2014). Overexpression of *ND42* or its co-chaperone *sicily* rescue complex I defects in *Pink1* but not *parkin* flies (Pogson *et al.*, 2014). Furthermore, *Drp1*, but not *parkin* overexpression rescues complex I defects in *Pink1* mutants (Liu *et al.*, 2011; Pogdson *et al.*, 2014), indicating a role for PINK1 in complex I maintenance, which involves mitochondrial morphology, but not Parkin-mediated MARF regulation and mitophagy.

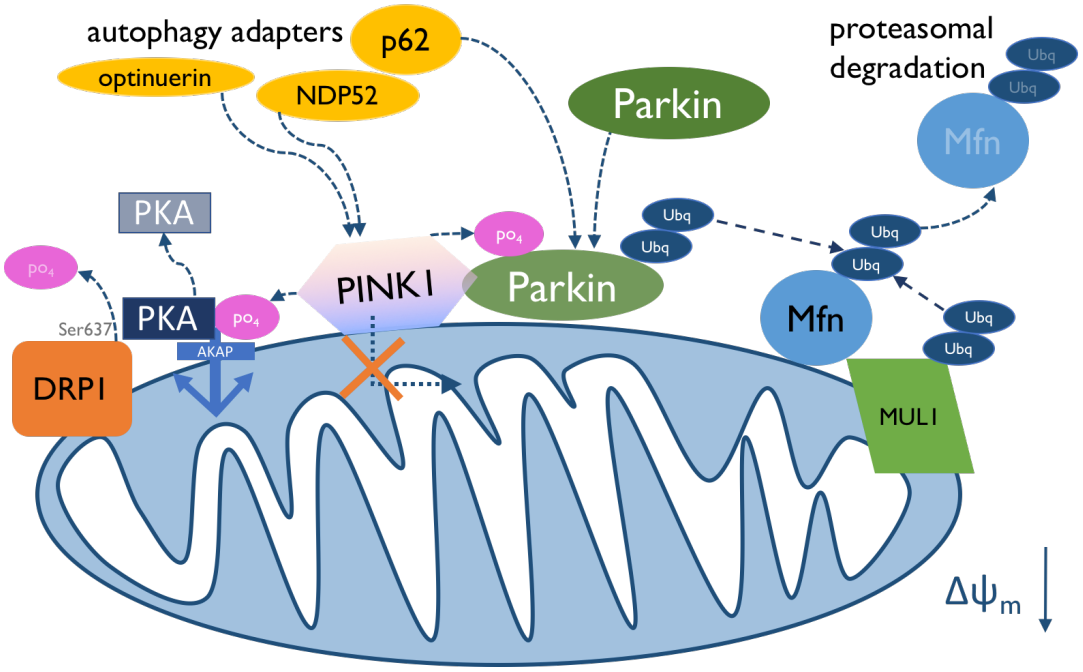

Figure 1.7. An overview of mitophagy and its influence on mitochondrial dynamics. Mitochondria damaged by depolarising agents or ETS dysfunction are unable to sustain polarisation of the MIM ($\Delta\Psi_m$). The dissipation of $\Delta\Psi_m$ inhibits the mitochondrial import of PTEN-induced kinase 1 (PINK1), which therefore accumulates on the MOM. PINK1 phosphorylates Ser65 of ubiquitin (Ubq) and Parkin Ubq-like domain, recruiting further Parkin to mitochondria and activating its E3 ubiquitin ligase activity. Parkin ubiquitinates a number of targets on the MOM, including Mfn1/2, targeting them for degradation through the ubiquitin proteasome system. Mfn1/2 can alternatively be ubiquitinated by mitochondrial ubiquitin ligase 1 (MUL1). PINK1 also phosphorylates A kinase anchoring protein (AKAP1), resulting in the untethering of protein kinase A (PKA) from the MOM and a decrease in dynamin related protein 1 (DRP1) phosphorylation at Ser637. The proteasomal degradation of Mfn1/2 and a reduction in DRP1 Ser637 act as anti-fusion / pro-fission stimuli, promoting the segregation of damaged portions of the organelle. The autophagy adapters optineurin, NDP52 and p62 are recruited to damaged mitochondria by PINK1 and Parkin, leading to their autophagic clearance from the cell.

Upon mitochondrial depolarization, release of Ca^{2+} into the cytosol activates calcinuerin, which dephosphorylates DRP1 at Ser637 (Cereghetti *et al.*, 2008). In studies of stress-induced mitophagy that utilise mitochondrial toxins such as CCCP, which causes mass depolarization of the mitochondrial network, the rapid mitochondrial fragmentation observed is therefore likely to be due to increased cytosolic Ca^{2+} and calcineurin-induced DRP1 activity. However, it has been argued that this is unlikely to be the mechanism that governs basal mitophagy *in vivo*, where only portions of mitochondria become damaged and selectively segregated for autophagic clearance. In these instances, Ca^{2+} release from these areas would rapidly diffuse into the cytosol and be strongly buffered by neighbouring ER and polarised mitochondria, thus preventing the specific targeting of damaged areas (Schon & Przedborski, 2011; Pryde *et al.*, 2016). Pryde *et al.,* (2016) showed that in addition to phosphorylating Ubq and Parkin, PINK1 also phosphorylates AKAP1, which results in the displacement of PKA from the MOM and a subsequent reduction in DRP1 Ser637 phosphorylation, thus promoting DRP1 GTPase activity at sites of mitochondrial depolarisation, where PINK1 accumulation occurs. In HeLa cells overexpressing dominant negative $Drp1^{K38A}$, YFP-Parkin recruitment to damaged mitochondria was enhanced, but the selective removal of damaged regions of mitochondria was abolished (Burman *et al.*, 2017). DRP1 may thus restrict PINK1/Parkin induced mitophagy to damaged portions of mitochondria, protecting undamaged regions of the network from unnecessary clearance. This hypothesis clarifies discrepancies between studies reporting that DRP1 facilitates mitophagy by dividing mitochondria into autophagasome engulfable segments (Twig *et al.,* 2008; Tanaka *et al.,* 2010; Gomes *et al.*, 2011; Rambold *et al.*, 2011) and studies reporting that DRP1 is not essential for mitophagy to occur (Mendl *et al.*, 2011; Song *et al.*, 2015; Yamashita *et al.*, 2016).

In *Drosophila*, introduction of a dominant-negative *Drp1* allele or heterozygous LOF causes synthetic lethality in *Pink1* and *parkin* deficient flies (Poole *et al.*, 2008; Fernandes & Rao *et al.*, 2011). Overexpression of *Drp1* via the UAS-GAL4 system rescues mitochondrial morphology in *Pink1* and *parkin* mutants (Deng *et al.*, 2008), whereas introduction of an additional *Drp1* allele under its endogenous promoter results in rescue of additional phenotypes such as flight and climbing ability (Poole

et al., 2008, Yang *et al*., 2008). In a study utilising the inducible UAS-GAL4 system "GeneSwitch" (Osterwalder *et al*., 2001), overexpression of DRP1 in midlife flies (Day 30 – Day 37) resulted in a mitophagy (*Atg1*)-dependant increase in lifespan and respiratory capacity as well as a decrease in mitochondrial area, ubiquitinated protein aggregates and ROS levels (Rana *et al.,* 2017). This again highlights the ability of DRP1 to facilitate selective mitophagy of damaged segments of mitochondria, which can ultimately delay the ageing process. Constitutive or adult-onset overexpression of Parkin also has similar effects on lifespan, which are likely at least in part to be due to the normalisation of MARF levels, which increase with age (Rana *et al*., 2013).

In *Drosophila* S2R+ cells, Parkin is responsible for the ubiquitination and degradation of *Drosophila* MARF, promoting mitochondrial fission (Zivani *et al*., 2010). MARF levels are thus raised in *Pink1* and *parkin* mutant flies and *Marf* RNAi knockdown is sufficient to rescue mitochondrial elongation (Deng *et al*., 2008; Poole *et al*., 2008). Heterozygosity in *Opa1* also results in rescue of *Pink1* mutant phenotypes in *Drosophila* (Poole *et al*., 2008; Deng *et al*., 2008; Yang *et al*., 2008). An alternative E3 ligase, mitochondrial ubiquitin ligase (MUL1), or mitochondrial-anchored protein ligase (MAPL, Neuspiel *et al*., 2008), acts in parallel to Parkin in the ubiquitination and degradation of Mfn1/2 in mammals (Lokireddy *et al*., 2012; Yun *et al*., 2014) and MARF in *Drosophila* (Yun *et al*., 2014). *Mul1* deletion results in exacerbation of mitochondrial morphology phenotypes in *Pink1* and *Parkin* flies, whereas overexpression of *Mul1* is protective (Yun *et al*., 2014). MUL1 has also been demonstrated to SUMOylate DRP1, leading to its stabilisation, mitochondrial localisation and an increase in fission (Brachi *et al*., 2009).

Mitochondria-ER contacts, mediated by interaction between Mfn1/2 (MARF) and MIRO, are increased in *Pink1* and *Parkin Drosophila* mutants and *Marf* or *Miro* RNAi reverses this effect (Celardo *et al*., 2016; Lee *et al*., 2018a). The reduction of mitochondria-ER contacts as a result of *Marf* or *Miro* knockdown is accompanied by a normalisation of phosphorylated protein kinase R-like endoplasmic reticulum kinase (PERK) levels, an attribute of ER stress (Celardo *et al*., 2016) and calcium homeostasis (Lee *et al*., 2018a). Genetic and pharmacological inhibition of the

mitochondrial calcium uniporter (MCU) is protective in *Pink1* mutant zebrafish (Soman *et al.*, 2017) by inhibiting mitochondrial uptake of Ca^{2+} released by the ER (Rizzuto *et al.*, 1998). Modulating ER stress and calcium homeostasis through mitochondria-ER contacts could therefore be another way in which mitochondrial dynamics proteins are linked to mitochondrial quality control. Reduction in mitochondria-ER contacts can be compensated by an increase in mitochondria-vacuole interfaces, which are mediated by the MOM protein Mdm10-complementing protein 1 (MCP1) and the ubiquitin binding protein variable small protein 13 precursor (VPS13) (John Peter *et al.*, 2017). Defects in VPS13 impair mitophagy and result in enlarged mitochondria and impaired calcium homeostasis in human and *Drosophila* models (Anding *et al.*, 2018). In flies, VPS13 LOF can be reversed by *Marf* RNAi, providing another link between mitophagy, mitochondrial dynamics and contact-points between mitochondria and other organelles.

1.2.2 Mitochondrial dysfunction in neurological disorders

Mitochondrial function has been strongly linked to the pathology of many human diseases, in particular conditions which effect the nervous system. For example, Leigh syndrome, typically characterised by early post-natal onset of encephalopathy and respiratory defects, can be caused by mutations in both nuclear and mitochondrial encoded components of the ETS (Ruhoy and Saneto; 2014). Defects in mitochondrial dynamics proteins also lead to neurological disorders - mutations in *Mfn2* cause Charcot-Marie-Tooth disease, a hereditary neuropathy characterised by the degeneration of long peripheral axons (Züchner *et al.*, 2004), whereas mutations in *OPA1* cause dominant optic atrophy (Alexander *et al.*, 2000; Delettre *et al.*, 2000)

Mitochondrial dysfunction has also been strongly linked to the pathology of neurodegenerative disorders in which the KP has also been implicated, namely HD, PD and AD. One of the most well-defined relationships between mitochondria and neurodegenerative disease is in PD. The first evidence to suggest a link between mitochondrial dysfunction and PD pathology was discovered upon the accidental exposure of four individuals to 1-methyl-4-phenyl-1,2,3,6-tetrahydropyridine (MPTP), a contaminant of the illicit drug 1-methyl-4-phenyl-4-propionoxy-piperidine (MPPP), which led to the development of parkinsonian symptoms and the degeneration of dopaminergic (DA) neurons (Langston *et al.*, 1983). MPTP oxidises to MPP+, which selectively enters DA neurons, where it inhibits the function of complex I of the ETS (Javitch *et al.*, 1985; Nicklas *et al.*, 1985; Ramsay and Singer, 1986). Other complex I inhibitors, such as the pesticides paraquat and rotenone, which DA neurons are particularly sensitive to, cause parkinson-like phenotypes (Liou *et al.*, 1997; Betarbet *et al.*, 2000; Tanner *et al.*, 2011).

In 1997, a locus on chromosome 6 was identified as the cause of autosomal-recessive juvenile parkinsonism (ARJP) in a Japanese population (Matsumine *et al.*, 1997). The responsible gene, initially named *PARK2*, is now commonly referred to as *parkin* (Kitada *et al.*, 1998) and mutations in *parkin* are thought to cause approximately half of known cases of ARJP (Nuytemans *et al.*, 2010). Four years

later, a second locus was implicated in ARJP, named *PARK6* (Valente *et al.*, 2001) and the gene responsible was *Pink1* (Valente *et al.*, 2004). Much of the early work establishing mitochondrial functions of PINK1 and Parkin and their interaction in a common pathway (discussed in 1.2.1.2) was performed in *Drosophila*. LOF *parkin* mutant flies exhibit aberrant mitochondrial morphogenesis during spermatogenesis, defects in wing posture, flight and startle induced locomotion (climbing), as well as apoptotic degeneration of indirect flight muscle, increased sensitivity to oxidative stress and reduced lifespan (Greene *et al.*, 2003; Pesah *et al.*, 2004). These phenotypes are mirrored in *Pink1* LOF mutant or RNAi flies and are rescued by *parkin* overexpression (Clark *et al.*, 2006; Park *et al*; 2006; Yang *et al*; 2006). In the brain, *Pink1* and *parkin* mutants exhibit mitochondrial dysfunction and degeneration specially in DA neurons of the posterior lateral region 1 (PPL_1) cluster (Whitworth *et al.*, 2005; Park *et al.*, 2006; Yang *et al.*, 2006; Burman *et al.*, 2012), which are functionally homologous to neurons of the mammalian *substantia nigra pars compacta* (Strausfeld & Hirth; 2013), the region of the brain which degenerates in ARJP (Yokochi, 1997) and sporadic PD patients (Trétiakoff; 1919). A range of non-motor PD symptoms are also reflected in *Pink1* and *parkin* mutant flies, including defects in learning, memory and circadian rhythms (Julienne *et al.*, 2017; Valadas *et al.*, 2018). The identification of mitochondrial roles for other ARJP and PD associated proteins, such as aSyn (Guardia-Laguarta *et al.*, 2014), leucine-rich repeat kinase 2 (LRRK2) (Wang *et al.*, 2012; Niu *et al.*, 2012) and DJ-1 (Canet-Aviles *et al.*, 2004), and VSP13 (Lesage *et al.*, 2016, Jansen *et al.*, 2017) strongly implicate mitochondrial function in the pathology of PD. Post-mortem analysis of the *substantia nigra* of sporadic PD patients showed a significant reduction in the activity of complex I (Schapira *et al.*, 1989; Schapira *et al.*, 1990; Mann *et al.*, 1994; Janetzky *et al.*, 1994), suggesting that mitochondrial dysfunction is also a feature, if not a cause, of sporadic PD.

More recently, the involvement of impaired mitochondrial form and function in other neurodegenerative diseases has become apparent. A genome-wide association study (GWAS) in ~2000 HD patients identified variants in genes involved in the regulation of mitochondrial fission, as well as the release of cytochrome c from mitochondria (Hensman Moss *et al.*, 2017). In HD patient cells,

mHTT binds to DRP1, increasing its activity and an increase in mitochondrial fission (Song *et al.*, 2011; Shirendeb *et al.*, 2012). Treatment of HD model cells and mice with a peptide which blocks DRP1-FIS1 interactions restored mitochondrial morphology, also improving behavioural and survival defects in the mouse model (Guo *et al.*, 2013). However, removal of MFF from the R6/2 HD mouse model exacerbated neuronal loss and neuroinflammation, whilst shortening lifespan, without affecting mHTT aggregation (Chan *et al.*, 2018). PINK1 overexpression also rescued mitochondrial morphology, neurodegeneration and lifespan in HD model flies, in a manner dependent on Parkin and MARF (Khalil *et al.*, 2015).

Mitochondrial dysfunction is also a well described aspect of AD. Reduced cerebral metabolic rate is well documented and precedes both cognitive impairment and brain atrophy (Blass, 2000). Mitochondria with broken cristae have been reported in AD patient neurons (Hirai *et al.*, 2001) and mitochondrial elongation observed in in fibroblasts derived from AD patients (Wang *et al.*, 2008). DRP1 levels were also decreased in patient fibroblasts compared to controls (Wang *et al.*, 2008), although another study reported increased DRP1 expression in AD patient neurons (Manczak *et al.*, 2011). Both Aß (Cho *et al.*, 2009; Manczak *et al.*, 2011) and Tau (DuBoff *et al.*, 2012) have been shown to affect DRP1 localisation or activity, and overexpression of DRP1 improved climbing ability, increased ATP levels and prolonged lifespan in a *Drosophila* $Aß_{42}$ model (Lv *et al.*, 2017).

1.3 Functional links between the KP and mitochondria

The KP has been linked to mitochondrial function through the effect of KP metabolites on mitochondria, as well as the mitochondrial localisation of some KP enzymes, including KMO. Indeed, an isoform of KAT I (Malherbe *et al.*, 1995) and mitochondrial aspartate aminotransferase (miAAT or KAT IV) (Guidetti *et al.*, 2007b) identified in the mammalian brain are also both mitochondrially localised. Upregulated PGC1α in skeletal muscle in response to exercise has been shown to increase expression of KAT IV, raising KYNA and reducing L-KYN in blood plasma, demonstrating a link between mitochondrial biogenesis and the KP (Agudelo *et al.*, 2014; Schlittler *et al.*, 2016). This KAT has been demonstrated to play a role in the synthesis and transport of TCA intermediates in neurons and astrocytes (Schousboe *et al.*, 1993; Westergaard *et al.*, 1996; McKenna *et al.*, 2000). Furthermore, inhibitors of the ETS such as rotenone, malonate, 1-methyl-4-phenylpyridinium and 3-nitropropionic acid all decrease KYNA synthesis (Hodgkins and Schwarcz, 1998; Luchowski *et al.*, 2002). KYNA treatment has also been reported to reduce the respiratory capacity of mitochondria isolated from rat heart tissue, but not liver or brain tissue (Baran *et al.*, 2016). Intrastriatal injection of 3-HK or 3-HANA caused a decrease in $\Delta\Psi_m$ and the activity of complex II of the ETS (Reyes-Ocampo *et al.*, 2015).

KMO has been shown to localise to the MOM in yeast (Bandlow, 1972) and mammals (Okamoto *et al.*, 1967). Localisation of mammalian KMO is dependent on a hydrophobic region and two putative transmembrane domains in the C-terminal region; truncation of the C-terminal 20 amino acids (ΔC20D) of pig liver KMO expressed in COS-7 cells results in cytosolic localisation, whereas a ΔC10D truncated form maintains mitochondrial localisation (Hirai *et al.*, 2010). The requirement of the C-terminal domain for maintaining catalytic activity is debatable; a C-terminal truncation of 66 amino acids (ΔC66D) in *S. cerevisiae* KMO produces an enzymatically active protein (Amaral *et al.*, 2013), whereas ΔC50D and ΔC70D truncated pig liver KMO expressed in COS-7 cells displayed >90% reduced activity compared to full length, ΔC10D, ΔC20D and ΔC30D proteins (Hirai *et al.*, 2010). C-terminal truncated forms of KMO have also shown reduced activity in insect (Han *et*

al., 2003) and other mammalian systems (Hirai *et al*., 2010; Wilson *et al*., 2014; Amaral; 2013; Kim *et al*., 2018). This is thought to be due to the blocking of KMO active site by a disrupted C-terminal α-helix, which does not occur in *S. cerevisiae* KMO (Kim *et al*., 2018).

The mitochondrial localising domain is highly similar to the tail-anchor domain of other MOM proteins such as monoamine oxidase B (MAO-B), cytochrome b_5 (OM b_5) and FIS1 (Hirai *et al*., 2010). In FIS1, the hydrophobic C-terminal domain is also responsible for the assembly and stabilization of functional oligomers (Habib *et al*., 2003); KMO forms oligomers as well (Uemura & Hirai, 1998), however the mechanism by which it does so has not yet been characterised. KMO purified from the MOM of pig liver tissue has proven difficult to separate from MAO-B without losing enzymatic activity (Uemura & Hirai, 1998; Hirai *et al*., 2010). MAO-B has also been implicated in the regulation of Parkin recruitment to the MOM and its E3 ligase activity (Siddiqui *et al*., 2012). MAO-B overexpression in PC12 cells causes an increase in mitochondrial Parkin, as does treatment with FCCP. When both an increase in MAO-B and FCCP treatment are combined, the effect on the abundance of mitochondrial Parkin is additive. However, an increase in MAO-B activity results in a decrease in mitophagy because of inhibition of Parkin E3 ubiquitin ligase activity and a reduction in mitochondrial complex I respiratory capacity (Siddiqui *et al*., 2012).

In the KMO knockout mouse, the nuclear encoded complex I subunit *NDUFAF4* is upregulated ~1.2-fold in the liver compared to littermate controls (Repici & Giorgini, unpublished) whereas the mitochondrial encoded subunit *MT-ND5* is downregulated ~1.3-fold in the cerebellum (Erhardt *et al*., 2017). In the cerebral hemisphere, the complex II subunit *SDHC* and the complex IV subunit *COX8B* are downregulated (Erhardt *et al*., 2017), indicating that KMO could influence ETS regulation. Perhaps the most compelling evidence for a mitochondrial role for KMO has emerged from *Drosophila*. Like in yeast and mammals, *Drosophila* KMO localises to mitochondria (Ghosh & Forrest, 1967; Sullivan *et al*., 1974). In a genome-wide screen for modifiers of *Pink1* and *parkin* mutant phenotypes, deletion of the 42E;44C genomic region which includes *cn,* using the *Df(2R)cn9* deficiency strain,

enhanced the penetrance of a wing posture phenotype observed upon ubiquitous RNAi knockdown of *Pink1* or *parkin*, or in a *Pink1*-null mutants (Fernandes & Rao, 2011). In a genome-wide RNAi screen, knockdown of *cn* in *Drosophila* S2R+ cells resulted in more elongated mitochondria compared to cells expressing endogenous levels of *cn* (Ivatt *et al*., 2014). Furthermore, *cn* RNAi also caused a reduction in CCCP and paraquat-induced Parkin-GFP translocation to mitochondria (Ivatt *et al*., 2014), providing evidence that KMO could play a role in the context of mitochondrial dynamics and PINK1/Parkin-mediated mitophagy.

Given the potential therapeutic applications of KMO inhibition for the treatment of neurological disorders, many of which also feature compromised mitochondrial function, any involvement of KMO in mitochondrial function or quality control warrants thorough investigation. *Drosophila* was used extensively as a model organism in this study, not only because of the aforementioned indication of a mitochondrial role for KMO in this species, but also a number of other advantages that the model organism offers. Kept at 25^{o}C, the development of *Drosophila* from egg to adult takes approximately 10 days, allowing for rapid generation of desired genotypes to study. Furthermore, the toolkit that is available to use in the organism make genetic manipulations very straightforward. Genes can be expressed under the control of binary systems such as LexA/LexAop or GAL4-UAS. GAL4 is a transcription factor endogenous to yeast and not endogenously expressed in *Drosophila*. Transgenic introduction of GAL4 under the control of enhancer and promoter regions of *Drosophila* genes, commonly referred to as enhancer traps, facilitates the expression of GAL4 in specific tissues of interest. GAL4 binds to a specific upstream activation sequence (UAS), which can be inserted upstream of a genetic sequence which one wishes to express. GAL4 binding to UAS initiates transcription, driving expression of the desired mRNA in tissues of choice. Binary systems can be used to overexpress genes by placing coding sequences downstream of UAS, or can be used to silence gene expression through the expression of RNAi constructs. Chromosomes carrying large genomic rearrangements such as inversions, referred to as balancer chromosomes, suppress meiotic recombination and also carry visible markers, allowing easy tracking of inheritance of chromosomes carrying specific transgenes or genetic variants.

The range of possibilities in *Drosophila* genetic manipulation allowed the employment of powerful genetic epistasis experiments, exploring functional interactions between *cinnabar* and genes involved in mitochondrial quality control, such as *Pink1* and *parkin*. The conservation of this mechanism between flies and mammals, alongside the high sequence similarity between *Drosophila* and human KMO, gave reason to hypothesise that the meaning inferred from these epistasis experiments could be translatable to human, clinically relevant systems.

1.4 Aims and Objectives

This project arose out of the desire to better characterise what mitochondrial roles KMO might play. The following objectives were therefore established:

1) Identify mitochondrial phenotypes in KMO deficient models.

KMO knockdown and deletion was performed in *Drosophila* and mammalian cell models to probe for consequences in mitochondrial form and function.

2) Investigate interplay between KMO and mitochondrial quality control proteins PINK1 and Parkin

Given the identification of *cn* as a modulator of Parkin recruitment to mitochondria (Ivatt *et al.*, 2014), functional interplay between KMO and PINK1/Parkin was investigated. This was approached through genetic epistasis experiments, as well as microscopy and immunoprecipitation techniques.

3) Assess involvement of KMO in regulation of mitochondrial dynamics

Mitophagy is strongly linked to the regulation of mitochondrial dynamics. Given the elongated mitochondria observed upon *cn* knockdown and the implication of an involvement in mitophagy (Ivatt *et al.*, 2014), the effects of KMO on known regulators of mitochondrial morphology, MARF and DRP1, were investigated.

2. Materials and Methods

2.1. Materials

2.1.1. *Drosophila* stocks

Table 2.1. List of *Drosophila* stocks used in this work

Stock	Description	Supplier
Canton S	Wildtype strain	Bloomington *Drosophila* Stock Center, Indiana (stock #64349)
+ ; cn^3 ; +	*cn* null allele	Bloomington *Drosophila* Stock Center, Indiana
y^1.w^*; P{Act5CGAL4}/CyO; +	Ubiquitous GAL4 driver	Bloomington *Drosophila* Stock Center, Indiana (stock #25374)
y^1.w^*;+; P{Act5CGAL4}/TM6B	Ubiquitous GAL4 driver	Bloomington *Drosophila* Stock Center, Indiana (stock #3954)
+; {pKC43}VIE-260B; + (*3M*)	Empty vector control for kk RNAi lines	Dr. Carlo Breda, University of Leicester
w^*; cn^{RNAi}; +	*cn* RNAi expressing KK line	Vienna *Drosophila* Resource Center (KK stock #105854)
y^1.w. $Pink1^{B9}$/FM6; + ; +*	*Pink1* null allele	Dr. Alex Whitworth; MRC Mitochondrial Biology Unit, Cambridge
w; + ; $park^{25}$/TM6B.GFP.w^+*	*parkin* null allele	Dr. Miguel Martins, MRC Toxicology Unit, Leicester

Stock	Description	Supplier
w; UAScn [attP40] / SM6a; +*	*cn cDNA* overexpression	Microinjection Service, University of Cambridge
w; UAScn [attP51c] / SM6a; +*	*cn cDNA* overexpression	Dr. Christopher Elliot, University of York
w; UAShKMO [attP40] / SM6a; +*	*hKMO* cDNA overexpression	Microinjection Service, University of Cambridge
w; +; P{UAS-park.FLAG.COX-IV}*	*parkin* cDNA overexpression	Bloomington *Drosophila* Stock Center (Stock #34746)
w; + ; P{w[+mC]=UASDrp1.D}3*	*Drp1* UAS ovexpression	Bloomington *Drosophila* Stock Center (Stock #51647)
y^1.w; +; FLAG-FlAsH-HA-Drp1. Ki^1*	Genomic *Drp1* overexpression	Bloomington *Drosophila* Stock Center (Stock #42208)
w; $Marf^{RNAi}$; +*	*Marf* RNAi expressing KK line	Vienna *Drosophila* Resource Centre (KK stock #105261)
w; + ; P{$Drp1^{RNAi}$} /TM3*	*Drp1* RNAi expression GD line	Vienna *Drosophila* Resource Centre (GD stock #44156)

2.1.2. Cell lines

Table 2.2. List of cell lines used in this work

Cell lines	Supplier
Drosophila Schneider's S2	Prof. Charalambos Kyriacou, University of Leicester
Murine N9 (2 x scramble shRNA, 2 x KMO shRNA)	Dr. Aisha Swaih, University of Leicester
Human embryonic kidney (HEK293)	Dr. Mahdieh Hassanjani, University of Leicester
YFP-Parkin expressing HeLa (Nardena *et al.*, 2008)	Dr. Alexander Whitworth, MRC Mitochondrial Biology Unit, Cambridge

2.1.3. Antibodies

Table 2.3. List of antibodies used in this work

Antigen	Supplier (catalogue #)	Host species	Dilution
ß-Actin	Abcam (ab1801)	Rabbit	1:1000
DRP1	Cell Signalling (#8570)	Rabbit	1:1000
DRP1 pSer616	Cell Signalling (#3455)	Rabbit	1:1000
DRP1 pSer637	Cell Signalling (#4867)	Rabbit	1:1000
GAPDH	Santa Cruz Biotechnology (sc32233)	Mouse	1:200
GFP	Abcam (ab6556)	Rabbit	1:1000
KMO	Proteintech (10698-1-AP)	Rabbit	1:1000
MARF	Dr. Alex Whitworth, MRC Mitochondrial Biology Unit, Cambridge	Rabbit	1:1000
Tubulin	Developmental Studies Hybridoma Bank (AA4.3)	Mouse	1:1000
VDAC1	Abcam (ab14734)	Mouse	1:1000
VDAC1	Cell Signalling (#4866)	Mouse	1:1000

2.1.4. Plasmids

Table 2.4. List of plasmids used in this work

Name	Supplier	Application
pcDNA3.1/Zeo	Invitrogen	Control for hKMO overexpression experiments
pcDNA3.1-hKMO	Dr. Aisha Swaih University of Leicester	DRP1 phospho-status and mitochondrial morphology
pcDNA3.1-hKMO-RFP	Dr. Aisha Swaih University of Leicester	Immunoprecipitation
pMK33-dParkin-GFP	Dr. Alex Whitworth MRC Mitochondrial Biology Unit, Cambridge	Parkin mitochondrial recruitment assay, immunoprecipitation
pUASt-attB	Dr. Ane Martin-Anduaga University of Leicester	Molecular cloning of *cn* and *hKMO* for *Drosophila* microinjection
Act5C-GAL4	Dr. Alex Whitworth MRC Mitochondrial Biology Unit, Cambridge	Overexpression of pUASt-attB plasmids in S2 cells

2.1.5. Oligonucleotides

Table 2.5. List of oligonucleotide used in this work.
T7 promotor sequence is italicised. Restriction enzyme recognition sites are underlined. Non-specific nucleotides to increase efficiency of restriction enzyme digestion are in lower case.

Name	Forward sequence	Reverse Sequence
cn dsRNA	*TAATACGACTCACTATAGGG*GAGGGTATGCAGAGCTCCAG	*TAATACGACTCACTATAGGG*TTTGTACGAGTACCGGGAGG
f.luc dsRNA	*TAATACGACTCACTATAGGG*CCTGGTTCCTGGAACAATTGC	TAATACGACTCACTATAGGGCGGAGTTCATGATCAGTGC
Drp1 dsRNA	TAATACGACTCACTATAGGGACATCATGGCCACGCAATT	TAATACGACTCACTATAGGGCCTGCTGCACTTCGTTG
Marf dsRNA	TAATACGACTCACTATAGGGTGAGCAAATACCCCCAAAAG	TAATACGACTCACTATAGGGGATCTGGAGCGGTGATTTGT
Pink1 dsRNA	*TAATACGACTCACTATAGGG*GCCATGTACAAGGAGACGGT	*TAATACGACTCACTATAGGG*ATTGAGTACGGCAAACGGAC
Parkin dsRNA	*TAATACGACTCACTATAGGG*TATTCAGACGCTCCTCGCTT	*TAATACGACTCACTATAGGG*TTTTGTACGCAAAATGCTGG
cn qPCR	TACCATTTACTGCCCATCTGACA	CCTCCTGGCTAACGATTCCTG
Drp1 qPCR	ATGGAGGCCCTAATTCCGGT	GCTCTGACTGCCTAGAACAACA
Pink1 qPCR	AAGCGAGGCTTTCCCCTAC	GCACTACATTGACCACCGATTT
parkin qPCR	ATTTGCCGGTAAGGAACTAAGC	AAGTGGCCGACTGGATTTTCT
cn cDNA (full length)	gatcCTCGAGATGAGCCCAGGAATCGTTAGCCA	gaTCTAGATTAGCAACAACAATTAAGTCGGAAATGA

cn cDNA (full length with N or C terminal HA tag)	gatcCTCGAGATGTACCCATACGATGTTCCAGATTACGCTAGC CCAGGAATCGTTAGCCA	gaTCTAGATTAAGCGTAGTCTGGGACGTCGTATGGGTAGC AACAACAATTAAGTCGGAAATGA
hKMO (full length)	gaGCGGCCGCATGGACTCATCTGTCATTCAAAG	gaTCTAGATCACCTGCTAATGAGATTGGAAATTT

2.2. Methods

2.2.1. *Drosophila* husbandry and compound supplementation

All experimental flies were maintained at 25 ^{o}C on maize-based medium (yellow cornmeal (72 g/l), glucose (79.3 g/l), brewer's Yeast (50 g/l), agar (8.5 g/l), propionic acid (0.3 % v/v), 20 % Nipagen in EtOH (1.35 % v/v)), under a 12:12 light:dark regime. For feeding experiments, 3-HK (Sigma) and KYNA (Sigma) were dissolved in ddH_2O. Ro 61-8048 (Sigma) was dissolved in DMSO. Each compound was added to ~50 ^{o}C medium at the desired concentration and mixed thoroughly before dispensing into vials.

2.2.2. Cell culture

Drosophila Schneider's S2 cells were cultured in Hyclone SFX-Insect Medium (GE Healthcare) supplemented with 10 % (v/v) fetal bovine serum (FBS) (Gibco), 100 U/mL penicillin and 100 µg/mL streptomycin. Cells were incubated at 25 ^{o}C and passaged every 3 - 4 days, when they reached a confluence of ~1 x 10^7 cells/mL. The cells are semi-adherent, attaching loosely to culture materials, but also grow in suspension at higher densities. Adhered cells were readily detached by gentle agitation.

Human embryonic kidney (HEK293), HeLa and Murine N9 cells were routinely cultured in GlutaMAX Dulbecco's Modified Eagle Medium (DMEM) (Gibco) supplemented with 10 % (v/v) FBS (Gibco), 100 U/mL penicillin and 100 µg/mL streptomycin. Cells were incubated at 37 ^{o}C, 5 % CO_2 and passaged every 3 - 4 days, when they reached a confluence of ~80 %. Cells were detached by incubation for 3 - 5 min at 37 ^{o}C in 5mM EDTA-PBS. Scraping required to detach N9 cells. For experiments involving N9 cells, medium was switched to Macrophage - Serum Free Medium (SFM) (Gibco) 7 days before experiments, ensuring an endotoxin free environment in which microglia were not immunoactive.

2.2.3. *Drosophila* behavioural and morphological experiments

2.2.3.1. Rapid iterative negative geotaxis (RING) assay

Flies were aged for 7 – 35 days, transferred to fresh medium every 3 – 4 days. Flies were placed 10 per cohort in 18.4 x 2.3 cm transparent plastic cylinder, with a threshold marked 8 cm vertically. Flies were startled by firm tapping on a rubber mat. 10 s later, the number of flies above the 8 cm threshold was counted. The procedure was repeated 10 times per cohort of flies, with 60 s recovery time between iterations. Experiments were performed in a 25 ^{o}C controlled room, between 1100 and 1300 hrs, to control for any metabolic or circadian influence on performance.

2.2.3.2. TriKinetics Drosophila Activity Monitoring (DAM) system assay

Individual male flies were placed inside 5 x 65 mm Pyrex vials with standard medium at one end and a cotton bung at the other. 32 vials were loaded per monitor (TriKinetics) and kept in a 25 ^{o}C incubator with light-control. Flies were entrained for 4 days under a 12:12 light:dark (LD) regime and then subjected to constant darkness (DD) for a further 5 days. Locomotor activity during this time was recorded as the number of times each fly broke an infrared beam bisecting the vial, which is recorded by monitors at 60 s intervals. Average total activity in LD and DD regimes was calculated by summing the total activity counts over a 24 hrs period. The first days of LD and DD regimes were discounted from analysis. Nocturnal activity was calculated by dividing average total activity during the 12 hrs dark phase of the LD regime by the total activity in 24 hrs. Average free-running period of activity in DD regime was calculated by spectral analysis using the CLEAN algorithm.

2.2.3.3. Longevity

0 - 24 hrs post-eclosion, male flies were placed 10 per cohort in normal or supplemented medium. Flies were counted and transferred to fresh medium (without anaesthetisation) every 2 - 3 days.

2.2.3.4. Defective thorax scoring

0 – 24 hrs post-eclosion, male *Pink1*^{B9} or *park*$^{25/25}$ flies were anaesthetised and thoraces were assessed using a dissection microscope. The assay was binary, in the sense that flies were scored as either possessing the phenotype or not.

2.2.4. High-resolution respirometry

Single flies were homogenised in 80 µl of MiR05 respiration medium (EGTA (0.5 mM), $MgCl_2 \cdot 6\ H_2O$ (3 mM), K-lactobionate (60 mM), Taurine (20 mM), KH_2PO_4 (10 mM), HEPES (20 mM), sucrose (110 mM), BSA (1 g/l)) using a motorised mortar and disposable pestles. The homogenate from each fly was added to 1920 µl of MiR05 medium in a single chamber of the Oroboros 2k Oxygraph. Complex I-coupled respiration was initiated by the addition of substrates malate (final concentration 5 mM) and either pyruvate (final concentration 2 mM) or glutamate (final concentration 5 mM) with ADP (final concentration 1 - 5 mM). Complex I + II-linked respiration was activated through the addition of succinate (10 mM). ETS capacity was measured by uncoupling of oxygen reduction from ATP synthase activity via the addition of ~6 0.1 µM titrations of the protonophore CCCP. Complex II ETS was measured after the addition of the complex I inhibitor rotenone (0.5 µM) followed by the addition of complex IV inhibitor sodium azide (100 mM) to measure extracellular (non-mitochondrial) oxygen consumption.

2.2.5. Citrate Synthase activity assay

The citrate synthase (CS) assay is a widely employed assay for interpreting total mitochondrial mass. Five whole flies were homogenised for 60 s in 100 µl CellLytic MT Cell Lysis Reagent (Sigma) and debris was cleared from the lysate by centrifugation at 10,000x g for 10 mins. The lysate was diluted 5-fold in lysis reagent, stored at -80 ^{o}C, and used for both CS and BCA protein content assays. Six biological replicates were used for each group.

CS activity was assayed using the Citrate Synthase Assay Kit (Sigma) on a 96 well plate according to manufacturer's instructions, with each sample measured in triplicate. CS is an enzyme which catalyses a key reaction in the TCA cycle, where citrate is produced from acetyl CoA and oxaloacetate. A by-product of this reaction is coenzyme A (CoA-SH), which reacts with 5,5'-dithiobis-(2-nitrobenzoic acid) (DTNB) in this assay to produce TNB. The concentration of TNB in each sample was measured by light absorbance at 412 nm. A FLUOstar plate reader (Omega) was used to monitor the change in absorption of 412 nm wavelength light after addition of oxaloacetate to each sample and the rate of change in absorbance during the linear phase of the reaction was used to calculate CS activity (µM / ml / min). CS activity of each sample was normalised to total protein content, quantified by BCA assay (Thermo Fisher).

2.2.6. Transmission electron microscopy (TEM)

The heads from newly eclosed flies were dissected in PBS at room temperature (RT) and proboscises were removed with sharp forceps, to aid penetration of fixative. Heads were fixed in 4 % paraformaldehyde (PFA), 2.5 % glutaraldehyde, 0.1 M sodium cacodylate buffer (pH 7.4) and secondarily fixed in 1 % osmium tetroxide / 1.5 % Potassium ferricyanide. Fixed heads were washed three times in de-ionised H_2O, followed by dehydration steps in ethanol (30 %, 50 %, 70 %, 90 % and 100 %). Heads were embedded in modified Spurr's low viscosity resin, which was polymerised at 60 ^{o}C for 16 hrs. Ultra-thin (~70 nm) sections of the retina were cut

using a Ultracut E Ultramicrotome (Reichert), collected onto copper mesh grids and stained first with 2 % aqueous uranyl acetate for 30 mins, then lead citrate for 2 min. Sections were viewed on a JEOL JEM-1400 TEM at an acceleration voltage of 100 kV and images of 10,000x magnification were captured using a Megaview III digital camera with iTEM software.

Mitochondria were traced manually in FIJI and measured using the *"Measure"* function, which calculated aspect ratio (major axis/minor axis), circularity (4π x (area/perimeter^2) and Feret's diameter (the greatest distance between two points) of each organelle. Form factor was calculated as 1/circularity, so that a perfect circle gives a form factor = 1, and the less circular an object is, the higher its form factor.

2.2.7. RNA isolation

RNA was isolated using TRIzol reagent (Ambion), according to manufacturer's instructions. Briefly, samples (10 whole flies or 1 well of 6-well plate cells) were homogenised/lysed in 1mL TRIzol. 200µL chloroform was added and samples were shaken vigorously before centrifugation at 13, 000 g for 15 mins at 4 ^{o}C. The aqueous phase was carefully separated and thoroughly combined with equal volumes of isopropanol. Precipated RNA was pelleted by centrifugation at 13,000g for 10 mins at 4 ^{o}C. Pellets were twice washed in 70% EtOH and allowed to dry before resuspension in nuclease-free H_2O. Concentration and quality of RNA was assessed by spectrophotometry using the Nanodrop 8000 (Thermo Fisher).

2.2.8. cDNA synthesis

Removal of any remaining genomic DNA from RNA was achieved using the TURBO DNAse kit (Ambion). cDNA was synthesised using the QuantiTect Reverse Transcription kit (Qiagen) according to the manufacturer's protocols, by random priming.

2.2.9. dsRNAi synthesis

A *cn* dsRNA template was obtained from the Sheffield RNAi Screening Facility. Other dsRNAi template sequences were obtained from the Heidlberg H2 library and amplified from *Drosophila* cDNA, using the T7 flanked primers listed in Table 2.4 and Phusion taq polymerase, according to the following polymerase chain reaction (PCR) cycling conditions:

	Temperature (°C)	Time (s)	Cycles
Denaturation	98	10	40
Annealing	~60	30	40
Extension	72	30	40
Final extension	72	60	1

Template size was assessed by agarose gel electrophoresis. Templates were used to synthesise dsRNA by *in vitro* transcription reactions, using the T7 Megascript kit (Ambion), according to manufacturer's instructions. Concentration and quality of RNA was assessed by spectrophotometry using the Nanodrop 8000 (Thermo Fisher).

2.2.10. Quantitative PCR (qPCR)

qPCR reactions were performed on a LightCycler 480 system (Roche) using Maxima SYBR Green master mix (Thermo Fisher). Total reaction volume was 10 µl, with forward and reverse primer concentrations of 330 nM. Four technical replicates were used for each sample and a control reaction in which no reverse transcription was carried out was also included. The following thermal cycle was used for reactions and acquisitions were made during the extension phase:

	Temperature (°C)	Time (s)	Cycles
Initial denaturation	95	600	1
Denaturation	95	15	45
Annealing	~62	30	45
Extension	72	30	45
Melt curve	60 - 95	-	1

Crossing points (Cp) were determined by the second derivative method using LightCycler 480 Software (Roche). For relative expression quantification, raw fluorescence data of technical replicates with Cp values within 0.5 cycles of each other were averaged for each sample. The amplification efficiency of each reaction was calculated using the qpcR package in R Studio (Ritz & Spiess, 2008) by fitting sigmoidal curves to the raw fluorescence data, using the *pcrbatch* function. The fold-change ratio of expression was calculated using the *ratiobatch* function, using the following calculation:

$$\frac{E(gc)^{cp(gc)}}{E(gs)^{cp(gs)}} \Big/ \frac{E(rc)^{cp(rc)}}{E(rs)^{cp(rs)}}$$

E = amplification efficiency; gc = target gene of experimental sample; gs = target gene of control sample; rc = reference gene of experimental sample; rs = reference gene of control sample, cp = crossing point.

Statistical significance was calculated using a pairwise fixed random reallocation test, similar to that used by REST software (Pfaffl, 2002). Briefly, efficiency values are tied to Cp values and randomly shuffled between experimental and control samples for 1000 permutations. For each permutation, a fold-change expression ratio is calculated and compared to the value generated from the original data. The number of permutations which produce a fold-change greater than, equal to or smaller than the original data is used to produce a *P* value, representing the probability that the fold-change calculated from the original data is due to chance.

2.2.11. Molecular Cloning

cinnabar coding sequence was amplified from cDNA produced from S2 cells using the primers listed in Table 2.5 and Phusion polymerase (Thermo Fisher), to produce untagged, N-terminal or C-terminal HA constructs. hKMO was amplified from the pcDNA3.1-hKMO expression vector listed in Table 2.4. Primers were designed to incorporate XhoI (5') or XbaI (3') restriction sites for digestion and ligation into the pUAStattB vector. PCR products were separated by size by agarose-gel electrophoresis and purified using the MinElute Gel Extraction Kit (Qiagen), according to manufacturer's instructions. Purified products were blunt-end ligated into the pJET1.2 subcloning vector using the CloneJET PCR Cloning Kit (Thermo Fisher). 100 ng of pJET subcloning construct was added to 80 µL chemically competent DH5α *E. coli* (Invitrogen) on ice for 30 min, heat-shocked at 42 °C for 45 seconds and returned to ice for 2 min. 1 mL Luria broth (LB) (0.5% (w/v) yeast extract, 1% (w/v) tryptone & 0.5% (w/v) NaCl), was added to cells and incubated at 37 °C with gentle agitation for 1 hr. Cell suspension was plated onto LB-agar containing ampicillin and incubated at 37 °C overnight.

Colonies were isolated from LB-agar plates and grown in 4 mL LB-ampicillin for 12-16 hrs at 37 °C. Plasmid DNA was isolated from cells using the Plasmid Mini Kit (Omega). Purified plasmids were sequenced using the Big Dye v3.1 kit (Applied Biosystems). 10 µL reactions consisted of ~500 ng DNA, 2 µL 5x Sequencing Buffer, 1 uL Big Dye v3.1 and 2 µL pJET sequencing primer. Sequences were validated by alignment to open reading frame (ORF) sequences for *cn* and *hKmo* using NCBI blast. 1 µg of pJET plasmid containing correct sequence constructs was digested in 50 µL reactions with 1 µL of XhoI & XbaI (NEB) for *cn* constructs, NotI & XbaI (NEB) for *hKMO*, using CutSmart buffer (NEB) for 2 hrs at 37 °C. 1 µg pUASt-attB plasmid was also digested with the same restriction enzymes. Digested DNA was separated by size by agarose-gel electrophoresis and purified using the MinElute Gel Extraction Kit (Qiagen), according to manufacturer's instructions. A ~3 : 1 molar ratio of construct : pUASt-attB plasmid DNA (40 ng : 75 ng) was used in ligation reactions. Reactions were 20 µL total and contained 2 µL T4 ligase buffer (NEB) and

1 µL T4 ligase (NEB). Ligation reactions were incubated at 16 °C for ~16 hrs and subsequently purified using the Cycle Pure Kit (Omega).

Ligations were transformed into DH5α *E. coli* and plated on LB-agar amplicillin plates as above. DNA from isolated colonies was prepared as above and diagnostically digested and size-separated by gel electrophoresis. Plasmid DNA from clones demonstrating the expected pUASt-attB and insert sizes were again sequenced and validated as above. These clones were used to produce glycerol stocks and to prepare DNA for *Drosophila* microinjection or S2 cell transfection.

2.2.12. *Drosophila* microinjection

Untagged *cn* and *hKMO* containing pUASt-attB plasmids were prepared using the Plasmid Mini Kit (Omega) and eluted in 20 µL nuclease-free H_2O. DNA quality was verified by spectrophotometry (260/280 absorbance ratio of 1.80 - 1.90). Samples were diluted to ~0.4 µg/µL and sent to the University of Cambridge, Department of Genetics, Fly Facility. Plasmids were injected into the *y^1.w* M{vasint.Dm}ZH2A; attP40* line and surviving transformants were selected based on *mini-white (mw^+)* expression from the incorporated pUASt-attB vector. Two isogenic lines for each construct were established, with the construct-carrying chromosome balanced over the SM6a chromosome.

2.2.13. Mitotracker Red FM staining, laser confocal imaging and image processing

For S2 cell RNAi experiments, cells were transfected with dsRNA using Effectene reagent. When *cn* was overexpressed, the *pUAStattB-UAScn* (0.6 µg) and *Act5CGAL4* (0.2 µg) plasmids were added to the transfection mix. 60 hrs post-transfection, cells were seeded at 2 x 10^5/dish in glass-bottomed 35mm dishes (Ibidi) coated with Concanavalin A. 12 hrs later, cells were stained with Mitotracker Red FM (100 nM in complete Schneider's medium) for 30 mins. Medium was replaced with fresh

complete medium (without Mitotracker) and cells were imaged live at 25°C on an Olympus FV1000 scanning confocal microscope (60x objective, zoom = 4, Kalman = 6).

7 days before imaging, N9 microglial cells were washed twice in PBS and media was changed from complete Glutamax DMEM (Gibco) to serum-free Macrophage-SFM (Gibco). Cells were passaged every 3 - 4 days and were then seeded at 2 x 10^5 cells per dish in glass-bottomed 35 mm dishes (Ibidi) coated with poly-l-orthanine, in Macrophage-SFM. 24 hrs later, cells were stained with Mitotracker Red FM (100 nM in Macrophage-SFM) for 30 mins. Medium was replaced with fresh Macrophage-SFM and cells were imaged live at 37 °C, 5 % CO_2 on an Olympus FV1000 scanning confocal microscope (60x objective, zoom = 4, Kalman = 6).

HEK293 cells were seeded at 1 x 10^5 cells per dish in glass-bottomed dishes coated with poly-l-ornathine. 48 hrs post-transfection, cells were washed in PBS and given fresh complete DMEM. 72 hrs post-transfection, cells were stained with Mitotracker Red FM (100nM in complete DMEM) for 30 mins. Medium was replaced with fresh complete DMEM and cells were imaged live at 37 °C, 5 % CO_2 on an Olympus FV1000 scanning confocal microscope (60x objective, zoom = 4, Kalman = 6). Images were deconvolved using Huygen's Professional, then processed in FIJI using the following macro code:

```
run("Z Project...", "projection=[Max Intensity]");
run("Subtract Background...", "rolling=10");
run("Enhance Contrast...", "saturated=0.001");
```

For quantification of mitochondrial parameters, the following macro was applied:

```
run("Make Binary");
run("Analyze Particles...", " circularity=0-0.99 show=[Bare Outlines] display exclude summarize");
```

Aspect ratio (major axis/minor axis) and circularity (4π x (area/perimeter^2) values were produced by the *Analyze Particles* function. Form factor was calculated as 1/circularity, so that a perfect circle gives a form factor = 1, and the less circular an object is, the higher its form factor.

2.2.14. Parkin-GFP mitochondrial recruitment assay

pMK33-Parkin-GFP plasmid was transfected into S2 cells using Effectene Reagent (Qiagen), according to manufacturer's protocol. Cells were selected in complete media containing 300 µM Hygromycin B. Clonal cell line was established by serially diluting the mixed population of cells in a 96-well plate and expanding wells which contained individual colonies derived from single cells.

Cells were seeded at 2.5 x 10^5 cells per well of a 24-well plate in 0.5 mL of complete media. dsRNA treatment (*cinnabar* or *Pink1*) was applied according to Zhou *et al.*, (2013) using Effectene reagent (Qiagen). After 24 hrs, $CuSO_4$ was added to each well at 500 µM final concentration to induce expression of the Parkin-GFP construct. 12 hrs before CCCP treatment, cells were replated in a 24-well plate coated with concanavalin A at 1 x 10^5 cells per well to allow cells to properly adhere and spread to the dish at the desired confluence for imaging. 70 hrs after dsRNA transfection, cells were treated with CCCP (20 mM in DMSO) at a final concentration of 20 µM, or DMSO for 2 hrs. Media was then aspirated, cells washed in PBS and fixed in 4 % PFA in PBS for 20 mins at room temperature. Cells were washed twice more in PBS and finally covered by 0.5 mL of PBS. Before imaging, cells were stained with Hoechst 33342 dye (Invitrogen) 0.5 µg/mL in PBS for 15 mins.

Imaging was performed using the Olympus scanR system with a 40x objective. 49 positions were imaged per well. Individual cells were detected by Hoechst nuclear staining and the number of Parkin-GFP foci per cell was automatically counted by the scanR analysis software.

2.2.15. Co-immunoprecipitation (CoIP) assays

YFP-Parkin cells were seeded at 1 x 10^6 cells per 100 mm dish in 7 mL complete DMEM. 24 hrs later, cells were transfected with 2 µg pcDNA3.1(empty or RFP-KMO) plasmid DNA (300µL EC buffer, 16µL Enhancer, 16µL Effectene, 3mL complete DMEM). GFP-Parkin S2 cells were seeded at 1 x 10^7 cell per 100mm dish in 7 mL complete Schneider's medium. Shortly after, cells were transfected with 1 µg pUAStattB-hKMO and 1 µg Act5CGAL4 plasmid DNA (300 µL EC buffer, 16 µL Enhancer, 16 µL Effectene, 3 mL complete DMEM). 48 hrs post-transfection, cells were treated with CCCP (20 µM) or DMSO for 2 hrs. For fixed samples, PFA (1 % final concentration) was added to medium and incubated at RT for 10 min with gentle agitation. PFA was quenched by 125 mM glycine for 5 mins. Cells were detached by agitation and washed twice in RT PBS, centrifuged at 200x g for 5 min before each wash, then resuspended in either 200µL ice-cold CoIP lysis buffer (10mM Tris/Cl pH 7.5; 150 mM NaCl; 0.5 mM EDTA; 0.5 % NP-40, 1 X protease inhibitor cocktail (Roche)). Cells were lysed on ice for 30 mins with disruption by pipetting every 10 mins. Lysates were centrifuged at 16, 000x g for 10 mins at 4 ^oC. Supernatants were diluted in 300µL dilution buffer (10 mM Tris/Cl pH 7.5; 150 mM NaCl; 0.5 mM EDTA).

YFP-hParkin (HeLa cells) or dParkin-GFP (S2 cells) were immunoprecipitated using GFP-trap magnetic beads (Chromotek), according to manufacturer's instructions, with the modification that samples were incubated with GFP-trap beads for 2 hrs at 4 ^oC. Immunocomplexes were dissociated from beads by incubation with Laemli buffer for 10 min at 95 ^oC and loaded onto Novex Tris-glycine 10% gels (Invitrogen).

2.2.16. Mitochondrial fractionation

Mitochondria were isolated from cells using the Mitochondrial Isolation Kit for Cultured Cells (Mitosciences), according to manufacturer's protocol. Cells were pelleted at 200x g for 5 min at RT, media aspirated, cell pellets snap frozen in lN_2. Pellets were thawed at 37^oC for 1 min, resuspended in Kit Buffer A and ruptured

using a dounce homogeniser (30 strokes). Nuclear fraction was removed by centrifugation, then mitochondrial and cytosolic fractions were separated by a second centrifugation. For CoIP experiments, the mitochondrial pellet was resuspended in CoIP lysis buffer (see 2.1.14) and for phospho-specific immunoblotting, was suspended in RIPA (see 2.1.14) supplemented with Halt Phosphatase Inhibitor Cocktail (Thermo Fisher).

2.2.17. SDS-PAGE & Immunoblotting

Proteins were separated on Novex 10 % Tris-glycine gels (Invitrogen) in Running buffer (250 mM Tris, 1.9 M glycine, 0.5 % (w/v) SDS) at constant voltage (225 V) for ~45 mins. Proteins were transferred to nitrocellulose membrane by wet transfer in Transfer buffer (20mM Tris, 0.149 M Glycine, 0.1 % (w/v) SDS and 12 % (v/v) methanol) for 90 mins at constant current (400 mA). Post-transfer, membranes were blocked with 5 % (w/v) milk protein (or bovine serum albumin (BSA) for phospho-sensitive assays) in TBS-T (0.1 % TWEEN20) for at least 1 hr. Membranes were incubated with antibodies in 5 % (w/v) milk or BSA TBS-T (0.1 % TWEEN20) at 4 ^{o}C for 16 - 24 hrs (primary antibodies) and 1 hr RT (secondary antibodies), with gentle agitation. Membranes were washed 3 x 10 min in TBS-T (0.1 % TWEEN20) after primary and secondary antibody incubations. HRP-conjugated secondary antibodies were detected using SuperSignal West PICO Plus Chemilluminescent substrate (Thermo Fisher) and imaged with the GeneGnome XRC imaging system (Syngene).

2.2.18. Statistical analysis

Aside from qPCR analysis which was performed in R Studio, all other statistical analyses were performed in Prism 7 (GraphPad). Details of tests performed on individual experiments are described in figure legends.

3 Exploring mitochondrial phenotypes in KMO deficient models

3.1 Introduction

Although KMO is localised to the mitochondrial outer membrane (MOM), a mitochondrial function for the protein has not been described in detail. However, the KMO encoding gene *cinnabar* (*cn*), was identified in a genome-wide RNAi screen of *Drosophila melanogaster* immortalised S2R+ cells, as a positive regulator of CCCP and paraquat-induced Parkin-GFP translocation to mitochondria (Ivatt *et al.,* 2014). In the same study, *cn* knockdown also affected mitochondrial morphology under basal conditions. These findings imply a role for KMO in Parkin-mediated mitophagy and mitochondrial dynamics, mechanisms via which a healthy mitochondrial population is maintained. In order to investigate a potential role for KMO in maintaining mitochondrial health, the primary approach taken in this chapter was the study of phenotypes linked to mitochondrial function and energy metabolism in KMO deficient models.

I first attempted to replicate the finding of Ivatt *et al*., (2014) that mitochondrial morphology is affected by *cn* knockdown *in vitro* using immortalised *Drosophila* cells. *Drosophila* is an attractive model to study KMO deficiency *in vivo*, due to the availability of *cn* RNAi expressing lines (Dietzl *et al*., 2007; Campesan *et al*., 2011; Breda *et al*., 2016), in addition to *cn* amorphic alleles such as cn^3 (Warren *et al*., 1996; Campesan *et al*., 2011; Green *et al*., 2012). The cn^3 allele contains a 0.5 kb deletion and a 7.5 kb insertion located about 5 kb distally (Warren *et al*., 1996). Flies homozygous for this mutation do not express any functional KMO, reflected in the bright red eyes of these flies, due to the lack of synthesis of 3-HK and thus its downstream product, the brown eye pigment xanthommatin. Since genetic background is not identical between cn^3 and the wildtype Canton S strain, I also investigated *cn* knockdown by RNAi, utilizing a KK line from the Vienna Drosophila Resource Center (VDRC) and an isogenic control. KK lines feature RNAi constructs

inserted into the genome at a specific landing site using the phiC31 site-specific integrase, thereby eliminating insertional and positional effects (Dietzl *et al.*, 2007). Comparison of flies in which *cn*-targeting RNAi was expressed to flies in which an empty UAS vector was incorporated into the same VIE-260B landing site, allowed for uniformity in genetic background as well as controlling for potential issues caused by GAL4 titration by multiple UAS binding sites.

I also assessed mitochondrial morphology in a mammalian model of KMO knockdown. KMO has a highly tissue specific expression pattern in mammals, with highest expression levels detected in the liver, kidney and placenta (Erickson *et al.*, 1992). However, the widely used and readily available human embryonic kidney 293 (HEK293) cell model does not express detectable levels of KMO (Alberati-Giani *et al.*, 1997b; Swaih; 2016), therefore knockdown experiments could not be performed in these cells. In the CNS, KMO expression is limited to microglial cells (Guillemin *et al.*, 2003a, Giorgini *et al.*, 2008) and is upregulated upon immune activation (Giorgini *et al.*, 2008; Connor *et al.*, 2008; Wang *et al.*, 2010; Molteni *et al.*, 2013). Given the relevance of both KMO and mitochondrial function to numerous neurological disorders, a CNS model was desirable. N9 murine microglial immortalised cell lines, stably expressing KMO-targeting shRNA constructs were produced by another member of my group (Swaih & Giorgini, unplublished) and were utilised to assess if findings in *Drosophila* are translatable to a mammalian CNS model.

3.2 Results

3.2.1 Assessing mitochondrial morphology in *cinnabar* knockdown *Drosophila* S2 cells

I first sought to replicate the observation from Ivatt *et al.,* (2014) of aberrant mitochondrial morphology upon *cn* knockdown in *Drosophila* S2R+ cells. I used the S2 cell line, which differs from S2R+ in the expression of some cell surface receptors (Yanagawa *et al*., 1998). dsRNA targeting *parkin* was used as a positive control, as it has been previously shown that *parkin* dsRNA causes a more elongated, connected mitochondrial network in *Drosophila* S2R+ cells (Ziviani *et al.,* 2010, Pogson *et al.,* 2014). dsRNA was synthesised *in vitro* using template sequences taken from the second generation Heidelberg library (Horn *et al.,* 2010). dsRNA complementary to the *Photinis pyralis* (firefly) *luciferase (luc*) gene (*f.luc*), was used as a negative control.

A serum-starvation approach was initially employed for delivery of dsRNA, which is usually sufficient for uptake of dsRNA by S2 cells (Clemens *et al*., 2000; Rogers & Rogers, 2008; Zhou *et al*., 2014). However, assessment of *cn* mRNA levels by qPCR revealed that significant knockdown was not achieved at 48 or 72 hrs post-dsRNA treatment (Figure 3.1A). The dsRNA delivery strategy was therefore changed to the use of a lipid-based transfection reagent Effectene (Qiagen), which can also be used for delivery of dsRNA to S2 cells (Zhou *et al*., 2013). The knockdown efficiency of *cn* and *parkin* 72 hrs post-transfection was ~78% and ~99% respectively (Figure 3.1B), therefore this method of dsRNA delivery was employed in subsequent experiments. *parkin* dsRNA cells showed elongated, aggregated mitochondria, whereas the control *f.luc* dsRNA cells showed more punctate organelles. *cn* dsRNA cells appeared to display an intermediate phenotype, with more elongated structures compared to the negative control group, but less aggregated clusters of organelles than observed in *parkin* dsRNA cells (Figure 3.2) An attempt was made to quantify mitochondrial morphology via the "analyse particles" function within FIJI. However, it was not possible to distiniguish individual organelles and therefore quantification was not performed on mitochondrial morphology in S2 cells.

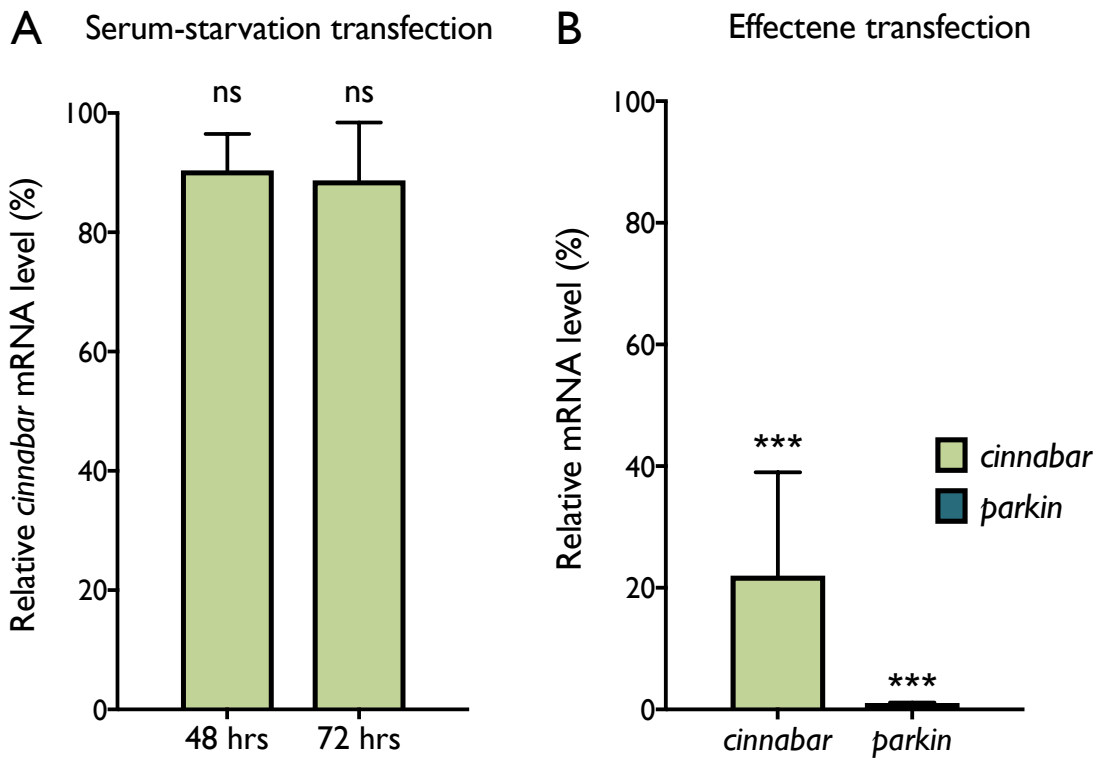

Figure 3.1. Knockdown efficiency of *Drosophila* S2 cells treated with dsRNA is dramatically improved by using a chemical transfection-based approach as opposed to serum starvation.

A) Cells were seeded at 1 x 10^6 cells per well of a 6 well plate and transfected with 20 µg of dsRNA in serum-free medium. After 1 hr, medium was replaced with 10 % FBS medium. After 48 and 72 hrs, total RNA was extracted and used to reverse-transcribe cDNA. qPCR was performed to quantify *cn* mRNA levels normalised to the *rp49* reference mRNA. Values represent the level of normalised *cn* mRNA relative to untreated cells. **B)** Cells were seeded at 1 x 10^6 cells per well of a 6 well plate and transfected with 2 µg of dsRNA targeting either firefly *luciferase* (*f. luc*), *cinnabar* or *parkin,* using Effectene transfection reagent mix. RNA was extracted 72 hrs post-transfection. Values represent normalised mRNA levels of target gene (*cinnabar* or *parkin*) in dsRNA treated cells compared to *f.luc* dsRNA treated controls (mean ± SD; pairwise fixed reallocation randomization test, *** $P < 0.001$, ns = not significant. n = 3).

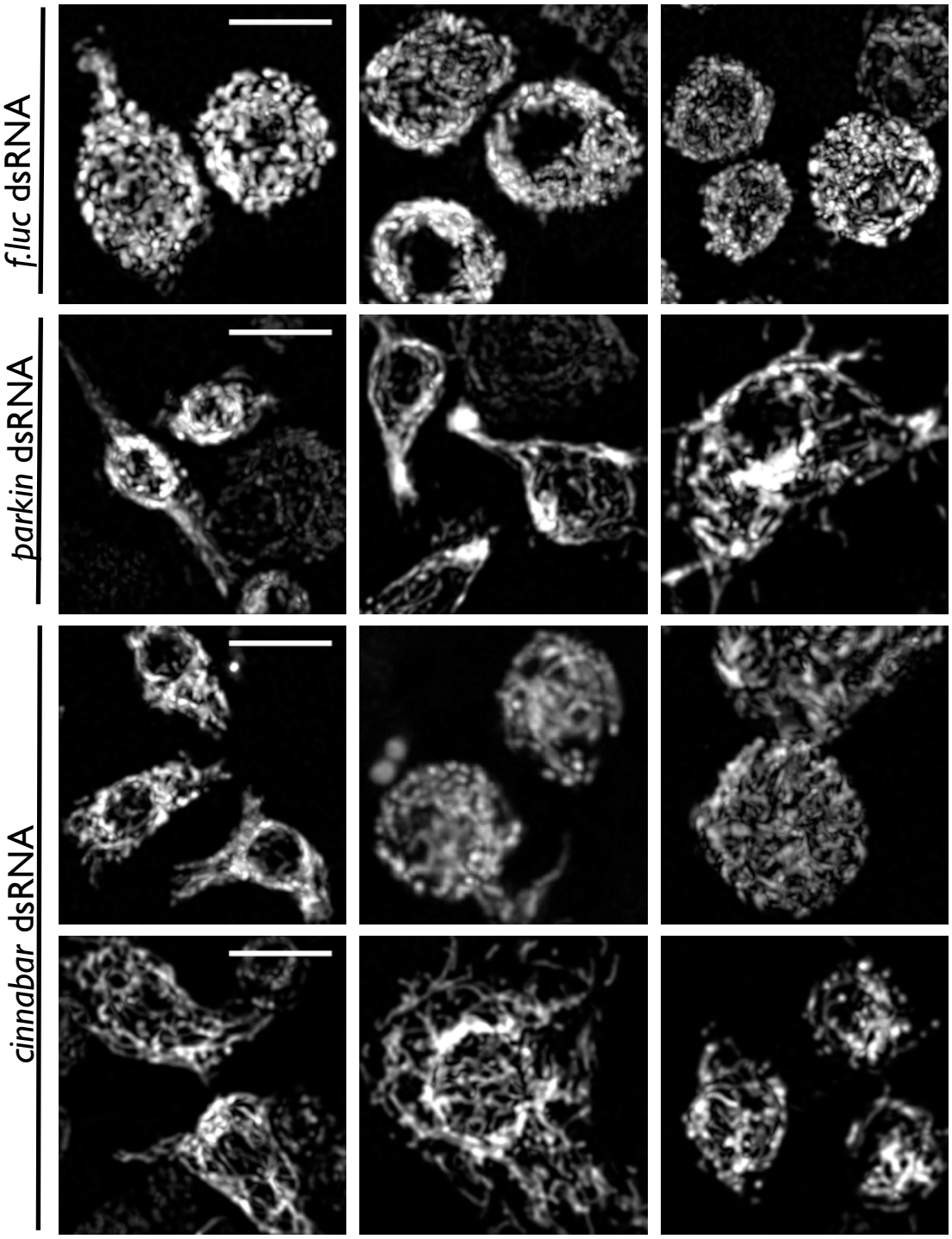

Figure 3.2. Mitochondrial morphology appears affected in *cinnabar* and *parkin* dsRNA treated *Drosophila* S2 cells.

Drosophila S2 cells were seeded at 1 x 10^6 cells per well in 6-well plates and transfected with dsRNA targeting firefly *luciferase (f.luc), parkin* or *cinnabar,* using Effectene reagent. 60 hrs post-transfection, cells were plated in glass bottomed dishes coated with concanavalin A. 12 hrs later, cells were stained with Mitotracker Red FM and imaged live at 25 ^oC (scale bars = 5 μm).

3.2.2 Assessing mitochondrial morphology upon *KMO* knockdown in a murine N9 microglial cell line

To assess if KMO loss leads to elongated mitochondria in a mammalian CNS model, N9 murine immortalised microglial cells stably expressing *Kmo*-targeting shRNA constructs (Swaih & Giorgini, unpublished) were utilised. I first tested the efficiency of KMO knockdown by qPCR in cells expressing one of two *Kmo*-targeting shRNA constructs, compared to two scramble control shRNAs. Control shRNA expressing cells showed no significant difference in *Kmo* mRNA levels between each other (Figure 3.3). Both cell types had Cp values of *Kmo* amplification (see Chapter 2) of ~35 over a total of 45 cycles, compared to ~ 18 and ~ 22 for the two reference genes, indicating that basal *Kmo* expression levels are very low in this cell type. In *Kmo* shRNA-expressing cells, *Kmo* amplification above the Cp threshold was not detected (Figure 3.3).

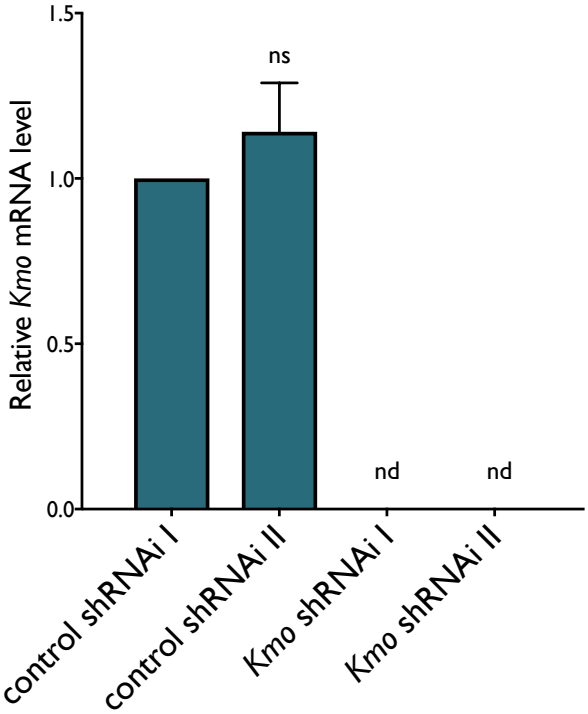

Figure 3.3. *Kmo* mRNA expression is abolished in shRNAi expressing N9 cells. Cells were seeded at 1 x 10^6 cells per well of a 6-well plate. 24 hrs later, total RNA was extracted and reverse transcribed to produce cDNA. *Kmo* mRNA levels relative to the reference genes *RpLP0* & *Ppib* were assessed by qPCR, and normalised to the control shRNAi I cell line (mean ± SD, pairwise fixed reallocation randomization test, nd = not detected, ns = not significant. n = 3)

N9 cells with control or *Kmo* shRNA were stained with Mitotracker Red FM and imaged live. No observable difference in mitochondrial morphology was observed in *Kmo* shRNAi cells compared to controls (Figure 3.4).

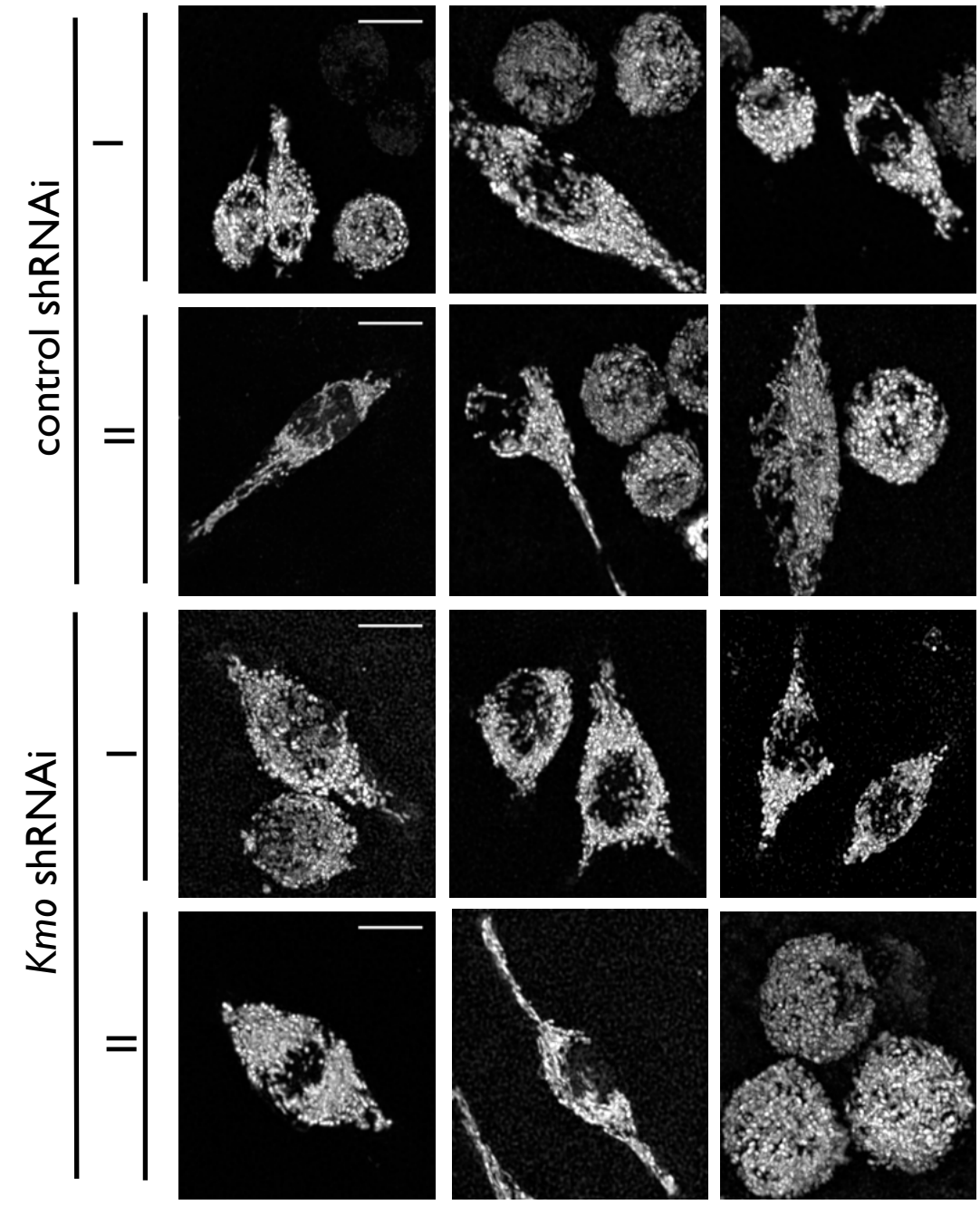

Figure 3.4. Mitochondrial morphology is unaffected in *Kmo* shRNAi N9 cells.
Cells were plated in glass-bottomed dishes coated with poly-l-ornathine. 24 hrs later, cells were stained with Mitotracker Red FM and imaged live at 37 ^{o}C, 5 % CO_2 (scale bars = 5 μm).

3.2.3 Modulating KMO expression by immune activation in N9 microglial cells

KMO expression is dramatically upregulated in the CNS upon immune activation *in vivo* (Connor *et al.*, 2008; Molteni *et al.*, 2013) and in primary and immortalised microglial cells *in vitro* (Giorgini *et al.*, 2007; Wang *et al.*, 2010; Alberati-Giani *et al.*, 1996). Given the low levels of *Kmo* mRNA observed in the N9 cells expressing control shRNA, I investigated the possibility of upregulating KMO by immune activation. Lipopolysaccharide (LPS) supplemented in the media of N9 cells resulted in immune activation, as indicated by the raised concentration of nitrites in media 24 hrs post-treatment (Figure 3.5A). At the same time media was sampled, total RNA was extracted from cells and *Kmo* mRNA levels were assessed by qPCR. No *Kmo* mRNA was detected in *Kmo* shRNA cells, in PBS or LPS-treated conditions. In the LPS-treated control shRNA I line, *Kmo* mRNA was significantly increased ~2.5-fold compared to PBS-treated controls. However, in the control shRNA II line, *Kmo* mRNA was not significantly increased (Figure 3.5B). At this stage it was decided to discontinue experiments using the N9 cell model.

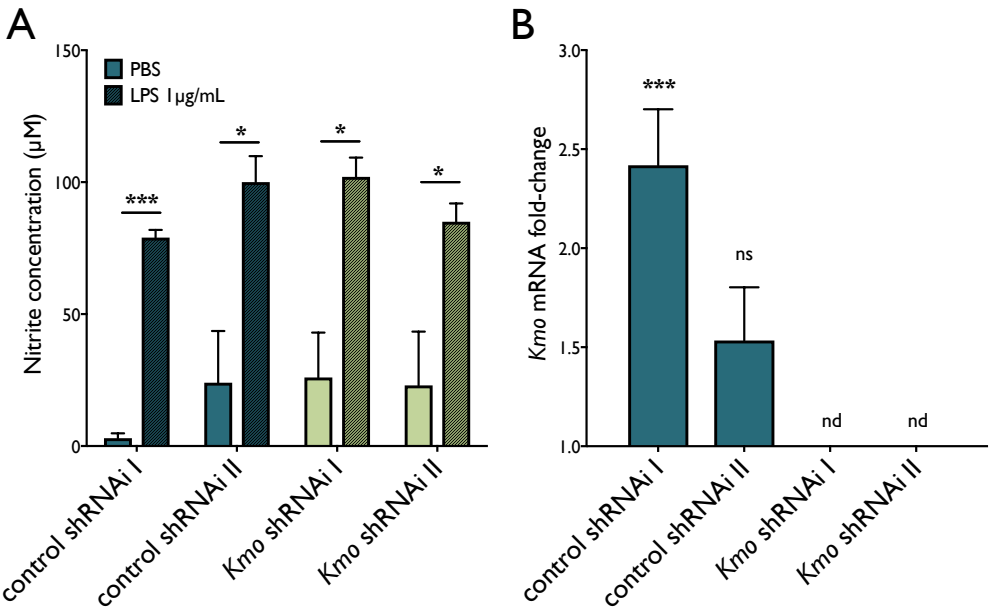

Figure 3.5. **LPS treatment of N9 microglial cells causes activation of nitrite production and modest upregulation of KMO activiry in the control shRNAi I cell line**

A) Nitrite concentration in cell media 24 hrs post-treatment with LPS (1 µg/mL) (mean ± SD, multiple t tests, * $P < 0.05$, *** $P < 0.001$. n = 3). **B)** Fold-change in *Kmo* mRNA level between LPS and PBS treated N9 cell lines (mean ± SD, pairwise fixed reallocation randomization test, *** $P < 0.001$).

3.2.4 *cinnabar* transcript levels in RNAi knockdown and amorphic *Drosophila*

In order to investigate if the mitochondrial morphology phenotype observed in *Drosophila* cells *in vitro* is reflected *in vivo, cn* deficient *Drosophila* models were employed. Flies homozygous for the cn^{3} allele showed no detectable levels of *cn* mRNA (Figure 3.6). As expected, cn^{3} heterozygotes express ~50% *cn* mRNA compared to the Canton S wildtype strain. The balancer chromosome II, Curly of Oster (CyO), carries several mutant alleles including $duox^{cy}$, resulting in a curly wing phenotype and cn^{2}, a hypomorphic *cinnabar* allele. Thus, cn^{3}/CyO flies exhibit a further reduction in *cn* mRNA levels, with ~30% of Canton S levels.

Given the different genetic background between cn^{3} and Canton S flies, an additional KMO deficient fly model was used, in which *cn* was knocked-down ubiquitously using a UAS-RNAi construct from the KK library (Vienna Stock Center) and the *Act5CGAL4* driver. The 3M control group contains an empty 10XUAS construct used to generate all KK RNAi lines, incorporated into the same landing site. The 3M line crossed to *Act5CGAL4* was used as a control in RNAi experiments, in this way controlling for GAL4 titration and genetic background. Any differences observed between *3M; Act5CGAL4* and $cn^{RNAi;}$ *Act5CGAL4* flies can thus be attributed to a reduction in *cn* expression. *Act5CGAL4* driven expression of cn^{RNAi} resulted in ~65% knockdown in whole body homogenates. *cn* mRNA levels of the *3M; Act5CGAL4* control group were not significantly different from the Canton S wildtype group (Figure 3.6).

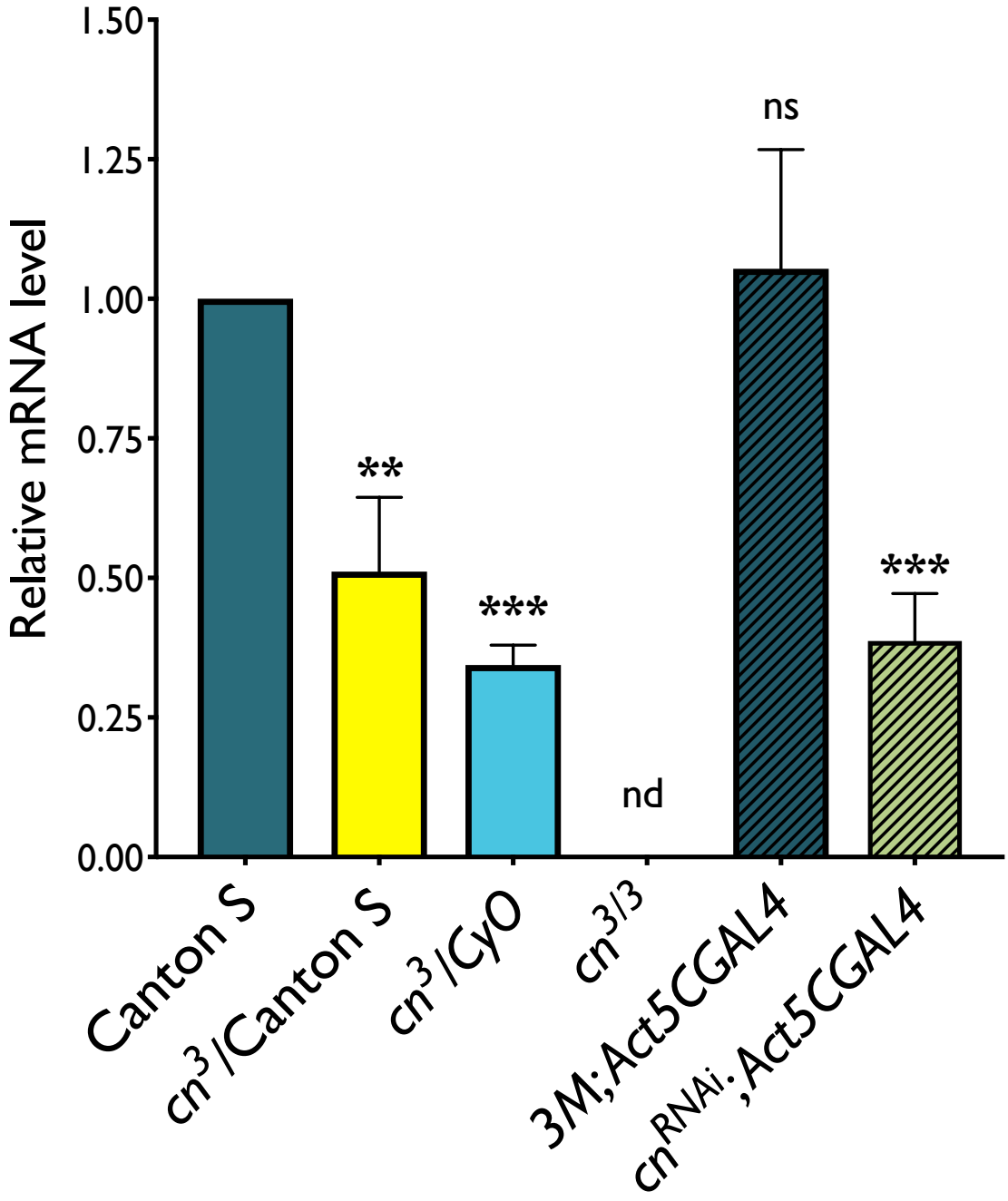

Figure 3.6. *cinnabar* mRNA levels are modulated in *Drosophila* experimental lines. Newly eclosed flies were snap frozen in liquid nitrogen before RNA extraction and cDNA synthesis. qPCR was employed to determine *cn* mRNA level relative to the reference gene *rp49*, normalised to that of the Canton S wildtype group (mean ± SD, pairwise fixed reallocation randomization test, ** $P<0.01$, *** $P<0.001$, nd = not detected, ns = not significant. Ten flies per n, n = 3).

3.2.5 Elongated mitochondria and increased mitochondrial area coverage in *cn* flies

To investigate if loss of *cinnabar* affected mitochondrial morphology *in vivo*, transmission electron microscopy (TEM) was performed on the compound eye. This tissue was selected based on spatial expression data available for *cn*, which indicates the eye has higher *cn* mRNA levels than other adult tissues (Chintapalli *et al.,* 2007). The *Drosophila* compound eye consists of ~800 multiple repeating units called ommatidia. Each ommatidium consists of 8 photoreceptor neurons called rhabdomeres, surrounded by 4 cone cells, 2 primary and 6 secondary pigment cells, as well as tertiary pigment cells and mechano-sensory bristles (Kumar, 2012).

In transverse sections of the retina in which 7 rhabdomeres were visible per ommatidium, the majority of mitochondria were visible in the transverse plane (Figure 3.7A), making analysis of mitochondrial length uninformative. Longitudinal sections gave a much better representation of mitochondrial length (Figure 3.7B) and were used to calculate mitochondrial size and area coverage (Figure 3.8). Due to the high degree of contrast between the electron dense pigment granules and surrounding cell cytoplasm, it was challenging to take images that had the optimum contrast for capturing features of mitochondrial ultrastructure, such as organization and density of cristae. Nonetheless, I did not observe any difference in ultrastructure between $cn^{3/3}$ flies and Canton S controls.

Mitochondria were traced and dimensions quantified using longitudinal sections where the entire outer membrane was visible. In $cn^{3/3}$ flies, the aspect ratio and Feret's diameter were increased compared to Canton S, reflecting elongated mitochondria in KMO deficient flies (Figure 3.8A & B; Mann-Whitney test, $P < 0.0001$). Form factor was also increased in $cn^{3/3}$ flies (Figure 3.8C; Mann-Whitney test, $P = 0.0013$), indicative of a more branched mitochondrial network. Mitochondria also covered a higher percentage of the total area measured in $cn^{3/3}$ flies compared to Canton S (Figure 3.8D, Welch's t test, $P = 0.0460$).

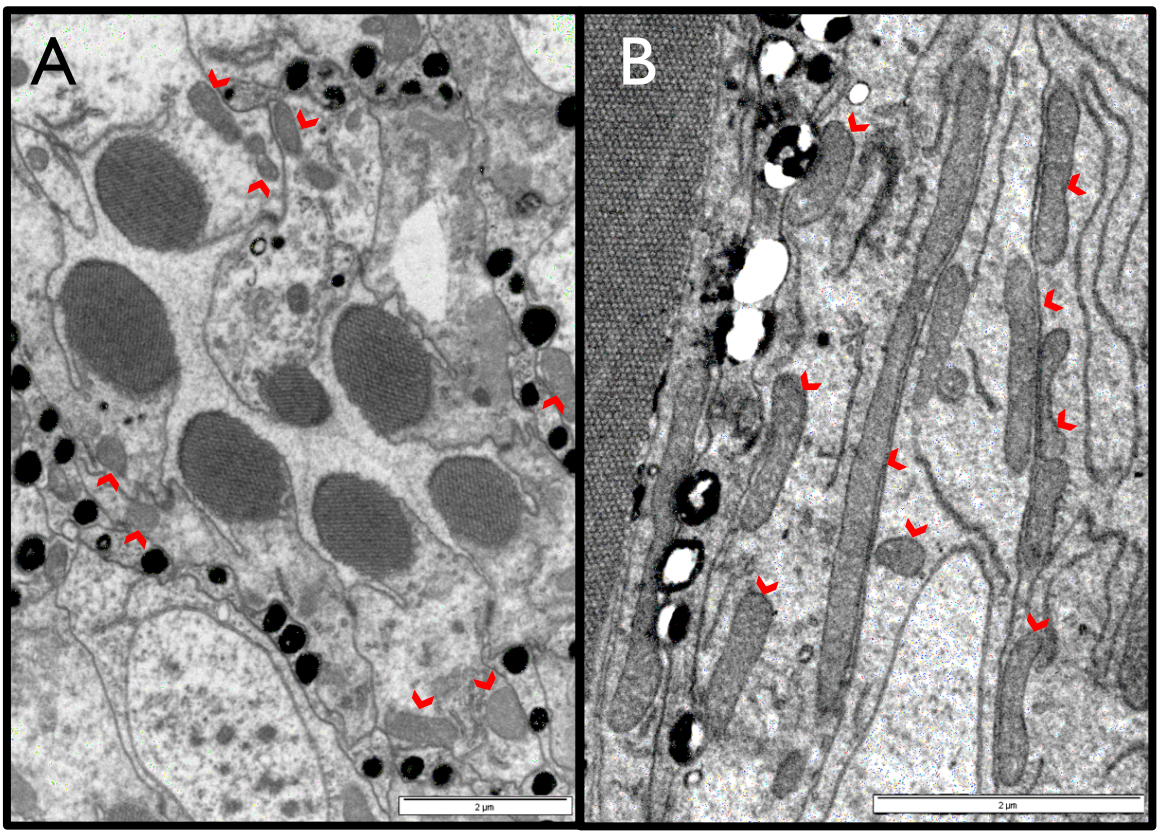

Figure 3.7. Transmission electron microscopy images from eye tissue of *cn*$^{3/3}$ flies reflect mitochondrial length better in longitdunal than transverse sections.
A) Transverse sections of the *Drosophila* eye, in which 7 rhabdomeres are visible. Due to the long structure of eye cells and subsequent orientation of mitochondria, transverse sections resulted in the majority of mitochondria being visible in the transverse plane. **B)** Longitudinal sections were selected, using rhabdomere structures as a reference point. Sections in this plane resulted in more longitudinal sections of mitochondria, allowing a more accurate analysis of mitochondrial length. Mitochondria are labelled by red arrowheads (scale bars = 2 µm).

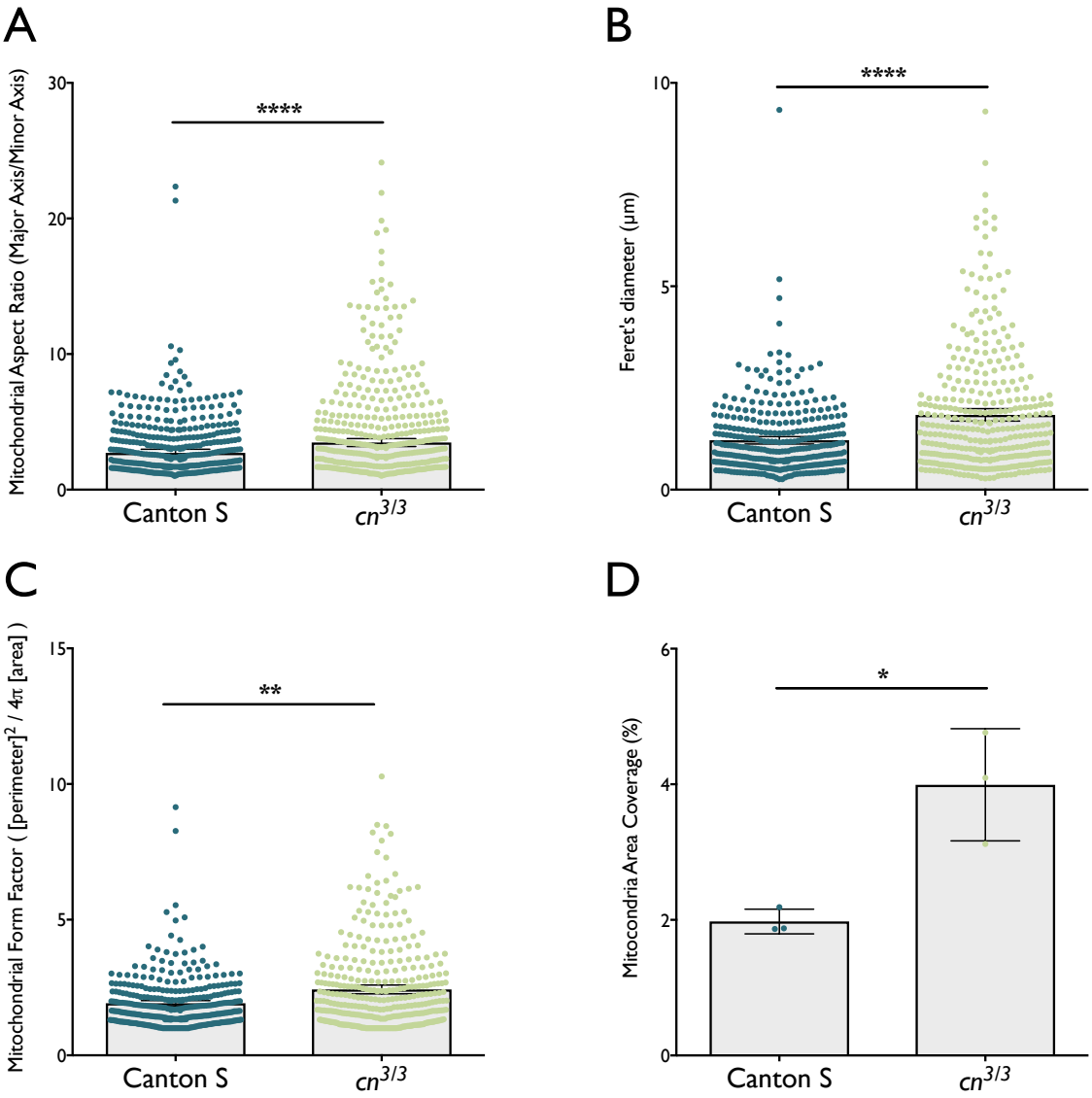

Figure 3.8. Mitochondrial length and area coverage are increased in *cn*$^{3/3}$ flies compared to the Canton S wildtype strain.

Longitudinal sections of the compound eye of *cn*$^{3/3}$ and Canton S flies were examined by transmission electron microscopy. Mitochondria of which the entire outer membrane was visible were manually traced. The following parameters were quantified in FIJI: **A)** Aspect ratio (major axis length / minor axis length). **B)** Feret's diameter (distance between two most distal points). **C)** Form factor (degree of branching, calculated as the inverse of circularity) (median ± 95% CI, n = 3, >350 total mitochondria analyzed per group, Mann-Whitney U test, ** $P < 0.01$, **** $P < 0.0001$). **D)** Mitochondrial area coverage (percentage of total area analyzed covered by mitochondria). All identified mitochondria, regardless of whether the entire outer membrane was visible were used for this calculation (mean ± SD, Welch's t test, * $P < 0.05$. n = 3).

3.2.6 Citrate synthase is increased in *cn*^{3} flies

In order to validate the findings by TEM that mitochondrial content was increased in *cn*^{3} flies, whole fly homogenates were subjected to the citrate synthase assay. The assay measures the conversion of oxaloacetate to citrate by citrate synthase, widely used as an indicator of mitochondrial content (Larsen *et al.*, 2012; Costa *et al.*, 2013; Pryde *et al.*, 2016). An increase in citrate synthase activity was observed in *cn*$^{3/3}$ flies compared to Canton S controls. To assess if the increase in mitochondrial content is due to the loss of KMO enzymatic activity and hence a result of altered KP metabolism, *cn*$^{3/3}$ flies were supplemented with 3-HK in their diet at a concentration (0.8 mg/mL), previously shown to restore this metabolite to endogenous levels (Campesan *et al.,* 2011), as well as Canton S flies. Newly emerged progeny reared on 3-HK supplemented food had notably darker eyes, indicating the uptake of the metabolite, which acts as a precursor for the brown ommochrome xanthommatin (Figure 3.9). 3-HK supplementation made no significant difference to citrate synthase activity in either *cn*$^{3/3}$ or Canton S flies (Figure 3.10A). Act5CGAL4-driven *cn*^{RNAi} flies were also assessed, however they showed no significant different in citrate synthase activity compared to the 3M control group (Figure 3.10B). These data indicate that altered mitochondrial morphology in cinnabar deficient flies is not due to the enzymatic activity of KMO.

Figure 3.9. 3-HK supplementation restores wildtype eye colour of *cn*$^{3/3}$ flies.
Newly emerged *cn*$^{3/3}$ flies reared on standard (left) or 3-HK (0.8 mg/mL) supplemented (right) medium. The darker eye colour of the 3-HK supplemented fly indicates the uptake of 3-HK, which is converted into the brown ommochrome xanthommatin.

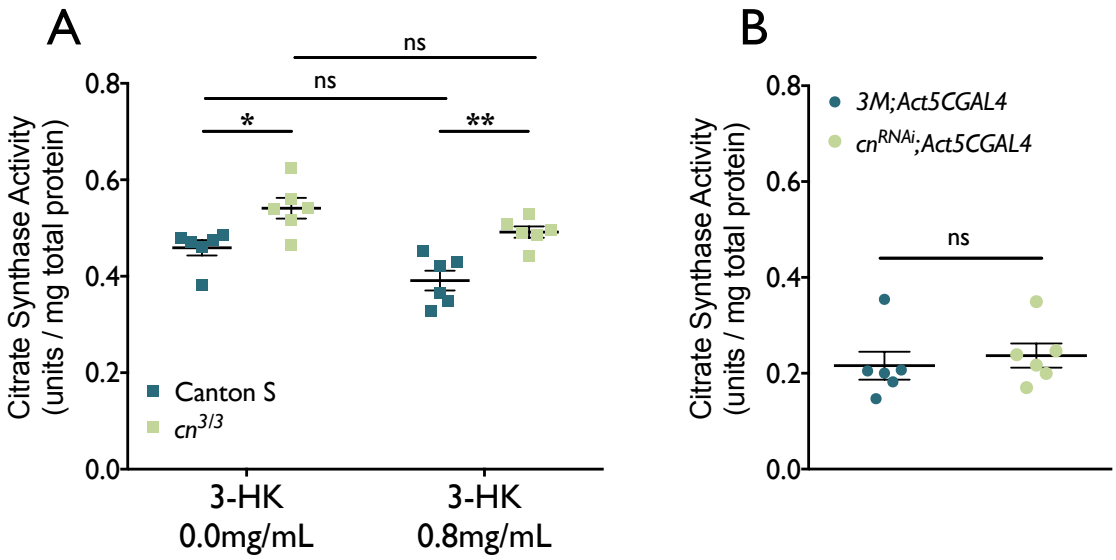

Figure 3.10. Citrate synthase activity is increased *cn³* amorphs but not *cn³* knockdown flies.

Flies were homogenised in lysis buffer. Lysis was enhanced by one freeze-thaw cycle. Homogenates were diluted 5-fold for the assay. Activity was assessed by colorimetric change due to the conversion of oxaloacetate to citrate. Activity was normalised to total protein content, measured by BCA assay **A)** Activity of $cn^{3/3}$ flies compared to Canton S wildtype controls. Both groups were supplemented with 3-HK at a concentration that restores it to physiological levels in $cn^{3/3}$ flies (mean ± SEM; two-way ANOVA, Tukey *post hoc* * $P < 0.05$, ** $P < 0.01$ ns = not significant. n = 6). **B)** Activity of cn^{RNAi} flies compared to 3M controls (t test, ns = not significant. Five flies per n, n = 6).

3.2.7 Respiratory capacity of KMO deficient flies

To assess if the differences in mitochondrial morphology observed in *cn* flies are reflected in altered mitochondrial respiratory function, respirometry experiments were performed on whole fly homogenates. The Oroboros 2K respirometer was used to assess respiratory capacity of electron transfer system complexes I & II, in both an ATP synthase-coupled (OXPHOS capacity) and uncoupled state (ETS capacity). Initial experiments used malate and glutamate (M-G) as substrates for complex I of the ETS (Costa *et al.,* 2013; Lehmann *et al*., 2016). In the presence of M-G, cn^{3} fly homogenates showed no significant difference in respiratory capacity in comparison to the Canton S wildtype strain (Figure 3.10A). However, upon the use of pyruvate alongside malate (M-P) (Liu *et al*., 2011; Scialó *et al*., 2016; Rana *et al*., 2017), a significant reduction in the capacities of complex I, as well as complex I & II combined, was observed in both an ATP synthase coupled and uncoupled state (Figure 3.10B). Upon inhibition of complex I with rotenone, no significant difference in oxygen flux was observed, indicating that complex I is responsible for the respiratory deficit.

To ascertain if the reduced respiratory capacity observed in *cn* flies was due to loss of KMO enzymatic activity, cn^{3} flies were supplemented with 3-HK (0.8 mg/mL). There was no significant difference in respiratory capacity between 3-HK treated and untreated flies, indicating that the mitochondrial phenotype observed was independent of 3-HK levels (Figure 3.10C). cn^{RNAi} flies displayed similar deficits in complex I and complex I + II capacities compared to controls (Figure 3.10D).

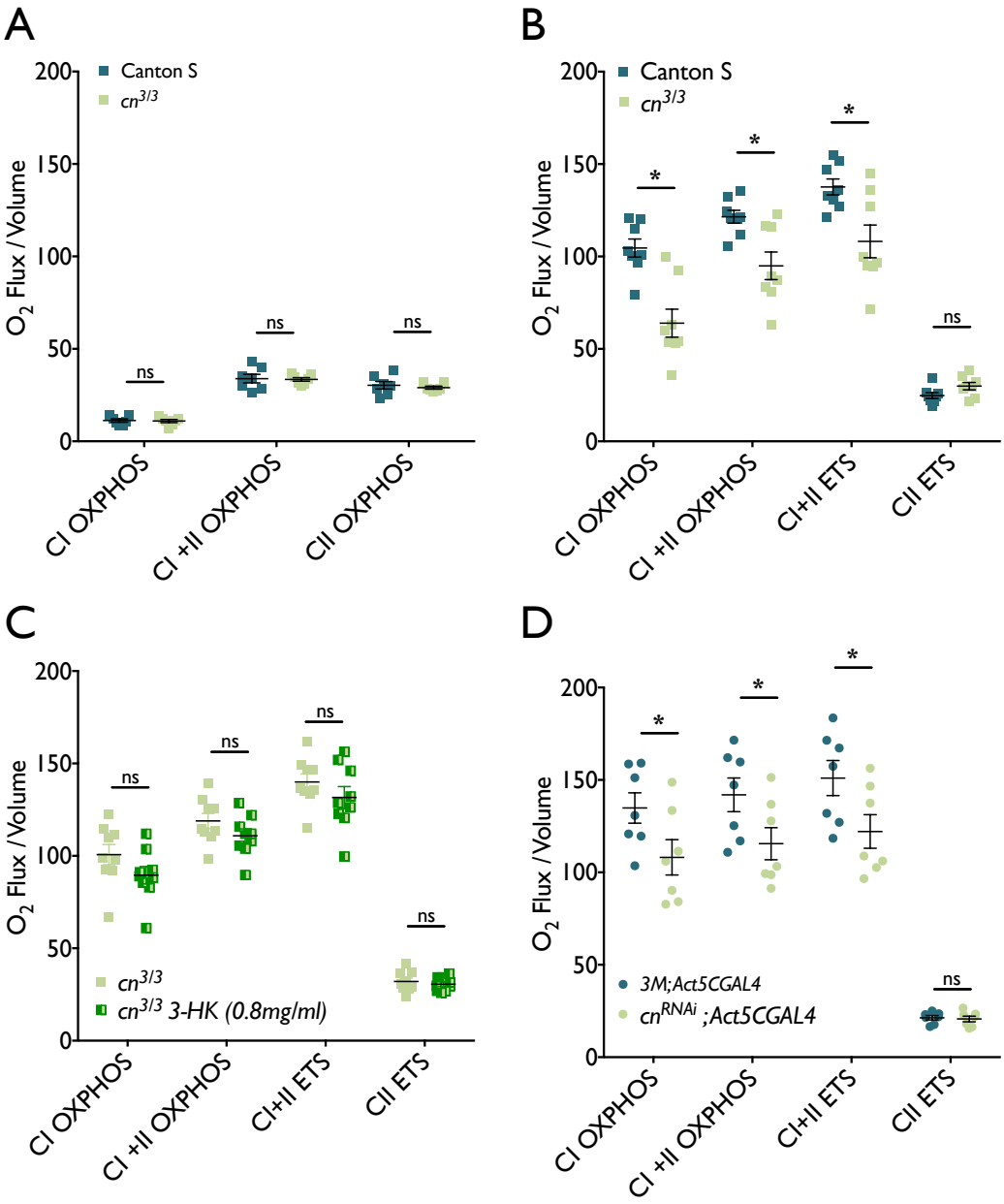

Figure 3.11. Respiratory capacity is reduced in *cinnabar* flies.

Individual Day 3 female flies were homogenised in Miro5 respiration buffer and loaded into chambers of the Oroboros 2K Respirometer. **A)** Complex I OXPHOS was measured in the presence of malate, glutamate and ADP. Complex I + II OXPHOS was measured after the addition of succinate. Complex II was measured after addition of complex I inhibitor rotenone. **B-D)** Complex I OXPHOS was measured in the presence of malate, pyruvate and ADP. Complex I + II OXPHOS was measured after the addition of succinate. Complex I + II ETS was measured by adding titrations of CCCP until maximal oxygen flux was reached. Complex II ETS was measured after the addition of Complex I inhibitor rotenone. Due to high inter-experimental variability, a pairwise statistical comparison for each experiment was performed (mean ± SEM; paired t test, Holm-Sidak *post hoc*, * $P < 0.05$. n = 7 - 9).

3.2.8 Locomotor ability of KMO deficient flies

Locomotor ability was assessed using the Trikinetics monitoring system, by which the activity of individual flies is logged based upon the number of times an infrared beam is crossed (Rosato & Kyriacou, 2006). This apparatus is commonly used to explore circadian phenotypes in *Drosophila*, as activity can be monitored under different light and temperature cycles. Flies were monitored in both a 12:12 light:dark (LD) cycle and in also in constant darkness (DD). Flies in which *cn* was ubiquitously knocked down with RNAi showed significantly reduced total locomotor activity in both LD and DD conditions (Figure 3.12A & B). Activity was also monitored in the context of the null cn^{3} allele; flies homozygous for the null allele showed a significant decrease in total locomotor activity, compared to Canton S wild type control group in both LD and DD conditions, while $cn^{3}/+$ flies showed an intermediate phenotype (Figure 3.12C & D).

Given that the KP is implicated in neurodegenerative and psychiatric disorders, both of which are associated with aberrant circadian rhythms and sleep behaviours, activity data from these experiments were also analysed to investigate circadian phenotypes. Nocturnal / diurnal (N / D) ratio (the proportion of locomotor activity during the dark phase over a full 24 hr cycle) and mean free-running period (length in hrs of 1 "day" in terms of rhythmic behaviour in constant dark conditions) were analysed. Canton S flies showed a significantly higher nocturnal activity compared to other groups tested, however this is likely caused by a background effect of this strain, and not based on levels of *cn* expression, as the *3M; Act5CGAL4* control group showed no significant difference in N / D ratio compared to either cn^{RNAi}*; Act5CGAL4* or cn^{3} flies (Figure 3.12E). No significant difference in free-running period was observed between any of the lines (Figure 3.12F).

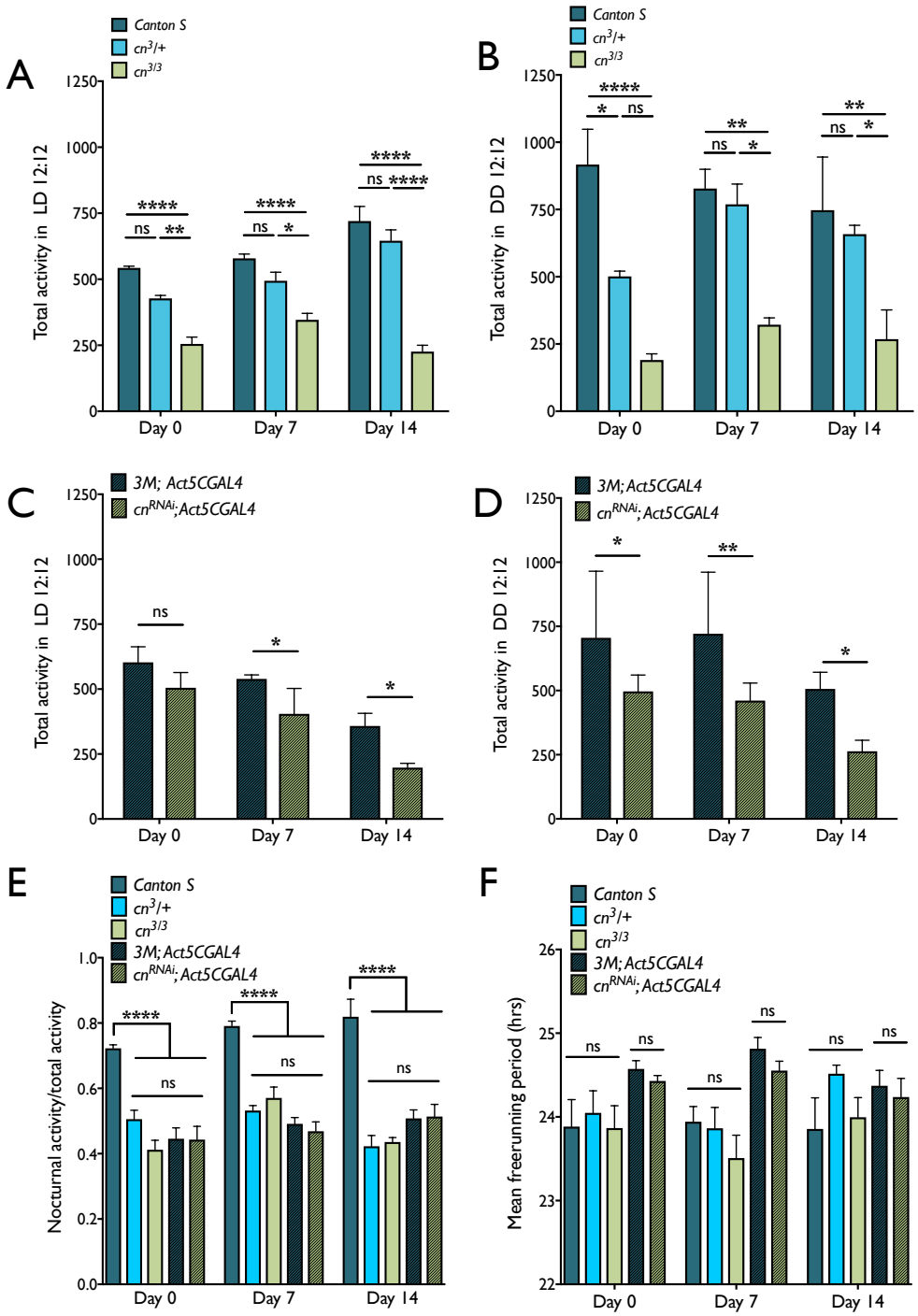

Figure 3.12. Locomotor activity is reduced in *cinnabar* flies.

Newly eclosed, 7 or 14 day old flies were loaded into Trikinetics monitors, in which activity of individual flies is counted by the number of times the animal crosses an infrared beam. **A-D)** Total activity per 24 hrs was counted for 5 days of LD (12:12), followed by 10 days of DD. (Mean ± SEM; Two-way ANOVA, Tukey *post hoc*, * P <0.05, ** P<0.01, ** P<0.001, **** P<0.0001. n=32). **E)** Nocturnal diurnal ratio was calculated across 5 days of LD as the total activity during the dark phase as a proportion of total activity per 24 hour day (one - way ANOVA, Tukey *post hoc,* ** P <0.01. n = 32). **F)** Freerunning period in constant darkness was calculated by spectral analysis (mean ± SEM, two – way ANOVA, Tukey *post hoc*).

To further explore the locomotor deficit observed in *cn* flies, an additional assay was also employed. The rapid iterative negative geotaxis (RING) assay (Gargano *et al.,* 2005) is an established method of monitoring motor function in *Drosophila,* particularly when modelling diseases in which deficiency in such traits are prominent, such as neurodegeneration (Liu *et al.*, 2015; Breda *et al.,* 2016). Flies show an age associated decrease in fitness with this assay (Liu *et al.*, 2015; Rhodenizer *et al.,* 2008), which we observed in Canton S and *3M; Act5CGAL4* control groups (Figure 3.13). $cn^{3/3}$ flies showed a significantly lower climbing ability than Canton S at Day 7 and 14 (Figure 3.13A). At Day 21, the climbing ability of both genotypes dramatically decreased and there was no significant difference between them. cn^{RNAi} flies showed reduced climbing ability compared to the 3M control group at all ages investigated (7-35 days old) (Figure 3.13B).

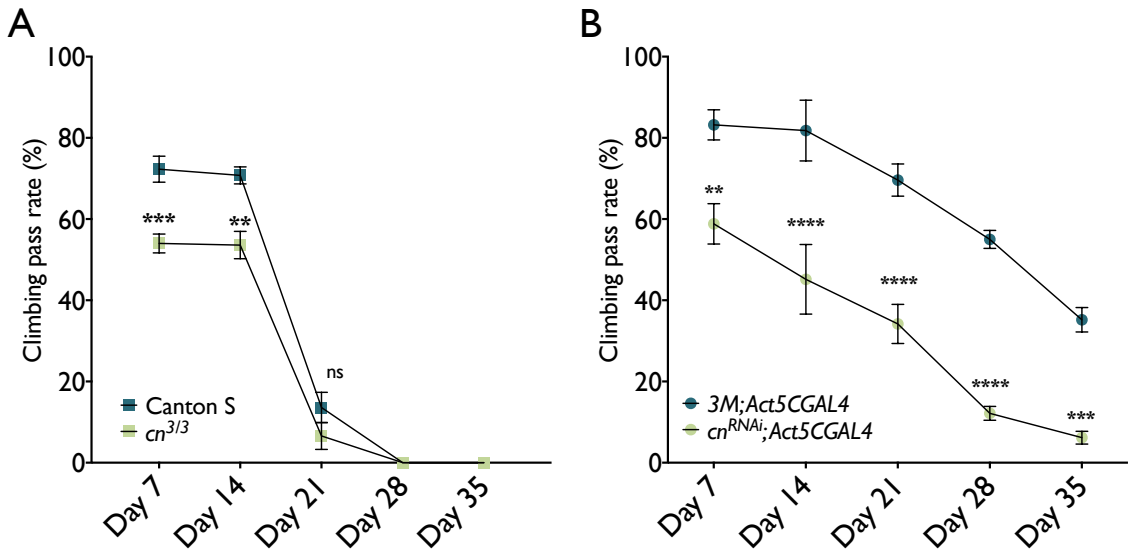

Figure 3.13. Climbing ability is reduced in *cinnabar* flies.
A) $cn^{3/3}$ flies compared to the Canton S wildtype strain. **B)** cn^{RNAi}; *Act5CGAL4* compared to the *3M; Act5CGAL4* control group. Ability was assessed using the rapid iterative negative geotaxis (RING) assay. 10 flies were placed inside a 20 cm vial and tapped to the bottom. The percentage of flies that passed a 8 cm threshold line after 10 s was counted (mean ± SEM; two-way ANOVA, Sidak *post hoc*, * $P < 0.05$, ** $P < 0.01$, *** $P < 0.001$, **** $P < 0.0001$. Ten flies per n, n = 5-10).

3.2.9 NAD+ and NADH levels are unaffected by *cn* RNAi

In mammals, the KP is one of the major routes for NAD+ biosynthesis, which occurs through the central branch of the pathway where KMO operates. NAD+ supplementation has been shown to rescue mitochondrial defects in *Pink1* and *parkin* mutants (Lehmann *et al.*, 2016). Given the reduced locomotor ability and complex I respiratory capacity of *cn* flies, and the essential role of NAD+ redox reactions in glycolysis and oxidative phosphorylation, a reduction in NAD+ production could be responsible for the phenotypes observed in KMO deficient flies. However, *Drosophila* have no known homologues of the genes encoding the enzymes acting downstream of KMO (3-HAAO and QPRT), thus the KP is thought to be uncoupled from QUIN and NAD+ synthesis in flies (Rongvaux *et al.*, 2003). Nonetheless, to confirm that NAD+ and NADH levels are unaffected by loss of *cn*, enzymatic assays were conducted to quantify NAD+ and NADH in fly homogenates. NAD+ and NADH concentrations, thus also NAD+/NADH ratio, were all unaffected in cn^{RNAi}*; Act5CGAL4* flies compared to flies lacking *Act5CGAL4* (Figure 3.14). This corroborates that the KP is uncoupled from NAD+ synthesis in *Drosophila* and also that the mitochondrial and locomotor phenotypes observed in *cn* flies are independent from NAD+ levels.

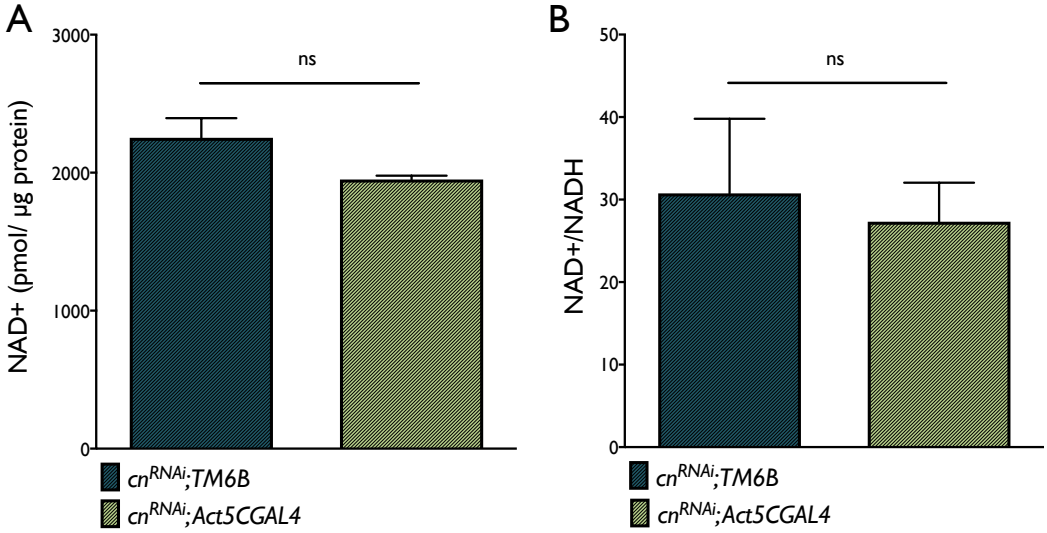

Figure 3.14. NAD+ concentration and NAD+/NADH ratio are unaffacted cn^{RNAi} flies. Samples consisted of homogenised flies in extraction buffer which were deproteinised by centrifugation through 10 kDa molecular weight filters. NAD+ and total NAD (NAD+ & NADH) were quantified by separate colorimetric reactions and normalised to total protein content (t test, ns = not significant. Twenty flies per n, n = 5)).

3.2.10 Lifespan of KMO deficient flies

Given the implication of mitochondrial dysfunction in ageing and age associated disease, the effect of *cn* knockdown or deletion on longevity was investigated. There was no significant difference in lifespan between cn^{RNAi} and 3M lines, with a median lifespan of 56 and 58 days respectively (Table 3.1, Figure 3.15). The median lifespan of $cn^{3/3}$ and Canton S flies was 32 and 39 days respectively. There was no significant difference in survival between $cn^{3/3}$ and Canton S groups, however both of these groups were significantly different from the *3M; Act5CGAL4* control group (Table 3.1).

Table 3.1. Survival data summary of *cn* males.
Summary of the data used to generate survival curves (Figure 3.15), median survival and curve comparison significance computed by Prism 7. P values were calculated by Mantel-Cox test as a comparison between each genotype and either Canton S or *3M; Act5CGAL4* control groups.

	Canton S	$cn^{3/3}$	*3M; Act5CGAL4*	cn^{RNAi}*; Act5CGAL4*
# deaths/events	100	100	100	100
Median survival (days)	39	32	58	56
P value (compared to Canton S)	NA	0.3231	<0.0001	<0.0001
P value (compared to *3M; Act5CGAL4*)	<0.0001	<0.0001	NA	0.0823

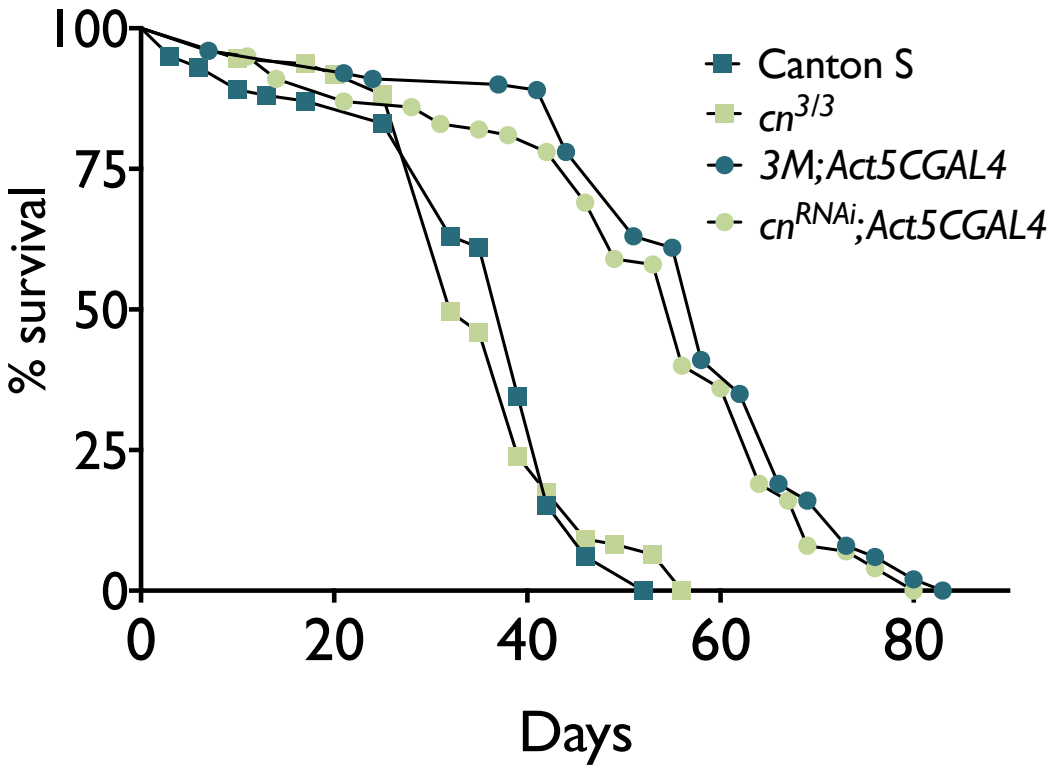

Figure 3.15. Lifespan of *cinnabar* amorph or knockdown flies are not significantly different from corresponding control genotypes.
Newly emerged males were placed 10 per vial and transferred to fresh medium every 3 - 4 days (n = 100).

3.3 Discussion

The primary aim of this chapter was to probe for a mitochondrial role of KMO using a reverse genetics approach. *Drosophila melanogaster* proved to be a valuable model for this investigation, due to the ease by which the KMO encoding gene *cinnabar* could be knocked down by RNAi *in vitro* and *in vivo*, as well as the availability of fly lines carrying amorphic alleles (e.g. cn^3). Although unquantified, elongated mitochondria were observed in S2 cells in which *cn* was knocked down, an observation previously made in an S2R+ cell RNAi screen (Ivatt *et al.,* 2014). However, this observation was not extended to the murine N9 microglial cell line. This could be due to the low basal level of *Kmo* expression observed in this cell line, meaning that KMO might not have an important role in mitochondrial dynamics in inactivated microglia. LPS-induced activation of the N9 cells caused a significant increase in *Kmo* expression in only one of the control shRNAi lines used, and the ~2.5-fold change was still very small compared to the ~400-fold increase previously reported in LPS-treated primary microglia (Wang *et al*., 2010). This could have been due to the time-point chosen to measure *Kmo* expression, as the peak of upregulation was found to be ~8 hrs by Wang *et al* (2010), and closer to baseline at 24 hrs. Although I did not pursue these experiments any further, given the finding that LPS-treated primary microglia exhibit an increase in DRP1 pSer616 phosphorylation and a decrease in mitochondrial length (Katoh *et al*., 2017), it would be interesting to use this model to further investigate a role for KMO in mitochondrial dynamics in activated microglia. This experiment could also be performed in peripherally derived mammalian cells in which KMO is expressed more highly, for example the SK-Hep1 and MHCC-97H hepatocyte cell lines in which *Kmo* RNAi has been previously performed (Jin *et al*., 2015). KMO knockout mice (Giorgini *et al*., 2013) could also utilised to assess mitochondrial phenotypes in a mammalian *in vivo* context. Given the tissue specific nature of KMO expression, it would be interesting to compare the effects on mitochondrial morphology in KMO expressing and non-expressing tissues in these mice. This could provide insight into the properties of these cells that might require additional regulation of mitochondrial morphology.

Longitudinal sections of the *Drosophila* eye were selected for the quantification of mitochondrial parameters in *cn*-null mutants *ex vivo*, due to the fact that *cn* is expressed in the eye of adult flies and the longitudinal sections gave the best indication of mitochondrial length. The manual tracing of mitochondria from TEM images was also prone to artefacts, the most notable being that many mitochondria are not visible in their entirety in a single section. Only organelles in which the entire MOM was visible were traced, which means that mitochondria from both Canton S and cn^3 flies, particularly more elongated structures, were excluded from analysis. Of the mitochondria that could be traced, there was a significantly greater median length, aspect ratio and degree of branching (form factor) in cn^3 flies. Given the shift in distribution towards elongated mitochondria in cn^3 flies, excluding mitochondria in which the whole MOM could not be traced from the analysis it is likely to have given a conservative estimate of this effect, rather than overestimating it. For total area coverage of mitochondria, all visible organelles were selected, regardless of whether the entire MOM was visible. An increase in total area coverage was also observed in cn^3 flies.

An increase in mitochondrial content was corroborated by the increase in citrate synthase activity observed in the cn^3 flies. However, this finding is not replicated in cn^{RNAi} flies compared to the 3M control group. This could be due to the fact that *cn* mRNA levels are ~35% that of the 3M control group, whereas $cn^{3/3}$ flies do not express any *cinnabar.* RNAi knockdown could therefore be insufficient to induce the significant increase in citrate synthase activity observed in cn^3 flies. An increase in sample size could reduce the error in significance calculations and show a significant increase in the RNAi flies. Alternatively, the difference observed between cn^3 and Canton S could be a genetic background effect. These doubts could be overcome by backcrossing the cn^3 allele into the genetic background of the Canton S flies, or by producing a complete *cn* knockout line by CRISPR/Cas9 editing (Zhang *et al.,* 2014).

Respirometry experiments employing malate and glutamate (M-G) as substrates for complex I of the ETS show no significant difference in respiratory capacity between cn^3 and Canton S fly homogenates. However, when malate and pyruvate (M-P)

substrates are used, not only is the oxygen flux of both Canton S and *cn*^{3} significantly higher compared to glutamate and malate, but *cn*^{3} flies also demonstrate significantly lower respiratory capacity compared to wild type. The difference in efficacy between pyruvate and glutamate as substrates is possibly due to differences in the transport of these compounds into the mitochondrial matrix, where they are utilised in the TCA cycle to produce NADH, which acts as electron donor to complex I (Teulier *et al.,* 2016). As demonstrated by M-P experiments, the oxygen flux observed using malate and glutamate does not reflect true respiratory capacity of samples, which could be why no difference is observed between *cn* deficient samples and controls in M-G experiments. However, significant differences in complex I respiratory capacity have been previously demonstrated in *Pink1* mutants using malate and glutamate as substrates (Costa *et al.,* 2013; Lehmann *et al*., 2016). The reason that they are not observed in *cn*^{3} flies could be simply due to the mildness of the phenotype. Experiments by Costa *et al*. and Lehmann *et al*. were performed at 37^{o}C, whereas those in this study were performed at 25^{o}C. *Pink1* mutants exhibit a decrease in resistance to a number of stresses (Clark *et al*., 2006). The stress caused by a shift in temperature above levels physiological in *Drosophila* could be another reason why an effect was observed using malate and glutamate as substrates in *Pink1* flies.

Locomotion of *cn*-null or RNAi flies at several different ages was assessed over several days by Trikinetics monitoring. No significant correlation between *cn* deficiency and aberrant circadian phenotype was observed, indicating that KMO does not play an important role in biological rhythms in *Drosophila.* A significant decrease in total locomotor activity was observed in *cn*^{3} flies, with an intermediate effect in *cn*$^{3/+}$ heterozygotes compared to Canton S. *cn*^{RNAi} flies also showed a significant decrease in total locomotor activity compared to 3M controls. *cn*^{3} flies also showed a significantly reduced climbing ability in the RING assay compared to Canton S at Day 7 and Day 14. By Day 21, the effect was lost, as both groups show a dramatic reduction in climbing ability compared to Day 14. Age-associated decreases in climbing performance are well documented (Gargano *et al*., 2005; Rhodeniser *et al.,* 2008), however the inability to climb at Day 21 in both Canton S and *cn*^{3} is more dramatic than expected in wildtype flies. This is enforced by the

behaviour of cn^{RNAi} and 3M control groups, of which a proportion are still capable of climbing at Day 35. cn^{RNAi} flies show a significantly decreased climbing ability compared to *3M* at the earliest age assayed (7 day old) and the difference between *cn* RNAi and *3M* controls does not correlate with age, suggesting that the effect of *cn* knockdown on climbing is not age-associated.

A decrease in locomotor activity in larvae of the *cn*-null mutant (cn^1) compared to Canton S was previously reported (Zakharov *et al.,* 2012). In this study, *vermillion* mutants were also assayed and also showed a locomotor phenotype, which was thus attributed to aberrant KP metabolite levels. However, the *cn* mutant phenotype was more severe than *v,* which was hypothesised by the authors to be due to the greater accumulation of KYNA observed in *cn* mutants, leading to inhibition of NAChRs. In my work neither respiratory nor citrate synthase activity phenotypes were reversed by supplementing cn^3 flies with 3-HK at concentrations known to restore it to physiological levels (Campesan *et al*., 2011), suggesting that these effects are independent of 3-HK production by KMO. However, the effect of KYNA on the mitochondrial phenotypes reported in this chapter should also be further investigated. 1mM KYNA treatment reduced the respiratory capacity of mitochondria isolated from rat heart tissue, but not liver or brain tissue (Baran et al., 2016). Mitochondria express NAChRs on the MOM, where they regulate mitochondrial Ca^{2+} uptake and cytochrome c release (Gergalova *et al*., 2012). Nicotine treatment of hippocampal neurons resulted in an increase in mitochondria fission, which was attributed to increased DRP1 Ser616 phosphorylation (Godoy *et al.,* 2018). The elongated mitochondria observed in *cn* flies could therefore be due to inhibition of NAChRs by elevated KYNA.

Supplementing Canton S or *3M; Act5CGAL4* flies with KYNA at a concentration that elevated it to the levels observed in *cn* mutants or knockdown flies, would reveal whether the phenotypes observed here are due to increased KYNA levels. Flies overexpressing human KATII, in which KYNA levels are significantly raised (Breda *et al.,* 2016) could also be investigated for phenotypes related to mitochondrial morphology, respiratory capacity and locomotion. An alternative strategy for distinguishing between functions of KMO that are dependent or independent of its

catalytic activity would be to treat wildtype flies with KMO inhibitors, such as the Ro 61-8048 compound, which has been previously been effectively used in *Drosophila* (Campesan *et al.*, 2011). Alternatively, a mutation to remove either enzymatic activity or mitochondrial localization could be knocked-in using CRISPR/Cas9 editing. Creating a mutation that affects enzymatic activity without affecting mitochondrial localization, or *vice versa,* could prove technically challenging, as both of these properties require the C-terminal region in both insect (Han *et al.*, 2003) and mammalian KMO (Hirai *et al.*, 2010; Wilson *et al.*, 2014; Amaral & Scrutton; unpublished; Kim *et al.*, 2018). However, the R83 residue of *S. cerevisiae* KMO, which when mutated leads to a loss of KMO enzymatic activity (Amaral et al., 2013) is conserved in humans and flies. Introducing the R83M point-mutation at the corresponding *Drosophila* residue would allow the separation of KMO enzymatic activity from independent mitochondrial functions.

This chapter has revealed that KMO deficiency in *Drosophila* leads to mitochondrial phenotypes, which are similar to, but milder than those observed in *Pink1* and *Parkin* mutant *Drosophila*. The RNAi screen which identified *cn* as a modulator of mitochondrial morphology also found that *cn* knockdown impaired the recruitment of GFP-tagged Parkin to mitochondria exposed to CCCP and paraquat (Ivatt *et al.,* 2014). Damaged mitochondria are unable to sustain the proton gradient across the MIM therefore membrane potential ($\Delta\psi_m$) dissipates, inhibiting the import of PINK1 through the TOM complex and resulting in its accumulation on the MOM. Parkin can then be recruited from the cytosol to dysfunctional mitochondria by PINK1, although Parkin overexpression is sufficient to rescue *Pink1* mutant phenotypes in *Drosophila*, indicating that PINK1 is not essential for Parkin function in flies. Recruited Parkin ubiquitinates multiple mitochondrial targets including Mitofusins MAO-B, voltage dependant ion channels (VDACs) 1, 2 & 3 and MIRO (Sarraf *et al.*, 2013, Wang *et al.*, 2011). Once ubiquitinated, these targets are preferentially degraded at the proteasome. The degradation of ubiquitinated MFNs leads to a shift in mitochondrial dynamics towards the promotion of fission, therefore resulting in shorter, more punctate organelles. The elongated mitochondria observed in *cn* deficient models could therefore be due to a decrease in Parkin recruitment and thus an increase in MARF.

Ubiquitination of MOM proteins also leads to the recruitment of p62 (re(f2)P) and LC3 (Atg8) resulting in the autophagic clearance of damaged mitochondria from the cell (Geisler *et al.*, 2010; Okatsu *et al.*, 2010; Narendra *et al.*, 2010b; Wong & Holzbaur, 2014; Lazarou *et al.*, 2015). The increase in mitochondrial content in cn^3 flies could therefore be due to a mitophagy deficit, also caused by a reduction in Parkin recruitment. However, a recent study quantifying mitophagy in *Drosophila* using the pH-dependant dye-quenching system mt-Keima (Katayama *et al.*, 2011) demonstrated that basal mitophagy is not detectably different in young *Pink1* and *parkin* mutants compared to wildtype controls (Lee *et al.*, 2018b), whereas another study found that mitophagy deficits in these flies were age-dependent (Cornelissen *et al.*, 2018). This indicates that defects in mitophagy may not be the major factor underlying phenotypes observed in young *Pink1* and *parkin* mutants. Given that the TEM and citrate synthase assays were performed in young cn^3 flies, it is thus unlikely that the increased mitochondrial content observed is due to a defect in PINK1 / Parkin – linked mitophagy.

PINK1 also maintains mitochondrial health through Parkin-independent mechanisms such as regulation of complex I (Morais *et al.*, 2014; Pogson *et al.*, 2014). Complex I defects and mitochondrial morphology in *Pink1* mutant flies are rescued by overexpression of the CI subunit NDUFA10/ ND42, or its co-chaperone *sicily* (Pogson *et al.,* 2014). PINK1 regulates mitochondrial DRP1 activity via displacement of protein kinase A (PKA) from its MOM tether OMM-bound A-kinase anchoring protein 1 (AKAP1), leading to a reduction in mitochondrial DRP1 phosphorylated at the pSer637 site, resulting in an increase in DRP1 GTPase activity (Pryde *et al.*, 2016). Overexpression of DRP1 also rescues complex I defects in *Pink1*-null *Drosophila* (Liu *et al.*, 2011). The elongated mitochondria and CI respiratory defects observed in KMO deficient models could be due to a role of KMO in DRP1-mediated fission.

If KMO influences mitochondrial dynamics and/or mitophagy through PINK1 and/or Parkin-dependent pathways, one might expect *cn* deletion to modify *Pink1* or *parkin* mutant phenotypes, which have been well characterised in *Drosophila*

(Greene *et al.*, 2003; Park *et al.*, 2006; Clark *et al.*, 2006). Furthermore, overexpression of *cn* or human *KMO* might be sufficient to rescue *Pink1* or *parkin* mutant phenotypes. Overexpression of *Drp1* or knockdown of *Marf* could also reverse the phenotypes observed in *cn* flies, as has previously been shown in *Pink1* and *parkin* mutant *Drosophila* (Deng *et al.*, 2008; Poole *et al.*, 2008; Yang *et al.*, 2008, Liu *et al.*, 2011).

3.4 Conclusions

Elongated mitochondria, reduced complex I respiratory capacity and reduced locomotion are all observed in KMO deficient *Drosophila*. This implicates KMO in mitochondrial quality control mechanisms such as mitochondrial dynamics and mitophagy. Interactions between KMO and proteins involved in these mechanisms will be explored in the coming chapters of this thesis.

4 Investigation of potential functional interactions between KMO and PINK1

4.1 Introduction

My observation in Chapter 3 that KMO deficient *Drosophila* exhibit elongated mitochondria corroborates the similar findings by Ivatt *et al.*, (2014). Furthermore, an increase in mitochondrial content and a decrease in respiratory capacity and locomotor activity were observed in *cn* RNAi and *cn* null flies, indicating a defect in the mechanisms that maintain a functional mitochondrial network. Ivatt *et al.*, (2014) identified that *cn* knockdown in S2 cells not only modulates mitochondrial morphology, but also impairs recruitment of Parkin to mitochondria damaged by treatment with the protonophore CCCP, or the oxidative stress-inducer paraquat. Such mitochondria are targeted for degradation via a mechanism involving two familial PD-associated proteins, PINK1 and Parkin. Upon depolarisation, the import of PINK1 into the mitochondrial intermembrane space through the TOM complex is blocked (Lazarou *et al.*, 2012), causing it to accumulate on the MOM. There, PINK1 phosphorylates both Parkin and ubiquitin, creating a feed-forward signal that promotes the activity of Parkin as an E3 ubiquitin-ligase (Shiba-Fukishima *et al.*, 2012; Koyano *et al.*, 2014). Parkin ubiquitinates a number of targets on the MOM, including Mfn (MARF in *Drosophila*) (Ziviani *et al.*, 2010), labelling them for proteasomal degradation. Parkin ubiquitination of the MOM also results in the recruitment of autophagy adapters p62 (Ref(2)P in *Drosophila*) and LC3 (Atg8), facilitating autophagic clearance of damaged organelles (Kawajiri *et al.*, 2010).

Upon accumulation on the MOM, PINK1 also phosphorylates AKAP1, resulting in the untethering of PKA from mitochondria. This causes a reduction in the levels of mitochondrial DRP1 phosphorylated at its Ser637 residue, therefore an increase in DRP1 GTPase activity which promotes mitochondrial fission (Pryde *et al.*, 2016). The elongated mitochondria observed upon *cn* knockdown could therefore be due to involvement of KMO in PINK1 dependent mechanisms, such as the recruitment of

Parkin and subsequent degradation of MARF or Parkin-independent regulation of DRP1 activity.

To investigate if KMO functionally interacts with PINK1, genetic epistasis experiments were performed in *Drosophila*. The fruit fly has been used extensively to study the function and interaction of PINK1 and Parkin, and the phenotypes observed in flies mutant for either of the two genes have been well characterised (Greene *et al*, 2003; Greene *et al*., 2005; Park *et al*., 2006; Clark *et al*., 2006; Yang *et al*., 2006). The *Pink1*^{B9} mutant line displays several behavioural, morphological and molecular phenotypes, such as reduction in locomotor activity (including negative geotaxis), degeneration of flight muscle in the thorax, aberrant wing posture and reduction in respiratory capacity, ATP production and lifespan (Park *et al*., 2006; Clark *et al*., 2006; Yang *et al*., 2006). Such phenotypes were explored in *Pink1*^{B9} flies in which *cn* was knocked down or deleted, to investigate any link between the phenotypes observed in *cn* flies in Chapter 3 and PINK1 mediated mitochondrial quality control. Flies overexpressing *cn* and *hKMO* were also utilised to investigate a functional interaction between KMO and PINK1.

4.2 Results

4.2.1 *cn* deletion causes semi-lethality in *Pink1*-null *Drosophila*

To investigate functional interplay between PINK1 and KMO, crosses were first set up to produce *Pink1^{B9}; cn^{3}* flies. *Pink1* is located on the X chromosome, therefore males carrying the *Pink1^{B9}* are hemizygous for the mutation. *Pink1^{B9}* hemizygosity affects male fertility (Park *et al.*, 2006), so the mutant allele-carrying chromosome is balanced over the FM6 balancer chromosome in the *Pink1^{B9}* stock. The *cn^{3}* allele was balanced over the CyO chromosome because in a *w* background *cn^{3}* cannot be used as a visible marker. As well as the *duox^{cy}* allele, which causes a curly wing phenotype that serves as an easily observed marker, the CyO chromosome carries a hypomorphic *cn^{2}* allele and thus *cn^{3}/CyO* flies have similar levels of *cn* mRNA as *cn^{RNAi}; Act5CGAL4* flies (Chapter 3, Figure 3.6).

From the final experimental cross, there were four expected genotypes in the male progeny (Table 4.1, Figure 4.1). The *Pink1^{B9}* stock produces a ratio of approximately 1:1 *FM6* to *Pink1^{B9}* male adults. When *cn^{3}/ CyO* flies are self-crossed, the ratio of *cn$^{3/3}$* to *cn^{3}/CyO* males is 1:2 (Figure 4.2), the expected Mendelian frequency given that the CyO chromosome is homozygous lethal. The number of eclosed *FM6*; *cn^{3}* males was therefore expected to be equal to the number of *Pink1^{B9}; cn^{3}* males, and the number of FM6; *cn^{3}/CyO* equal to the number of *Pink1^{B9}*; *cn^{3}/CyO.* The proportion of *Pink1^{B9}; cn$^{3/3}$* males that emerged was only 34% that of *FM6; cn^{3}*. The number of *Pink1^{B9}; cn^{3}/CyO* flies was 98% that of *FM6; cn^{3}/CyO. Act5CGAL4*-driven 3M control and *cn* RNAi males were also crossed to *Pink1B9/FM6* females. The number of *Pink1^{B9}; 3M; Act5CGAL4* males and *Pink1^{B9}; cn^{RNAi}; Act5CGAL4* males was 116% and 104% respective to their corresponding *FM6* genotypes (Figure 4.2). This indicates that KMO can compensate for *Pink1* LOF and by complete absence of *cn* expression, partial lethality is uncovered in the *Pink1^{B9}* hemizygous males.

Table 4.1. Experimental cross to generate *Pink1^{B9}; cn^{3}* flies.
Females carrying the *Pink1^{B9}* mutant allele on the X chromosome, balanced over FM6 and *cn^{3}* on chromosome II, balanced over *CyO*, were crossed to *cn^{3}/CyO* males. Parental gamete and male progeny genotypes are detailed. *CyO* is homozygous embryonic lethal.

	FM6; cn^{3}	***FM6; CyO***	***Pink1^{B9}; cn^{3}***	***Pink1^{B9}; CyO***
Y; cn^{3}	*FM6; cn$^{3/3}$*	*FM6; cn^{3}/CyO*	*Pink1B9; cn$^{3/3}$*	*Pink1^{B9}; cn^{3}/CyO*
Y; CyO	*FM6; cn^{3}/CyO*	Lethal	*Pink1^{B9}; cn^{3}/CyO*	Lethal

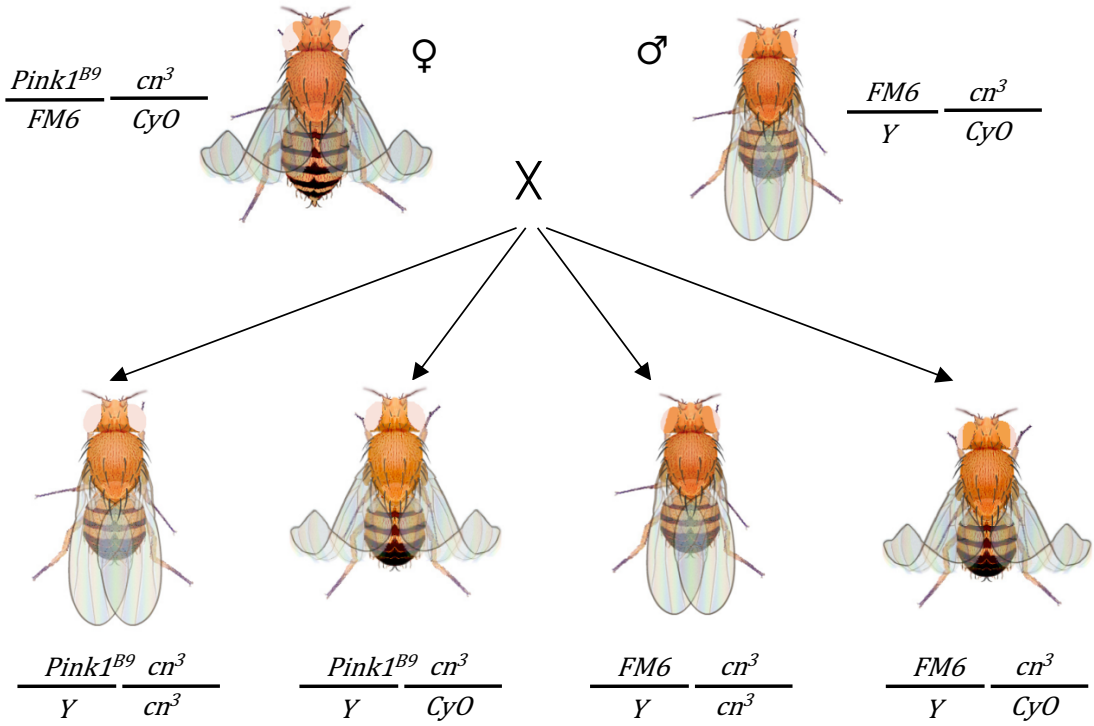

Figure 4.1. Crossing scheme to geneate *Pink1; cn* double mutants.
Virgin females carrying the null *Pink1^{B9}* allele on the X chromosome, balanced over the FM6 chromosome and *cn^{3}* balanced over *CyO*, were crossed to *FM6; cn^{3}/CyO* males. Male offspring were expected to receive the *Pink1^{B9}* or *FM6* X chromosomes at a 1:1 ratio and the ratio of *cn^{3}* homozygotes to *cn^{3}/CyO* heterozygotes was expected to be 1:2 (adapted from Otto, 2000)

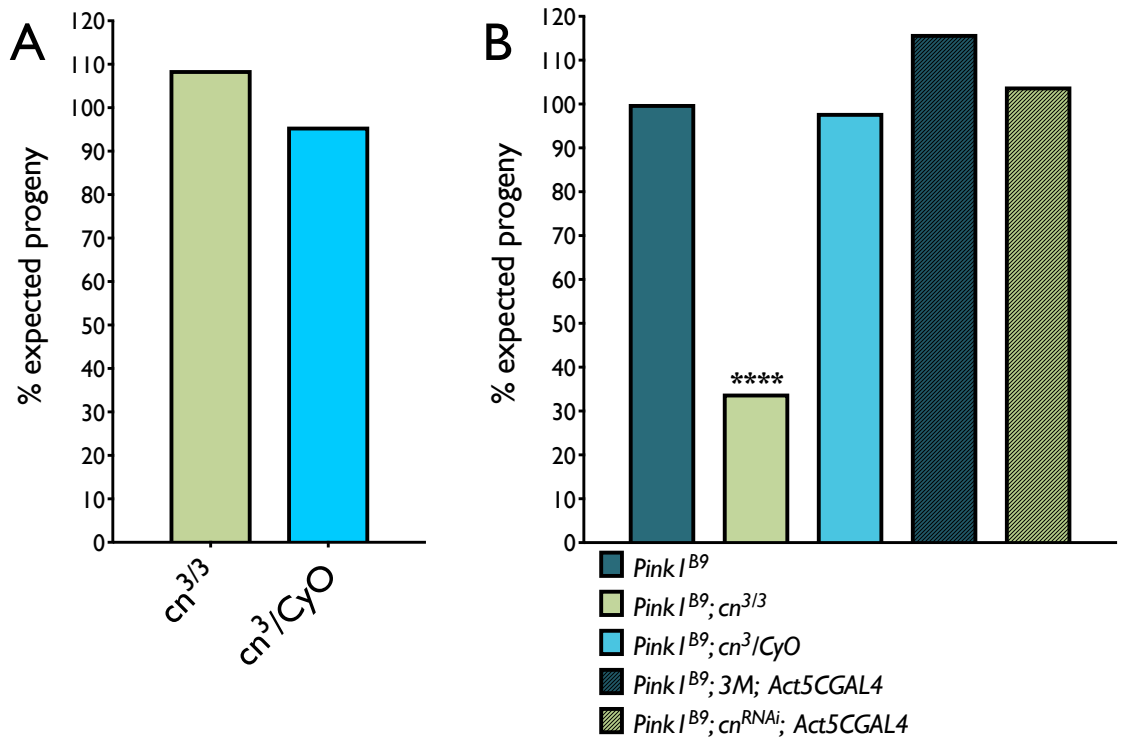

Figure 4.2. Homozygous *cn* LOF causes synthetic lethality in *Pink1^{B9}* male flies.
A) *cn^{3}/CyO* in a *w* wildtype background were self-crossed. According to mendelian inheritance, the expected ratio of *cn$^{3/3}$* flies to *cn^{3}/CyO* is 1:2. *CyO* is homozygous lethal. % expected progeny was calculated from the total number of progeny. **B)** Crosses were set up to produce *Pink1^{B9}* flies carrying the *cn^{3}* allele or expressing *cn^{RNAi}* driven by *Act5CGAL4.* The ratio of *Pink1^{B9}* to *FM6* flies is 1:1. % expected progeny was calculated as the proportion of *Pink1^{B9}* male progeny in relation to *FM6*, upon *cn* RNAi knockdown or deletion χ^2 test, 1 d.f., Bonferroni *post hoc*, *** $P < 0.005$.

4.2.2 *cn* deletion and knockdown increases penetrance of defective-thorax phenotype in *Pink1*-null *Drosophila*

A commonly studied phenotype in *Pink1* mutant flies is the degeneration of indirect flight muscles (IFMs) in the thorax, which is observed as early as the pupal stage (Clark *et al.*, 2006). The phenotype shows incomplete penetrance – in the *Pink1*^{B9} stock, the proportion of adult hemizygous mutant males displaying the phenotype in my hands is ~50% (Figure 4.3), although the figure previously reported in the literature is highly variable (Clark *et al.*, 2006; de Castro *et al.*, 2013; Celardo *et al.*, 2016). Both *Pink1*^{B9}*; cn*$^{3/3}$ and *Pink1*^{B9}*; cn*^{3}*/CyO* males showed an increase in penetrance of the defective thorax phenotype compared to *Pink1*^{B9} stock mutants, indicating that loss of *cn* enhances this phenotype (Figure 4.3, ~62%, χ^2 test, 1 d.f., $P < 0.05$). However, this modulation was not directly proportional to *cn* levels, as *cn*^{3}*/CyO* flies which express some *cn* (Chapter 3, Figure 3.6) showed a higher penetrance than *cn*^{3} homozygotes (Figure 4.3, ~85%, χ^2 test, 1 d.f., $P < 0.001$). *Pink1*^{B9}*; cn*$^{RNAi;}$ *Act5CGAL4* flies also showed a significant increase in penetrance compared to *Pink1*^{B9}*; 3M; Act5CGAL4* controls (Figure 4.3, ~60%, χ^2 test, 1 d.f., $P < 0.05$).

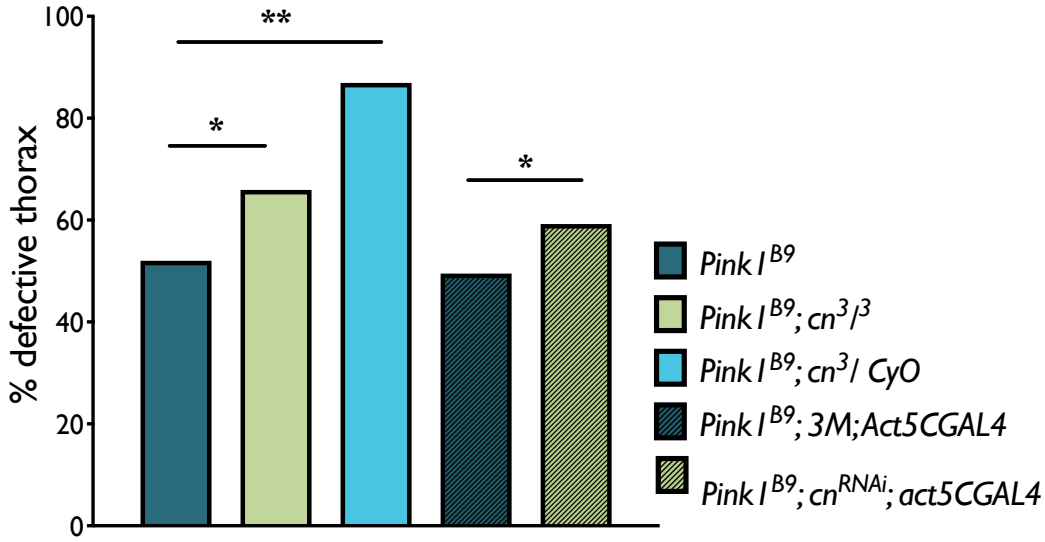

Figure 4.3. Reduced *cn* expression enhances penetrance of the defective thorax phenotype in Day 1 *Pink1*^{B9} males.
Penetrance in the *Pink1*^{B9}*; cn*$^{3/3}$ and *Pink1*^{B9}*; cn*^{3}*/CyO* genotypes was compared to the *Pink1*^{B9} stock. *Pink1*^{B9}*; cn*$^{RNAi;}$ *Act5CGAL4* was compared to *Pink1*^{B9}*; 3M; Act5CGAL4.* χ^2 test, 1 d.f., * $P < 0.016$, *** $P < 0.005$.

4.2.3 KMO inhibition and KYNA supplementation cause decreased penetrance of defective thorax phenotype

To investigate if the increase in penetrance of the defective thorax phenotype in KMO deficient *Pink1*^{B9} flies is due to changes in KP metabolites, the *Pink1*^{B9}/FM6 stock was reared on medium containing a range of concentrations of either the KMO inhibitor Ro 61-8048, or KYNA, which is known to be elevated in both *cn*^{3} and *cn*^{RNAi} flies. Supplementation with either 100 or 200 µM Ro 61-8048 in the food led to significantly higher eclosion of *Pink1*^{B9} males than untreated control flies (Figure 4.4A). Intriguingly, this pharmacological inhibition of KMO was the opposite effect observed upon genetic inhibition of *cn* (*cn*$^{3/3}$), which leads to a significant reduction in the eclosion of *Pink1*^{B9} males (Figure 4.1). KYNA supplementation had no significant effect on the eclosion of *Pink1*^{B9} males (Figure 4.4B). Both Ro 61-8048 and KYNA treatment caused a significant reduction in penetrance of the defective thorax phenotype compared to untreated controls, with an optimal concentration of 100 µM Ro 61-8048 and 100 mg/mL KYNA (Figure 4.4C & D). Again, this effect was the opposite to that observed by *cn* deletion or knockdown, which caused a significant increase in penetrance of the phenotype (Figure 4.4). The effect caused by Ro 61-8048 is likely due to an increase in KYNA caused by KMO pharmacological inhibition. The fact that this protection is not observed in *cn*^{3}, *cn*^{3}*/CyO* and *cn*^{RNAi}*;* flies, in which KYNA levels are also increased (Campesan *et al.*, 2011; Breda *et al.*, 2016) indicates that loss of KMO protein has an additional effect on this phenotype independent from an increase in KYNA.

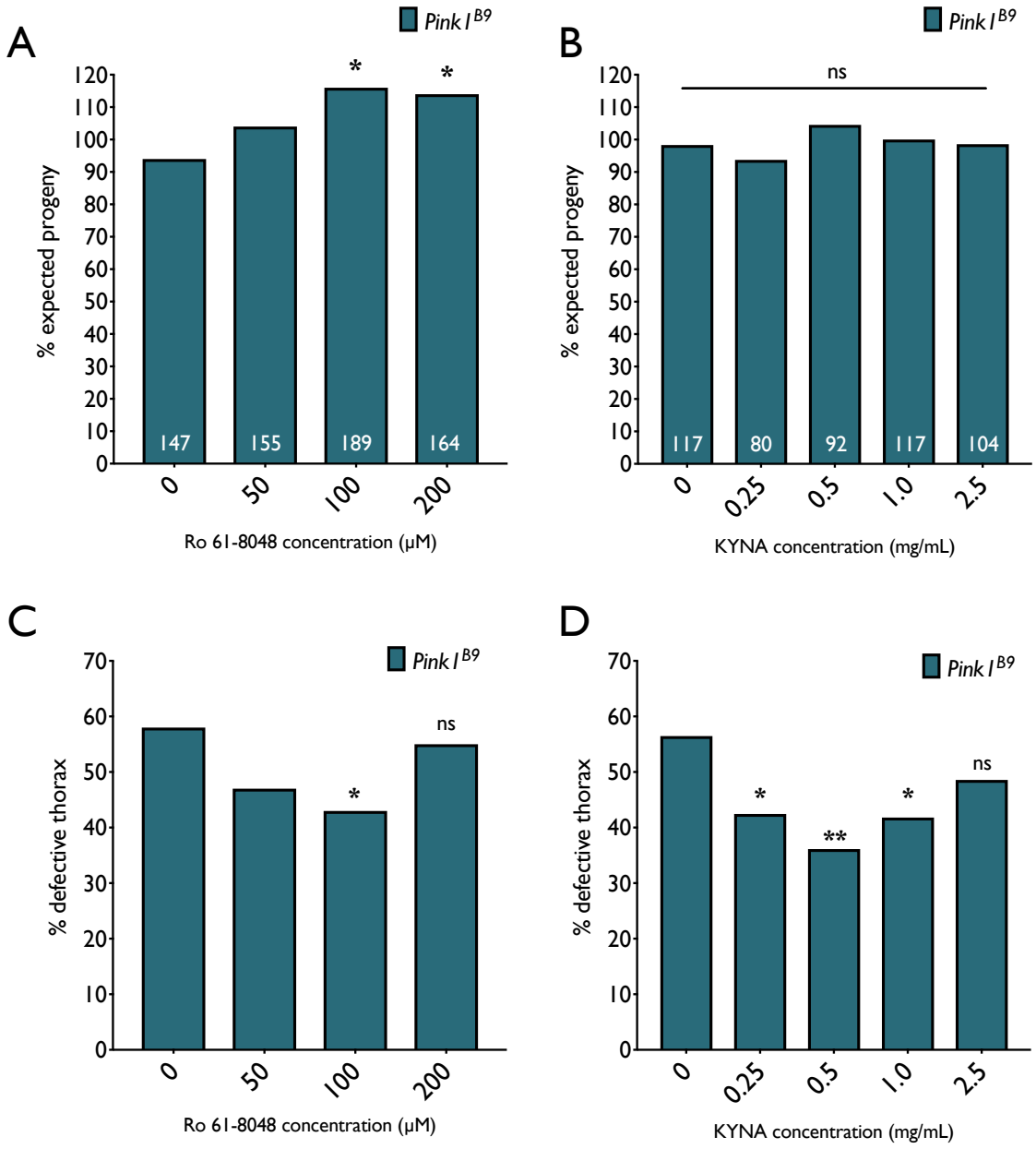

Figure 4.4. Eclosion and penetrance of defective thorax phenotypes are modulated by KMO inhibitor Ro 61-8048 or KYNA supplementation in *Pink1*^{B9} males.

Four *Pink1*^{B9}/FM6 virgin females were mated with four FM6 males on medium containing a range of concentrations of Ro 61-8048 or KYNA. **A & B)** % expected *Pink1*^{B9} male progeny in relation to *FM6*. **C & D)** Penetrance of the defective thorax phenotype is compared to flies reared on medium containing vehicle alone (DMSO for Ro 61-8048, H_2O for KYNA). χ^2 test, 1 d.f., Bonferroni *post hoc,* * $P < 0.0125$, ** $P < 0.0025$.

4.2.4 *cn* deletion but not RNAi knockdown reduces lifespan of *Pink1*-null *Drosophila*

In order to investigate if loss of KMO affects the fitness of *Pink1* mutant adult flies, the lifespan of progeny from the cross detailed in Table 4.1 was assessed (Table 4.2, Figure 4.5). Males carrying the *FM6* X chromosome had a median lifespan of 50 days, compared to 47 days for *FM6; $cn^{3/3}$* flies, which was not significantly different (Mantel-Cox test, $P = 0.1527$). *FM6; cn^{3}/CyO* flies had a 42 day median lifespan, which was significantly – though only modestly - different from both *FM6* ($P < 0.0001$) and *FM6; $cn^{3/3}$* flies. Males carrying the *$Pink1^{B9}$* mutation on their X chromosome had a median lifespan of 41 days. Both *$Pink1^{B9}$; $cn^{3/3}$* and*; $Pink1^{B9}$; cn^{3}/CyO* genotypes had a significantly reduced median lifespan of 34 days. However, *Act5CGAL4* driven RNAi knockdown of *cn* had no significant effect on lifespan in either *FM6* or *$Pink1^{B9}$* flies (Table 4.3, Figure 4.6).

Table 4.2. Survival data summary of *FM6* and *$Pink1^{B9}$* males carrying the *cn^{3}* allele.
Summary of the data used to generate survival curves (Figure 4.5), median survival and curve comparison significance computed by Prism 7. P values were calculated by Mantel-Cox test as a comparison between *FM6* or *$Pink1^{B9}$* carrying males and corresponding *$cn^{3/3}$* or *cn^{3}/CyO* genotypes.

	FM6	*FM6; $cn^{3/3}$*	*FM6; cn^{3}/CyO*
# deaths/events	100	100	100
Median survival (days)	50	47	42
P value (compared to *FM6*)	NA	0.1527	<0.0001

	$Pink1^{B9}$	*$Pink1^{B9}$; $cn^{3/3}$*	*$Pink1^{B9}$; cn^{3}/CyO*
# deaths/events	100	100	100
Median survival	41	34	34
P value (compared to *$Pink1^{B9}$*)	NA	0.0094	0.0132

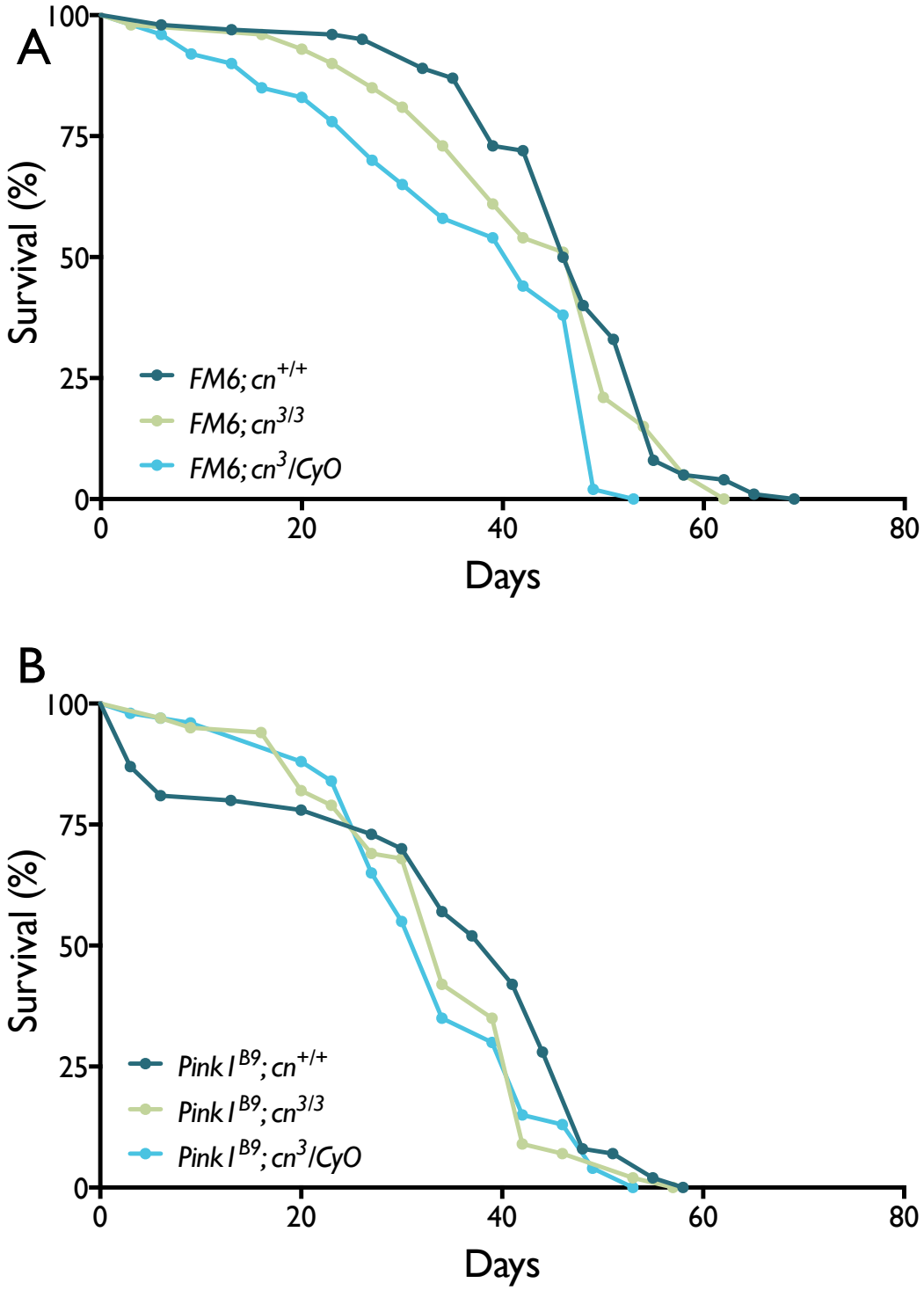

Figure 4.5. Lifespan of *FM6* or *Pink1^{B9}* males is modulated by *cn$^{3/3}$* or *cn^{3}/CyO*. Newly emerged *FM6* **(A)** or *Pink1^{B9}* **(B)** males were placed 10 per vial and transferred to fresh medium every 2 - 3 days (n = 100).

Table 4.3. Survival data summary of *FM6* and *Pink1^{B9}* males upon *cn* knockdown. Summary of the data used to generate survival curves (Figure 4.6), median survival and curve comparison significance computed by Prism 7. P values were calculated by Mantel-Cox test as a comparison between *cn$^{RNAi;}$ Act5CGAL4* males and *3M; Act5CGAL4* controls, carrying either *FM6* or *Pink1^{B9}* chromosomes.

	FM6		*Pink1^{B9}*	
	3M; Act5CGAL4	*cn^{RNAi}; Act5CGAL4*	*3M; Act5CGAL4*	*cn^{RNAi}; Act5CGAL4*
# deaths/events	100	100	100	100
Median survival	48	48	41	41
P value (compared to *3M; Act5CGAL4*)	NA	0.4860	NA	0.6894

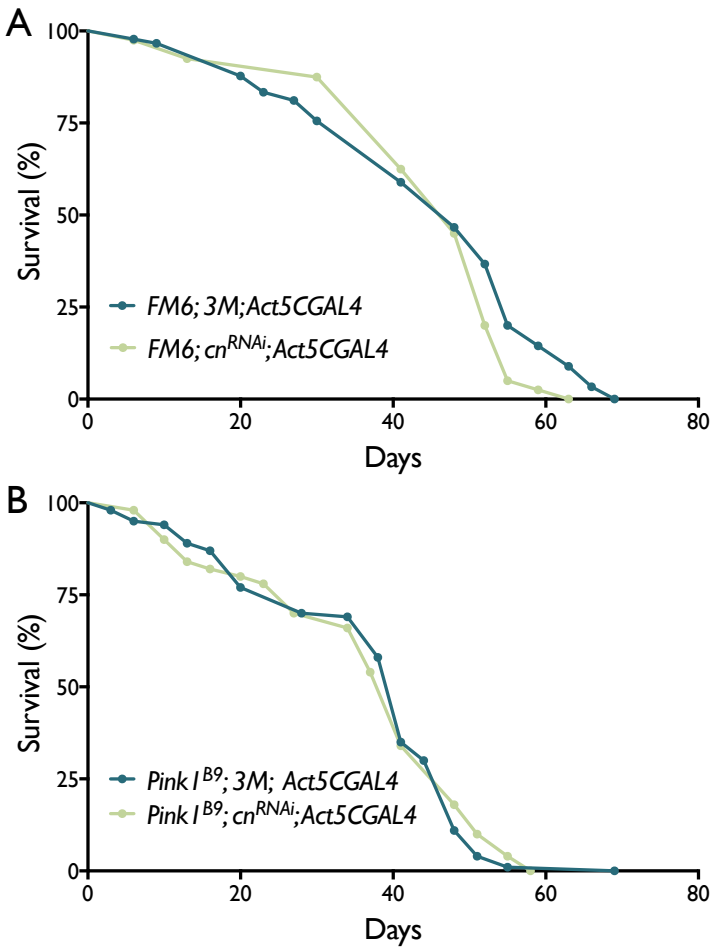

Figure 4.6. Lifespan *FM6* and *Pink1^{B9}* males is unaffected upon *cn* RNAi knockdown. Newly emerged *FM6* **(A)** or *Pink1^{B9}* **(B)** males were placed 10 per vial and transferred to fresh medium every 2 - 3 days (n = 100).

4.2.5 KYNA supplementation prolongs lifespan in *Pink1*-null *Drosophila*

To investigate if elevated KYNA might affect lifespan, *FM6* and *Pink1*^{B9} flies were supplemented with 0.5 mg/mL KYNA during development and adulthood. KYNA supplementation had no significant effect on the lifespan of *FM6* male flies (Table 4.4., Figure 4.7A). However, KYNA supplementation did lead to a small but significant increase in longevity of *Pink1*^{B9} males, increasing median lifespan from 41 to 42.5 days (Table 4.4., Figure 4.7B, $P = 0.0393$).

Table 4.4. Survival data summary of *FM6* and *Pink1*^{B9} males supplemented with KYNA.
Summary of the data used to generate survival curves (Figure 4.7), median survival and curve comparison significance computed by Prism 7. *P* values were calculated by Mantel-Cox test as a comparison between KYNA supplemented (0.5 mg/mL) flies and controls, carrying either *FM6* or *Pink1*^{B9} chromosomes.

	FM6		*Pink1*^{B9}	
	KYNA (0.0 mg/mL)	KYNA (0.5 mg/mL)	KYNA (0.0 mg/mL)	KYNA (0.5 mg/mL)
# deaths/events	100	100	100	100
Median survival	47	48	41	42.5
P value (compared to 0.0mg/mL KYNA)	NA	0.8186	NA	0.0393

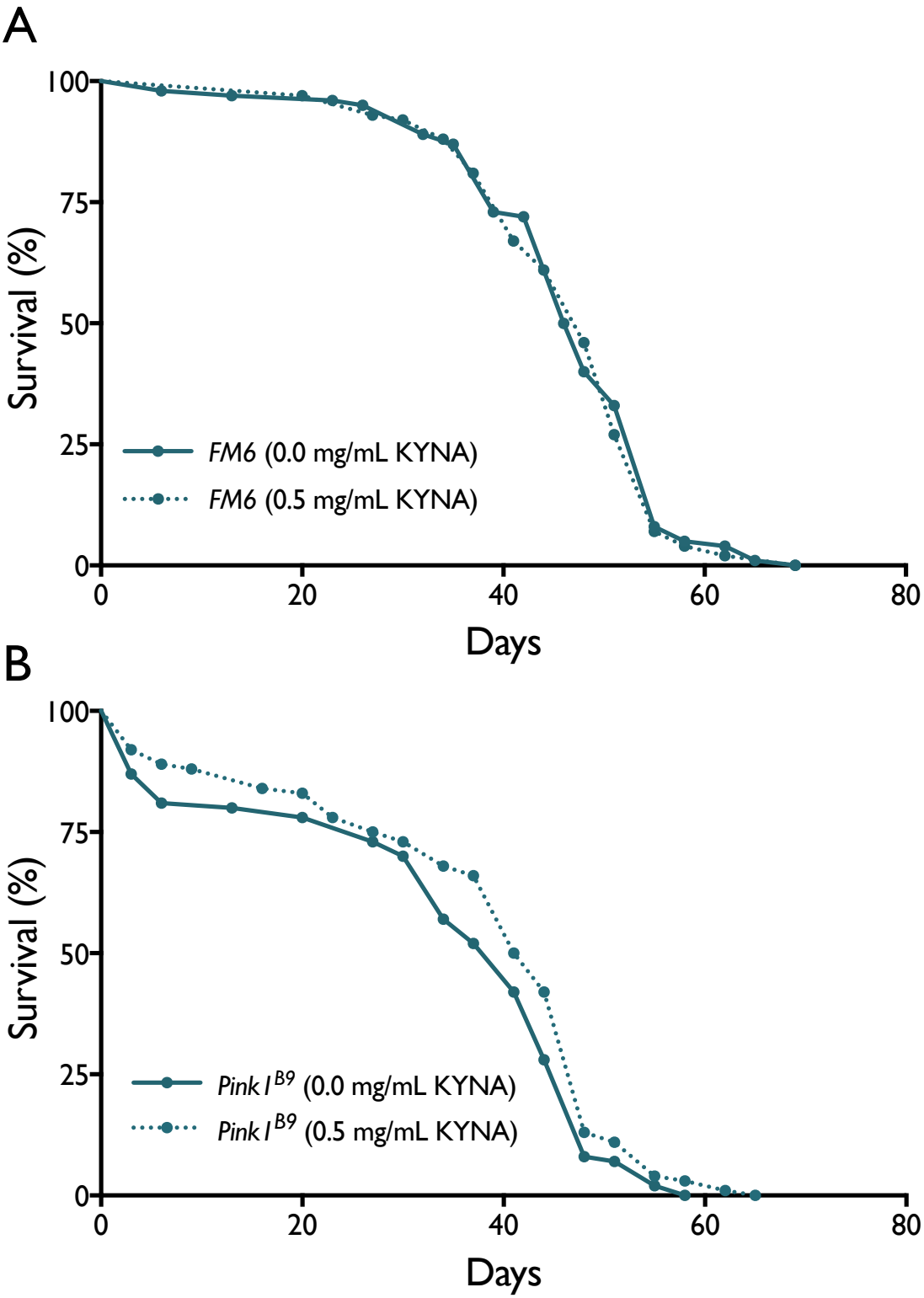

Figure 4.7. Lifespan of *Pink1*^{B9} males is increased upon 0.5 mg/mL KYNA supplementation.

Newly emerged *FM6* **(A)** or *Pink1*^{B9} **(B)** males were placed 10 per vial and transferred to fresh medium every 2 - 3 days (n = 100).

4.2.6 Generation of *cn and* human *KMO* overexpressing *Drosophila*

Given the enhancement of phenotypes in *Pink1*^{B9} flies due to *cn* reduction seen above, I next investigated whether overexpression of *cn* or human *KMO (hKMO)* modulates *Pink1* mutant phenotypes. *cn* and *hKMO* cDNA were sub-cloned into the *pUASt-attB* vector and microinjected into the *phiC31vas-int; attP40* line. Two individually derived *UAScn[attP40]* lines were assessed. An additional line kindly donated by Dr. Christopher Elliot (University of York), in which *UAScn* was incorporated into the *attP51C* landing site on chromosome II (Furmston, 2016), was also utilised.

The levels of *cn* mRNA in *Act5CGAL4*-driven whole fly homogenates were assessed by qPCR. In *UAScn[attP51c]*; *Act5CGAL4* flies, *cn* mRNA levels are ~4-fold higher than in *3M; Act5CGAL4* control flies. In the two *UAScn[attP40]* lines, *cn* mRNA levels are ~50-fold higher than *3M; Act5CGAL4* and ~12-fold higher than *UAScn[attP51c]*; *Act5CGAL4* flies (Figure 4.8A). The *UAScn[attP40](1)* line, which showed a slightly higher expression level than *UAScn[attP40](2),* was used for further experiments and is herein referred to as *UAScn[attP40]*. The vast difference in expression strength of the *UAScn[attP51C]* and *UAScn[attP40]* lines permitted titration of *cn* expression levels, in the investigation of modulation of *Pink1* mutant phenotypes. Given the availability of human KMO specific antibodies (Proteintech Group), *Act5CGAL4*-driven *hKMO* expression was evaluated by immunoblotting. *UAShKMO; Act5CGAL4* flies showed a ~55 kDa molecular weight band, which corresponds to the expected molecular weight of KMO, as well as some other lower molecular weight bands (Figure 4.8B). These lower molecular weight bands were also present in *UAShKMO* flies that lack *Act5CGAL4,* but not *3M; Act5CGAL4* flies, suggesting some leaky expression of the *UAShKMO* construct. As *3M; Act5CGAL4* flies express *cinnabar,* the lack of the lower molecular weight bands in this line excluded the possibility that the hKMO antibodies recognise *Drosophila* KMO. These bands are therefore possibly hKMO that have been post-translationally modified or partially degraded by proteases.

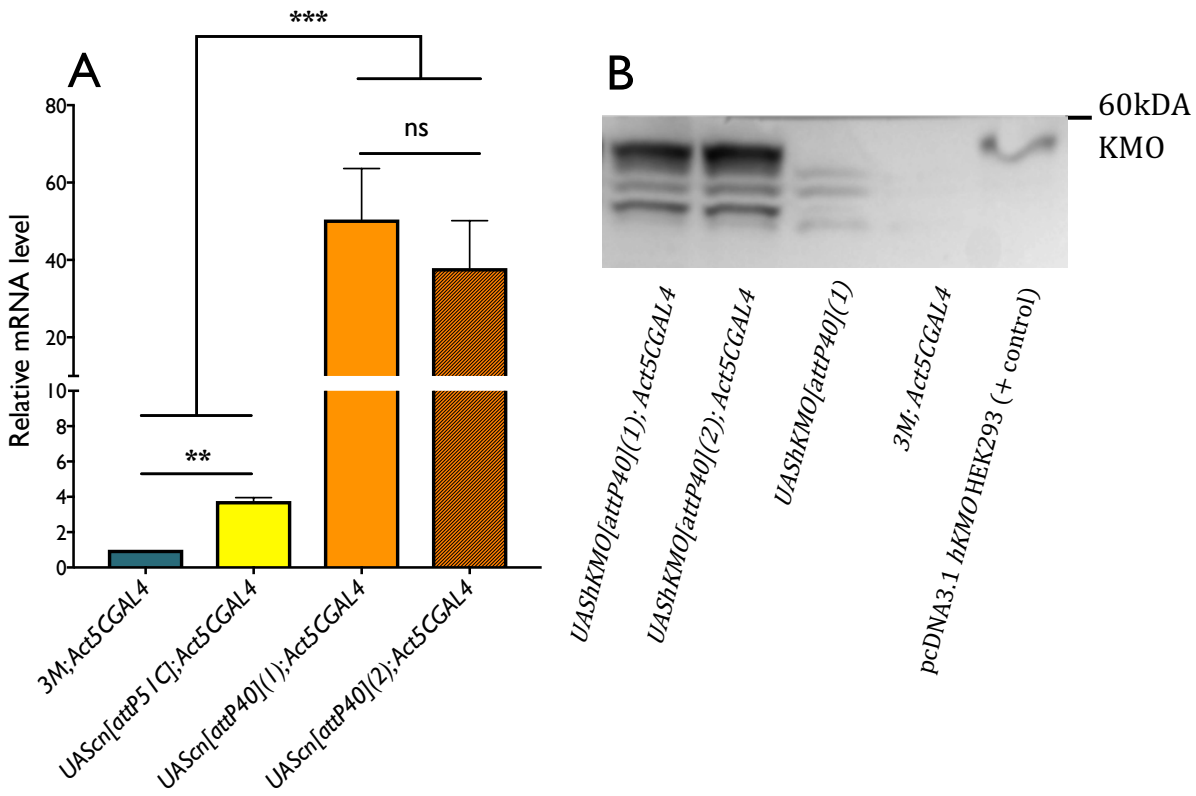

Figure 4.8. *cinnabar* and *hKMO* are expressed in *Drosophila* overexpression lines. **A)** *cinnabar* overexpression lines were evaluated by qPCR. *cinnabar* mRNA was normalised to the reference gene *rp49* and mRNA levels are displayed relative to the *3M; Act5CGAL4* control genotype (mean ± SD, pairwise fixed reallocation randomization test, ** $P < 0.01$, *** $P < 0.001$, nd = not detected, ns = not significant. Ten flies per n, n = 3)). **B)** *hKMO* overexpression lines evaluated by immunoblot. 20 µg of total protein extracted from whole flies was separated by SDS-PAGE (10 flies per sample) and probed with hKMO antibodies.

4.2.7 Overexpression of *cn* and *hKMO* rescues defective thorax, climbing and longevity phenotypes in *Pink1*-null *Drosophila*

Firstly, to assess whether KMO overexpression affects viability of *Pink1* mutant flies, the proportion of *FM6* to *Pink1*^{B9} males was scored. *Act5CGAL4*-driven overexpression of *cn* (either landing-site) or *hKMO* has no significant effect on the eclosion of *Pink1*^{B9} males relative to FM6 (Figure 4.9A), suggesting no effect on viability. Next, the effect of KMO overexpression on the degeneration of IFMs in *Pink1*^{B9} males was assessed. *Act5CGAL4*-driven overexpression of *UAScn* from the attP51C site causes a significant decrease in penetrance of the defective thorax phenotype in *Pink1*^{B9} mutants compared to *Pink1*^{B9}*; 3M; Act5CGAL4* controls, from ~50% to ~35% (Figure 4.9B, χ^2 test, $P < 0.016$). *UAScn* and *UAShKMO* overexpression from the *attP40* site had no significant effect on the penetrance of the phenotype (Figure 4.9B). This effect negatively correlates with KMO expression levels, as expression from the *attP40* site is ~10-fold higher than from the *attP51C* site (Figure 4.8).

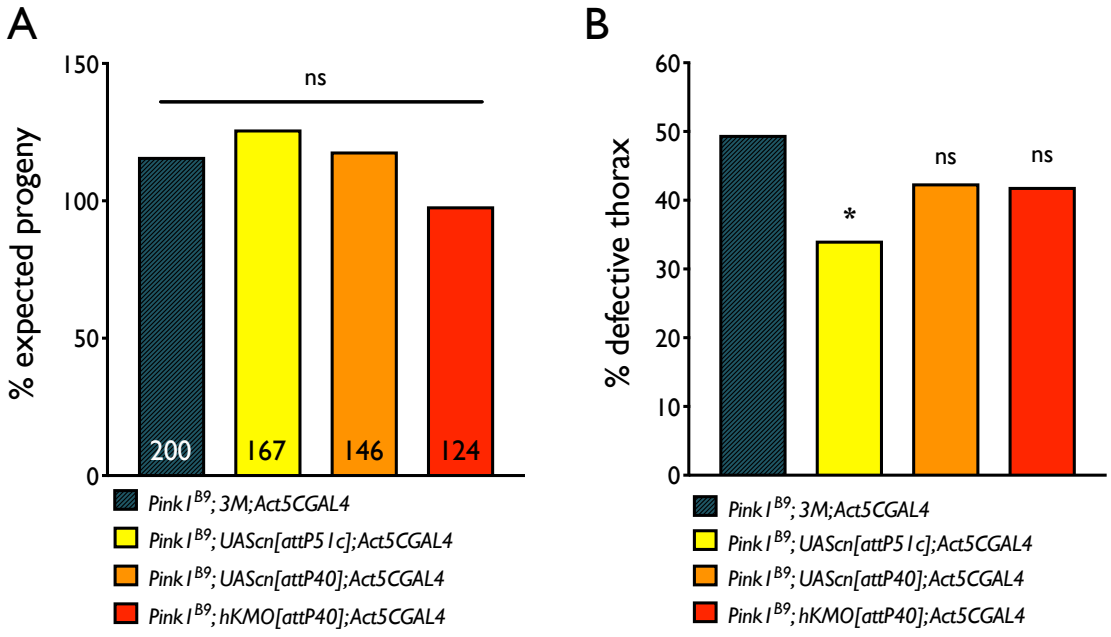

Figure 4.9. KMO overexpression modulates defective thorax penetrance but not eclosion in *Pink1*^{B9} male flies.
A) Eclosion rate of adult *Pink1*^{B9} male flies as a percentage of the corresponding *FM6* chromosome carrying genotypes. **B)** Penetrance of the defective thorax phenotype in newly eclosed *Pink1*^{B9} males (χ^2 test, 1 d.f., ns = not significant, * $P < 0.016$).

Pink1^{B9} flies show a severe reduction in their startle induced locomotor (climbing) response. *Act5CGAL4*-driven overexpression of *cn* (either landing-site) or *hKMO* significantly rescues the climbing defects observed in Day 7 *Pink1*^{B9}*; 3M; Act5CGAL4* flies (Figure 4.10, two-way ANOVA, $P < 0.0001$). The rescue is more robust in the *cn[attP40]* (~70%) and *hKMO[attP40]* (72%) lines than the *cn[attP51C]* line (~52%), restoring climbing ability to wildtype levels. This effect positively correlates with expression, as *cn* is expressed more highly from the *attP40* than the *attP51c* site (Figure 4.8).

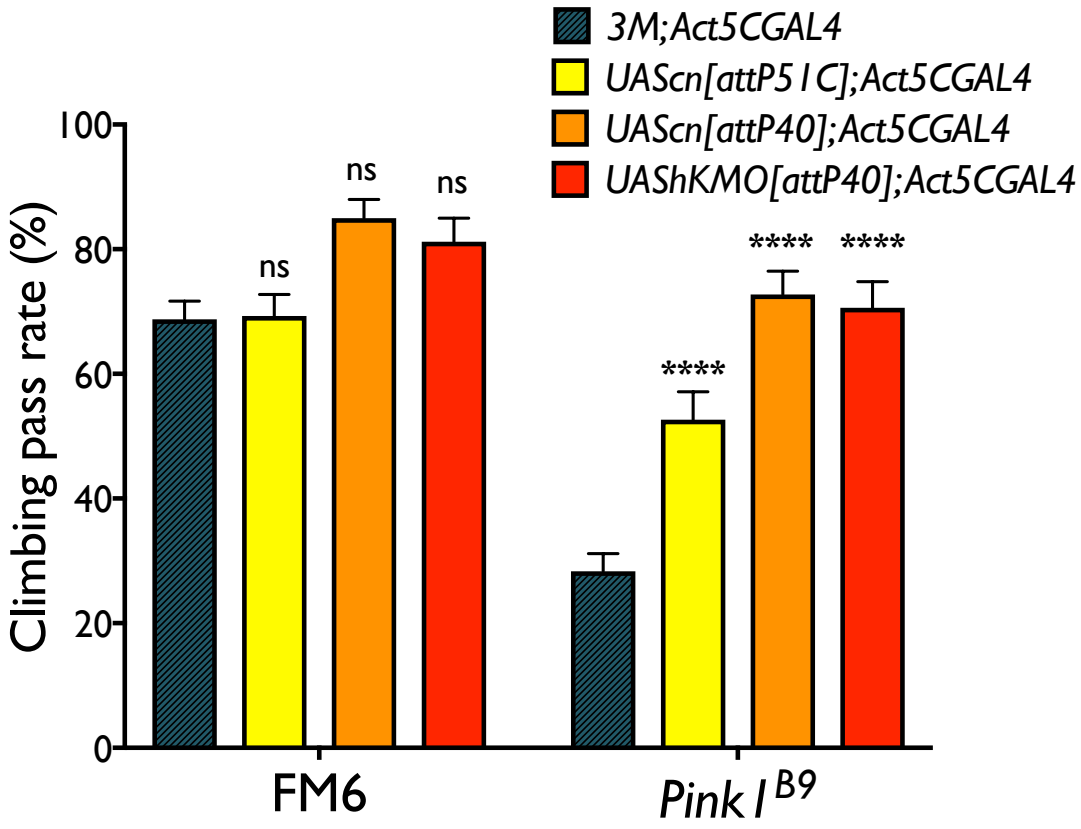

Figure 4.10. *cn* or *hKMO* overexpression rescues climbing ability in *FM6* or *Pink1*^{B9} male flies.

Ability was assessed using the rapid iterative negative geotaxis (RING) assay. 10 Day 7 flies were placed inside a 20 cm vial and tapped to the bottom. The percentage of flies that passed an 8 cm threshold line after 10 s was counted (mean ± SEM; Two-way ANOVA, Tukey *post hoc*, ns = not significant, **** $P < 0.0001$. Ten flies per n, n = 8 - 10).

Overexpression of *cn* (either landing site) or *hKMO* from the *attP40* site had no significant effect on the lifespan of *FM6* controls (Table 4.5, Figure 4.11A). However, *cn* and *hKMO* overexpression from the *attP40* site caused a significant increase in median lifespan of $Pink1^{B9}$ male flies by 3 (Mantel-Cox test, $P = 0.0183$) and 7 ($P = 0005$) days respectively (Table 4.5, Figure 4.11B). Overexpression of *cn* from the *attP51C* site had no significant effect on the lifespan of $Pink1^{B9}$ males. This again represents a dose-dependent correlation between KMO expression and protection against a *Pink1* mutant phenotype.

Table 4.5. Survival data summary of *FM6* and $Pink1^{B9}$ males overexpressing *cn* or *hKMO*.

Summary of the data used to generate survival curves (Figure 4.11). Median survival and curve comparison significance computed by Prism 7. *P* values were calculated by Mantel-Cox test as a comparison between *FM6* or $Pink1^{B9}$ carrying *3M; Act5CGAL4* males and corresponding *cn* or *hKMO* overexpressing flies.

FM6	***3M; Act5CGAL4***	***UAScn[attP51C]; Act5CGAL4***	***UAScn[attP40]; Act5CGAL4***	***UAShKMO[attP40]; Act5CGAL4***
# deaths/events	100	100	100	100
Median survival	48	45	48	50
P value (compared to *3M; Act5CGAL4*)	NA	0.4465	0.4339	0.1720

$Pink1^{B9}$	***3M; Act5CGAL4***	***UAScn[attP51C]; Act5CGAL4***	***UAScn[attP40]; Act5CGAL4***	***UAShKMO[attP40]; Act5CGAL4***
# deaths/events	100	100	100	100
Median survival	41	41	44	48
P value (compared to *3M; Act5CGAL4*)	NA	0.4068	0.0183	0.0005

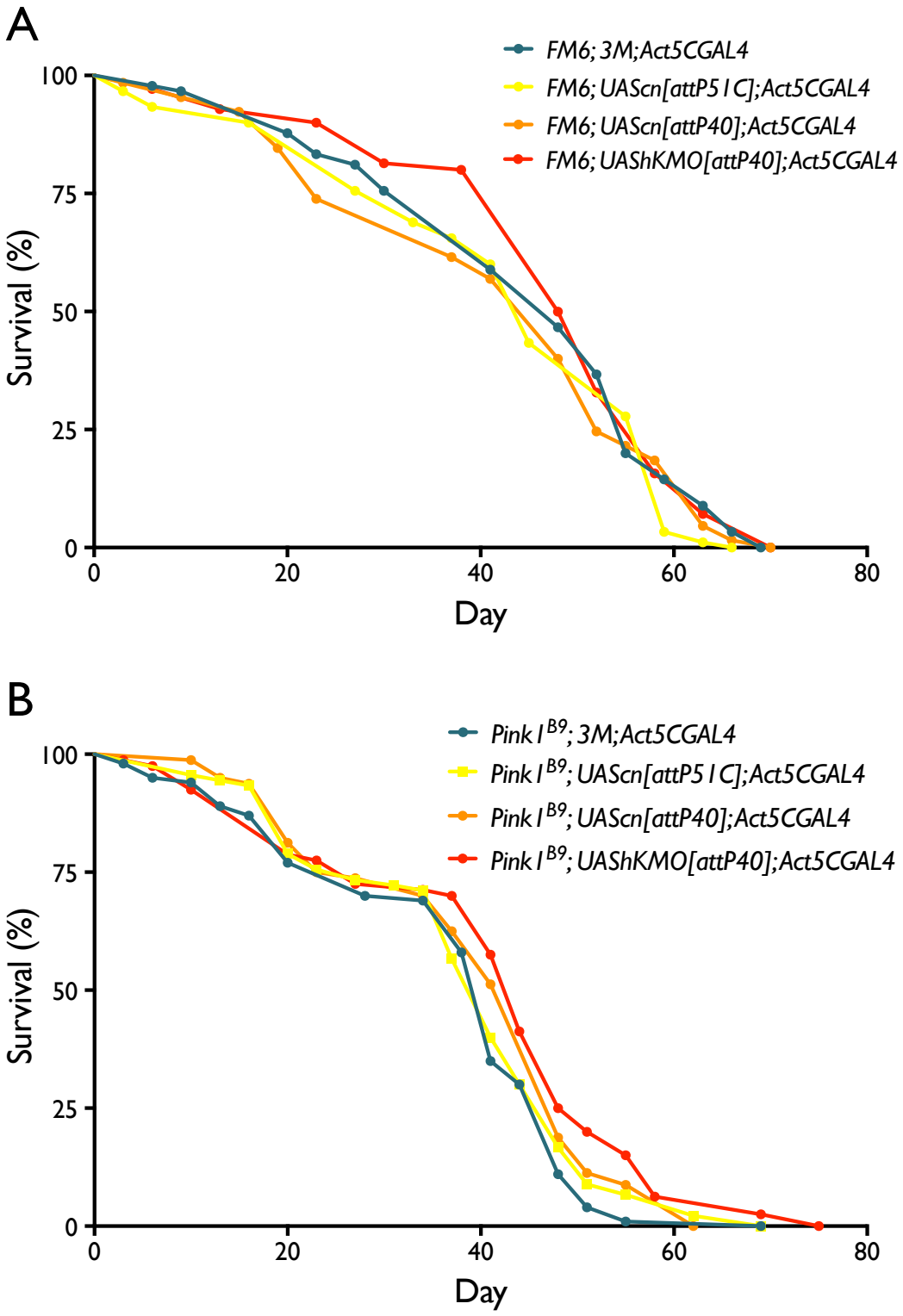

Figure 4.11. *cn* or *hKMO* overexpression modulates lifespan in *Pink1*^{B9} male flies
Newly emerged *FM6* **(A)** or *Pink1*^{B9} **(B)** males were placed 10 per vial and transferred to fresh medium every 2 - 3 days (n = 100).

4.2.8 Overexpression of *cn* and *hKMO* does not rescue respiratory capacity in *Pink1*-null *Drosophila*

Whole-fly homogenates of *FM6* and *Pink1*^{B9} carrying *UAScn[attP40]; Act5CGAL4* flies were compared to *3M; Act5CGAL4* in respirometry experiments, to assess if the striking improvement in climbing ability (Figure 4.10) could be correlated to an increase in respiratory capacity. As previously reported (Liu *et al.*, 2011; Costa *et al.*, 2013), *Pink1*^{B9} flies (Figure 4.12B) had a lower complex I respiratory capacity compared to control flies (Figure 4.12A) However, no significant increase in the respiratory capacity of Day 7 *FM6* or *Pink1*^{B9} males was observed upon *cn* overexpression (Figure 4.12), suggesting that the improvement in climbing performance was not achieved through an increase in oxidative phosphorylation.

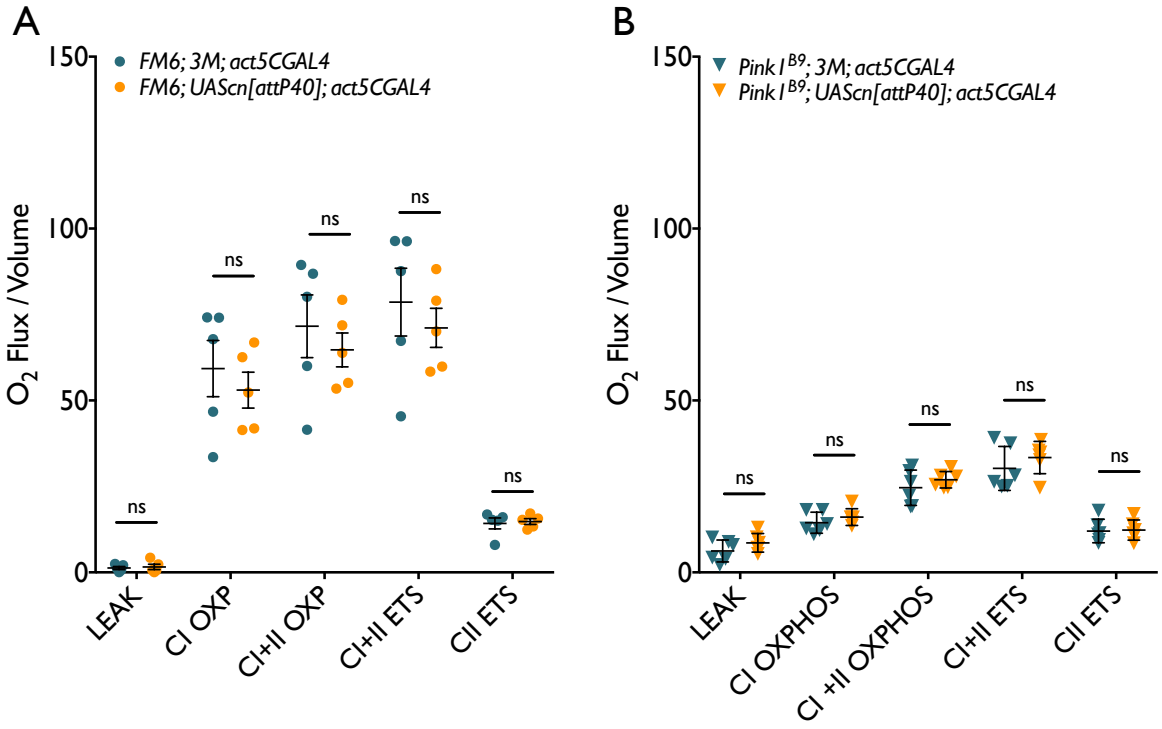

Figure 4.12. Respiratory capacity of *FM6* or *Pink1*^{B9} whole-fly homogenates is not affected by overexpressing *cn*.
Leak was measured in the presence of malate and pyruvate but the absence of ADP. Complex I OXPHOS was measured upon addition of ADP, then Complex I + II OXPHOS was measured after the addition of succinate. Complex I + II ETS was measured by adding titrations of CCCP until maximal oxygen flux was reached. Complex II ETS was measured after the addition of Complex I inhibitor rotenone. Due to high inter-experimental variability, a pairwise statistical comparison for each experiment was performed (mean ± SEM; paired t test, Holm-Sidak *post hoc*, ns = not significant, * $P < 0.05$. n = 5).

Given the association between PINK1 and PD, which is primarily considered a disease of the nervous system, it is possible that the rescue of climbing ability conveyed by *cn* overexpression was caused by protection specifically in neurons. To investigate this, homogenates were prepared from the heads of *FM6* and *Pink1*^{B9} flies, which are enriched for neuronal tissue. Notably, there was also no observable defect in *Pink1B9* heads compared to *FM6* controls, indicating that the complex I defects observed in *Pink1* flies are predominantly in body tissue, most likely in the IFMs, which are packed with mitochondria in wildtype flies, but degenerate in *Pink1* mutants. Overexpression of *cn* did not affect respiratory capacity in *FM6* or *Pink1*^{B9} backgrounds (Figure 4.13). Thus, it appears that the complex I deficiencies observed in *Pink1* mutant flies are predominantly in the body rather than the head, and *cn* overexpression is insufficient to rescue this phenotype.

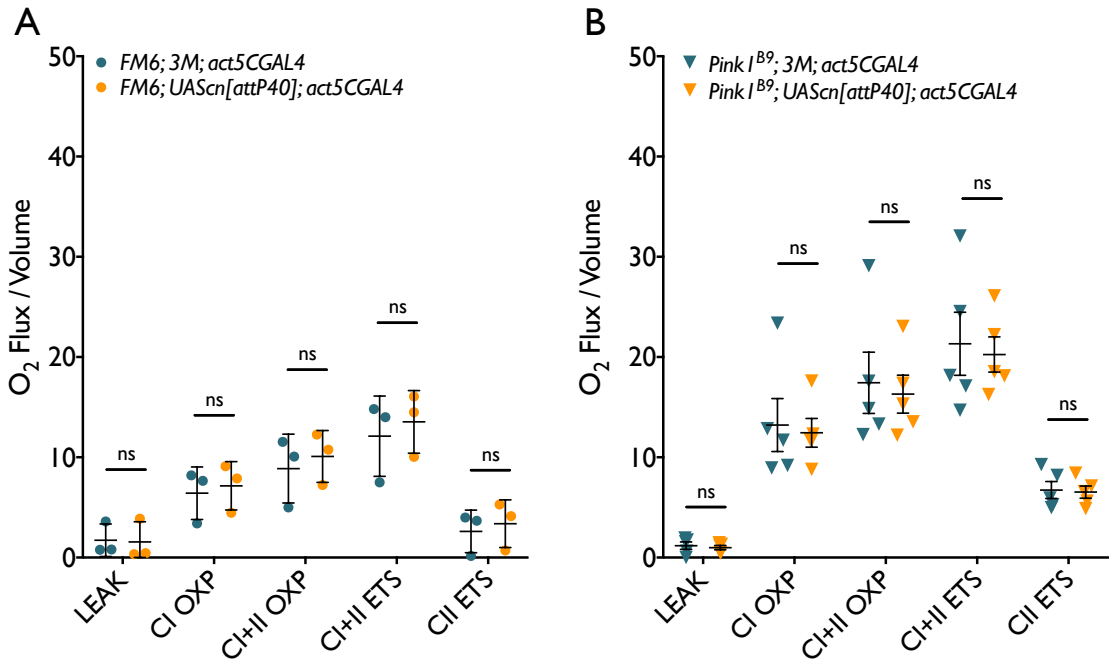

Figure 4.13. Respiratory capacity of *FM6* or *Pink1*^{B9} head homogenates overexpressing *cn*.

Leak was measured in the presence of malate and pyruvate but the absence of ADP. Complex I OXPHOS was measured upon addition of ADP, then Complex I + II OXPHOS was measured after the addition of succinate. Complex I + II ETS was measured by adding titrations of CCCP until maximal oxygen flux was reached. Complex II ETS was measured after the addition of Complex I inhibitor rotenone. Due to high inter-experimental variability, a pairwise statistical comparison for each experiment was performed (mean ± SEM; paired t test, Holm-Sidak *post hoc*, ns = not significant. Five male heads per n, n = 3 – 6,).

4.2.9 Overexpression of *cn* alters mitochondrial morphology in *Pink1* knockdown S2 cells

Given the aberrant mitochondrial morphology caused by *cn* deficiency (Chapter 3), I next investigated whether *cn* overexpression could rescue mitochondrial morphology in *Pink1* knockdown S2 cells. *Pink1* knockdown in *Drosophila* cells has been previously shown to cause elongated mitochondria (Ziviani *et al.*, 2010; Pogson *et al.*, 2014), but also the opposite in another study (Lutz *et al.*, 2009). *Pink1* dsRNA was transfected into S2 cells using Effectene Reagent as in Chapter 3, resulting in knockdown efficiency of ~78% (Figure 4.14). This resulted in notably elongated mitochondria compared to *f. luc* dsRNA treated cells, although this was not quantified, for the reasons stated in 3.2.1 (Figure 4.15). The *pUASt-attB cn* plasmid used to generate overexpression flies was transfected into *f. luc* or *Pink1* knockdown S2 cells alongside an *Act5CGAL4* plasmid. In *f. luc* dsRNA cells, *cn* overexpression had no notable effect on mitochondrial morphology. In *Pink1* dsRNA cells however, *cn* overexpression appeared to restore mitochondrial morphology to similar that of *f.luc* dsRNA cells.

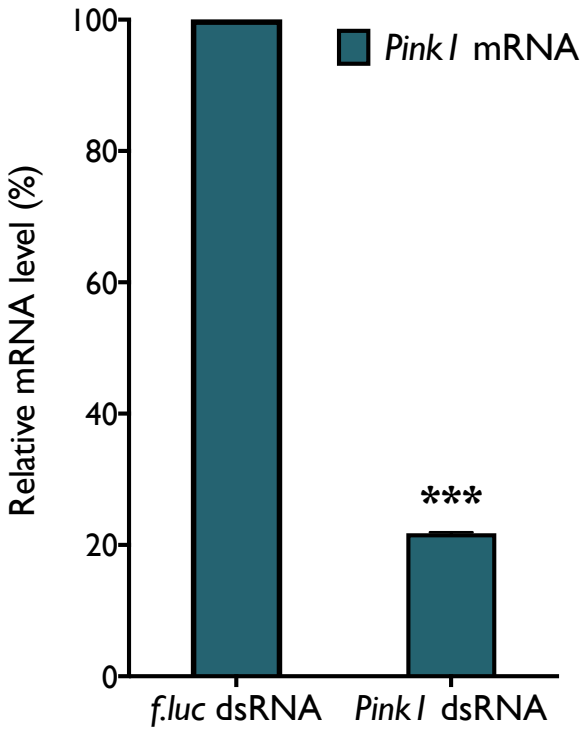

Figure 4.14. *Pink1* is knocked down in *Drosophila* S2 cells upon dsRNA treatment. Cells were seeded at 1 x 10^6 cells per well of a 6 well plate and transfected with 2 µg of dsRNA targeting either firefly *luciferase* (*f. luc*) or *Pink1,* using Effectene transfection reagent mix. RNA was extracted 72 hrs post-transfection. Values represent normalised mRNA levels of *Pink1* in dsRNA treated cells compared to *f. luc* dsRNA treated controls (mean ± SD; pairwise fixed reallocation randomization test, *** $P < 0.001$, n = 3).

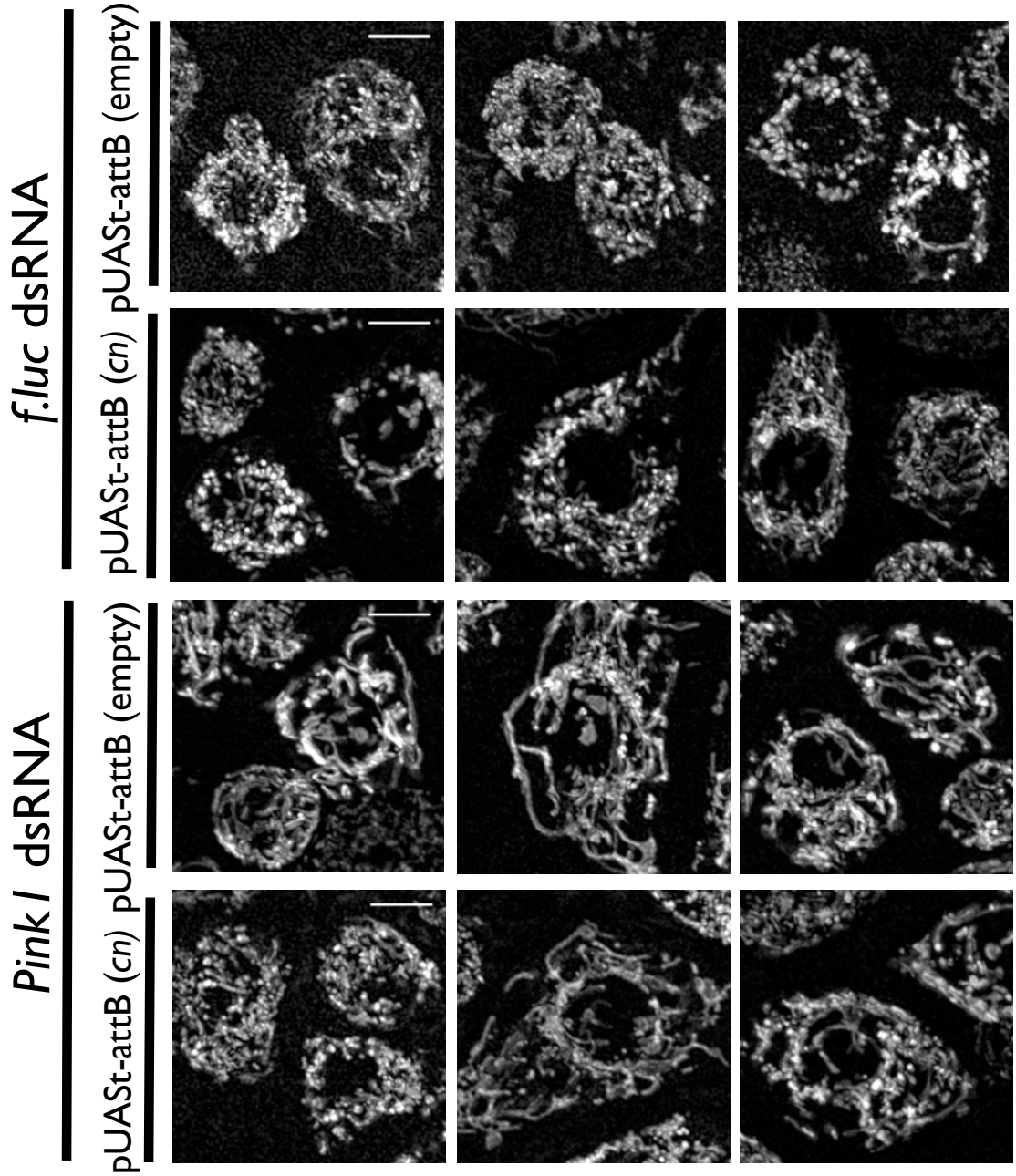

Figure 4.15. Mitochondrial morphology in *Pink1* dsRNA treated *Drosophila* S2 cells appears to be modulated by *cn* overexpression.

Drosophila S2 cells were seeded at 1 x 10^6 cells per well in 6-well plates and transfected with dsRNA targeting firefly *luciferase (f.luc)* or *Pink1*, alongside pUASt (empty or *cn*) and *Act5CGAL4* plasmids, using Effectene reagent. 60 hrs post-transfection, cells were plated in glass bottomed dishes coated with concanavalin A. 12 hrs later, cells were stained with Mitotracker Red FM and imaged live at 25°C (scale bars = 5 μm).

4.3 Discussion

In this chapter, I demonstrated that manipulation of KMO expression modulates well-characterised phenotypes in *Pink1* mutant flies. Although *Pink1^{B9}* hemizygous males usually eclose at an expected Mendelian frequency of 1:1 in relation to FM6 chromosome carriers, complete *cinnabar* deletion resulted in semi-lethality in *Pink1^{B9}* males, with ~35% of the expected number of *Pink1^{B9}; cn$^{3/3}$* adult flies eclosing compared to *FM6; cn$^{3/3}$*. An eclosion defect in *cn^{3}* flies has been previously reported, with a significantly lower than expected number of *cn^{3}* homozygotes eclosing compared to heterozygotes, when *cn$^{3/3}$* flies were crossed to *cn$^{3/+}$* (Green *et al.,* 2012). However, in the present work the *cn^{3}* chromosome was balanced over the CyO chromosome, which carries the hypomorphic *cn^{2}* allele (see Chapter 3). When *cn^{3}/CyO* flies were self-crossed, *cn$^{3/3}$* flies eclosed at a Mendelian frequency of 50% relative to *cn^{3}/CyO*, indicating that there is no fitness cost to *cn^{3}* homozygotes compared to *cn^{3}/CyO*. Thus, from the experiments performed in this chapter, it is deduced that whilst *cn^{3}* homozygosity or *Pink1^{B9}* hemizygosity alone do not confer an eclosion phenotype, the combination of these two genotypes is sufficient to cause semi-lethality, indicating a potential functional overlap between KMO and PINK1. A similar effect has been previously reported in *Pink1^{B9}* flies in which dominant-negative *Drp1* alleles have been introduced (Poole *et al*., 2008). In that study, a single copy of the dominant negative allele was sufficient to induce semi-lethality, whereas here, *cn^{3}* homozygosity was necessary, as demonstrated by *cn3/CyO* or *cn^{RNAi}; Act5CGAL4* having no significant effect on the eclosion of *Pink1^{B9}* males. PINK1 regulates DRP1 activity by phosphorylating AKAP1 on the MOM, resulting in inhibition of PKA tethering to mitochondria. This leads to a decrease in DRP1 phosphorylated at the Ser637 residue, resulting in an increase in mitochondrial fission (Pryde *et al*., 2016). Given the mitochondrial elongation observed upon *cn* knockdown or deletion in *Drosophila* models, the partial lethality observed could be due to an interaction between KMO and DRP1.

Both *cn^{3}* homo- and heterozygosity was sufficient to increase the penetrance of the defective thorax phenotype in *Pink1^{B9}* males, as well as *Act5CGAL4*-driven *cn* RNAi knockdown. This phenotype, which is also observed in *parkin* mutant flies (Greene

et al., 2003), is caused by degeneration of the mitochondria-dense, highly ATP-demanding indirect flight muscle of flies, and is apparent as early as the late-pupal stage (Greene *et al*., 2005; Clark *et al*., 2006). This is before the onset of basal mitophagy defects in *Pink1* and *parkin* mutants (Lee *et al*., 2018b*;* Cornelissen *et al*., 2018), which would indicate that mitophagy-independent functions of PINK1 and Parkin are responsible for this phenotype. Conversely, however, overexpression of the autophagy adapter Ref(2)P causes a significant decrease in penetrance of the defective thorax phenotype (Costa *et al*., 2013), meaning that autophagy/mitophagy cannot be excluded from the responsible mechanism(s).

$Pink1^{B9}$*;* $cn^{3/3}$ and $Pink1^{B9}$*;* cn^{3}*/CyO* flies also displayed a decrease in lifespan compared to $Pink1^{B9}$*;* $cn^{+/+}$, however *cn* RNAi had no significant effect on longevity. Given that cn^{3}*/CyO* flies show a similar level of *cn* expression to cn^{RNAi}*; Act5CGAL4* flies (Chapter 3), it is unclear why cn^{3}*/CyO* causes a decrease in lifespan of *Pink1* mutants but not *cn* RNAi knockdown. One explanation could be that, like the eclosion phenotype, total *cn* deletion is necessary to cause the effect and that the change in lifespan observed in $Pink1^{B9}$*;* cn^{3}*/CyO* flies is due to a cinnabar independent effect of the CyO chromosome. This is supported by the fact that lifespan was also reduced in *FM6;* cn^{3}*/CyO* flies compared to *FM6;* $cn^{+/+}$, but no effect was observed in *FM6;* $cn^{3/3}$ or *FM6;* $cn^{RNAi;}$ *Act5CGAL4* flies.

As in Chapter 3, the question as to whether the effects observed by *cn* deficiency were due to changes in KP metabolite levels needed to be addressed. As *cn* deficiency also results in an increase in KYNA production, $Pink1^{B9}$ flies were supplemented with KYNA at a range of concentrations which have previously replicated the neuroprotective effects of *cn* deletion or knockdown (Campesan *et al*., 2011; Breda *et al*., 2016). KYNA supplementation had no significant effect on the eclosion of $Pink1^{B9}$ males in proportion to control flies at all doses tested. KYNA supplementation did, however, have a significant dose-dependent effect on the penetrance of the defective thorax phenotype, but the opposite effect to that of *cn* deletion or knockdown. A reduction in penetrance was observed at 0.25, 0.50 and 1.00 mg/mL KYNA, with the most significant effect caused by 0.50 mg/mL. This concentration was subsequently used to examine effects of KYNA on lifespan in

Pink1^{B9} mutants. Again, the opposite effect of *cn* deletion was observed, with a small but significant increase in lifespan of *Pink1*^{B9}, but not FM6 males. A decrease in penetrance of the defective thorax phenotype was also observed in *Pink1*^{B9} flies upon inhibition of KMO enzymatic activity via Ro 61-8046, indicating that the exacerbation of *Pink1* mutant phenotypes induced by *cn* deletion or knockdown, comes as a result of a functional overlap between KMO and PINK1, which is independent from KMO enzymatic activity. This is in concordance with the respiratory capacity decrease in *cn*^{3} and *cn* RNAi flies observed in Chapter 3, which was not rescued by restoring 3-HK to physiological levels.

cn and *hKMO* overexpressing lines were generated for the purpose of exploring whether *Pink1*^{B9} mutant phenotypes could be compensated for by increased levels of KMO. The *UAScn[attP51C]* line (Furmston, 2016) showed *cn* transcript levels ~4-fold greater than newly eclosed controls when driven with *Act5CGAL4*, in concordance with previous reports of weak expression from the *attP51C* site (Kharazmi *et al.*, 2012) and the low level of expression of the *mini-white* transgenic marker which results in these flies have light-orange eyes (Bischof *et al.*, 2007). *Act5CGAL4* driven expression of *UAScn[attP40]* resulted in *cn* transcript levels ~10-fold higher than the *UAScn[attP51C]* line, which allowed for titration of *cn* overexpression. Unlike *cn* deletion, *cn* or *hKMO* overexpression had no significant effect on the eclosion of *Pink1*^{B9} males, indicating no negative consequences for viability. *UAScn[attP51C]; Act5CGAL4* flies exhibited significantly decreased penetrance of the defective thorax phenotype. A small but non-significant decrease was also observed in *UAScn[attP40]; Act5CGAL4* and *UAShKMO[attP40]; Act5CGAL4* flies compared to controls. This could be interpreted as high KMO in the *attP40* lines, leading to a reduction in the level of rescue of this phenotype.

Overexpression of *cn* from both landing sites or *hKMO* was sufficient to robustly rescue the climbing defect observed in *Pink1*^{B9} males compared to controls. Expression from the *attP40* site resulted in a greater rescue, restoring climbing ability to approximately the same level as *FM6* control genotypes. This indicates that different levels of KMO expression are required for higher rescue of the various phenotypes, as *UAScn[attP51C]* provided better rescue of the defective thorax

phenotype. Overexpression of *cn* or *hKMO* from the *attP40* site resulted in a significant increase in lifespan of *Pink1*^{B9} males but not *FM6* controls, whereas expression of *cn* from the *attP51C* site had no significant effect on lifespan in either *Pink1*^{B9} or FM6.

Together, the results of this chapter indicate that KMO and PINK1 have a functional interaction, as *cn* deletion or knockdown exacerbated *Pink1* mutant phenotypes, whereas *cn* or *hKMO* overexpression rescued them. Rescue appears to correlate with modulation of mitochondrial morphology, as *cn* overexpression in S2 cells reversed the elongated mitochondrial phenotype induced by *Pink1* dsRNA silencing. However, *cn* overexpression did not rescue respiratory capacity defects in whole body extracts of *Pink1* mutants. Parkin overexpression in a *Pink1* mutant background also rescues mitochondrial morphology and climbing ability in a *Pink1*-null background (Clark *et al.*, 2006; Park *et al.*, 2006) but does not rescue complex I activity (Pogson *et al.*, 2014), suggesting that the two phenotypes are not caused through the same mechanism. The protection conveyed by KMO could be due to Parkin-related mechanisms, rather than Parkin-independent functions of PINK1. An appropriate next step in this investigation is to discern how KMO interacts with PINK1 and in particular, given the suggestion that KMO might play a role in Parkin recruitment (Ivatt *et al.*, 2014), if this interaction occurs via Parkin-dependant or independent mechanisms.

4.4 Conclusions

Genetic epistasis experiments in *Drosophila* have revealed a functional interaction between KMO and PINK1. Exacerbation of *Pink1*-null phenotypes was observed upon *cn* deletion or knockdown. Furthermore, overexpression of *cn* or *hKMO* was sufficient to robustly rescue climbing ability in *Pink1* mutants and caused a modest improvement in lifespan. However, overexpression of *cn* or *hKMO* was not sufficient to rescue complex I defects, a similar effect to that observed by *parkin* overexpression. The mechanism through which KMO and PINK1 functionally interact requires further investigation. This will be addressed in the subsequent chapters by investigation of functional relationships between between KMO and

Parkin, as well as DRP1, which PINK1 regulates in a Parkin independent fashion (Pryde *et al.*, 2016).

5. Investigating the interplay between KMO and Parkin

5.1. Introduction

The phenotypes observed in *cn* deficient *Drosophila* models in Chapter 3 are comparable to phenotypes previously reported in *Pink1* or *parkin* deficient models (Greene *et al*., 2003; Clark *et al*., 2006; Park *et al*., 2006; Yang *et al*., 2006; Ziviani *et al*., 2010; Costa *et al*., 2013). In *Drosophila*, *parkin*-null flies have very similar phenotypes to *Pink1* mutants and epistasis analysis revealed that Parkin operates downstream of PINK1 in a common pathway (Clark *et al*., 2006; Park *et al*., 2006; Yang *et al*., 2006). Upon mitochondrial damage, the import of PINK1 into the intermembrane space is blocked, causing it to accumulate on the mitochondrial outer membrane. PINK1 phosphorylates both ubiquitin and Parkin's ubiquitin-like domain at the Ser65 residue, leading to the recruitment of Parkin to mitochondria and activation of its E3 ubiquitin-ligase activity (reviewed by Pickrell & Youle, 2015). Parkin ubiquitinates a number of targets on the MOM, including the fission factor Mfn1/2 (MARF in *Drosophila*) and MIRO, which facilities mitochondrial motility. Interestingly, overexpression of a Ser94Ala (corresponding to human Ser65Ala) phospho-mutant isoform of Parkin in *Drosophila* is sufficient to rescue mitochondrial and physiological defects in a *Pink1* or *parkin*-null background, suggesting that phosphorylation at this Parkin residue is not crucial for function in the fly (Shiba-Fukushima *et al*., 2014). In Chapter 4, a functional interaction between KMO and *Pink1* in *Drosophila* was detailed. The next step is to establish whether this interaction occurs upstream, downstream or independent of the PINK1/Parkin mitophagy pathway.

In this Chapter, I describe genetic epistasis experiments in *Drosophila,* similar to those performed in Chapter 4, employed to probe for an interaction between KMO and Parkin. Eclosion, degeneration of IFMs, climbing ability and lifespan were all assessed in *parkin* flies in which *cn* was either deleted or knocked down and in which *cn* or *hKMO* were overexpressed. *cn* was also overexpressed in *parkin* dsRNA S2 cells to investigate the effect on mitochondrial morphology. As in previous

chapters, the changes caused by *cn* deficiency were differentiated from changing levels of KP metabolites by supplementing *parkin*-null flies with the KMO inhibitor Ro 61-8048 or with KYNA.

cn knockdown has been shown to modulate the recruitment of Parkin to damaged mitochondria in a genome-wide RNAi screen in *Drosophila* S2R+ cells (Ivatt *et al*, 2014). I attempted to replicate the assay performed in this study by measuring Parkin-GFP foci in *cn* dsRNA S2 cells under basal conditions or upon mitochondrial depolarisation caused by the protonophore CCCP. A physical interaction between KMO and Parkin was also explored via immunoprecipitation experiments in *Drosophila* S2 cells and human HeLa cells, under basal conditions and upon mitochondrial depolarisation. A downstream indicator of Parkin recruitment to mitochondria – the ubiquitination and degradation of MARF, was also assessed.

5.2. Results

5.2.1. *cn* deletion causes semi-lethality in *parkin* deficient *Drosophila*

Crosses were set up to produce cn^{3}; $park^{25}$ flies. *Parkin* is located on chromosome III and was balanced over the TM6B chromosome, which carries the $Tubby^{1}$ marker. As in Chapter 4, the crosses were performed in a *w* background, therefore the cn^{3} carrying chromosome was balanced over the *CyO* chromosome, which carries the $duox^{cy}$ and cn^{2} alleles. From the final experimental cross, four genotypes were expected in the progeny due to the homozygous lethality of *CyO* and *TM6B* chromosomes (Table 5.1, Figure 5.1). As $cn^{3/3}$ exhibits no eclosion phenotype in relation to cn^{3}/CyO (Chapter 4, Figure 4.1A), and $park^{25/25}$ flies eclose at a Mendelian frequency when balanced over the *TM6B* chromosome (Poole *et al.*, 2008; Celardo *et al.*, 2017), the expected ratio of progeny from the cross outlined in Table 5.1 is 1:2:2:4 of $cn^{3/3}; park^{25/25}$: $cn^{3/3}; park^{25}/TM6B$: $cn^{3}/CyO; park^{25}/park^{25}$: $cn^{3}/CyO; park^{25}/TM6B$.

In order to make a direct comparison to the results of Chapter 4 in which $Pink1^{B9}$ hemizygous males were analyzed, only male progeny were counted. The number of expected male progeny for each genotype was calculated based on the number of double heterozygote males which emerged. When self-crossed, $park^{25}/TM6B$ flies produced a ratio of 1 : 2 $park^{25}$ homozygote : heterozygote progeny, the expected proportion predicted by Mendelian inheritance. Similar to the results obtained in Chapter 4 in the context of $Pink1^{B9}$ hemizygous males, the number of $cn^{3/3}; park^{25/25}$ double homozygous males was significantly lower than expected in proportion to $cn^{3/3}; park^{25}/TM6B$, with only ~50% the expected number of flies eclosing (Figure 5.2, χ^2 test, $P < 0.0001$). However $cn^{3}/CyO; park^{25/25}$ males eclosed at the expected frequency in proportion to double heterozygotes, indicating that, as with the $Pink1^{B9}$ allele, cn^{3} homozygosity is required in order to cause an eclosion phenotype in *parkin* mutants. $3M/Act5CGAL4; park^{25/25}$ males eclosed at the expected rate in proportion to $3M/Act5CGAL4; park^{25}/TM6B$, whereas ~90% of $cn^{RNAi}/Act5CGAL4; park^{25/25}$ males eclosed compared to $cn^{RNAi}/Act5CGAL4; park^{25}/TM6B$ (Figure 5.2). However, the reduction in $cn^{RNAi}/Act5CGAL4; park^{25/25}$ progeny did not deviate

significantly from the expected number, as calculated by χ^2 test. Only complete loss of KMO is therefore sufficient to induce semi-lethality in *parkin*-null flies.

Table 5.1. Experimental cross to generate *cn³; park²⁵* flies.
cn³/CyO; TM6B/park²⁵ flies were crossed - parental gamete and male progeny genotypes are detailed. CyO and TM6B chromosomes are homozygous embryonic lethal.

	cn³; park²⁵	***cn³; TM6B***	***CyO; park²⁵***	***CyO; TM6B***
cn³; park²⁵	*cn³/³; park²⁵/²⁵*	*cn³/³; park²⁵/TM6B*	*cn³/CyO; park²⁵/park²⁵*	*cn³/CyO; park²⁵/TM6B*
cn³; TM6B	*cn³/³; park²⁵/TM6B*	Lethal	*cn³/CyO; park²⁵/TM6B*	Lethal
CyO; park²⁵	*cn³/CyO; park²⁵/park²⁵*	*cn³/CyO; park²⁵/TM6B*	*Lethal*	Lethal
CyO; TM6B	*cn³/CyO; park²⁵/TM6B*	Lethal	Lethal	Lethal

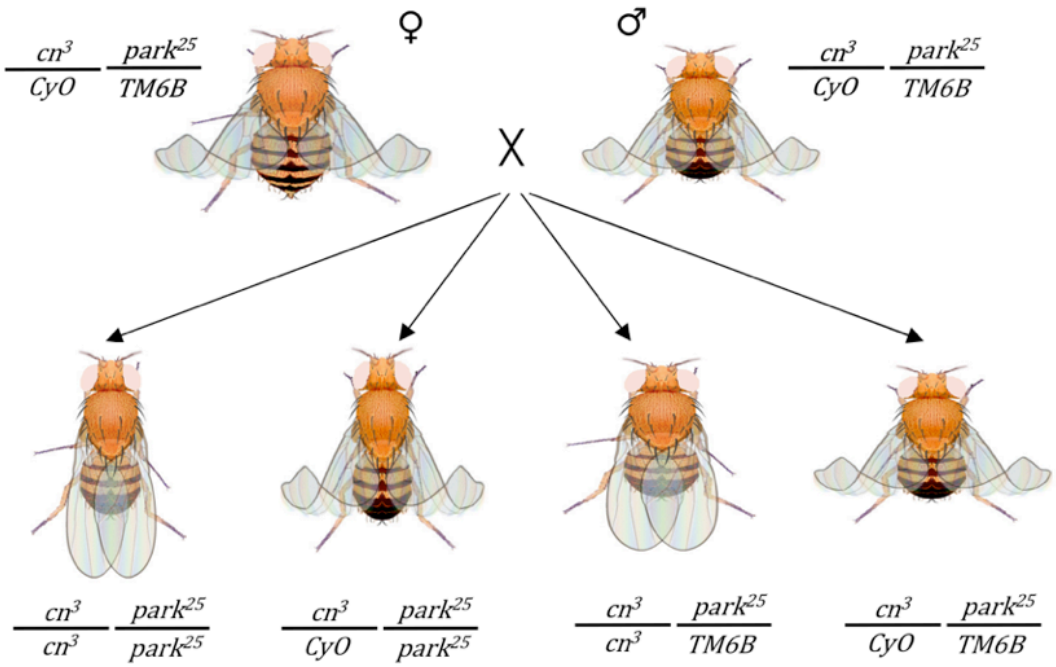

Figure 5.1. Crossing scheme used to generate *cn³; park²⁵* flies.
cn³/CyO; park²⁵/TM6B virgin females were crossed to males of the same genotype. Four different genotypes were expected in the F1 progeny, due to the homozygous lethality of *CyO* or *TM6B* chromosomes (adapted from Otto, 2000).

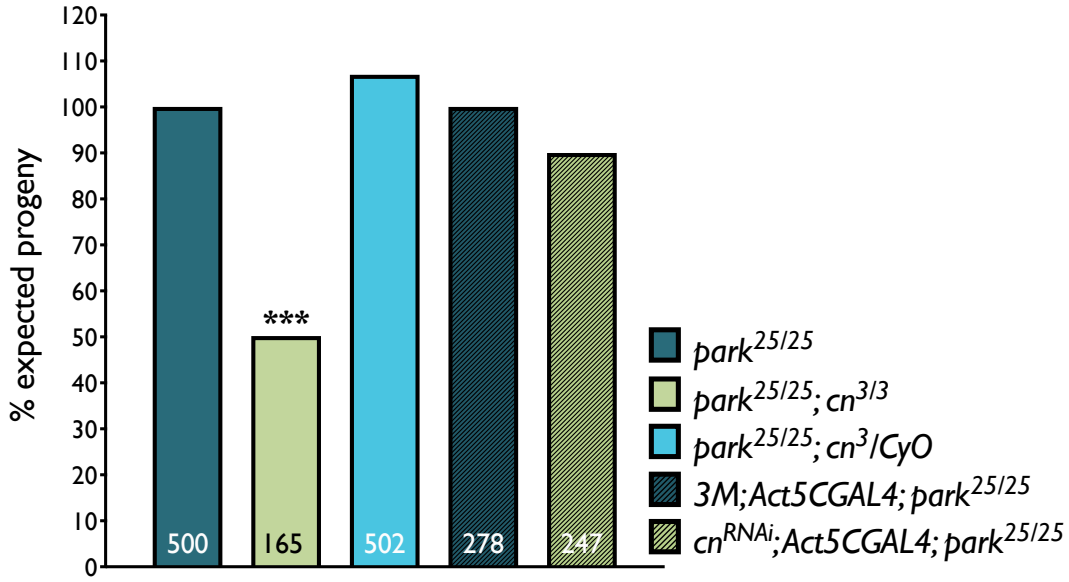

Figure 5.2. Eclosion is impaired in *cn³; park²⁵* flies, but not *cn³; CyO; park²⁵* or *cn^{RNAi}/Act5CGAL4; park²⁵*.

Expected progeny was calculated in proportion to the number of corresponding *park²⁵/TM6B* flies that eclosed. χ^2 test, 1 d.f., **** $P < 0.0001$.

5.2.2. *cn* deletion decreases penetrance of defective-thorax phenotype in *parkin* deficient *Drosophila*

The defective thorax phenotype, which is observed in both *Pink1* and *parkin* mutant flies, was next scored in newly eclosed adult $park^{25/25}$ males in which *cn* was deleted or knocked down. Like in $Pink1^{B9}$ flies, the defective thorax phenotype shows incomplete penetrance and the proportion of flies exhibiting the phenotype varies greatly (Poole *et al.*, 2008; Costa *et al.*, 2013; Celardo *et al.*, 2016). I found ~50% of newly emerged $park^{25/25}$ males exhibited the phenotype. When combined with $cn^{3/3}$, a significant reduction in penetrance was observed, with only ~13% of eclosed males exhibiting the phenotype (Figure 5.3, χ^2 test, $P < 0.001$). $cn^3/CyO; park^{25/25}$ flies also showed reduced penetrance of the phenotype compared *to* $cn^{+/+}; park^{25/25}$ (Figure 5.3, χ^2 test, $P < 0.01$). Although $cn^{RNAi}/Act5CGAL4; park^{25/25}$ males showed a significant reduction in penetrance compared to $park^{25/25}$ flies, a similar reduction was interestingly also observed in $3M/Act5CGAL4; park^{25/25}$ flies (Figure 5.3, χ^2 test, $P < 0.001$). LOF in *cn* therefore modulates the degeneration of IFMs in $park^{25}$ flies, but has the opposite effect to that observed in $Pink1^{B9}$ flies.

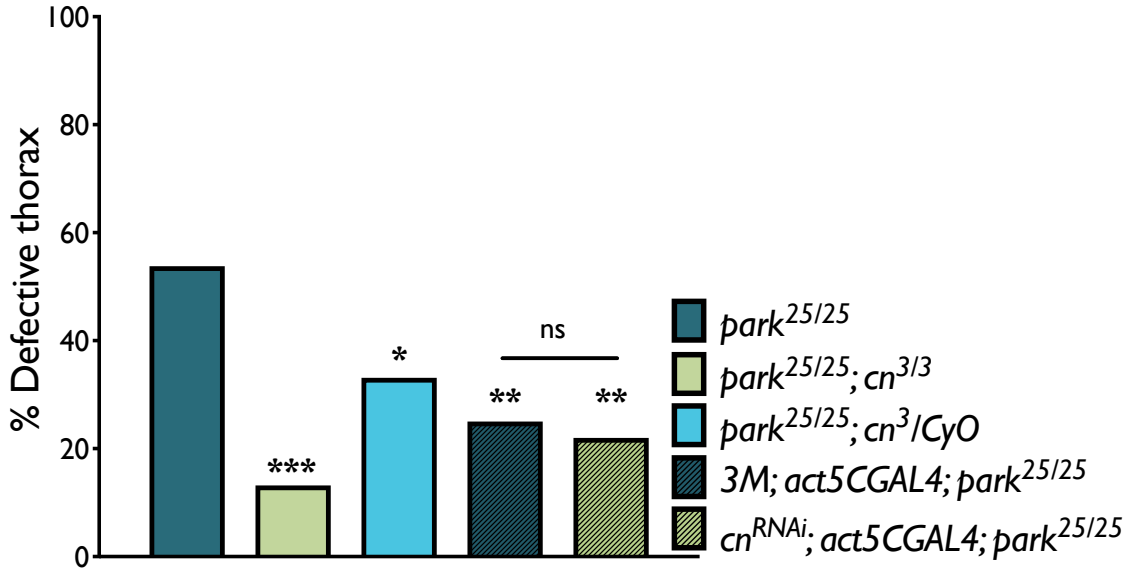

Figure 5.3. Penetrance male defective thorax phenotype of Day 1 $park^{25/25}$ males combined with *cn* deletion or knockdown.
Penetrance in the $cn^{3/3}; park^{25/25}$ and $cn^3/CyO; park^{25/25}$ genotypes was compared to the $park^{25}$ stock. $cn^{RNAi}/Act5CGAL4; park^{25/25}$ was compared to $3M/Act5CGAL4; park^{25/25}$. χ^2 test, 1 d.f., ** $P < 0.0125$, ** $P < 0.0025$, *** $P < 0.00025$.

5.2.3. KMO inhibition or KYNA supplementation cause a reduction in eclosion of *park*$^{25/25}$ flies but a decrease in penetrance of defective thorax phenotype

To investigate if the modulation of eclosion and defective thorax phenotypes caused by *cn* deficiency is due to a change in KP metabolites, the *park*^{25}*/TM6B* stock was reared on medium containing a range of concentrations of either the KMO inhibitor Ro 61-8048, or KYNA, which is known to be elevated in both *cn*^{3} and *cn*^{RNAi} flies (Campesan *et al.*, 2011, Breda *et al.*, 2016). Inhibition of KMO enzymatic activity by supplementation with a concentration of Ro 61-8048 known to inhibit KMO activity (Campesan *et al.*, 2011) did not significantly affect the proportion of *park*$^{25/25}$ male flies that emerged in proportion to *park*^{25}*/TM6B* (Figure 5.4A). However, supplementation with 2.5 mg/mL KYNA resulted in a significant decrease in eclosion of *park*$^{25/25}$ males, with ~75% the expected number of flies eclosing (Figure 5.4B, χ^2 test, $P < 0.05$), while lower concentrations of KYNA (0.25 – 1.0 mg/mL) had no significant effect on eclosion. The phenotype observed with 2.5 mg/mL KYNA supplementation was considerably milder than that of complete *cn* deletion, as only ~50% the expected number of *cn*$^{3/3}$*; park*$^{25/25}$ flies eclosed (Figure 5.2, χ^2 test, $P < 0.0001$).

Notably, treatment with Ro 61-8048 or KYNA resulted in a decrease in penetrance of the defective thorax phenotype in newly eclosed *park*$^{25/25}$ males (Figure 5.4C & D). A significant decrease in penetrance was observed with 50 - 200µM Ro 61-8048 and 0.25 – 1.0 mg/mL KYNA. The percentage of flies with the phenotype was reduced from ~50% in untreated controls to ~26– 40 %, with the maximum effect observed upon 1.0 mg/mL KYNA supplementation, upon which only ~26 % of flies had the phenotype (Figure 5.4D, χ^2 test, $P < 0.001$). This was still a more modest effect in comparison to *cn*$^{3/3}$*; park*$^{25/25}$ flies of which only ~13 % had the phenotype (Figure 5.2, χ^2 test, $P < 0.001$). This could suggest either that due to the eclosion phenotype, the *cn*$^{3/3}$*; park*$^{25/25}$ flies that do eclose are fitter and thus exhibit a more modest penetration of the defective thorax phenotype, or that the increase in KYNA caused by KYNA supplementation or inhibition of KMO enzymatic activity through Ro 61-8048 is not as great as that caused by complete *cn* deletion. Nonetheless, it appears that the decrease in penetrance of the defective thorax phenotype caused

by *cn* LOF in *park*^{25} flies could be due to an increase in KYNA, caused by a reduction in the conversion of KYN to KYNA by KMO.

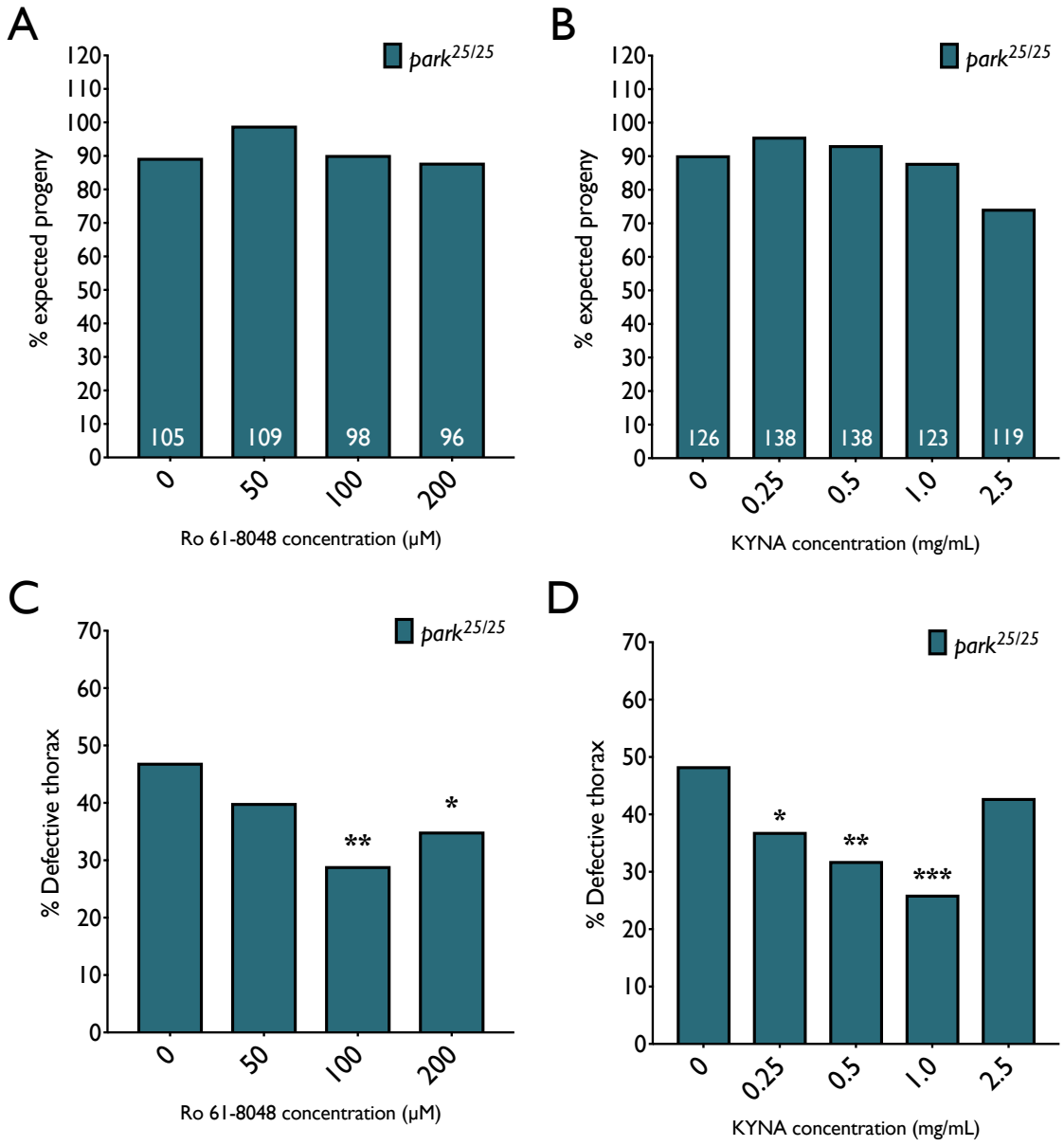

Figure 5.4. Eclosion and penetrance of defective thorax phenotypes in *park*^{25} males supplemented with KMO inhibitor Ro 61-8048 or KYNA.

Four *park*^{25}*/TM6B* virgin females were mated with four *park*^{25}*/TM6B* males at 25°C, on medium containing a range of concentrations of Ro 61-8048 or KYNA, or vehicle alone (DMSO for Ro 61-8048, H_2O for KYNA). Eclosing progeny were counted for 10 days and scored for defective thorax on Day 1 post-eclosion. **A & B)** % expected *park*$^{25/25}$ male progeny in relation to *park*^{25}*/TM6B.* **C & D)** Penetrance of the defective thorax phenotype in newly eclosed *park*$^{25/25}$ adult males. χ^2 test, 1 d.f., * $P < 0.0125$, ** $P < 0.0025$, *** $P < 0.00025$.

5.2.4. *cn* deletion and knockdown reduces lifespan in *park^{25}* flies

In order to investigate if loss of KMO affected the fitness of *parkin* mutant adult flies, the lifespan of progeny from the cross detailed in Table 5.1 was assessed (Table 5.2, Figure 5.5). Males carrying the *park^{25}/TM6B* males had a median lifespan of 37 days, compared to 38 days in *cn$^{3/3}$; park^{25}/TM6B* and *cn^{3}/CyO; park^{25}/TM6B* flies, which were not significantly different (Mantel-Cox test, $P = 0.3605$ & $P = 0.3168$). Male *park$^{25/25}$* flies had a median lifespan of 27 days. Both *cn$^{3/3}$; park$^{25/25}$* and *cn^{3}/CyO; park$^{25/25}$* genotypes had reduced median lifespans of 24 days. This was significant in *cn$^{3/3}$; park$^{25/25}$* flies (Mantel-Cox test, $P = 0.0015$) but not *cn^{3}/CyO; park$^{25/25}$* ($P = 0.203$). *Act5CGAL4* driven RNAi knockdown of *cn* also decreased median lifespan of *park$^{25/25}$* males to 24 days compared to 27 in *3M/Act5CGAL4; park$^{25/25}$* (Table 5.3, Figure 5.6A, $P = 0.03$), but had no significant effect on the lifespan of *park^{25}/TM6B* males (Table 5.3, Figure 5.6B, $P = 0.1887$). Loss of KMO thus has a detrimental effect on the lifespan of *parkin*-null flies, but not *parkin* LOF heterozygotes.

Table 5.2. Survival data summary of *park^{25}* heterozygote and homozygote males carrying *cn^{3}* allele.
Summary of the data used to generate survival curves (Figure 5.5), median survival and curve comparison significance computed by Prism 7. P values were calculated by Mantel-Cox test as a comparison between *park^{25}/TM6B* or *park$^{25/25}$* carrying males and corresponding *cn$^{3/3}$* or *cn^{3}/CyO* genotypes.

	park^{25}/TM6B	*park^{25}/TM6B; cn$^{3/3}$*	*park^{25}/TM6B; cn^{3}/CyO*
# deaths/events	100	100	100
Median survival (days)	37	38	38
P value (compared to *park^{25}/TM6B*)	NA	0.3605	0.3168

	park$^{25/25}$	*park$^{25/25}$; cn$^{3/3}$*	*park$^{25/25}$; cn^{3}/CyO*
# deaths/events	100	100	100
Median survival (days)	27	24	24
P value (compared to *park$^{25/25}$*)	NA	0.0015	0.2030

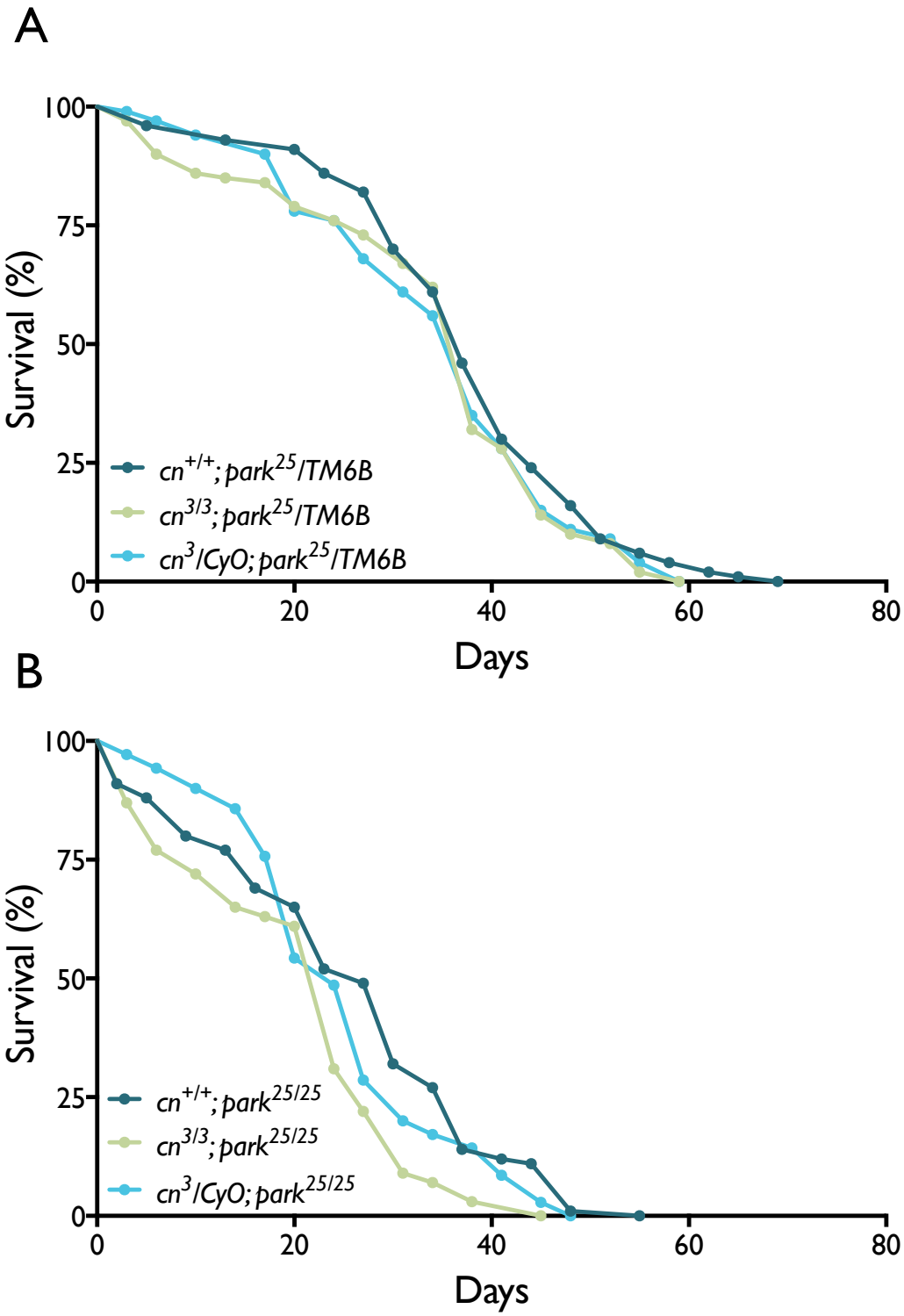

Figure 5.5. *cn* deletion reduces lifespan of *park*$^{25/25}$ males.
Survival curves of *park*^{25}*/TM6B* **(A)** and *park*$^{25/25}$ **(B)** male flies carrying the *cn*^{3} allele. Newly emerged males were placed 10 per vial and transferred to fresh medium every 2 - 3 days (n = 100).

Table 5.3. Survival data summary of *park^{25}* heterozygous and homozygous males upon *cn* knockdown.

Summary of the data used to generate survival curves (Figure 5.6), median survival and curve comparison significance computed by Prism 7. *P* values were calculated by Mantel-Cox test as a comparison between *cn^{RNAi}; Act5CGAL4* males and *3M; Act5CGAL4* controls, either homozygous or heterozygous for the *park^{25}* allele.

	park^{25}/TM6B		*park$^{25/25}$*	
	3M/ Act5CGAL4	*cn^{RNAi}/ Act5CGAL4*	*3M/ Act5CGAL4*	*cn^{RNAi}/ Act5CGAL4*
# deaths/events	100	100	100	100
Median survival	38	38	28	24
P value (compared to *3M/Act5CGAL4*)	NA	0.1887	NA	0.0030

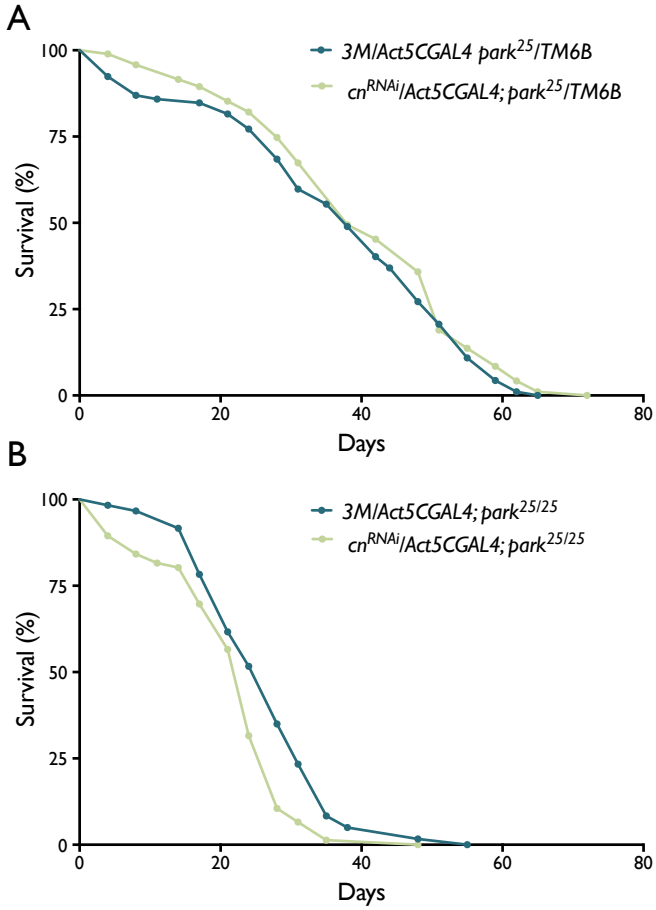

Figure 5.6. Ubiquitous *cn* knockdown reduces lifespan of *park$^{25/25}$* males.

Survival curves of *park^{25}/TM6B* **(A)** and *park$^{25/25}$* **(B)** male flies upon *Act5CGAL4*-driven *cn* knockdown. Newly emerged males were placed 10 per vial and transferred to fresh medium every 2 - 3 days (n=100).

5.2.5. KYNA prolongs lifespan in *park$^{25/25}$* flies

To investigate if the decrease in lifespan observed in *cn^{3}* and *cn^{RNAi}/Act5CGAL4; park$^{25/25}$* males was due to an increase in KYNA, *park^{25}* flies were supplemented with KYNA. In order to make a direct comparison to the results in Chapter 4, the lifespan was assessed upon treatment with 0.5 mg/mL KYNA. KYNA supplementation increased the median lifespan of *park^{25}/TM6B* from 36 to 37 days (Table 5.4, Figure 5.7A, Mantel-Cox test, $P = 0.0940$) and *park$^{25/25}$* males from 27 to 30 days (Table 5.4, Figure 5.7B, Mantel-Cox test, $P = 0.0015$). As lifespan was decreased in *cn$^{3/3}$; park$^{25/25}$* and *cn^{RNAi}/Act5CGAL4; park$^{25/25}$* flies, the increase in lifespan caused by KYNA supplementation indicates either that KMO has an overlapping function with Parkin independent of KMO enzymatic activity, or that *cn* deletion or knockdown results in an increase in KYNA levels drastically different from that achieved through 0.5 mg/mL supplementation.

Table 5.4. Survival data summary of *park^{25}* heterozygous and homozygous males supplemented with KYNA.
Summary of the data used to generate survival curves (Figure 5.7), median survival and curve comparison significance computed by Prism 7. *P* values were calculated by Mantel-Cox test as a comparison between KYNA supplemented (0.5 mg/mL) flies and controls, carrying either *park^{25}/TM6B* or *park$^{25/25}$* chromosomes.

	park^{25}/TM6B		*park$^{25/25}$*	
	KYNA (0.0 mg/mL)	**KYNA (0.5 mg/mL)**	**KYNA (0.0 mg/mL)**	**KYNA (0.5 mg/mL)**
# deaths/events	100	100	100	100
Median survival	36	37	27	30
P value (compared to 0.0mg/mL KYNA)	NA	0.0940	NA	0.0015

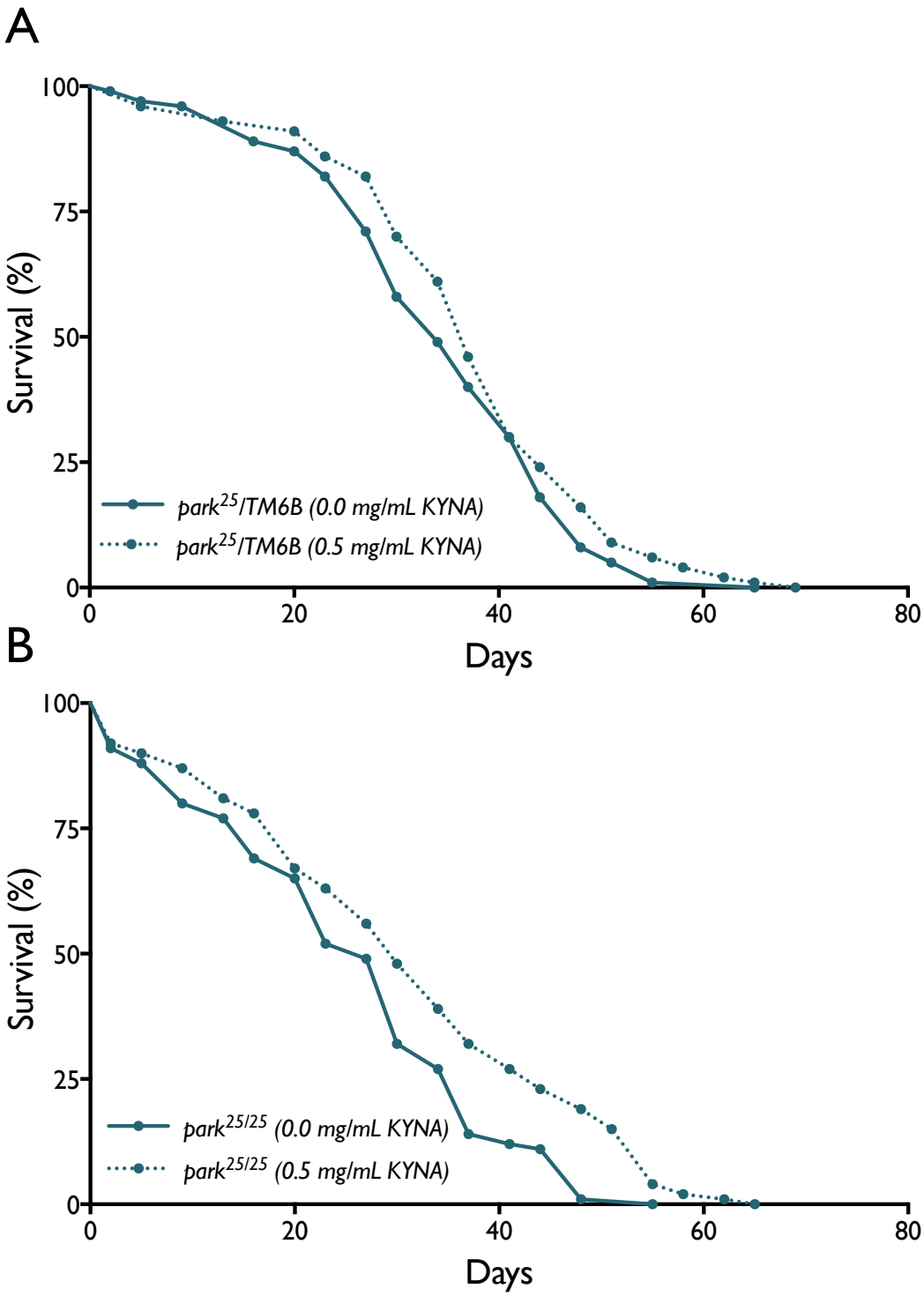

Figure 5.7. KYNA supplementation (0.5 mg/mL) extends lifespan of *park$^{25/25}$* males. Survival curves of *park^{25}/TM6B* **(A)** and *park$^{25/25}$* **(B)** male flies upon KYNA supplementation. Flies were reared on medium supplemented with 0.5 mg/mL KYNA or vehicle (H_2O). Newly emerged males were placed 10 per vial on fresh medium (KYNA or H_2O) and transferred to fresh medium every 2 - 3 days (n = 100).

5.2.6. *cn* deletion improves climbing performance in *parkin* overexpressing flies

In the epistasis experiments which defined the PINK1/Parkin mitophagy pathway in *Drosophila*, overexpression of *parkin* was sufficient to rescue *Pink1* mutant phenotypes, revealing that Parkin acted downstream of PINK1 (Clark *et al*., 2006; Park *et al*., 2006; Yang *et al*., 2006). Due to the genetic link between *cn* and *Pink1* described in Chapter 4, alongside the similar findings in *cn/parkin* double mutants shown above, I next investigated whether Parkin overexpression could rescue *cn* mutant phenotypes. The easily scored climbing assay was employed in 7 day old *Act5CGAL4* driven *UASparkin* flies, in a wildtype or $cn^{3/3}$ background. +; *UASparkin/Act5CGAL4* flies showed a significant decrease in climbing performance compared to both Canton S and $cn^{3/3}$ flies (Figure 5.8), whereas $cn^{3/3}$; *UASparkin/Act5CGAL4* flies climbed significantly better than +; *UASparkin/Act5CGAL4*. However, $cn^{3/3}$; *UASparkin/Act5CGAL4* flies showed no significant difference in climbing performance compared to $cn^{3/3}$ animals. This could suggest that loss of KMO compensates for the detrimental effect of Parkin overexpression, but Parkin overexpression is not sufficient to rescue the cn^{3} climbing phenotype. Although difficult to interpret, these results support a functional interaction between KMO and Parkin.

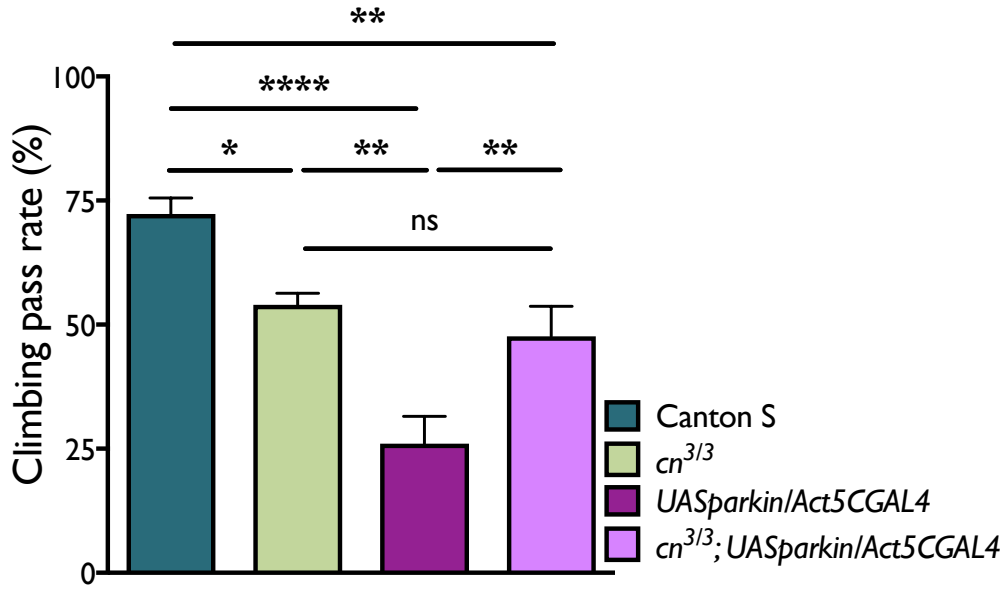

Figure 5.8. Parkin overexpression does not rescue *cn*^{3} climbing phenotype, but *cn*^{3}*; UASparkin/Act5CGAL4* climb better than *+; UASparkin/Act5CGAL4.*
Ability was assessed using the rapid iterative negative geotaxis (RING) assay. Ten Day 7 flies were placed inside a 20 cm vial and tapped to the bottom. The percentage of flies that passed a 8 cm threshold line after 10 s was counted (mean ± SEM; One-way ANOVA, Tukey *post hoc*, *** $P < 0.001$. Ten flies per n, n = 5 - 7,).

5.2.7. Overexpression of *cn* or *hKMO* in *park*^{25} flies

Considering that loss of KMO causes a reduction in viability of *Pink1* and *parkin* mutant flies, it appears that there is a functional overlap between KMO and the two familial PD associated proteins. In addition, a significant decrease in penetrance of the crushed thorax phenotype in *Pink1* mutant flies was observed when *cn* was overexpressed by *Act5CGAL4*-driven expression of *UAScn* from the *attP51C* landing site (Chapter 4, Figure 4.8B). Furthermore, overexpression of either *cn* or *hKMO* robustly rescued the climbing defect of Day 7 *Pink1*^{B9} flies (Chapter 4, Figure 4.10) and also increased their lifespan (Chapter 4, Figure 4.11B). This indicates that KMO functions downstream or in parallel with PINK1, allowing overexpression to rescue *Pink1* mutant phenotypes through complementation. To investigate if KMO operates upstream, downstream or in parallel with Parkin, *cn* and *hKMO* were overexpressed in *parkin* mutant flies.

Homozygous *park*^{25} flies eclose at a Mendelian frequency when balanced over the TM6B chromosome, but cn deletion induces partial lethality (Figure 5.2). Overexpression of *cn* or *hKMO* in *park*^{25} flies had no significant effect on eclosion of *park*$^{25/25}$ males as a proportion of total progeny (Figure 5.9A). To investigate the potential effects of an increase of KMO on *parkin* mutant phenotypes, first the penetrance of the defective thorax phenotype was assessed. The penetrance of defective thorax was ~25 % in newly eclosed *3M/Act5CGAL4; park*$^{25/25}$ males (Figure 5.3, Figure 5.9B), which interestingly is significantly lower than the ~50 % penetrance observed in *park*$^{25/25}$ males (Figure 5.3). Notably, *Act5CGAL4*-driven *hKMO* overexpression caused a significant increase in the penetrance of defective thorax in *park*$^{25/25}$ flies compared to *3M/Act5CGAL4; park*$^{25/25}$*;* with a penetrance of ~38 % (Figure 5.9B, χ^2 test, $P < 0.05$). *UAScn[attP51C]/Act5CGAL4* or *UAScn[attP40]/Act5CGAL4* had no significant effect on the penetrance of the defective thorax phenotype.

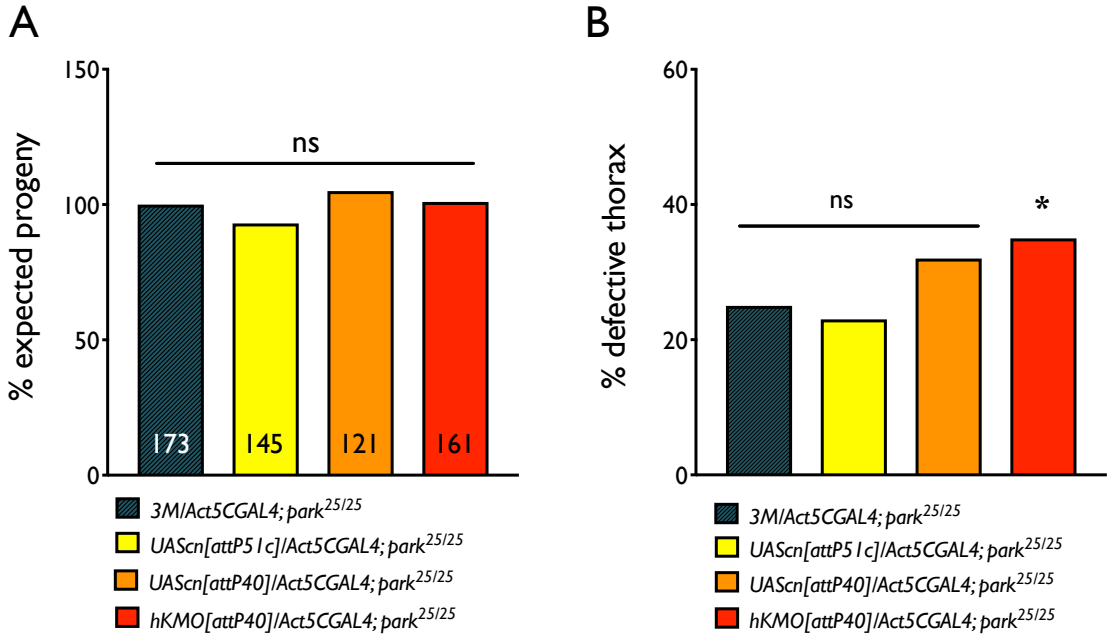

Figure 5.9. *cn* or *hKMO* overexpression does not affect eclosion in *park*^{25} male flies but has a modest effect on defective thorax phenotype.
A) Eclosion rate of adult *park*$^{25/25}$ male flies as a percentage of expected progeny, in relation to *park*^{25}*/TM6B* progeny. **B)** Penetrance of the defective thorax phenotype in newly eclosed *park*$^{25/25}$ males. χ^2 test, 1 d.f., ns = not significant, * $P < 0.05$.

Act5CGAL4-driven overexpression of *cn* from either *attP40* or *attP51C* landing sites did not rescue the climbing phenotype observed in *park*$^{25/25}$ males compared to *park*^{25}*/TM6B* heterozygotes (Figure 5.10). Overexpression of *hKMO* did however significantly improve the climbing performance of *park*$^{25/25}$ flies, improving climbing pass rate from ~8 % in *3M/Act5CGAL4; park*$^{25/25}$ controls to ~22 % (Figure 5.10, $P < 0.001$). Although strongly significant, this rescue was not as robust as the rescue of *Pink1*^{B9} males by *cn* or *hKMO* overexpression, which was restored to almost the level of *FM6* controls (Chapter 4, Figure 4.10).

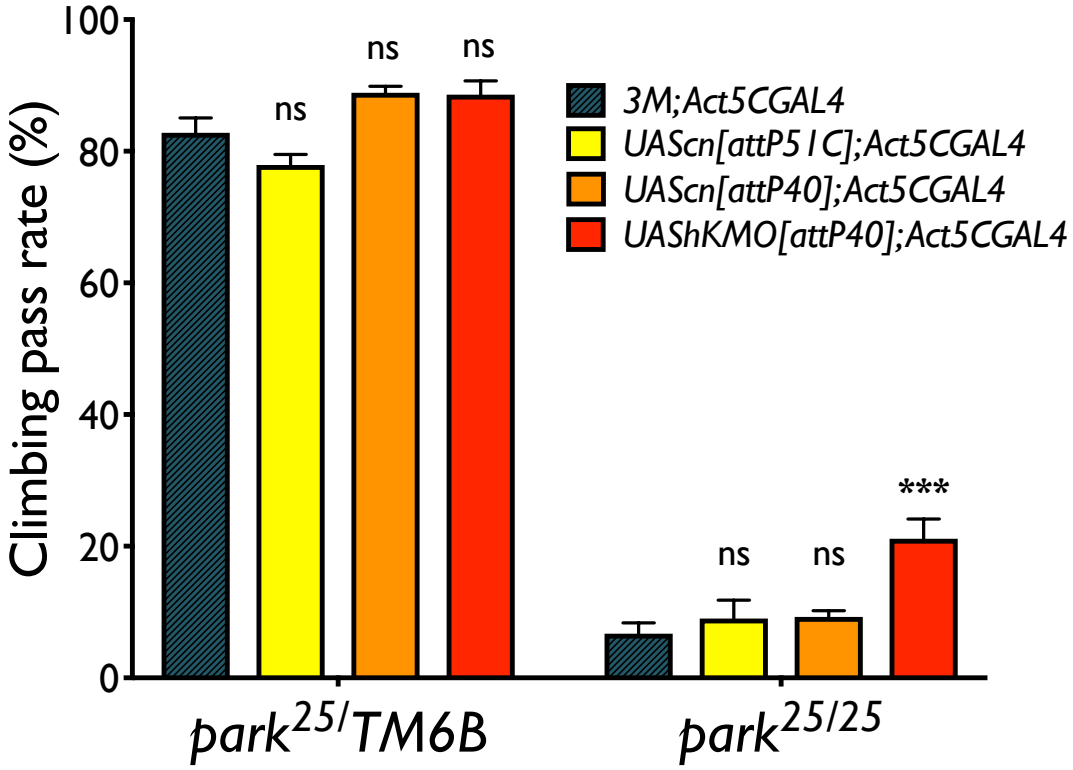

Figure 5.10. *cn* or *hKMO* overexpression does not robustly rescue climbing defects in *park*$^{25/25}$ male flies.

Ability was assessed using the rapid iterative negative geotaxis (RING) assay. 10 Day 7 flies were placed inside a 20 cm vial and tapped to the bottom. The percentage of flies that passed a 8 cm threshold line after 10 s was counted (mean ± SEM; Two-way ANOVA, Tukey *post hoc*, *** $P < 0.001$. Ten flies per n, n = 7 - 10).

Overexpression of *cn* or *hKMO* caused a significant extension in lifespan of *park^{25}/TM6B* flies, with a median lifespan of 48 days in *UAScn[attP51c]* and *hKMO[attP40]* flies and 44 days in *UAScn[attP40]* flies, compared to 38 days in *3M/Act5CGAL4; park$^{25/25}$* (Table 5.5, Figure 5.11A). However, the lifespan of *park$^{25/25}$* flies was not affected by overexpression of *cn* or *hKMO* (Table 5.5, Figure 5.11B). This suggests that some Parkin is required in order for KMO to provide a protective effect on lifespan.

Table 5.5. Survival data summary of *park^{25}* heterozygote and homozygote males overexpressing *cn* or *hKMO*.

Summary of the data used to generate survival curves (Figure 5.11). Median survival and curve comparison significance computed by Prism 7. *P* values were calculated by Mantel-Cox test as a comparison between *park^{25}/TM6B* or *park$^{25/25}$* carrying males and the corresponding UAS construct.

park^{25}/TM6B	*3M/Act5CGAL4*	*UAScn[attP51c]/Act5CGAL4*	*UAScn[attP40]/Act5CGAL4*	*UAShKMO[attP40]/Act5CGAL4*
# deaths/events	100	100	100	100
Median survival	38	48	44	48
P value compared to *3M/Act5CGAL4*	NA	0.0040	0.0035	0.0020

park$^{25/25}$	*3M/Act5CGAL4*	*UAScn[attP51c]/Act5CGAL4*	*UAScn[attP40]/Act5CGAL4*	*UAShKMO[attP40]/Act5CGAL4*
# deaths/events	100	100	100	100
Median survival	28	21	28	26
P value compared to *3M/Act5CGAL4*	NA	0.251	0.400	0.686

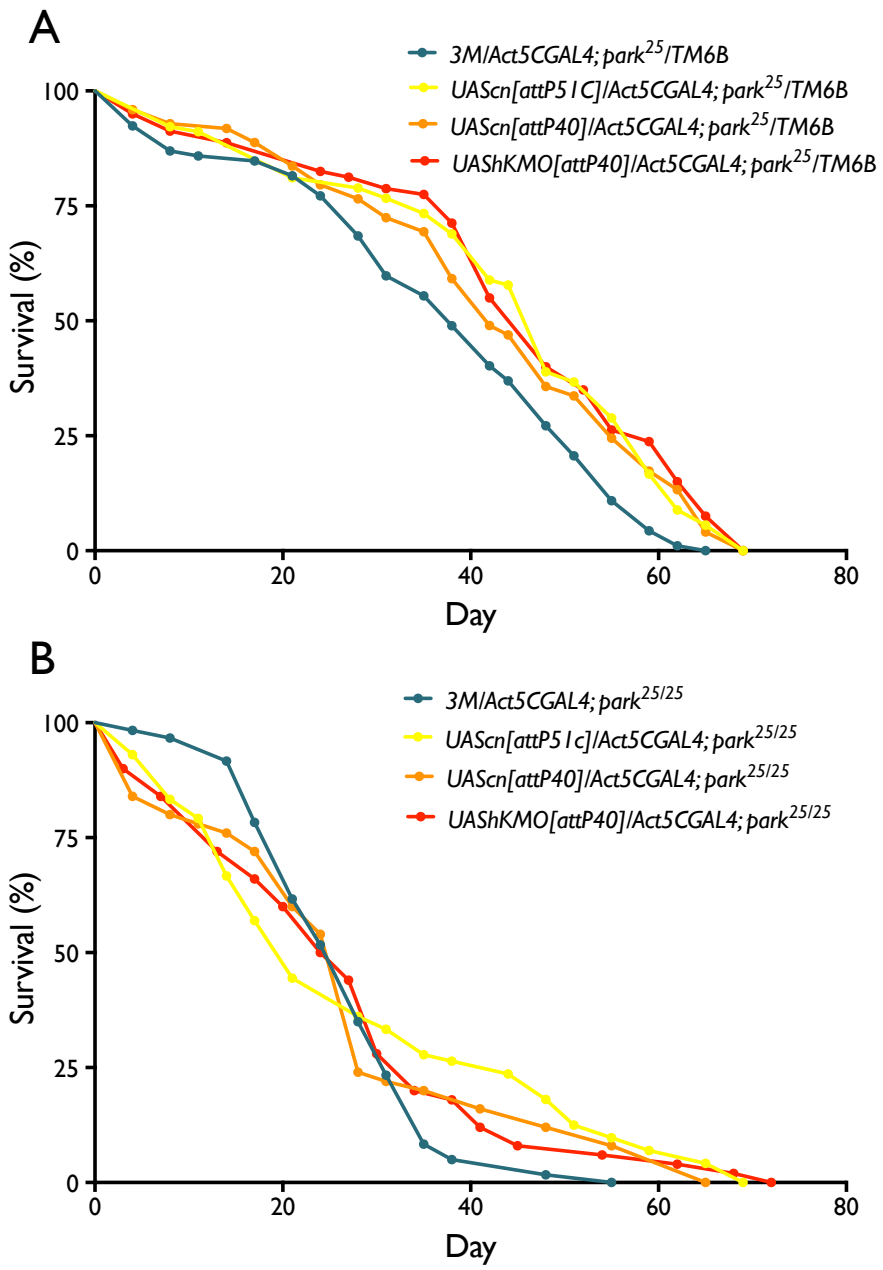

Figure 5.11. Ubiquitous overexpression of *cn* or *hKMO* increases lifespan of *park^{25}/TM6B* but not *park$^{25/25}$* males.

Survival curves of *park^{25}/TM6B* **(A)** and *park$^{25/25}$* **(B)** male flies upon *Act5CGAL4*-driven *cn* knockdown. Newly emerged males were placed 10 per vial and transferred to fresh medium every 2 - 3 days (n = 100).

5.2.8. KMO overexpression modulates mitochondrial morphology in *parkin* knockdown S2 cells

In Chapter 3, dsRNA knockdown of *cn* and *parkin* in S2 cells caused a similar elongation of mitochondrial morphology. This effect has been previously observed upon *parkin* (Ziviani *et al.*, 2010; Pogson *et al.*, 2014; Ivatt *et al.*, 2014) and *cn* (Ivatt *et al.*, 2014) knockdown. In Chapter 4, overexpression of *cn* appeared to rescue the elongated mitochondrial phenotype of *Pink1* dsRNA cells (Chapter 4, Figure 4.15). Here, *cn* was overexpressed in *parkin* knockdown cells to assess if this could also modulate mitochondrial morphology, to ascertain if KMO operates downstream or independently of Parkin. As observed in *Pink1* knockdown cells, *cn* overexpression appeared to reduce mitochondrial elongation in *parkin* knockdown cells (Figure 5.12).

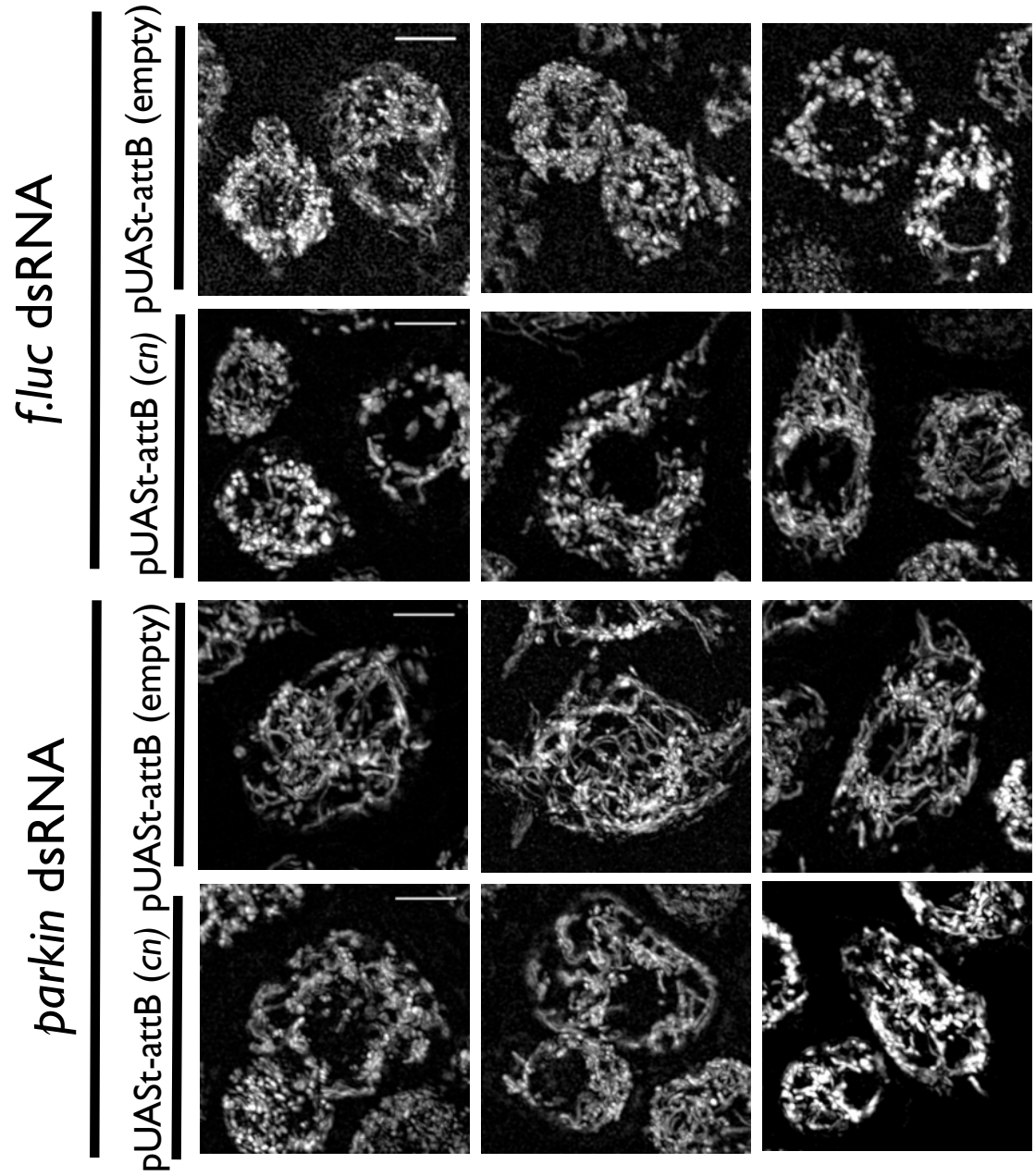

Figure 5.12. Mitochondrial morphology in *parkin* dsRNA treated *Drosophila* S2 cells appears to be modulated by *cn* overexpression.

Drosophila S2 cells were seeded at 1 x 10^6 cells per well in 6-well plates and transfected with dsRNA targeting firefly *luciferase (f.luc)* or *parkin*, alongside *pUAStattB* (empty or *cn*) and *Act5CGAL4* plasmids, using Effectene reagent. 60 hrs post-transfection, cells were plated in glass bottomed dishes coated with concanavalin A. 12 hrs later, cells were stained with Mitotracker Red FM and imaged live at 25°C (scale bars = 5 μm).

5.2.9. Knockdown of *cn* reduces the formation of Parkin-GFP foci upon mitochondrial depolarisation

The genetic epistasis experiments performed in *Drosophila* were not conclusive as to whether KMO might act upstream, downstream or independent of Parkin function; like in *Pink1* mutants, *cn* deletion results in an eclosion phenotype in *parkin* mutants. However, of those that eclosed, a significantly lower proportion of $cn^{3/3}$; $park^{25/25}$ males exhibited the defective thorax phenotype compared to $cn^{+/+}$; $park^{25/25}$. Defective thorax penetrance was also reduced in cn^{RNAi}/*Act5CGAL4*; $park^{25/25}$ flies compared to $park^{25/25}$, however a similar effect was observed in *3M/Act5CGAL4;* $park^{25/25}$, therefore this effect cannot be attributed specifically to *cn* knockdown, rather than a background effect, such as the introduction of the *mini-white* gene in both of these genotypes. Similar effects were also observed in $park^{25/25}$ flies raised on media supplemented with KMO inhibitor Ro 61-8048 or KYNA, therefore unlike in Chapter 3 and Chapter 4, here the influence of KP metabolites cannot be excluded. However, KYNA treatment enhanced lifespan in $park^{25/25}$ flies, whereas *cn* deletion or RNAi knockdown both significantly decreased lifespan.

Whereas both *cn* and *hKMO* overexpression robustly rescued climbing defects and modestly improved lifespan in *Pink1* mutants, here overexpression was sufficient to only extend lifespan in $park^{25}$/*TM6B* heterozygotes, and climbing was improved in *hKMO*, but not *cn* overexpressing flies. Due to the more modest nature of these findings - and to investigate if KMO might play a role in the recruitment of Parkin - the Parkin-GFP recruitment assay (Ivatt *et al.*, 2014), was next employed to test any KMO-related function. The pMK33-Parkin-GFP plasmid used in the original study (Ziviani *et al.*, 2010; Ivatt *et al.*, 2014) was thus transfected into the S2 cell line used in Chapters 3 & 4. Four clonal stable cell lines were selected and imaged live under control conditions or 2 hrs post-treatment with 20 μM CCCP, to promote Parkin-GFP recruitment to mitochondria. The clonal population with the highest level of GFP signal and clearest foci post-CCCP treatment (Figure 5.13) was selected and used for further experiments.

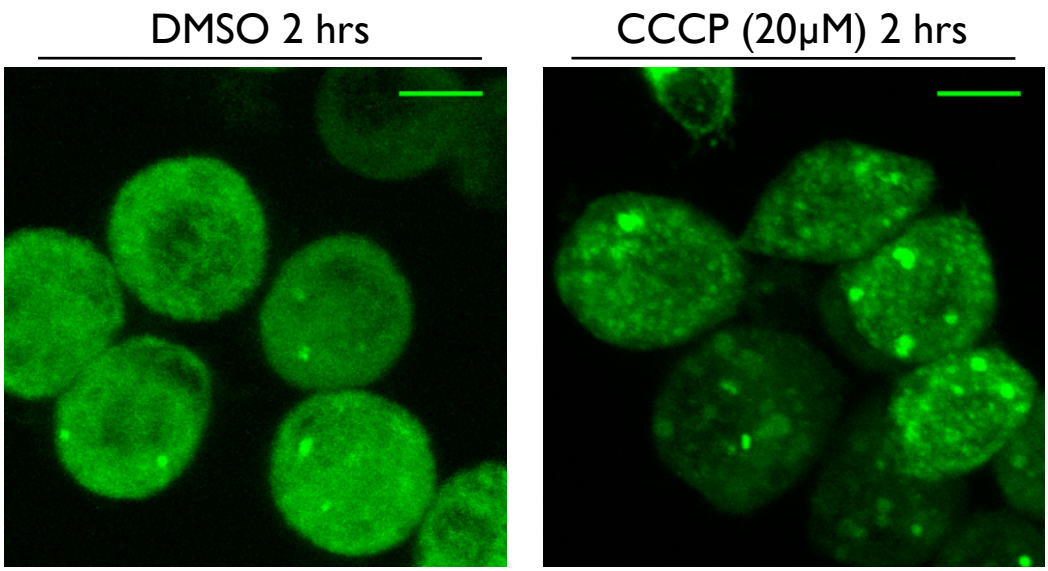

Figure 5.13. Parkin-GFP distribution in stable S2 cell line is cytosolic under control conditions and forms foci upon CCCP treatment.
Cells were seeded 24 hrs before imaging at 2 x 10^5 cells per 35 mm glass-bottomed dish. Parkin-GFP expression under the metallothionein (MT) promoter was induced by treating cells with 500 μM $CuSO_4$. 2 hrs before imaging, cells were treated with DMSO or CCCP (20 μM) and imaged live at 25°C by confocal microscopy. Scale bars = 5 μm.

The *Drosophila* Parkin-GFP expressing cell line was transfected with dsRNA targeting *f.luc, cn,* or *Pink1* 72 hrs before imaging. The knockdown efficiency of *cinnabar* and *Pink1* was ~84% and ~78% respectively (Figure 5.14A). 24 hrs before imaging, cells were re-seeded into 12-well plates and Parkin-GFP expression was induced using 500 μM $CuSO_4$. Cells were counterstained with Hoescht and automatically imaged using the Olympus scanR system. The mean number of GFP foci per cell was detected using dedicated scanR software, with the thresholds to distinguish between background signal and genuine foci optimised by eye. Knockdown of *cn* or *Pink1* had no significant effect on the number of GFP foci in DMSO-treated cells compared to *f.luc* RNAi controls (Figure 5.14B). In CCCP treated cells, the number of foci per cell was significantly higher than in corresponding DMSO controls, in *f.luc, cn* and *Pink1* RNAi treated cells. In CCCP treated cells, the number of foci per cell was significantly lower in *cn* RNAi treated condition than *f.luc* RNAi. However, *Pink1* RNAi, which was employed in this experiment as a positive control for negative regulation of Parkin recruitment, showed no significant difference in GFP foci per cell compared to *f.luc* RNAi cells. In Ivatt *et al.*, (2014),

CCCP treatment resulted in a mean ~4 GFP foci per cell in controls, whereas in this study, mean foci per cell was < 2. I therefore attempted to increase the induction of Parkin-GFP expression by modulating the concentration of $CuSO_4$ used to treat cells. However, this did not make a significant impact on the mean foci observed in DMSO or CCCP conditions in *f.luc* treated cells (Figure 5.15).

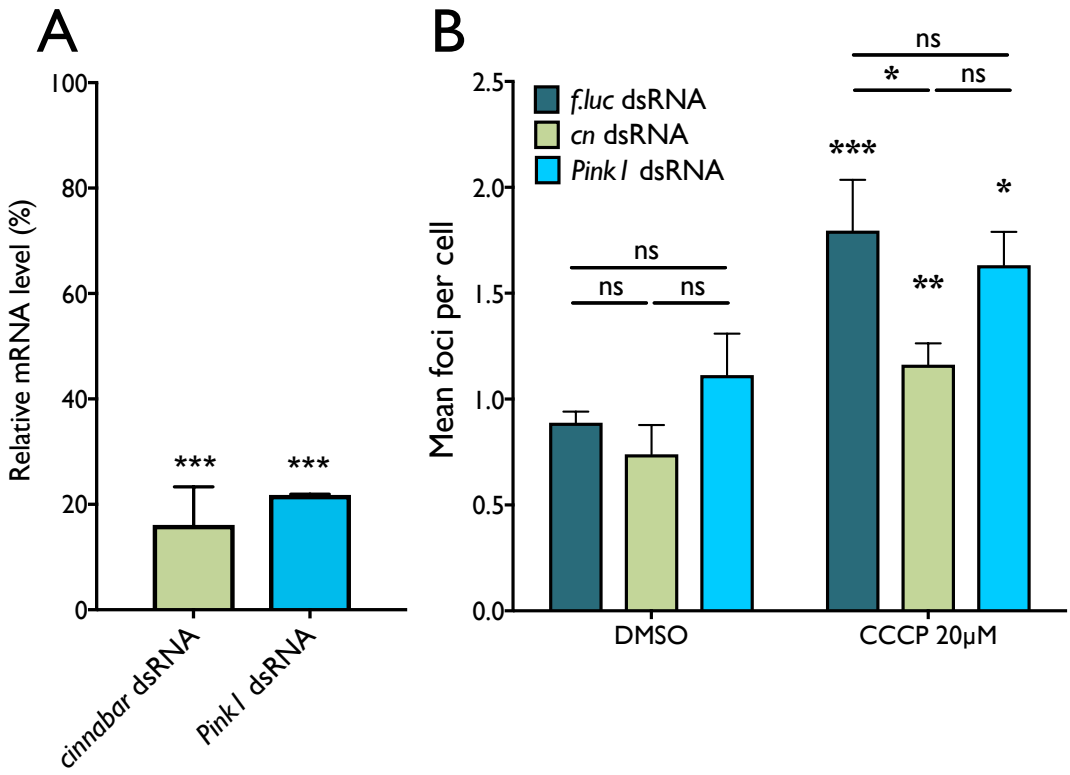

Figure 5.14. *cn* knockdown reduces mitochondrial Parkin-GFP recruitment.
A) Cells were seeded at 1 x 10^6 cells per well of a 6 well plate and transfected with 2 μg of dsRNA targeting either firefly *luciferase* (*f. luc*), *cn* or *Pink1,* using Effectene transfection reagent mix. RNA was extracted 72 hrs post-transfection. Values represent normalised mRNA levels of *cn* or *Pink1* in dsRNA treated cells compared to *f. luc* dsRNA treated controls (mean ± SD; pairwise fixed reallocation randomization test, *** $P < 0.001$, n = 3). **B)** Cells were transfected with dsRNA with Effectene 72 hrs before fixation, as described above. 24 hrs before fixation, cells were reseeded at 5 x 10^4 cells per well of a 24-well plate. Parkin-GFP expression under the metallothionein (MT) promoter was induced by treating cells with 500 μM $CuSO_4$. 2 hrs before fixation, cells were treated with CCCP (20 μM) or DMSO. Cells were fixed with 4 % PFA-PBS for 15 min, then counterstained with Hoescht-PBS. Cells were stored in the dark at 4 °C for ~72 hrs before imaging on the Olympus Scan R microscope (mean ± SD; Two-way ANOVA, Tukey *post hoc*, ns = not significant, * $P < 0.05$. n = 3).

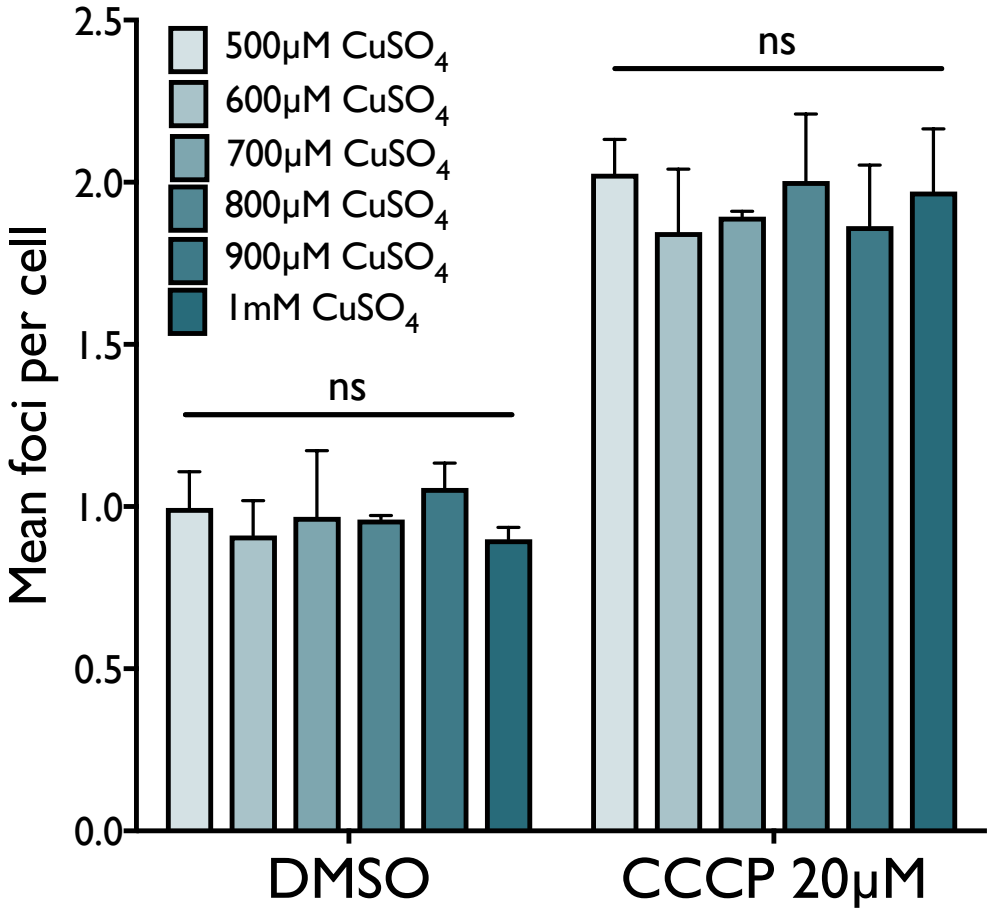

Figure 5.15. Modulation of $CuSO_4$ treatment has no effect on the level of Parkin-GFP foci per cell under control or CCCP conditions.

$CuSO_4$ concentration used to induce Parkin-GFP expression from the MT promoter was increased incrementally within the range that does not impede cell growth (Bunch *et al.*, 1988). Cells were transfected with *f.luc* dsRNA 72 hrs before fixation. 24 hrs before fixation, cells were reseeded at 5 x1 0^4 cells per well of a 24-well plate. Parkin-GFP expression under the metallothionein (MT) promoter was induced by treating cells with 500 – 1000 μM $CuSO_4$. 2 hrs before fixation, cells were treated with CCCP (20μM) or DMSO. Cells were fixed with 4 % PFA-PBS for 15 min, then counterstained with Hoescht-PBS. Cells were stored in the dark at 4°C for ~72 hrs before imaging on the Olympus Scan R microscope (mean ± SD; Two-way ANOVA, Tukey *post hoc*, ns = not significant. n = 2).

5.2.10. Exploring possible physical interactions between KMO and Parkin

Although the lack of effect caused by *Pink1* RNAi treatment leaves some doubt upon the reliability of the assay, *cn* RNAi did lead to a reduction in the number of Parkin-GFP foci formed as a result of CCCP treatment, corroborating the finding of Ivatt *et al.*, (2014). To investigate the possibility that KMO, also localised to the MOM, might play a direct role in Parkin recruitment, I sought to undertake Parkin-GFP immunoprecipitation experiments. Due to a lack of antibodies available that specifically bind *Drosophila* KMO (dKMO), *HA*-tagged *cn* constructs were cloned into the pUAStattB vector. As it was unknown what effect epitope tagging might have on dKMO localization to mitochondria, both N and C-terminus tagged cn clones were generated. Either N or C-terminus tagged cn constructs were transfected into S2 cells alongside an *Act5CGAL4* plasmid. 48 hrs post-transfection, cells were lysed and total protein extracted. Proteins were size-separated by SDS-PAGE and membranes probed with an anti-HA antibody. However, no HA-tagged proteins were detected, despite the antibody specifically detecting HA-Cryptochrome in a control fly-head lysate (Figure 5.16).

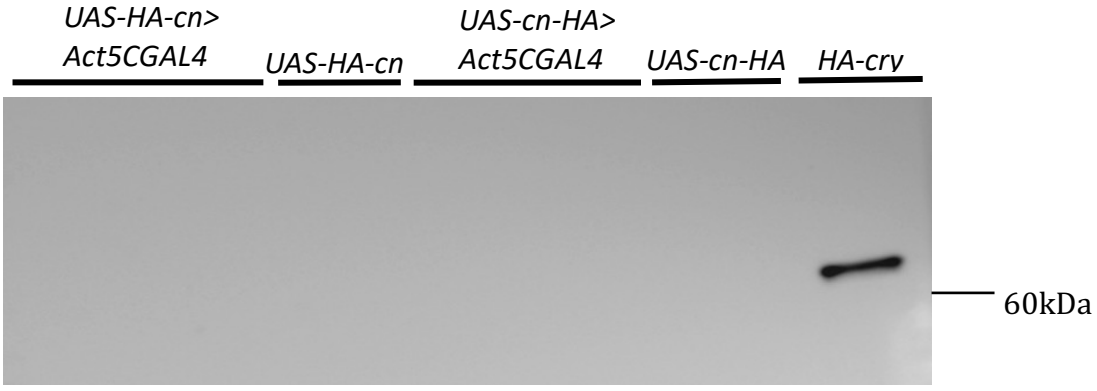

Figure 5.16. *UAS HA-cn* or *cn-HA* constructs are not expressed in S2 cells
Cells were transfected with *UAS HA-cn* or *cn-HA* constructs (1.5 or 1 µg) along with *Act5CGAL4* (0.5 or 1 µg), or *UAS* constructs alone (1.5 µg). 72 hrs post-transfection, cells were lysed and total protein extracted. 20 µg protein (quantified by BCA assay) was size-separated by SDS-PAGE. Total protein extract from the heads of *HA-cry; timGAL4* was used as a positive control for HA epitope recognition. HA was not detected in *HA-cn or cn-HA ; Act5CGAL4* samples.

For this reason, the *pUAStattB-hKMO* plasmid was transfected into S2 cells alongside *Act5CGAL4*. 48 hrs post-transfection, cells were treated with 20 μM CCCP or DMSO for 2 hrs, before lysis with a mild detergent (NP40) buffer. Lysates were incubated with magnetic beads conjugated to an anti-GFP antibody at 4 ^{o}C with gentle rotation. After 2 hrs, beads were isolated and boiled in SDS-buffer along with input lysate and flow-through. Proteins from input, pull-down and flow-through samples were size separated by SDS-PAGE and probed for KMO. KMO was detected in the pull-down fraction of both DMSO and CCCP treated cells - with increased KMO detected in CCCP treated cells - indicating a physical interaction between Parkin-GFP and hKMO (Figure 5.17A). However, the intensity of the KMO band in the pull-down fraction compared to input and flow-through fractions suggests that only a small proportion of total hKMO was associated with Parkin-GFP. This was underlined by probing the same membrane for MARF, a known Parkin interactor. The proportion of MARF in the pull-down fraction compared to input and flow-through fractions was much greater than the proportion of KMO pulled-down (Figure 5.17A), indicating either that the Parkin - KMO interaction is much more transient than Parkin - MARF, or that there is no true interaction and simply the high level of hKMO expression has resulted in a small residual proportion present in the pull-down fraction. However, it should be noted that the increased pull-down of KMO upon CCCP treatment gives an indication that the interaction is real and functional.

To test if a transient interaction between KMO and Parkin-GFP could be stabilised, the experiment was repeated, with cells treated with 1 % PFA to cross-link interacting proteins after 2 hrs treatment with 20μM CCCP or DMSO. Fixation did not affect the proportion of KMO pulled-down with immunoprecipitated Parkin-GFP, which was relatively low, as observed in unfixed cells (Figure 5.17B). Similar to unfixed samples, the quantity of KMO in the pull-down fraction appeared to be greater after CCCP treatment upon fixation as well, indicating that the interaction is enhanced when Parkin translocates to mitochondria.

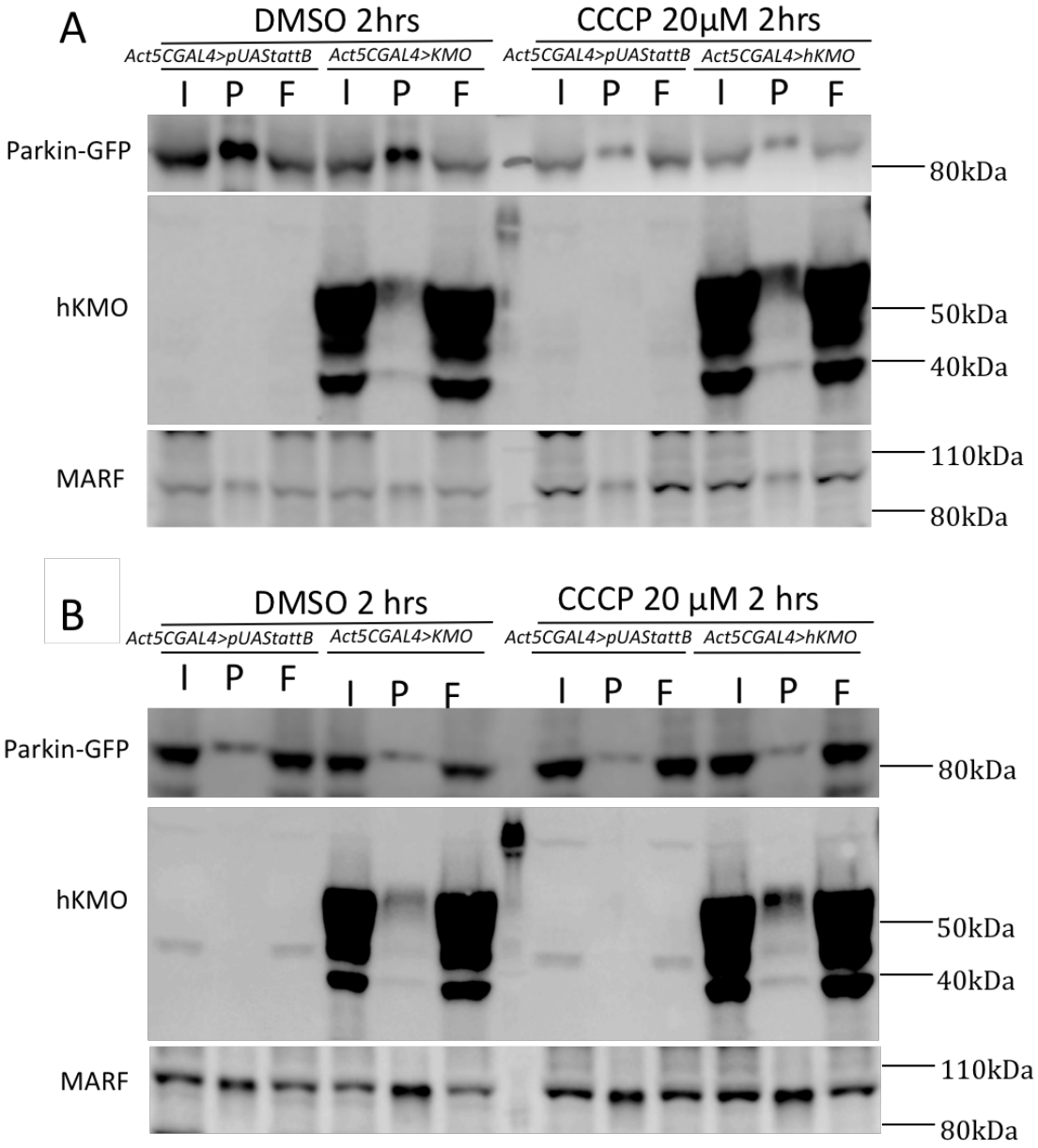

Figure 5.17. hKMO co-immunoprecipitates with Parkin-GFP in *Drosophila S2* cells. Stable dParkin-GFP expressing S2 cells were transfected with empty *pUAStattB* or *pUAStattB-hKMO* plasmids along with *Act5CGAL4*. 48 hrs post-transfection, cells were treated with DMSO or CCCP for 2 hrs. **A)** Unfixed cells were lysed with mild CoIP lysis buffer. **B)** Cells were fixed for 10 mins at RT with 1% PFA to cross-link interacting proteins before lysis with mild CoIP lysis buffer. Parkin-GFP was immunoprecipitated with GFP-Trap magnetic beads for 2 hrs at 4 ^{o}C with gentle rotation. Input, pull-down and flow-through fractions were boiled for 10 min at 95 ^{o}C and separated by SDS-PAGE (10% Tris-glycine gels). Proteins were transferred to nitrocellulose membrane, which was probed with anti-GFP, anti-KMO and anti-MARF antibodies. I = input, P = pull-down, F = flow-through.

To investigate if an interaction between Parkin-GFP and KMO occurs specifically at mitochondria, Parkin-GFP immunoprecipitation was performed with cytosolic and mitochondrial fractions of hKMO overexpressing S2 cells. The proportion of KMO in the mitochondrial Parkin-GFP pull-down fraction compared to input and flow-through fractions was similar between DMSO and CCCP treated cells (Figure 5.18). Although less than that observed in the mitochondrial input fraction, there was also a substantial quantity of KMO in the cytosolic input fraction. Intriguingly, the quantity of KMO in the cytosolic Parkin-GFP pull-down fraction was much greater in CCCP treated cells than in DMSO treated.

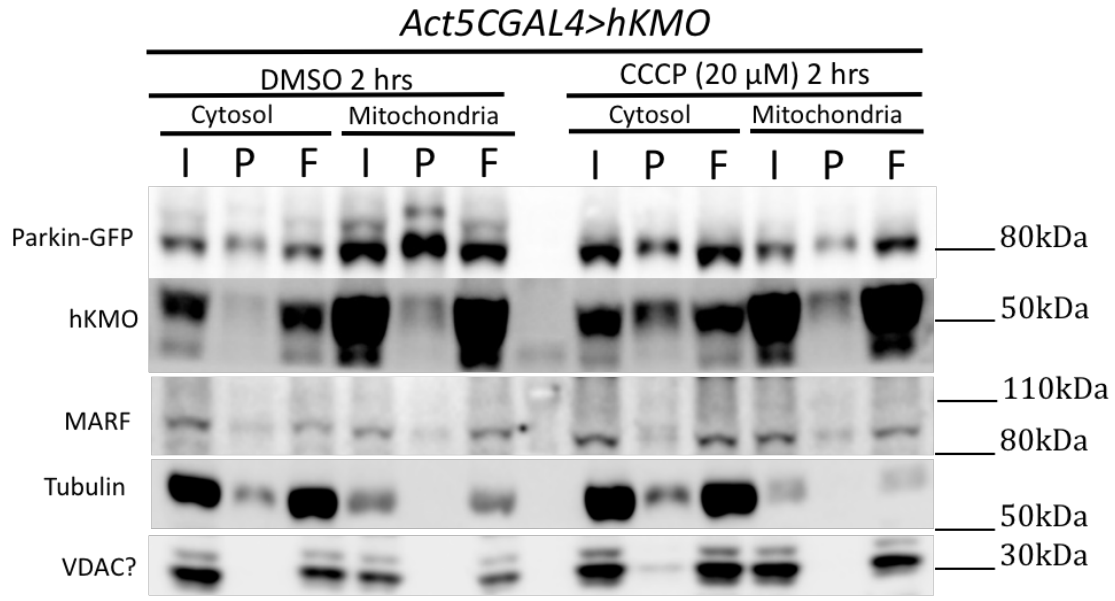

Figure 5.18. Co-immunoprecipitation of Parkin-GFP and hKMO in cytosolic and mitochondrial fractions of S2 cells treated with DMSO or CCCP.
Stable Parkin-GFP expressing S2 cells were transfected with *pUAStattB-hKMO* and *Act5CGAL4* plasmids. 48 hrs post-transfection, cells were treated with DMSO or CCCP (20 µM) for 2 hrs. Cells were pelleted and snap frozen in liquid nitrogen, then thawed at 25 °C for 1 min. Cytosolic and mitochondrial fractions were isolated by lysing cells with a dounce homogeniser, followed by centrifugations according to Mitosciences Mitochondrial Fractionation kit. Protein content of each fraction was quantified by BCA assay and 1.5 mg total protein was used for each immunoprecipitation reaction. Parkin-GFP was immunoprecipitated with GFP-Trap magnetic beads for 2 hrs at 4 °C with gentle rotation. Input, pull-down and flow-through fractions were boiled for 10 min at 95 °C and separated by SDS-PAGE (10% Tris-glycine gels). Proteins were transferred to nitrocellulose membrane, which was probed with anti-GFP, anti-KMO, anti-MARF anti-Tubulin and anti-VDAC antibodies. I = input, P = pull-down, F = flow-through.

An interaction between human Parkin and KMO was also investigated in a mammalian cell model, by transfecting a stable hParkin-YFP expressing HeLa cell line with RFP-hKMO. Cells were treated with DMSO or CCCP for 2 hrs and then fixed with 1% PFA. A band of ~70 kDa was detected in the YFP pull-down fraction, which closely corresponds to the size of RFP-hKMO. However, this band appeared in both empty vector and RFP-KMO transfected cells (Figure 5.19), indicating that it was a non-specific band not corresponding to RFP-KMO.

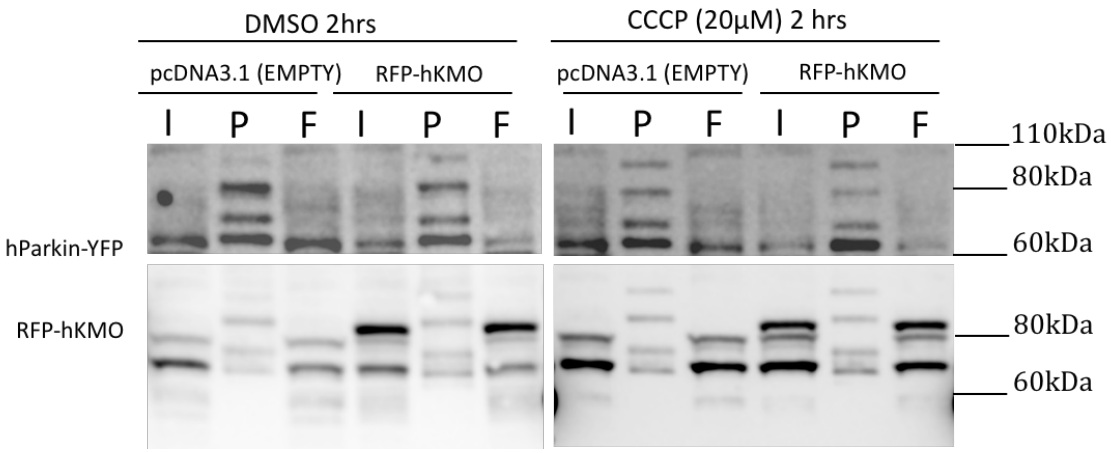

Figure 5.19. hKMO does not co-immunoprecipitate with hParkin-YFP in HeLa cells. Stable hParkin-YFP HeLa cells were transfected with RFP-hKMO using Effectene reagent. 48 hrs post transfection, cells were treated with DMSO or CCCP (20 μM) for 2 hrs. Cells were lysed and Parkin-YFP was pulled down with GFP-trap magnetic beads for 2 hrs at 4 ^{o}C with gentle rotation. Input, pull-down and flow-through fractions were boiled at 95 ^{o}C for 10 mins and separated by SDS-PAGE. Proteins were transferred to nitrocellulose membrane, which was probed with anti-GFP and anti-KMO antibodies. I = input, P = pull-down, F = flow-through.

5.2.11. Testing for changes in Parkin function as a result of KMO modulation

To further investigate whether KMO influences the recruitment of Parkin to depolarised mitochondria, an indirect effect of Parkin recruitment to mitochondria - the ubiquitination and degradation of MARF - was investigated. MARF levels are significantly higher in *Pink1* / *parkin* mutant flies (Poole *et al.*, 2010) and cells treated with *Pink1* / *parkin* dsRNA (Ziviani *et al.*, 2010) due to a lack MARF ubiquitination by mitochondrial-localised Parkin and thereby a reduction in MARF proteasomal degradation. Conversely, overexpression of either *Pink1* or Parkin causes a reduction in MARF compared to wildtype flies (Poole *et al.*, 2010). Investigating whether *cn* knockdown or overexpression could influence MARF levels would give an indication of whether KMO is involved in the recruitment of Parkin to mitochondria. First, MARF levels were assessed in S2 cells in which either *cn* or *parkin* was knocked down by dsRNA. In Chapter 3, silencing of either of these genes led to a more elongated mitochondrial network, therefore one possibility is that both of these effects were caused by a decrease in MARF degradation. Here, knockdown of Parkin caused an increase in MARF levels under basal conditions compared to *f.luc* dsRNA treated cells (Figure 5.20). After treatment with CCCP for 2 hrs, the difference in MARF levels between *parkin* and *f.luc* dsRNA treated cells was more pronounced. Knockdown of *cn* resulted in MARF levels which looked more similar to *f.luc* dsRNA cells than *parkin*. *Marf* dsRNA treated cells were used to ensure that the band interpreted corresponded to MARF.

Given that overexpression of *cn* rescued phenotypes of *Pink1* mutants in Chapter 4, I also assessed whether MARF levels were restored to wildtype levels in *cn* overexpression $Pink1^{B9}$ males. *Pink1B9; 3M; Act5CGAL4* males demonstrated a ~2-fold increase in MARF levels compared to *FM6; 3M; Act5CGAL4* (Figure 5.21), a similar fold-change to that previously observed in Pink1 mutants (Poole *et al.*, 2010). However, *Act5CGAL4*-driven overexpression of *cn* caused no significant difference in MARF levels in *FM6* or $Pink1^{B9}$ flies, indicating that the robust rescue of $Pink1^{B9}$ climbing defects caused by KMO overexpression is not due to the promotion of Parkin recruitment and ubiquitination of MARF.

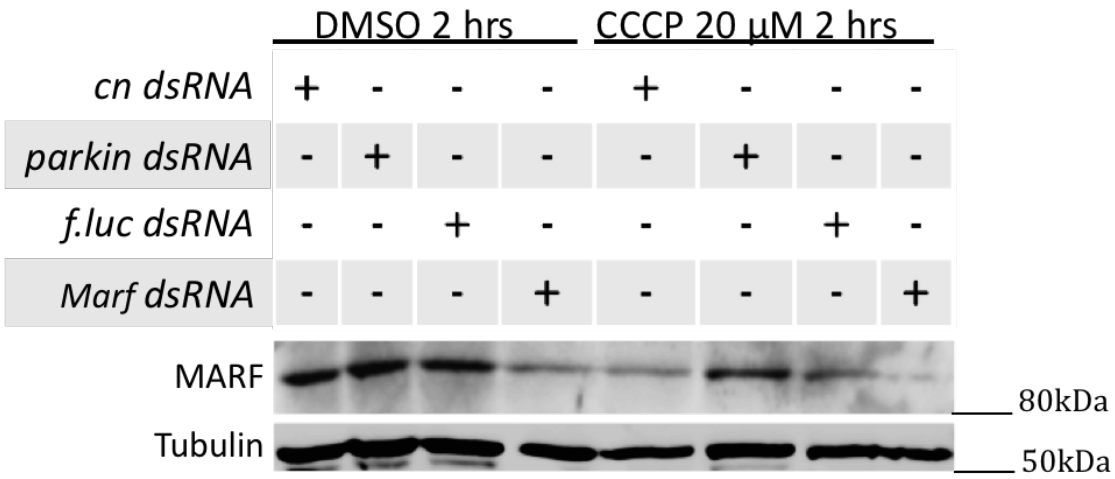

Figure 5.20. MARF levels are unaffected in *cn* knockdown S2 cells.
S2 cells were transfected with dsRNA targeting *cn, parkin, f.luc* or *Marf,* according to the Effectene protocol established in Chapter 3. 72 hrs post-transfection, cells were treated with DMSO or CCCP (20 µM) for 2 hrs. Cells were then pelleted and lysed in RIPA buffer with protease inhibitors. Total protein was quantified by BCA assay. 20 µg was loaded onto Tris-glycine gel and size separated by SDS-PAGE. Proteins were transferred to nitrocellulose membrane and probed for MARF and Tubulin.

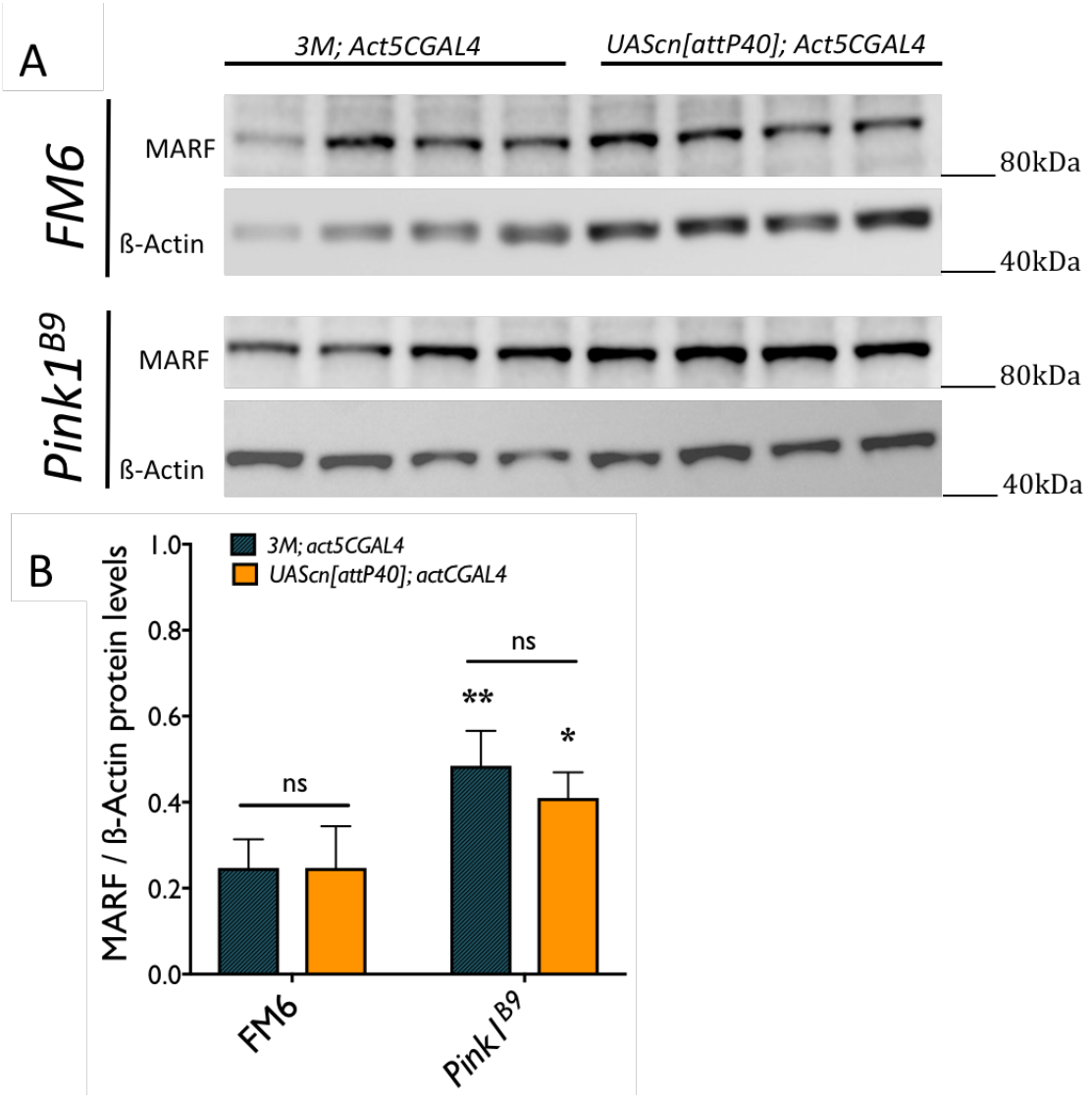

Figure 5.21. MARF levels are unaffected by *cn* overexpression in wildtype or *Pink1* mutant flies.

Day 7 flies (10 per n) were snap frozen and homogenised in RIPA buffer with protease inhibitors. Lysates were centrifuged at 13,000 g for 15 min at 4 °C to remove insoluble debris. Protein concentration of the supernatant was quantified by BCA assay. 20 µg protein was boiled at 95 °C in Laemmli buffer for 10 min and separated by SDS-PAGE (10 % Tris-glycine gel). **A)** Immunoblot of MARF and ß-Actin in *FM6* and *Pink1*^{B9} males (Day 7), with *Act5CGAL4* driven *UAScn* expression. **B)** Quantification of MARF levels in relation to ß-Actin, by densitometry of immunoblot bands (Two way ANOVA, Tukey *post hoc*, * $P < 0.05$, ** $P < 0.01$, ns = not significant, n = 4).

5.3. Discussion

Given the functional interaction between KMO and PINK1 detailed in Chapter 4, the aim of this chapter was to identify whether KMO plays a role upstream, downstream or independent of Parkin. Given the finding of Ivatt *et al.*, (2014) that *cn* knockdown negatively affects the recruitment of Parkin to mitochondria in S2 cells, the more likely hypothesis was that KMO acts upstream of Parkin in mitophagy. Firstly, genetic epistasis experiments similar to those performed in Chapter 4 were employed to assess the relationship between KMO and Parkin. Many of the results of these epistasis experiments mirrored those of Chapter 4: cn^{3} homozygosity induced an eclosion defect in $park^{25/25}$ males, whereas cn^{3}/CyO or $cn^{RNAi}/Act5CGAL4$; $park^{25/25}$ males eclosed at Mendelian frequencies. As discussed in Chapter 4 in relation to *Pink1*, synthetic lethality has also been previously observed in *parkin* mutant flies when a dominant-negative *Drp1* allele was introduced (Poole *et al.*, 2008). The current understanding of the relationship between DRP1 and Parkin is that DRP1 segregates damaged fragments of mitochondria from the mitochondrial network, which prevents the positive-feedback loop of Parkin recruitment and activation from ubiquitinating healthy fragments of mitochondria, which would lead to their unnecessary clearance (Burman *et al.*, 2017). However, this does not explain why loss of DRP1 function in a *parkin*-null background is detrimental to flies and how DRP1 overexpression can rescue *parkin*-null phenotypes (Deng *et al.*, 2008; Burman *et al.*, 2012). These effects may be linked instead to the elongated mitochondria observed in *parkin* mutant flies, thought to be due to the lack of degradation of MARF (Shiba-Fukushima *et al.*, 2014). As loss of KMO also causes elongated mitochondria (Chapter 3), the exacerbation of the mitochondrial morphology phenotype in *parkin* mutants could be the cause of the eclosion phenotype observed in $cn^{3}; park^{25}$ flies.

Deletion or knockdown of *cn* also modulated the defective thorax phenotype in $park^{25/25}$ flies, but the effect was opposite to that observed in $Pink1^{B9}$ flies. Both $cn^{3/3}$ and cn^{3}/CyO flies showed a decrease in the penetrance of the phenotype compared to $cn^{+/+}$. The reduction in eclosion of $cn^{3/3}; park^{25/25}$ flies could mean that those that did eclose are more resistant to *parkin* pathology, and this might explain why fewer

exhibit the defective thorax phenotype than *cn*$^{+/+}$; *park*$^{25/25}$ flies, which have no eclosion phenotype. However, *cn*^{3}*/CyO; park*$^{25/25}$ flies eclosed at the expected frequency in proportion to *cn*^{3}*/CyO; park*^{25}*/TM6B* and still showed a significant reduction in penetrance of defective thorax, suggesting that the effect is due to a reduction in KMO. A similar effect on penetrance of the phenotype was also observed in *cn*^{RNAi}*/Act5CGAL4; park*$^{25/25}$ flies, however it was also observed in *3M/Act5CGAL4*; *park*$^{25/25}$ controls and thus can't be attributed with certainty to *cn* knockdown. The cause of the reduction in penetrance in *3M/Act5CGAL4*; *park*$^{25/25}$ flies could be due to the introduction of the *mini-white (mw)* gene, which acts as a visible marker in the pMF3 vector used to generate the kk RNAi library (Dietzl *et al.*, 2007). The *white (w)* gene encodes an ABC-transporter subunit which is responsible for the translocation of a number of important substrates, including the KP metabolites tryptophan (Sullivan *et al.*, 1980), kynurenine (Sullivan and Sullivan, 1975) and 3-HK (Howells *et al.*, 1977). Flies carrying the loss of function *w*^{1118} allele show increased sensitivity to stress and an age-associated decrease in locomotion compared to *w*$^{+}$ flies (Ferreiro *et al.*, 2018), therefore the introduction of *mw* into *w*; *park*$^{25/25}$ flies could be responsible for conveying protection against the defective thorax phenotype. However, in *Pink1*^{B9} flies, introduction of *mw* in *3M; Act5CGAL4* flies had no significant effect on penetrance of defective thorax, and *cn*^{RNAi}*; Act5CGAL4* flies showed an increase in penetrance. Why *mw* might potentially cause protection in *parkin* but not *Pink1* mutants is unclear.

Given that either supplementing *parkin* mutants with KYNA or inhibiting KMO enzymatic activity via the KMO inhibitor Ro 61-8048 resulted in decreased penetrance of defective thorax, the effect observed in *cn*$^{3/3}$*; park*$^{25/25}$ and *cn*^{3}*/CyO; park*$^{25/25}$ flies could be due to a reduction in KMO enzymatic activity, and thereby a decrease in the production of 3-HK and an increase in the conversion of KYN to KYNA by KATs. KYNA supplementation also increased the lifespan of *park*^{25} homozygotes but did not affect heterozygotes. A screen for genetic modifiers of viability in *parkin* mutant flies has implicated oxidative stress response in *parkin* pathology (Greene *et al.*, 2005). Furthermore, overexpression of the antioxidant superoxide dismutases (SOD1 or SOD2) rescued *Pink1* and *parkin* in both flies and mammalian cells (Biosa *et al.*, 2018). Given the antioxidant properties of KYNA

within a particular concentration range (Lugo-Huitrón *et al.*, 2011), the protection conveyed by KYNA could be due to a reduction in ROS. Longevity was significantly reduced in $cn^{3/3}$; $park^{25/25}$ and cn^{RNAi}; *Act5CGAL4* flies, which might indicate that any beneficial effect of raised KYNA on lifespan is overcome by an additional cost of loss of KMO, or that KYNA levels are increased in cn^{3} or cn^{RNAi} flies beyond a level that is protective and may have toxic consequences.

Act5CGAL4-driven overexpression of *cn* or *hKMO* did not affect the eclosion of $park^{25}$ homozygotes, but *hKMO* did cause a significant increase in the penetrance of the defective thorax phenotype compared to *3M/Act5CGAL4*; $park^{25/25}$. A similar but not significant effect was also observed in flies overexpressing *cn* from the *attp40*, but not *attP51C* site. This could be due to an increase in the production of 3-HK, which can increase the generation of ROS (Okuda *et al.*, 1998). Conversely however, *hKMO* overexpression conveyed a small but significant improvement in the climbing performance of $park^{25}$ homozygotes, whereas overexpression of *cn* from either landing site did not. Overexpression of *cn* from both landing sites and *hKMO* significantly increased lifespan in $park^{25}$ heterozygotes but not homozygotes. Overexpression of *cn* also appeared to rescue elongated mitochondrial morphology in *parkin* knockdown S2 cells.

Although epistasis experiments indicate a link between KMO and Parkin, they did not clarify how the two might interact. I therefore sought to replicate the Parkin-GFP mitochondrial recruitment assay employed by Ivatt *et al.*, (2014) in which *cn* knockdown inhibited Parkin-GFP foci formation upon CCCP or paraquat treatment. Here, a significant reduction in Parkin-GFP foci upon CCCP treatment in *cn* knockdown cells was observed, however *Pink1* knockdown which was employed as a positive control, had no effect on the formation of Parkin-GFP foci, despite ~80% knockdown efficiency of both *cn* and *Pink1.* This makes these data difficult to interpret, as PINK1 is known to recruit Parkin to mitochondria (Ziviani *et al.*, 2010). However, Parkin overexpression is sufficient to rescue *Pink1* mutant flies, indicating that PINK1 is not essential for Parkin function in *Drosophila* (Clark *et al.*, 2006; Park *et al.*, 2006; Yang *et al.*, 2006; Shiba-Fukushima *et al.*, 2014). *Pink1* knockdown was previously shown to reduce Parkin-GFP recruitment to mitochondria (Ziviani *et al.*,

2010, Ivatt *et al.*, 2014). I thus attempted to enhance Parkin-GFP expression by increasing the concentration of copper sulphate used to induce expression from the MT promoter, in the hope that the number of foci per cell would increase upon CCCP treatment and therefore any reduction caused by *Pink1* knockdown might be magnified. However, no concentration of $CuSO_4$ within the tolerable range (Bunch *et al.*, 1988) enhanced the number of foci per control dsRNA cell, in DMSO or CCCP conditions. This assay could be pursued further in the future by selecting another positive control to use, from the ~70 genes identified by Ivatt *et al.*, (2014) as positive regulators of Parkin recruitment to mitochondria.

To investigate if a physical interaction might occur between MOM localised KMO and Parkin upon its recruitment to mitochondria, Parkin-GFP was immunoprecipitated from S2 cells under both control and CCCP-treated conditions. Notably, KMO was detected in pull-down fractions in both untreated and CCCP treated samples. The proportion compared to input and flow-through fractions was small, however, when compared to the proportion of MARF, a known Parkin interactor, that was pulled-down. Although the quantity of KMO pulled-down was not enhanced by chemical fixation, CCCP treatment did appear to have a positive effect – suggesting a functional relationship between these potential interaction partners. Upon separation of cytosolic and mitochondrial fractions, it was revealed that although enriched in mitochondrial fractions, KMO was also present in the cytosol, and that upon CCCP treatment more KMO was present in the cytosolic pull-down fraction than mitochondrial fraction. It is unclear why cytosolic KMO was more readily pulled-down with Parkin-GFP than mitochondrial KMO and also unclear why this occurred only in CCCP treated cells, when this treatment should cause mitochondrial translocation of Parkin. In HeLa cells, no RFP-KMO was pulled-down with Parkin-YFP, and so I was unable to further confirm my finding in S2 cells in a mammalian system. Nonetheless, given the findings both in this chapter and by Ivatt *et al.*, (2014) that *cn* knockdown reduces the mitochondrial translocation of Parkin-GFP, the influence of KMO over MARF levels - which is regulated by Parkin - was investigated. If *cn* knockdown reduces mitochondrial-localised Parkin, MARF levels should increase as a consequence, as they do in *parkin* mutant flies and knockdown cells. However, *cn* knockdown had no effect on MARF levels in S2 cells and

overexpression of *cn* did not restore MARF to wildtype levels in *Pink1* mutant flies, indicating that KMO does not influence MARF levels and thus Parkin ubiquitin ligase function at the MOM. This would suggest that the rescue achieved by overexpression of *cn* or *hKMO* in *Pink1* mutant flies and knockdown cells is due to a function of KMO downstream or in parallel with Parkin function.

5.4. Conclusions

Whether KMO acts downstream or independently from Parkin is difficult to conclude from the findings of this chapter; *cn* deletion resulted in a decrease in viability of *parkin* mutant flies, whereas overexpression of *cn* or *hKMO* extended the lifespan of $park^{25}$ heterozygotes but not homozygotes. Overexpression of *hKMO* but not *cn* improved climbing performance in *parkin* mutants, however this was considerably less robust than the rescue of *Pink1* mutants by *cn* or *hKMO* overexpression. A climbing defect caused by overexpression of *Parkin* was reversed by *cn* deletion and *cn* overexpression did appear to alter mitochondrial morphology in *parkin* knockdown but not control dsRNA cells. Although hKMO was pulled down with dParkin-GFP in S2 cells, the finding was not replicated in HeLa cells with hParkin-YFP. Furthermore, *cn* modulation did not affect MARF levels in S2 cells or in flies, indicating that KMO does not affect Parkin E3 ubiquitin ligase function at the MOM. Together, these results indicate that although KMO and Parkin might functionally interact, KMO does not appear to directly affect the role of Parkin at the MOM. Any interaction is likely to come therefore through KMO modulation of mitochondrial dynamics, independently from Parkin-mediated mitophagy.

6. Investigating the interplay between KMO and DRP1 in mitochondrial dynamics

6.1. Introduction

The elongated mitochondria observed in *cn* deficient flies and cells in Chapter 3, as well as by Ivatt *et al.*, (2014), indicates that KMO likely plays a direct role in mitochondrial dynamics. Furthermore, loss of *cn* reduces the viability of *Pink1* and *parkin* mutant flies, whereas overexpression of *cn* or *hKMO* is protective. As overexpression of *cn* did not restore MARF levels in Pink1 mutant flies, it appears more likely that KMO positively regulates mitochondrial fission than negatively regulates fusion. DRP1, which is primarily responsible for mitochondrial fission, has been strongly linked to PINK1 and Parkin function, particularly in *Drosophila*, and thus is a potential candidate for KMO action. Introduction of a dominant-negative *Drp1* transgene or heterozygous *Drp1* LOF causes synthetic lethality in *Pink1* and *parkin* deficient flies (Poole *et al.*, 2008; Fernandes & Rao, 2011). Furthermore, *Drp1* overexpression has rescued phenotypes in both *Pink1* and *parkin* mutant flies (Poole *et al.*, 2008; Deng *et al.*, 2008, Yang *et al.*, 2008; Park *et al.*, 2009). This is presumably due to DRP1 counterbalancing the increase in MARF levels caused by PINK1/Parkin loss. A dominant-negative *Drp1* allele restores mitochondrial morphology in Mfn2 deficient mouse embryonic fibroblasts (Chen *et al.*, 2003) and *Drp1* knockdown also improves viability of *Marf* knockdown flies (Trevisan *et al.*, 2018), demonstrating that mitochondrial morphology is maintained by retaining a balance in fission and fusion events, and that this is essential to viability.

DRP1 activity is governed by a number of post-translational modifications, including phosphorylation, ubiquitination, SUMOylation, S-nitrosylation and O-GlcNAcylation (Chang & Blackstone, 2010). Phosphorylation occurs at two distinct and highly conserved residues (Figure 6.1) Phosphorylation of hDRP1 Ser616 by CDK1/cyclin B occurs prior to mitotic cell division and causes an increase in DRP1-mediated mitochondrial fission (Taguchi *et al.*, 2007). However, phosphorylation at hDRP1 Ser637 by PKA causes a decrease in DRP1 GTPase activity and/or recruitment of

DRP1 to mitochondria, resulting in a decrease in mitochondrial fission (Chang & Blackstone, 2007; Cribbs & Strack, 2007). This site can also be phosphorylated by CaMKIα, although this was shown to have the opposite effect on mitochondrial fission (Han *et al.*, 2008). Phosphorylation at this site is also regulated through the phosphatase calcineurin, which removes phosphate groups from this residue and stimulates DRP1 translocation to mitochondria (Cereghetti *et al.*, 2008). PINK1 regulates this phosphorylation site via phosphorylation of AKAP1, resulting in untethering of PKA from mitochondria and therefore a decrease in mitochondrial Drp1 phosphorylated at the Ser637 residue (Pryde *et al.*, 2016).

To investigate a potential role for KMO in mitochondrial fission, genetic and functional interactions between KMO and DRP1 were explored in this chapter. Genetic epistasis experiments were performed in *Drosophila*, to assess the influence of *cn* on the viability of *Drp1* and *Marf* knockdown flies, as well as the effect of DRP1 overexpression on *cn* mitochondrial phenotypes. Mammalian cells were employed to assess the potential role of KMO on DRP1 post-translational modifications.

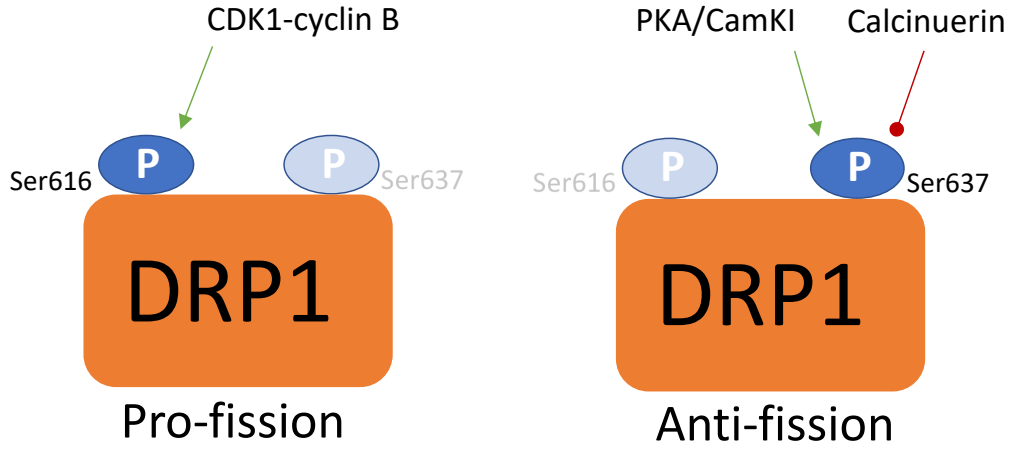

Figure 6.1. Phosphorylation of two highly conserved sites modulate DRP1 activity

DRP1 is phosphorylated at two Serine/Threonine residues which are conserved between flies and humans. Phosphorylation of hDRP1 Ser616 by CDK1/cyclin B occurs prior to mitosis, promoting mitochondrial fission, whereas phosphorylation of the Ser637 residue by PKA inhibits fission. Alignment between human and *Drosophila* DRP1 amino acid sequences was performed using Clustal X software.

6.2. Results

6.2.1. *Drp1* overexpression modulates climbing phenotype and mitochondrial morphology in *cn* flies

Given the ability of DRP1 to suppress phenotypes in *Pink1* and *parkin* mutants and the functional overlap between KMO and PINK1/Parkin, *Drp1* was overexpressed in cn^{RNAi}*; Act5CGAL4* flies to assess if the climbing defect observed in Chapter 3 could be rescued. *Drp1* was overexpressed via two strategies; firstly a *UASDrp1* construct (Bellen, 2013) was driven by *Act5CGAL4* in *cn* knockdown flies and 3M controls. However, this resulted in a significant decrease in climbing performance of both cn^{RNAi} and control flies at all ages assayed (7 – 28 days, Figure 6.2A). This is likely due to strong *Drp1* overexpression leading to excessive mitochondrial fission. *Drp1* was next overexpressed by introducing a *FLAG-FlAsH-HA-Drp1* (*FLAG-Drp1*) construct under its control of *Drp1* endogenous promoter (Verstreken *et al.*, 2005), essentially upregulating *Drp1* expression by 50 %, which is much milder than overexpression of a *UASDrp1* construct (DuBoff *et al.*, 2012). The *FLAG-Drp1* construct was previously used to rescue *Pink1* mutant flies (Poole *et al.*, 2008; Yang *et al.*, 2008). Introduction of this transgene into *3M; Act5CGAL4* flies significantly decreased climbing performance at all ages assayed (7 - 35 days, Figure 6.2B), however in cn^{RNAi} flies, it significantly improved climbing performance at ages 14 - 28 days. In comparison to *3M; FLAG-Drp1/Act5CGAL4* flies, cn^{RNAi}*; FLAG-Drp1/Act5CGAL4* flies climbed better at all ages assayed (7 - 35 days). Introduction of the transgenic *Drp1* allele in cn^{3} flies also improved climbing performance of cn^{3} flies from ages 7-28 days (Figure 6.3).

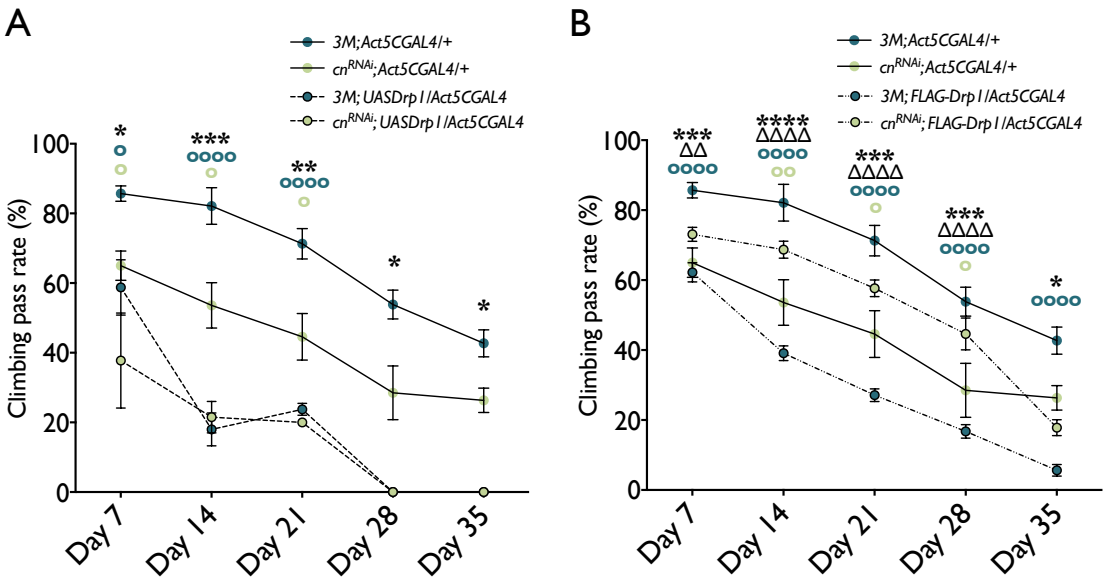

Figure 6.2. Overexpression of *Drp1* modulates the climbing phenotype of *cn* knockdown flies.

A) Overexpression of *UASDrp1* driven by the *Act5CGAL4* driver. Mean ± SEM, Two way ANOVA, Tukey *post hoc,* * $P<0.05$; ** $P< 0.01$; *** $P<0.001$; **** $P<0.0001$. * = *P* value *3M; Act5CGAL4/+* compared to *cn; Act5CGAL4/+.* o = *P* value *3M; Act5CGAL4/+* compared to *3M; Act5CGAL4/UASDrp1*; o = *P* value cn^{RNAi}*; Act5CGAL4/+* compared to cn^{RNAi}*; Act5CGAL4/UASDrp1.* n = 6 - 10 (10 flies per n).

B) Overexpression of *Drp1* by addition of *FLAG-Drp1* transgene under control of its endogenous promoter. Mean ± SEM, two way ANOVA, Tukey *post hoc,* * $P<0.05$; ** $P < 0.01$; *** $P <0.001$; **** $P <0.0001$. * = *P value 3M; Act5CGAL4/+* vs *cn; Act5CGAL4/+.* Δ = *P*value *3M; Act5CGAL4/FLAG-Drp1* vs cn^{RNAi}*; Act5CGAL4/FLAG-Drp1.* o = *P* value *3M; Act5CGAL4/+* vs *3M; Act5CGAL4/FLAG-Drp1.* o = *P* value cn^{RNAi}*; Act5CGAL4/+* vs cn^{RNAi}*; Act5CGAL4/FLAG-Drp1.* n = 8-10 (10 flies per n).

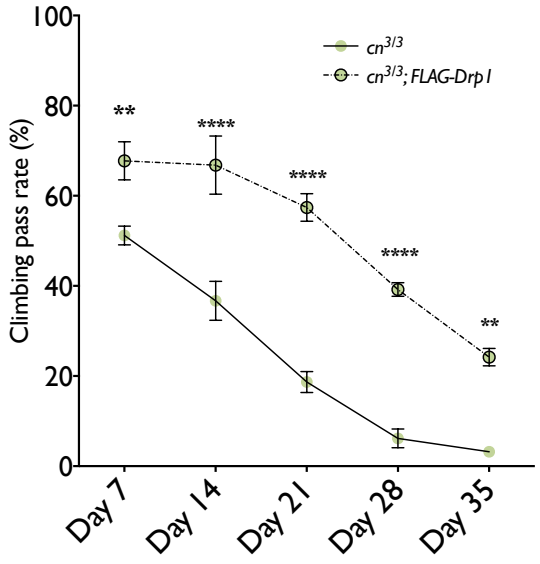

Figure 6.3. Overexpression of *Drp1* via the *FLAG-Drp1* transgene improves climbing ability in *cn³* flies.
The *FLAG-Drp1* transgene, under control of the endogenous *Drp1* promoter, was introduced into $cn^{3/3}$ flies. Climbing ability was assessed in flies aged 7 – 35 days (mean ± SEM, Two-way ANOVA, Tukey *post hoc*, * $P < 0.05$, ** $P < 0.01$, *** $P < 0.001$, **** $P < 0.0001$. n = 5 – 10, 10 flies per n).

To investigate if this locomotor improvement correlated with a change in mitochondrial morphology, eye tissue of $cn^{3/3}$; + and $cn^{3/3}$; *FLAG-Drp1* flies was assessed by TEM (Figure 6.4A & B). Overexpression of *Drp1* resulted in an increase in aspect ratio, form factor and Feret's diameter, indicating an increase in elongated and branched mitochondria (Figure 6.4C, D & E). Though this is the opposite of the hypothesised outcome given DRP1 function as mediator of mitochondrial fission, it nonetheless suggests an interplay between these proteins in mitochondrial dynamics. Notably, $cn^{3/3}$; *FLAG-Drp1* flies exhibited a significant decrease in total mitochondrial area compared to $cn^{3/3}$ flies (Figure 6.4F), suggesting that an increase in DRP1 could facilitate mitochondrial clearance in $cn^{3/3}$ flies leading to a normalization of mass.

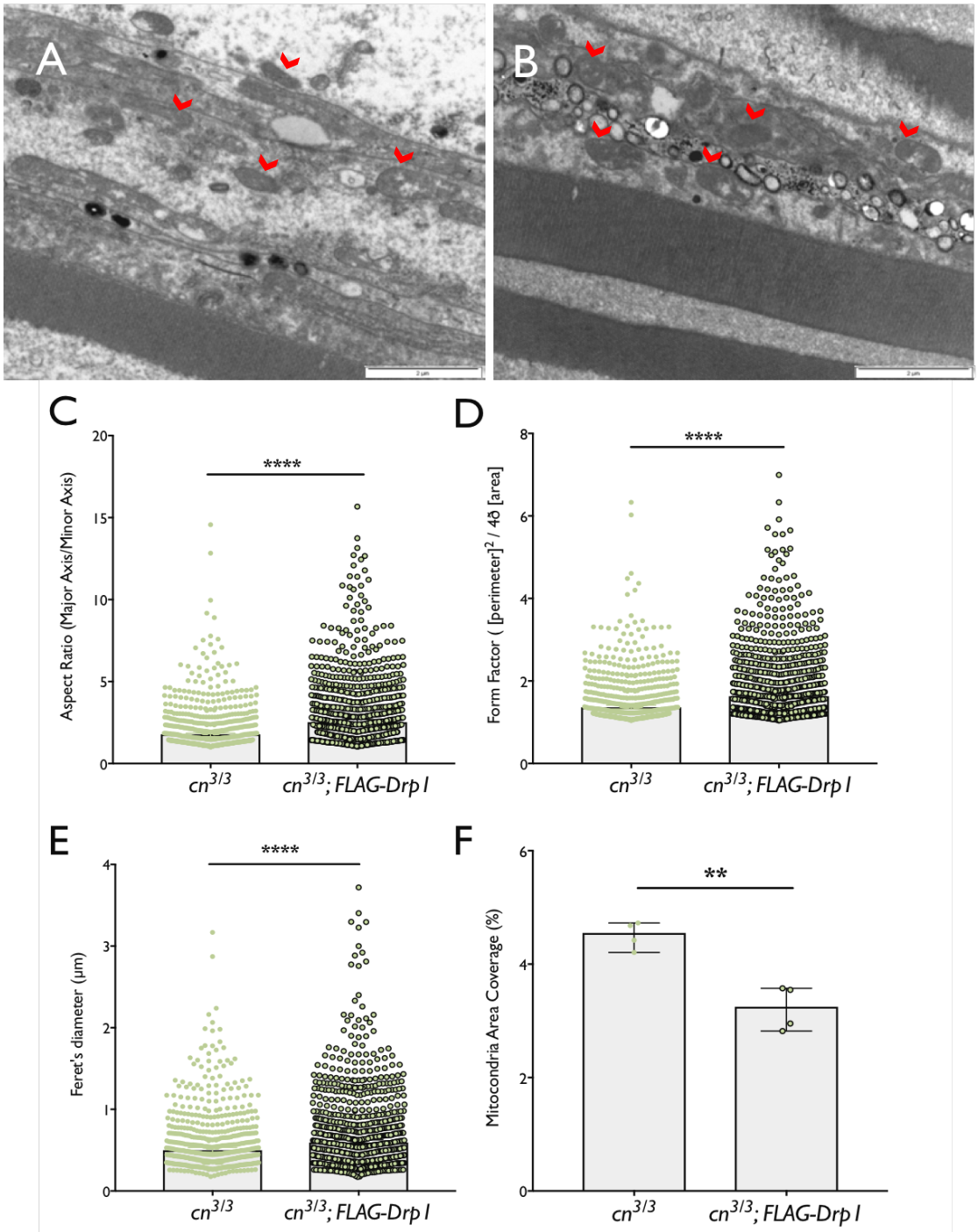

Figure 6.4. Mitochondria are more elongated and branched in *cn$^{3/3}$; FLAG-Drp1* flies compared to *cn$^{3/3}$*, but mitochondrial area coverage is decreased.

A & B) Longitudinal sections from the eye of newly eclosed *cn$^{3/3}$* **(A)** and *cn$^{3/3}$; FLAG-Drp1* **(B)** flies. Mitochondria are labelled by red arrowheads. **C)** Aspect ratio of traced mitochondria (median ± 95 % CI, Mann-Whitney test, **** $P < 0.0001$). **D)** Form factor of traced mitochondria (median ± 95 % CI, Mann-Whitney test, **** $P < 0.0001$, n= 4, >500 mitochondria analysed per group). **E)** Feret's diameter of traced mitochondria (median ± 95 % CI, Mann-Whitney test, **** $P < 0.0001$, n= 4, >500 mitochondria analysed per group). **F)** Aspect ratio of traced mitochondria (median ± 95 % CI, Mann Whitney test, **** $P < 0.0001$, n = 4, >500 mitochondria analysed

per group). **E)** % Area coverage of traced mitochondria (mean ± SD, t test, ** P <0.01, n= 4).

6.2.2. *cn* modulation does not affect viability of *Drp1* or *Marf* knockdown flies

The climbing defect in *3M; Act5CGAL4/FLAG-Drp1* flies is presumably due to an imbalance in mitochondrial dynamics. Knockdown of *cn* ameliorated the climbing defect indicating that loss of KMO likely negatively regulates Drp1 expression or function. *Drp1* RNAi has been used to increase the viability, respiratory capacity and ATP production of *Marf* RNAi flies (Trevisan *et al.*, 2018). To investigate if *cn* knockdown could have a similar effect on $Marf^{RNAi}$ flies, *3M; Act5CGAL4* and cn^{RNAi}; *Act5CGAL4* flies were crossed to $Marf^{RNAi}$ flies. However, these crosses gave rise to two 3M/$Marf^{RNAi}$ and four $cn^{RNAi}/Marf^{RNAi}$ flies of the >200 progeny counted over 10 days, indicating that ubiquitous *Marf* knockdown is developmental lethal and *cn* knockdown does not achieve the same robust protective effect observed upon *Drp1* knockdown (Figure 6.5A). *Drp1* loss of function mutations are recessive lethal in *Drosophila* (Littleton & Bellen, 1994) and RNAi driven by the *Mef2GAL4* driver is also lethal (Schnorrer *et al.*, 2010). Given that *cn* knockdown ameliorated the climbing defect of *Drp1* overexpressing flies, I next investigated whether *cn* overexpression could rescue lethality in *Drp1 RNAi* flies. *3M/3M; Act5CGAL4/TM6B* and *UAScn[attP40]/UAScn[attP40]; Act5CGAL4/TM6B* flies were crossed to $Drp1^{RNAi}$/$Drp1^{RNAi}$ flies. No *Act5CGAL4* carrying progeny emerged from either cross, indicating that ubiquitous *Drp1* knockdown is lethal and cannot be rescued by *cn* overexpression (Figure 6.5B).

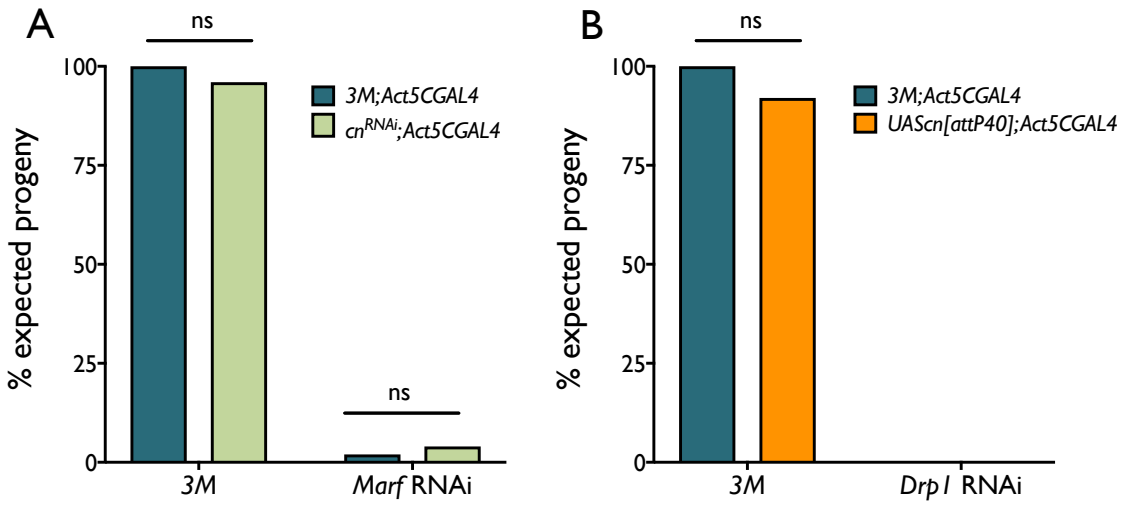

Figure 6.5. Eclosion of *Marf* RNAi flies is unaffected by *cn* knockdown.
A) *3M/3M; Act5CGAL4/TM6B* or cn^{RNAi}/cn^{RNAi}*; Act5CGAL4/TM6B* male flies were crossed to *3M/3M* or $Marf^{RNAi}/Marf^{RNAi}$ virgin females. **B)** *3M/3M; Act5CGAL4/TM6B* or *UAScn[attP40]/UAScn[attP40]; Act5CGAL4/TM6B* male flies were crossed to *3M/3M* or $Drp1^{RNAi}/Drp1^{RNAi}$ virgin females. The expected proportion of *Act5CGAL4* : *TM6B* carrying progeny was 1 : 1. > 200 progeny per cross were counted over 10 days post eclosion (χ^2 test, 1 d.f, ns = not significant).

6.2.2. Overexpression of KMO modulates mitochondrial DRP1 phosphorylation status in HEK293 cells

Given that knockdown of *cn* protected against *Drp1* upregulation (Figure 6.2), but *cn* overexpression did not rescue *Drp1* knockdown (Figure 6.5), it appears that KMO modulation of mitochondrial dynamics is dependent on the presence of DRP1 and therefore it is possible that KMO might regulate the activity of DRP1. DRP1 activity is regulated by a number of post-translational modifications including phosphorylation. To investigate if KMO might influence post-translational regulation of DRP1, KMO was overexpressed in HEK293 cells. Cells were treated with DMSO or CCCP, which causes mitochondrial depolarisation and is expected to cause a decrease in DRP1 Ser637 phosphorylation and an increase in mitochondrial DRP1 translocation (Cereghetti *et al.*, 2008; Losón *et al.*, 2008, Otera *et al.*, 2016). Cells lysates were separated into cytosolic and mitochondrial fractions, which were size separated by SDS-PAGE. Immunoblotting with anti-GAPDH (cytosolic marker) and anti-VDAC1 (mitochondrial marker) revealed the high purity of these fractions (Figure 6.6A) As expected, no KMO was detected in pcDNA3.1 vector transfected cells, whereas KMO was expressed robustly in pcDNA3.1-KMO transfected cells. KMO was present mainly in the mitochondrial fractions, although a small proportion was also detected in the cytosol, either indicating a low level mitochondrial contamination of the cytosolic fraction (unlikely given the absence of VDAC1), or that a small proportion of KMO has not integrated into the MOM.

Antibodies were also used to detect Drp1 (total, pSer616 and pSer637). Cytosolic DRP1 total levels (normalised to GAPDH) or phosphorylation status (normalised to total DRP1) were not significantly affected by KMO overexpression or CCCP treatment (Figure 6.6B - D). In the mitochondrial fraction, total DRP1 (normalised to VDAC1) was increased in KMO overexpressing cells in both DMSO and CCCP conditions, but this change was not significant in either condition (Figure 6.6E) Mitochondrial DRP1 pSer616 was not significantly affected by KMO overexpression or CCCP treatment. As expected, mitochondrial DRP1 pSer637 was reduced in CCCP treated cells transfected with empty vector, compared to DMSO (Figure 6.6G, $P = 0.0202$). Notably, KMO overexpression also significantly decreased mitochondrial

DRP1 pSer637 upon DMSO treatment compared to empty vector controls (Figure 6.6G, $P = 0.0426$), indicating that KMO can influence the post-translational regulation of DRP1 activity.

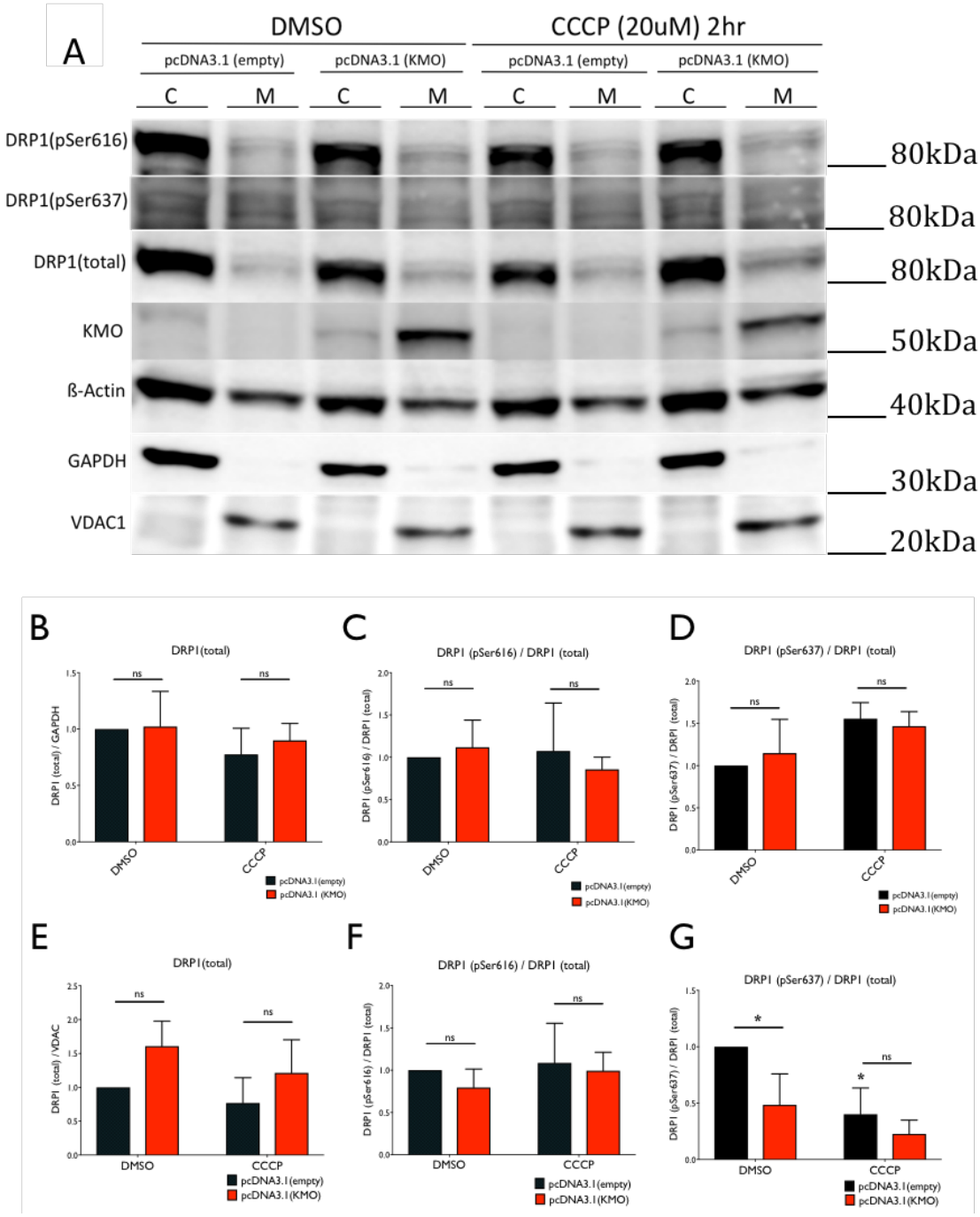

Figure 6.6. Mitochondrial DRP1 Ser637 phosphorylation is reduced by KMO overexpression.

HEK293 cells were transfected with pcDNA3.1 vector (empty or KMO). 46 hrs post-transfection, cells were treated with DMSO or CCCP (20µM) for 2 hrs. Cells were harvested in ice-cold PBS, washed three times in ice-cold PBS, pelleted and snap-frozen in LN_2, then thawed at 37 ^{o}C for 1 min. Cells were lysed by dounce homogeniser (30 strokes) and separated into cytosolic and mitochondria fractions using the mitochondrial fractionation kit (MitoSciences). Protein was quantified by BCA assay and 40µg per sample was size separated by SDS-PAGE. **A)** Proteins were transferred to nitrocellulose and probed for DRP11 (total, pSer616 and pSer637), KMO, ß-Actin, GAPDH and VDAC1. **B)** Total DRP1 was normalised to GAPDH levels

by densitometry of immunoblot bands. Cytosolic DRP1 pSer616 **(C)** and pSer637 **(D)** were normalised to total DRP1. **E)** Mitochondrial total DRP1 was normalised to VDAC1. Mitochondrial DRP1 pSer616 **(F)** and pSer637 **(G)** were normalised to total DRP1 (mean ± SD, Two-way ANOVA, Tukey *post hoc,* ns = not significant, * $P < 0.05$. n = 3).

6.2.3. Overexpression of KMO reduces mitochondrial length in HEK293 cells

To assess what effect KMO modulation of DRP1 phosphorylation might have on mitochondrial morphology, KMO overexpressing HEK293 cells were stained with Mitotracker Red FM and imaged live under basal conditions (Figure 6.7A & B). Mitochondrial morphology was assessed using the "*Make Binary*" and "*Analyse Particles*" functions of FIJI. Aspect ratio and form factor were both decreased in KMO overexpressing cells (Figure 6.7C & D), indicating that the decrease in mitochondrial DRP1 pSer637 observed in 6.2.2 is correlated to an increase in mitochondrial fission.

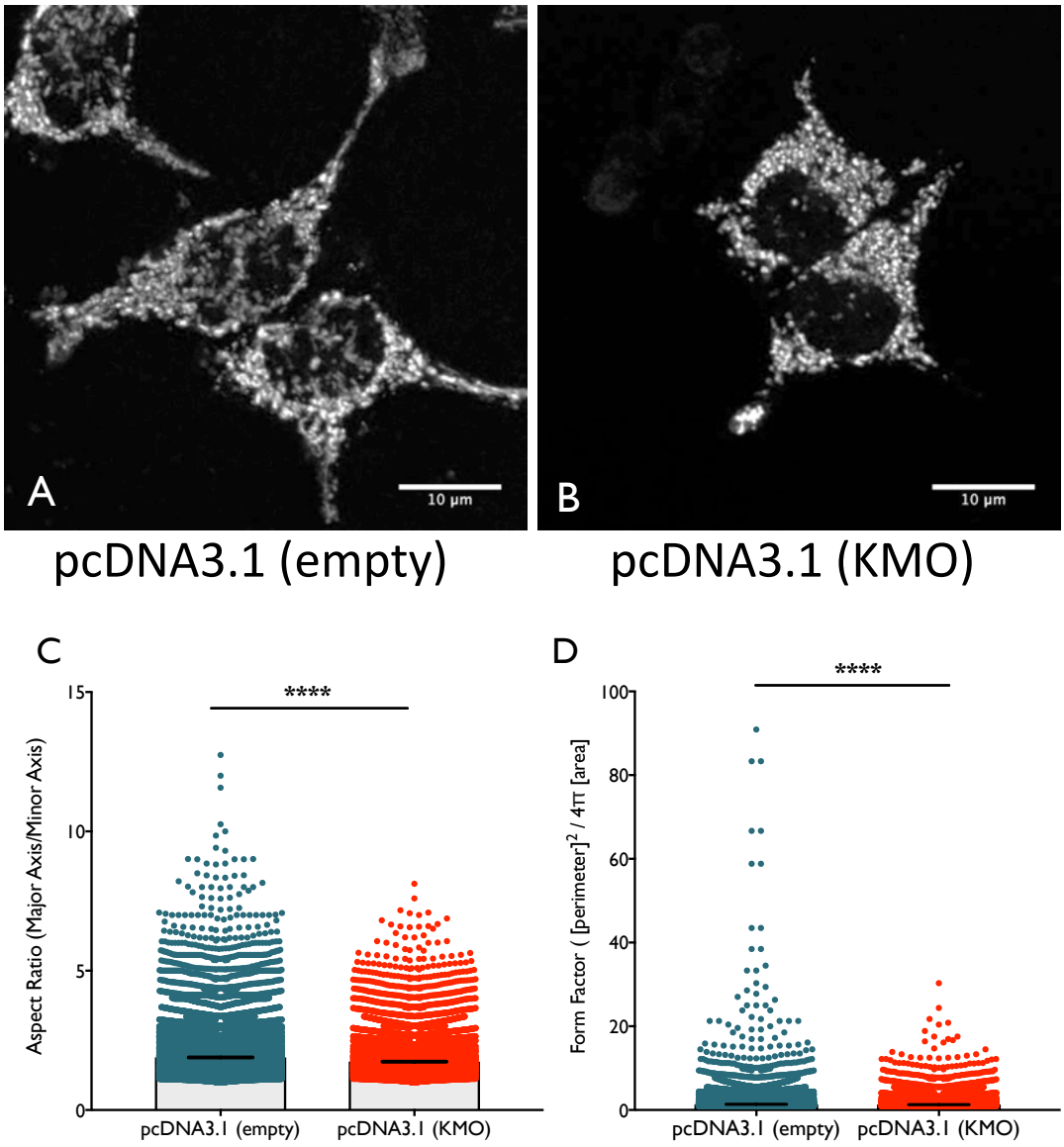

Figure 6.7. Mitochondrial morphology is affected in KMO overexpressing HEK293 cells.

Cells were seeded at 1 x 10^5 cells per well in poly-l-ornathine coated, glass bottomed 35 mm dishes. 24 hrs later, they were transfected with pcDNA3.1 (empty or KMO) plasmids, using Effectene reagent. **A & B)** 48 hrs post-transfection, cells were stained with Mitotracker Red FM for 30 mins, then imaged live at 37°C, 5% CO_2 using an Olympus FV1000 microscope, 60x magnification. n = 3 per group, > 10 FOV imaged per n. Scale bars = 10µM. **C & D)** Mitochondria were analysed in FIJI using the "*Analyse Particles"* function. > 10,000 mitochondria analysed per group (median ± 95%CI, Mann-Whitney test, **** $P < 0.0001$).

6.3. Discussion

As previously observed in *Pink1* and *parkin* mutant flies, overexpression of *Drp1* is sufficient to improve locomotor ability in *cn* mutant flies. Overexpression of a *UASDrp1* construct by *Act5CGAL4* had a detrimental effect on the climbing ability of both cn^{RNAi} and 3M control flies. This is likely due to the balance in mitochondrial dynamics being pushed too far towards pro-fission events by a large increase of DRP1. Introduction of a *FLAG-FlAsH-HA*-tagged *Drp1* transgene under control of the endogenous *Drp1* promoter (Verstreken *et al.*, 2005) increases Drp1 expression by ~50% and is a much more subtle approach to upregulating Drp1 expression than the *UAS-GAL4* system (DuBoff *et al.*, 2012). In the control *3M; Act5CGAL4* background, the *FLAG-Drp1* transgene caused a decrease in climbing performance, which may again be due to a shift in mitochondrial dynamics too far towards mitochondrial fission. However, in cn^{RNAi}*; Act5CGAL4* and cn^{3} flies, climbing performance was significantly improved. As climbing performance was enhanced in cn^{RNAi}*; Act5CGAL4* flies versus *3M; Act5CGAL4* flies at all ages tested, it can be interpreted that *cn* knockdown reduces the pro-fission impact of *Drp1* overexpression which is caused in *3M; Act5CGAL4* flies, again indicating that KMO has a negative effect on fission.

Unexpectedly however, TEM analysis of mitochondrial morphology in the eye found that the *FLAG-Drp1* transgene resulted in a decrease in mitochondrial aspect ratio, form factor and Feret's diameter in $cn^{3/3}$ flies. Why an increase in pro-fission DRP1 would cause an increase in mitochondrial length and branching is unclear, as it was expected that the opposite would be observed, especially given the behavioural improvements observed in these flies. However, the total mitochondrial area coverage was significantly reduced in $cn^{3/3}$*; FLAG-Drp1* flies indicating that the increase in DRP1 could be facilitating mitophagy and this could be the cause of improvements in climbing performance. It would be interesting to assess citrate synthase activity in these flies, as this was elevated in $cn^{3/3}$ flies compared to Canton S wild-type controls (Chapter 3) indicating an increase in mitochondrial mass.

As *cn* deletion causes elongated mitochondria and *cn* knockdown appears to counterbalance *Drp1* overexpression, this would indicate that KMO promotes mitochondrial fission. Relatedly, *Drp1* RNAi has been used to improve the viability of *Marf* RNAi flies (Trevisan *et al.,* 2018). I therefore hypothesised that *cn* knockdown could rescue *Marf* RNAi lethality similarly to *Drp1* RNAi. However, *cn* RNAi did not affect the viability of $Marf^{RNAi}$*; Act5CGAL4* flies. This suggests that loss of KMO does not have as strong an influence on mitochondrial fission as DRP1, which is to be expected, given that DRP1 is the main mediator of fission. *cn* overexpression did not rescue lethality in *Drp1* RNAi flies, suggesting that KMO acts upstream of DRP1. This led to the investigation of KMO influence on DRP1 post-translation modifications. Given that antibodies specific for phosphorylated DRP1 species are not immunoreactive in *Drosophila*, KMO was overexpressed in HEK293 cells. This resulted in a decrease in mitochondrial DRP1 phosphorylated at the Ser637 residue under basal conditions. Although total DRP1 in the mitochondrial fraction also appeared to be increased in KMO overexpressing cells under basal and CCCP treated conditions, this was not statistically significant. To further investigate if this effect is biologically relevant, the sample size could be increased to reduce the effect of standard error, as quantification by immunoblot is not a sensitive means of testing small fold-changes in protein abundance. DRP1 mitochondrial localisation could also be assessed using immunocytochemistry, by calculating the overlap in fluorescence of immunolabelled DRP1 with a mitochondrial-specific stain, such as Mitotracker red, or immunolabelling of a mitochondrial marker such as VDAC1. Not only should this be performed in KMO overexpressing HEK293 cells, it could also be assessed in *cn* or *hKMO* overexpressing *Drosophila*, utilizing the *FLAG-FlAsH-HA* epitope tagged *Drp1* transgene to probe for *Drosophila* DRP1, for which there are no commercially available antibodies. DRP1 localisation could also be assessed in a *cn* knockdown / null context in *Drosophila.* Given the mitochondrial phenotypes observed in *cn* deficient flies in Chapter 3 of this work, it is possible that a DRP1-related mechanism is implicated. Further *in vivo* validation could be performed by utilizing tissue from KMO KO mice (Giorgini *et al*., 2013) to assess DRP1 localisation and phosphorylation status, in tissues in which KMO is usually expressed at high levels, such as the liver.

The mechanism by which KMO is modulating mitochondrial DRP1 Ser637 phosphorylation should also be investigated further. A simple, but perhaps improbable explanation is that KMO interacts directly with DRP1 like MFF, FIS1, MiD49 & MiD51. This interaction might be influenced by DRP1 phosphorylation status, or might promote the dephosphorylation of DRP1 Ser637. A direct interaction between KMO and DRP1 could be investigated by immunoprecipitation experiments either in KMO overexpressing mammalian cells or hKMO overexpressing *Drosophila*, again utilizing the epitope tagged *Drp1* transgene. Given the lack of kinase or phosphatase-like domains present in KMO, direct modulation of phosphorylation status can be excluded as a possibility. Interestingly, a screen of KMO interactors in yeast identified a highly significant ($P = 6.2 \times 10^{-5}$) enrichment of these interactors also interact with calcinueurin subunit B (Thevandavakkam, 2011). Given calcineurin is responsible for the dephosphorylation of DRP1 Ser637 (Cereghetti *et al.*, 2008), it is possible that an increase in KMO abundance promotes calcineurin mitochondrial localization / activity through enhancement of interactions with other proteins.

It would also be interesting to investigate potential involvement of known DRP1 mitochondrial recruiters MFF, FIS1, MiD49 and MiD5. Interactions between DRP1 and these proteins could also be investigated in a KMO overexpression context in HEK293 cells, as KMO could cause a (de)stabilization of one or several of these interactions. An increase in mitochondrial DRP1 and DRP1 pSer637 was observed in HeLa cells overexpressing MiD49 or MiD51 (Losón *et al.*, 2008). These cells exhibited elongated mitochondria, but underwent rapid fission upon CCCP treatment. This was interpreted by the authors as the selective recruitment of inactive DRP1 pSer637 to mitochondria by MiD49/51, thus priming organelles for more efficient fission upon mitochondrial damage. This is further supported by the observation that MiD49/51 double knockout cells are resistant to CCCP induced mitochondrial fission (Osellame *et al.*, 2016). Conversely, MFF cannot bind DRP1 pSer637 and overexpression of MFF leads to increased mitochondrial fission under basal conditions, indicating that MFF recruits the active form of DRP1 (Zhang *et al.*, 2016). The interaction between DRP1 and MFF is enhanced upon UV-irradiation induced apoptosis and is accompanied by a decrease in DRP1 pSer637, a decrease

in DRP1-MiD51 interactions and an increase in FIS1-MiD51 interactions (Zhang *et al.*, 2016). This gives an insight into the complex interactions between DRP1 mitochondrial recruiters, in the priming and triggering of mitochondrial fission. Given the decrease in mitochondrial DRP1 pSer637 observed upon KMO overexpression, the interactions between MiD51 and DRP1/FIS1 could give further insight into the mechanisms by which KMO regulates DRP1. Intriguingly and counterintuitively, KMO overexpression in HEK293 cells has been shown to be protective against 3-HK mediated loss of mitochondrial membrane potential (Wilson *et al.*, 2016). This protection was abolished upon inhibition of KMO enzymatic activity, or knockdown of downstream enzymes KYNU and QPRT, both of which are upregulated upon KMO overexpression. It would be interesting to see if the effect on mitochondrial DRP1 in KMO overexpressing cells is abolished by KMO inhibition or knockdown of KYNU/QPRT. In previous chapters of this work, KMO-associated mitochondrial phenotypes appeared to be independent of KP metabolite changes. However, in the context of KMO-DRP1 interactions, this remains to be investigated.

This chapter also raises interesting questions as to the nature of KMO-inhibition in the context of protection in neurodegenerative disease models. KMO deletion or knockdown are protective in mHTT, Aß$_{42}$ and αSyn *Drosophila* models of neurodegeneration (Campesan *et al.*, 2011; Breda *et al.*, 2016) and an increase in KMO activity/expression has been observed in HD, AD and PD patients. In all three pathologies, aberrant mitochondrial morphology has also been reported. Furthermore, all three proteins has been reported to cause DRP1 mis-localisation or changes in activity (Cho *et al.*, 2009; Manczak *et al.*, 2011; Song *et al.*, 2011; Shirendeb *et al.*, 2012; Ordonez *et al.*, 2018). It is possible, therefore, that the protection conveyed in these models is at least in part due to a restoration in balance of DRP1 localization / activity and this warrants further investigation.

6.4. Conclusions

Mild overexpression of DRP1 improves locomotor defects in *cn* flies, corroborating the conclusions drawn from Chapter 3 that mitochondrial dynamics is implicated in

this phenotype. Although DRP1 overexpression did not lead to shorter, less branched mitochondria in *cn* flies, it did decrease mitochondrial area coverage, indicative of total mitochondrial mass. This indicates that an increase in DRP1 could enhance mitophagy in *cn* flies. Overexpression of KMO in HEK293 cells causes a significant decrease in mitochondrial DRP1 pSer637 under basal conditions and this correlates with shorter, less branched mitochondria. This likely explains the elongated mitochondria observed in *cn* deficient flies and S2 cells, and could explain the *cn/hKMO* mediated rescue of phenotypes in *Pink1* and *parkin* mutant flies observed in Chapters 4 and 5. Further research is required to elucidate the mechanisms via which KMO is regulating DRP1 post-translational modifications and whether these are dependant or independent of KP metabolite levels.

7 Discussion and Future Directions

7.1 A role for KMO in mitochondrial dynamics

KMO is a promising therapeutic target for the treatment of a number of human diseases, particularly those associated with inflammation such as neurodegenerative disorders (Schwarcz *et al.*, 2012; Maddison & Giorgini; 2015; Jacobs *et al.*, 2017). Given the emerging importance of mitochondrial function in the pathology of several disorders including HD, AD and PD, it is important to investigate potential mitochondrial functions of KMO, which localises to the MOM (Okamoto *et al.*, 1967). In an RNAi screen in Drosophila S2R+ cells, knockdown of the KMO encoding gene *cn* resulted in elongated mitochondria (Ivatt *et al.*, 2014). This observation was replicated in Chapter 3 of this thesis, both in S2 cells and in *cn*-null flies *ex vivo*. These flies also exhibit an increase in total mitochondrial mass, which is reflected by both an increase in total mitochondrial area coverage in *Drosophila* photoreceptors and an increase in citrate synthase activity of whole fly homogenates. Despite an increase in mitochondrial mass, *cn*-null and RNAi knockdown flies have a decreased respiratory capacity of ETS complex I. Citrate synthase activity and respiratory capacity were unaffected by supplementing flies with 3-HK at a concentration known to restore it to physiological levels (Campesan *et al.*, 2011), suggesting that these changes are independent of KMO-mediated production of 3-HK. However, the possibility that an increase in KYNA, as a consequence of *cn* deletion or knockdown (Campesan *et al.*, 2011; Breda *et al.*, 2016) could mediate these effects, should be investigated to establish whether the mitochondrial phenotype is truly independent from KP metabolite levels.

Changes in mitochondrial morphology and function are accompanied by a decrease in spontaneous and startle induced locomotor activity in *cn* knockdown and mutant flies. A decrease in locomotor activity has also been reported in adult cn^1 amorphs compared to the Oregon R wildtype strain (Cunningham *et al.*, 2018) and in cn^1 larvae compared to the Canton S wildtype strain (Zakharov *et al.*, 2012). *v* LOF mutant larvae were also assayed and also showed a locomotor phenotype, which

was thus attributed to aberrant KP metabolite levels (Zakharov *et al.*, 2012). The phenotype was more apparent in *cn* than *v* mutants, which was hypothesised by the authors to be due to the greater accumulation of KYNA and subsequent inhibition of NAChRs in *cn* mutants, although this was not tested. The increase in KYNA caused by KMO inhibition and the potential of this increase to affect mitochondrial form and function, as well as locomotor activity, warrants further investigation, as pharmacological inhibition of KMO, a potential therapeutic strategy for the treatment of neurodegenerative disorders, also causes an increase in KYNA (Zwilling *et al.*, 2011; Mole *et al.*, 2016).

The elongated mitochondrial phenotype observed in flies upon KMO knockdown was not mirrored in the murine N9 microglial cell line. This cell type was selected, as KMO expression in the CNS is limited to microglia (Guillemin *et al.*, 2003a; Giorgini *et al.*, 2008). However, KMO expression in control N9 lines was very low (Chapter 3) and expression in this cell type is much lower than peripheral tissues such as liver, kidney (Alberati-Giani *et al.*, 1997b) and monocyte-derived macrophages, which enter the CNS upon neuroinflammation (Heyes *et al.*, 1997; Chiarugi *et al.*, 2001; Guillemin *et al.*, 2003a). This could be the reason why no mitochondrial phenotype was observed in this cell type upon KMO knockdown. Activation of microglia by immune challenge is known to cause an upregulation in KMO levels and activity (Alberati-Giani *et al.*, 1996; Connor *et al.*, 2008; Giorgini *et al.*, 2008; Wang *et al.*, 2010; Molteni *et al.*, 2013) as well as an increase in mitochondrial fragmentation (Katoh *et al.*, 2017). In Chapter 3, KMO expression was not strongly upregulated in N9 cells 24 hrs post-immune challenge. It is possible that the peak of KMO upregulation might occur at an earlier time point (Wang *et al.*, 2008). A link between KMO, microglial activation and mitochondrial morphology could be further investigated by comparing mitochondrial morphology in LPS-treated KMO knockdown and control N9 cells, over a 24 hr time-course. Any difference in mitochondrial fragmentation caused by immune challenge between KMO knockdown and control lines would indicate a role for KMO in microglial mitochondria regulation, which would be of great interest, given the commonality of neuroinflammation, KP dysfunction and aberrant mitochondrial morphology in neurodegenerative disorders. The effect of KMO on other mammalian cell types in

which basal KMO expression is higher than in microglia should also be employed. For example, *Kmo* RNAi has previously been performed in SK-Hep1 and MHCC-97H hepatocyte cell lines (Jin *et al.*, 2015) and it would be interesting to compare mitochondrial morphology in these lines to controls. The availability of KMO KO mice (Giorgini *et al.*, 2013) also provides an *in vivo* mammalian model to address the potential human relevance of phenotypes observed in KMO deficient flies in Chapter 3.

An indication that KMO modulation may alter mitochondrial morphology in mammalian systems was provided in Chapter 6, where KMO overexpression led to a reduction in mitochondrial aspect ratio and form factor, indicating an increase in fission. Interplay between KMO and DRP1 was investigated by assessing DRP1 post-translational modifications in KMO overexpressing HEK293 cells. KMO overexpression caused a decrease in DRP1 pSer637 in the mitochondrial fraction of cells. Phosphorylation at this residue by PKA is generally considered to inhibit mitochondrial fission (Chang & Blackstone, 2007; Cribbs & Strack, 2007), although phosphorylation by CAMK1α was reported to have a pro-fission effect (Han *et al.*, 2008). Regulation of DRP1 by KMO might explain the elongated mitochondria observed in KMO deficient *Drosophila* models. This is supported by the rescue of startle-induced locomotion (climbing) in *cn*-null and knockdown flies by modest *Dp1* overexpression. Counterintuitively, assessment of mitochondrial morphology in the eye of *cn^3; FLAG-Drp1* flies revealed that mitochondria were more elongated and branched than in *cn^3* flies. However, total mitochondrial area coverage was decreased in *cn^3; FLAG-Drp1* flies, indicating that an increase in DRP1 could enhance mitophagic clearance in *cn^3* flies and this may be responsible for the improvement in locomotor ability. This is supported by the observation that Parkin and DRP1 are recruited to mitochondria in the proximity of PINK1 (Buhlman *et al.*, 2014) and DRP1 facilitates the selective mitophagy of damaged mitochondria in mammalian models (Burman *et al.*, 2017).

7.2 The interplay between the KP, PINK1, Parkin and mitophagy

The RNAi screen that identified *cn* as a modulator of mitochondrial morphology also found that *cn* knockdown impaired the recruitment of dParkin-GFP to mitochondria in *Drosophila* S2R+ cells treated with the protonophore CCCP or the oxidative stress inducing pesticide paraquat (Ivatt *et al.*, 2014). The increase in mitochondrial mass, accompanied by a decrease in respiratory capacity in *cn* deficient flies in Chapter 3 supports the hypothesis that KMO could be involved in mitochondrial quality control and turnover, which is governed by PINK1/Parkin-mediated mitophagy. As demonstrated in Chapters 4 and 5, homozygous *cn* LOF causes partial lethality in *Pink1* and *parkin* mutant flies. This suggests some functional overlap between KMO and the mitophagy pathway. Interestingly, the deficiency strain *Df(2R)cn9*, which contains a deletion on chromosome 2 including the *cn* gene, enhances the penetrance of a wing-posture phenotype in *parkin* and *Pink1* RNAi flies (Fernandes & Rao; 2011). This region contains ~80 genes of known function and the region contributing towards the enhancement of phenotype was not fine-mapped. The findings of this thesis suggest that loss of *cn* could in part have contributed towards this effect.

Heterozygous *Drp1* LOF or a dominant negative *Drp1* allele both cause lethality in *Pink1* and *parkin* mutants (Poole *et al.*, 2008). This is thought to be due to DRP1-mediated fission facilitating mitophagy, by producing smaller mitochondria that are easily engulfed by autophagosomes (Buhlman *et al.*, 2014; Burman *et al.*, 2017). This could mean that alternative routes to mitophagy, such as via the E3 ubiquitin ligase MUL1 (Yun *et al.*, 2014), are sufficient in the absence of PINK1 or Parkin in a $Drp1^{+/+}$, but not a $Drp1^{+/-}$ background. Given the elongated mitochondria observed in KMO deficient *Drosophila* both in Chapter 3 and by Ivatt *et al.*, (2014), and the interplay between KMO and DRP1 explored in Chapter 6, the partial lethality of *cn* LOF in *Pink1* and *parkin* mutants could be caused through a DRP1-dependant mechanism. This could be investigated by overexpressing *Drp1* in $Pink1^{B9}$; cn^{3} or cn^{3}; $park^{25}$ flies and assessing whether this is sufficient to rescue lethality.

cn LOF or RNAi knockdown also causes modulation of another phenotype in *Pink1* and *parkin* mutant flies – the apoptotic degeneration of IFMs in the thorax. In Chapter 4, homozygous and heterozygous cn^{3} carrying *Pink1* mutants exhibited an increase in penetrance of the defective thorax phenotype, which was also caused by *cn* RNAi knockdown. This again implies a functional overlap between *cn* and *Pink1*. Conversely, pharmacological inhibition of KMO using the Ro 61-8048 compound, which leads to increased KYNA and a decrease in 3-HK/KYNA ratio (Campesan *et al.*, 2011; Breda *et al.*, 2016), or KYNA supplementation over a range of concentrations, caused a decrease in phenotype penetrance. Like in Chapter 3, where 3-HK supplementation did not reverse phenotypes of *cn*-null flies, this finding indicates that mitochondria specific effects of KMO deficiency are at least partly independent from KP metabolites. Furthermore, the effect of *cn* depletion on the defective thorax phenotype in *Pink1* mutants is sufficient to reverse any positive effect caused by an increase in KYNA and decrease in 3-HK/KYNA ratio. The positive effect caused by an increase in KYNA and decrease in 3-HK/KYNA ratio could be caused by the antioxidant properties of KYNA (Lugo-Huitron *et al.*, 2011) relative to the oxidising properties of 3-HK (Vazquez *et al.*, 2000; Giles *et al.*, 2003). PINK1/Parkin pathology has been previously linked to oxidative stress in flies (Greene *et al.*, 2005) and mammalian models (Palacino *et al.*, 2004; Dagda *et al.*, 2009). Overexpression of superoxide dismutase (SOD1 or SOD2), or treatment with a SOD-mimetic compound rescued mitochondrial morphology in *PINK1* and *Parkin* knockdown SH-SY5Y cells, and improved locomotor ability in *Pink1* and *parkin* mutant flies, in which mitochondrial ROS is elevated (Biosa *et al.*, 2018). The effects of KYNA on mitochondrial ROS levels in *Pink1* and *parkin* mutants could be investigated via the mt-roGFP-Orp1 genetic reporter (Biosa *et al.,* 2018), or the dye reporter MitoSOX (Rana *et al.*, 2017).

In Chapter 5, both genetic and pharmacological KMO inhibition, as well as KYNA supplementation, all decreased the penetrance of the defective thorax phenotype in *parkin* mutants. In $cn^{3/3}; park^{25/25}$ flies which have a strong eclosion defect, it could be argued that the flies that emerged are predisposed to be resistant to pathology. However, cn^{3}/CyO (cn^{3}/cn^{2}); $park^{25/25}$ and $cn^{RNAi}/Act5CGAL4; park^{25/25}$ flies, which have no eclosion phenotype, also showed a significant decrease in penetrance of

defective thorax. This suggests that a reduction in KMO is protective against apoptotic muscle degeneration in *parkin* mutants. Given the potential use of KMO inhibitors in the treatment of PD, it is reassuring that pharmacological inhibition of KMO does not appear to mirror the partial lethality caused upon genetic KMO inhibition in *Pink1* and *parkin* mutants, or the exacerbation of apoptotic muscle degeneration in *Pink1* mutants.

Overexpression of *cn* or *hKMO* robustly rescued climbing defects in *Pink1* mutant flies, a phenotype which has previously been rescued by overexpression of *Drp1* (Liu *et al.*, 2011) and *parkin* (Clark *et al.*, 2006; Park *et al.*, 2006; Yang *et al.*, 2006). Overexpression of *cn* and *hKMO* also modestly improved lifespan in $Pink1^{B9}$ hemizygous and $park^{25}$ heterozygous males, but not in a *parkin*-null background - indicating that the protection conveyed by KMO is dependent on the presence of Parkin. However, overexpression of *cn* was not sufficient to rescue the respiratory capacity of complex I in *Pink1* mutants. Interestingly, although overexpression of Parkin rescues a number of mitochondrial and behavioural phenotypes in *Pink1* mutants (Clark *et al.*, 2006; Park *et al.*, 2006; Yang *et al.*, 2006), it is unclear whether it is sufficient to rescue complex I defects (Shiba-Fukushima *et al.*, 2014; Pogson *et al.*, 2014). However, complex I assembly and respiratory capacity in *Pink1* mutants have been rescued by overexpression of DRP1 (Liu *et al.*, 2011). Given the role of KMO in mitochondrial dynamics and its interplay with DRP1, it might have been expected that an increase in KMO could promote DRP1 activity sufficiently to rescue complex I defects. It would be interesting to investigate mitochondrial morphology in *Pink1* and *parkin* flies upon *cn* and *hKMO* overexpression. This could be achieved by expression and visualisation of mitochondrial-targeted GFP (mito-GFP) or electron microscopy in tissues where abnormal mitochondrial morphology has been previously reported, such as IFM in the thorax (Clark *et al.*, 2006; Park *et al.*, 2006; Yang *et al.*, 2006) or in DA neurons (Whitworth *et al.*, 2005; Park *et al.*, 2006; Yang *et al.*, 2006; Burman *et al.*, 2012). Quantification of mitophagy using the fluorescent reporter system mt-Keima (Katayama *et al.*, 2011) revealed that mitophagy defects in *Pink1* and *parkin* mutant flies are not apparent in young adults (Lee *et al.*, 2018b; Cornelissen *et al.*, 2018) but are apparent by Day 30 (Cornelissen *et al.*, 2018). It would be interesting to assess age-related changes in mitophagy in

KMO-overexpressing *Pink1* and *parkin* mutants, to further investigate if improvements in mitophagy facilitate the rescue of climbing defects in *Pink1* mutants and lifespan in *Pink1* and *parkin* mutants.

In Chapter 5, *cn* knockdown in S2 cells reduced dParkin-GFP recruitment to mitochondria in CCCP-treated S2 cells, corroborating the finding of Ivatt *et al*. (2014). Given KMO is localised to the MOM, it is possible that KMO and Parkin could physically interact and that KMO might directly recruit Parkin. Immunoprecipitation of dParkin-GFP also pulled-down hKMO in *Drosophila* S2 cells. The quantity of hKMO pulled-down as a proportion of total input hKMO was low, although it was increased upon CCCP treatment, a stimulus for Parkin recruitment to mitochondria. Immunoprecipitation of GFP-Parkin pulled-down hKMO in both cytosolic and mitochondrial fractions, but a greater quantity of hKMO was pulled down in the cytosolic fraction. In HEK293 cells, hKMO was not pulled down with YFP-hParkin. Together, these results are insufficient to confirm a physical interaction between KMO and Parkin. Neither *cn* knockdown in S2 cells, nor overexpression in FM6 control or $Pink1^{B9}$ flies was sufficient to modulate levels of MARF, which is ubiquitinated and degraded in a Parkin dependant fashion (Ziviani *et al*., 2010). This would suggest that any effect of KMO on mitochondrial Parkin recruitment does not influence MARF levels and thus indicates MARF levels do not influence mitochondrial morphology in KMO deficient flies. Furthermore it suggests that any role KMO might play in regulating mitophagy is independent of Parkin E3 ubiquitin ligase activity.

7.3 Future directions

The findings of this thesis support the involvement of KMO in mitochondrial dynamics through the regulation of DRP1. However, the mechanism by which this occurs is still not clear. Although mitochondrial phenotypes in KMO deficient *Drosophila* appear to be independent of KP metabolites, the effects of KP metabolites on DRP1 post-translational modification requires investigation. Furthermore, potential physical interaction between KMO and DRP1, or known

recruiters and modifiers of the pro-fission protein, should be explored in order to elucidate this mechanism. The decrease in complex I activity yet an increase in mitochondrial content suggest that KMO deficiency impairs mitophagic clearance of disfunctional mitochondria. Furthermore, DRP1 overexpression, which improved climbing performance in *cn* flies, also caused a reduction in mitochondrial area coverage in photoreceptors. It would be interesting to quantify mitophagy in *cn* flies using mt-Keima (Lee *et al.*, 2018b; Cornelissen *et al.*, 2018) and assess whether DRP1 overexpression modulates this. Given the tissue specificity of KMO expression in both flies and mammals, it warrants consideration as to why KMO modulation of mitochondrial morphology might be necessary in some tissues but not others. In flies, the assessment of mitochondrial morphology in *cn* amorphs, in tissues other than the eye, will give an indication of the tissue specific nature of KMO involvement in mitochondrial dynamics. Mitochondrial morphology, DRP1 localisation and activity, in KMO expressing and non-expressing tissues could also be explored in mice, in both a wildtype and KMO knockout context, in order to translate these findings to mammalian systems, giving greater relevance to human biology and disease pathology.

Previous studies have shown that *cn* knockdown is protective in mHTT, aSyn and $A\beta_{42}$ *Drosophila* models (Campesan *et al.*, 2011; Breda *et al.*, 2016). As compromised mitochondrial morphology and DRP1 function are known components of pathogensis of these three proteins, (Cho *et al.*, 2009; Manczak *et al.*, 2011; Song *et al.*, 2011; Shirendeb *et al.*, 2012; Ordonez *et al.*, 2018), it would be interesting to explore if this protection is, in part, due to modulation of mitochondrial dynamics. The rescue *Pink1* and *parkin* phenotypes by *cn* and KMO overexpression can be better understood through the use of tissue-specific GAL4 drivers to identify in which cells KMO expression is sufficient to rescue phenotypes, such as climbing ability in *Pink1* mutants and lifespan in $park^{25}$ heterozygotes. Overexpression of *cn* in *Pink1* and *parkin* dsRNA S2 cells appeared sufficient to normalise mitochondrial morphology. This effect should also be confirmed *in vivo*, to establish that protection is conveyed by modulation of mitochondrial morphology.

7.4 Concluding Remarks

This study has identified a number of mitochondrial phenotypes in KMO deficient *Drosophila*, including aberrant mitochondrial morphology, an increase in mitochondrial mass and yet a decrease in respiratory capacity. KMO is implicated in mitochondrial dynamics, through regulation of the fission protein DRP1, and interacts with the PINK1/Parkin mitophagy pathway. These effects appear to be largely independent of KP metabolite levels, although this requires further investigation. The findings of this investigation therefore support the hypothesis of a role for KMO in mitochondrial quality control, but indicate that this function would not be compromised through the pharmacological inhibition of KMO enzymatic activity.

Bibliography

Agudelo, L.Z., Femenia, T., Orhan, F., Porsmyr-Palmertz, M., Goiny, M., Martinez-Redondo, V., Correia, J.C., Izadi, M., Bhat, M., Schuppe-Koistinen, I., Pettersson, A.T., Ferreira, D.M.S., Krook, A., Barres, R., Zierath, J.R., Erhardt, S., Lindskog, M. and Ruas, J.L. (2014) 'Skeletal muscle PGC-1alpha1 modulates kynurenine metabolism and mediates resilience to stress-induced depression', *Cell,* 159(1), pp. 33-45.

Alberati-Giani, D., Malherbe, P., Ricciardi-Castagnoli, P., Kohler, C., Denis-Donini, S. and Cesura, A.M. (1997a) 'Differential regulation of indoleamine 2,3-dioxygenase expression by nitric oxide and inflammatory mediators in IFN-gamma-activated murine macrophages and microglial cells', *Journal of immunology (Baltimore, Md.: 1950),* 159(1), pp. 419-426.

Alberati-Giani, D., Cesura, A.M., Broger, C., Warren, W.D., Rover, S. and Malherbe, P. (1997b) 'Cloning and functional expression of human kynurenine 3-monooxygenase', *FEBS letters,* 410(2-3), pp. 407-412.

Alberati-Giani, D., Ricciardi-Castagnoli, P., Kohler, C. and Cesura, A.M. (1996) 'Regulation of the kynurenine metabolic pathway by interferon-gamma in murine cloned macrophages and microglial cells', *Journal of neurochemistry,* 66(3), pp. 996-1004.

Alexander, C., Votruba, M., Pesch, U.E., Thiselton, D.L., Mayer, S., Moore, A., Rodriguez, M., Kellner, U., Leo-Kottler, B., Auburger, G., Bhattacharya, S.S. and Wissinger, B. (2000) 'OPA1, encoding a dynamin-related GTPase, is mutated in autosomal dominant optic atrophy linked to chromosome 3q28', *Nature genetics,* 26(2), pp. 211-215.

Amaral, M. (2013) 'Structure and mechanism of Kynurenine 3-monooxygenase, a candidate Huntington's disease drug target', *PhD Thesis (Universidade de Lisboa),* .

Amaral, M., Levy, C., Heyes, D.J., Lafite, P., Outeiro, T.F., Giorgini, F., Leys, D. and Scrutton, N.S. (2013) 'Structural basis of kynurenine 3-monooxygenase inhibition', *Nature,* 496(7445), pp. 382-385.

Anderson, S., Bankier, A.T., Barrell, B.G., de Bruijn, M.H., Coulson, A.R., Drouin, J., Eperon, I.C., Nierlich, D.P., Roe, B.A., Sanger, F., Schreier, P.H., Smith, A.J., Staden, R. and Young, I.G. (1981) 'Sequence and organization of the human mitochondrial genome', *Nature,* 290(5806), pp. 457-465.

Andersson, S.G., Zomorodipour, A., Andersson, J.O., Sicheritz-Ponten, T., Alsmark, U.C., Podowski, R.M., Naslund, A.K., Eriksson, A.S., Winkler, H.H. and Kurland, C.G. (1998) 'The genome sequence of Rickettsia prowazekii and the origin of mitochondria', *Nature,* 396(6707), pp. 133-140.

Anding, A.L., Wang, C., Chang, T.K., Sliter, D.A., Powers, C.M., Hofmann, K., Youle, R.J. and Baehrecke, E.H. (2018) 'Vps13D Encodes a Ubiquitin-Binding Protein that Is Required for the Regulation of Mitochondrial Size and Clearance', *Current biology : CB,* 28(2), pp. 287-295.e6.

Austin, S. and St-Pierre, J. (2012) 'PGC1alpha and mitochondrial metabolism--emerging concepts and relevance in ageing and neurodegenerative disorders', *Journal of cell science,* 125(Pt 21), pp. 4963-4971.

Ball, H.J., Yuasa, H.J., Austin, C.J., Weiser, S. and Hunt, N.H. (2009) 'Indoleamine 2,3-dioxygenase-2; a new enzyme in the kynurenine pathway', *The international journal of biochemistry & cell biology,* 41(3), pp. 467-471.

Bandlow, W. (1972) 'Membrane separation and biogenesis of the outer membrane of yeast mitochondria', *Biochimica et biophysica acta,* 282(1), pp. 105-122.

Bandres-Ciga, S., Price, T.R., Barrero, F.J., Escamilla-Sevilla, F., Pelegrina, J., Arepalli, S., Hernandez, D., Gutierrez, B., Cervilla, J., Rivera, M., Rivera, A., Ding, J.H., Vives, F., Nalls, M., Singleton, A. and Duran, R. (2016) 'Genome-wide assessment of Parkinson's disease in a Southern Spanish population', *Neurobiology of aging,* 45, pp. 213.e3-213.e9.

Baran, H., Okuno, E., Kido, R. and Schwarcz, R. (1994) 'Purification and characterization of kynurenine aminotransferase I from human brain', *Journal of neurochemistry,* 62(2), pp. 730-738.

Baran, H. and Schwarcz, R. (1990) 'Presence of 3-hydroxyanthranilic acid in rat tissues and evidence for its production from anthranilic acid in the brain', *Journal of neurochemistry,* 55(3), pp. 738-744.

Baran, H., Staniek, K., Bertignol-Sporr, M., Attam, M., Kronsteiner, C. and Kepplinger, B. (2016) 'Effects of Various Kynurenine Metabolites on Respiratory Parameters of Rat Brain, Liver and Heart Mitochondria', *International journal of tryptophan research : IJTR,* 9, pp. 17-29.

Beadle, G.W., Mitchell, H.K. and Nyc, J.F. (1947) 'Kynurenine as an Intermediate in the Formation of Nicotinic Acid from Tryptophane by Neurospora', *Proceedings of the National Academy of Sciences of the United States of America,* 33(6), pp. 155-158.

Beaumont, V., Mrzljak, L., Dijkman, U., Freije, R., Heins, M., Rassoulpour, A., Tombaugh, G., Gelman, S., Bradaia, A., Steidl, E., Gleyzes, M., Heikkinen, T., Lehtimaki, K., Puolivali, J., Kontkanen, O., Javier, R.M., Neagoe, I., Deisemann, H., Winkler, D., Ebneth, A., Khetarpal, V., Toledo-Sherman, L., Dominguez, C., Park, L.C. and Munoz-Sanjuan, I. (2016) 'The novel KMO inhibitor CHDI-340246 leads to a restoration of electrophysiological alterations in mouse models of Huntington's disease', *Experimental neurology,* 282, pp. 99-118.

Beconi, M.G., Yates, D., Lyons, K., Matthews, K., Clifton, S., Mead, T., Prime, M., Winkler, D., O'Connell, C., Walter, D., Toledo-Sherman, L., Munoz-Sanjuan, I. and Dominguez, C. (2012) 'Metabolism and pharmacokinetics of JM6 in mice: JM6 is not a prodrug for Ro-61-8048', *Drug metabolism and disposition: the biological fate of chemicals,* 40(12), pp. 2297-2306.

Behan, W.M., McDonald, M., Darlington, L.G. and Stone, T.W. (1999) 'Oxidative stress as a mechanism for quinolinic acid-induced hippocampal damage: protection by melatonin and deprenyl', *British journal of pharmacology,* 128(8), pp. 1754-1760.

Bellen, H. (2013) 'Bellen insertions.', *Personal communication to FlyBase,* .

Bender, D.A. and McCreanor, G.M. (1982) 'The preferred route of kynurenine metabolism in the rat', *Biochimica et biophysica acta,* 717(1), pp. 56-60.

Betarbet, R., Sherer, T.B., MacKenzie, G., Garcia-Osuna, M., Panov, A.V. and Greenamyre, J.T. (2000) 'Chronic systemic pesticide exposure reproduces features of Parkinson's disease', *Nature neuroscience,* 3(12), pp. 1301-1306.

Biosa, A., Sanchez-Martinez, A., Filograna, R., Terriente-Felix, A., Alam, S.M., Beltramini, M., Bubacco, L., Bisaglia, M. and Whitworth, A.J. (2018) 'Superoxide dismutating molecules rescue the toxic effects of PINK1 and parkin loss', *Human molecular genetics,* 27(9), pp. 1618-1629.

Bischof, J., Maeda, R.K., Hediger, M., Karch, F. and Basler, K. (2007) 'An optimized transgenesis system for Drosophila using germ-line-specific phiC31 integrases', *Proceedings of the National Academy of Sciences of the United States of America,* 104(9), pp. 3312-3317.

Blanco Ayala, T., Lugo Huitron, R., Carmona Aparicio, L., Ramirez Ortega, D., Gonzalez Esquivel, D., Pedraza Chaverri, J., Perez de la Cruz, G., Rios, C., Schwarcz, R. and Perez de la Cruz, V. (2015) 'Alternative kynurenic acid synthesis routes studied in the rat cerebellum', *Frontiers in cellular neuroscience,* 9, pp. 178.

Blass, J.P. (2000) 'The mitochondrial spiral. An adequate cause of dementia in the Alzheimer's syndrome', *Annals of the New York Academy of Sciences,* 924, pp. 170-183.

Bonda, D.J., Mailankot, M., Stone, J.G., Garrett, M.R., Staniszewska, M., Castellani, R.J., Siedlak, S.L., Zhu, X., Lee, H.G., Perry, G., Nagaraj, R.H. and Smith, M.A. (2010) 'Indoleamine 2,3-dioxygenase and 3-hydroxykynurenine modifications are found in the neuropathology of Alzheimer's disease', *Redox report : communications in free radical research,* 15(4), pp. 161-168.

Bonen, L., Cunningham, R.S., Gray, M.W. and Doolittle, W.F. (1977) 'Wheat embryo mitochondrial 18S ribosomal RNA: evidence for its prokaryotic nature', *Nucleic acids research,* 4(3), pp. 663-671.

Braidy, N., Grant, R., Adams, S., Brew, B.J. and Guillemin, G.J. (2009) 'Mechanism for quinolinic acid cytotoxicity in human astrocytes and neurons', *Neurotoxicity research,* 16(1), pp. 77-86.

Breda, C., Sathyasaikumar, K.V., Sograte Idrissi, S., Notarangelo, F.M., Estranero, J.G., Moore, G.G., Green, E.W., Kyriacou, C.P., Schwarcz, R. and Giorgini, F. (2016) 'Tryptophan-2,3-dioxygenase (TDO) inhibition ameliorates neurodegeneration by modulation of kynurenine pathway metabolites', *Proceedings of the National Academy of Sciences of the United States of America,* 113(19), pp. 5435-5440.

Buhlman, L., Damiano, M., Bertolin, G., Ferrando-Miguel, R., Lombes, A., Brice, A. and Corti, O. (2014) 'Functional interplay between Parkin and Drp1 in mitochondrial fission and clearance', *Biochimica et biophysica acta,* 1843(9), pp. 2012-2026.

Bunch, T.A., Grinblat, Y. and Goldstein, L.S. (1988) 'Characterization and use of the Drosophila metallothionein promoter in cultured Drosophila melanogaster cells', *Nucleic acids research,* 16(3), pp. 1043-1061.

Burman, J.L., Pickles, S., Wang, C., Sekine, S., Vargas, J.N.S., Zhang, Z., Youle, A.M., Nezich, C.L., Wu, X., Hammer, J.A. and Youle, R.J. (2017) 'Mitochondrial fission facilitates the selective mitophagy of protein aggregates', *The Journal of cell biology,* 216(10), pp. 3231-3247.

Burman, J.L., Yu, S., Poole, A.C., Decal, R.B. and Pallanck, L. (2012) 'Analysis of neural subtypes reveals selective mitochondrial dysfunction in dopaminergic neurons from parkin mutants', *Proceedings of the National Academy of Sciences of the United States of America,* 109(26), pp. 10438-10443.

Calvo, S.E. and Mootha, V.K. (2010) 'The mitochondrial proteome and human disease', *Annual review of genomics and human genetics,* 11, pp. 25-44.

Campbell, B.M., Charych, E., Lee, A.W. and Moller, T. (2014) 'Kynurenines in CNS disease: regulation by inflammatory cytokines', *Frontiers in neuroscience,* 8, pp. 12.

Campesan, S., Green, E.W., Breda, C., Sathyasaikumar, K.V., Muchowski, P.J., Schwarcz, R., Kyriacou, C.P. and Giorgini, F. (2011) 'The kynurenine pathway modulates neurodegeneration in a Drosophila model of Huntington's disease', *Current biology : CB,* 21(11), pp. 961-966.

Canet-Aviles, R.M., Wilson, M.A., Miller, D.W., Ahmad, R., McLendon, C., Bandyopadhyay, S., Baptista, M.J., Ringe, D., Petsko, G.A. and Cookson, M.R. (2004) 'The Parkinson's disease protein DJ-1 is neuroprotective due to cysteine-sulfinic acid-driven mitochondrial localization', *Proceedings of the National Academy of Sciences of the United States of America,* 101(24), pp. 9103-9108.

Carroll, J., Fearnley, I.M., Skehel, J.M., Shannon, R.J., Hirst, J. and Walker, J.E. (2006) 'Bovine complex I is a complex of 45 different subunits', *The Journal of biological chemistry,* 281(43), pp. 32724-32727.

Celardo, I., Costa, A.C., Lehmann, S., Jones, C., Wood, N., Mencacci, N.E., Mallucci, G.R., Loh, S.H. and Martins, L.M. (2016) 'Mitofusin-mediated ER stress triggers neurodegeneration in pink1/parkin models of Parkinson's disease', *Cell death & disease,* 7(6), pp. e2271.

Cereghetti, G.M., Stangherlin, A., Martins de Brito, O., Chang, C.R., Blackstone, C., Bernardi, P. and Scorrano, L. (2008) 'Dephosphorylation by calcineurin regulates translocation of Drp1 to mitochondria', *Proceedings of the National Academy of Sciences of the United States of America,* 105(41), pp. 15803-15808.

Cha, M., Chen, H. and Chan, D. (2018) 'Removal of the Mitochondrial Fission Factor Mff Exacerbates Neuronal Loss and Neurological Phenotypes in a Huntington's Disease Mouse Model', *PLOS Currents Huntington Disease,* Edition 1. doi: 10.1371/currents.hd.a4e15b80c4915c828d39754942c6631f.

Chacinska, A., Pfannschmidt, S., Wiedemann, N., Kozjak, V., Sanjuan Szklarz, L.K., Schulze-Specking, A., Truscott, K.N., Guiard, B., Meisinger, C. and Pfanner, N. (2004) 'Essential role of Mia40 in import and assembly of mitochondrial intermembrane space proteins', *The EMBO journal,* 23(19), pp. 3735-3746.

Chang, C.R. and Blackstone, C. (2010) 'Dynamic regulation of mitochondrial fission through modification of the dynamin-related protein Drp1', *Annals of the New York Academy of Sciences,* 1201, pp. 34-39.

Chang, C.R. and Blackstone, C. (2007) 'Cyclic AMP-dependent protein kinase phosphorylation of Drp1 regulates its GTPase activity and mitochondrial morphology', *The Journal of biological chemistry,* 282(30), pp. 21583-21587.

Chang, D., Nalls, M.A., Hallgrimsdottir, I.B., Hunkapiller, J., van der Brug, M., Cai, F., International Parkinson's Disease Genomics Consortium, 23andMe Research Team, Kerchner, G.A., Ayalon, G., Bingol, B., Sheng, M., Hinds, D., Behrens, T.W., Singleton, A.B., Bhangale, T.R. and Graham, R.R. (2017) 'A meta-analysis of genome-wide association studies identifies 17 new Parkinson's disease risk loci', *Nature genetics,* 49(10), pp. 1511-1516.

Chaugule, V.K., Burchell, L., Barber, K.R., Sidhu, A., Leslie, S.J., Shaw, G.S. and Walden, H. (2011) 'Autoregulation of Parkin activity through its ubiquitin-like domain', *The EMBO journal,* 30(14), pp. 2853-2867.

Chen, H., Detmer, S.A., Ewald, A.J., Griffin, E.E., Fraser, S.E. and Chan, D.C. (2003) 'Mitofusins Mfn1 and Mfn2 coordinately regulate mitochondrial fusion and are essential for embryonic development', *The Journal of cell biology,* 160(2), pp. 189-200.

Chen, Y. and Guillemin, G.J. (2009) 'Kynurenine pathway metabolites in humans: disease and healthy States', *International journal of tryptophan research : IJTR,* 2, pp. 1-19.

Chiarugi, A., Calvani, M., Meli, E., Traggiai, E. and Moroni, F. (2001) 'Synthesis and release of neurotoxic kynurenine metabolites by human monocyte-derived macrophages', *Journal of neuroimmunology,* 120(1-2), pp. 190-198.

Chiarugi, A., Rapizzi, E., Moroni, F. and Moroni, F. (1999) 'The kynurenine metabolic pathway in the eye: studies on 3-hydroxykynurenine, a putative cataractogenic compound', *FEBS letters,* 453(1-2), pp. 197-200.

Chintapalli, V.R., Wang, J. and Dow, J.A. (2007) 'Using FlyAtlas to identify better Drosophila melanogaster models of human disease', *Nature genetics,* 39(6), pp. 715-720.

Cho, D.H., Nakamura, T., Fang, J., Cieplak, P., Godzik, A., Gu, Z. and Lipton, S.A. (2009) 'S-nitrosylation of Drp1 mediates beta-amyloid-related mitochondrial fission and neuronal injury', *Science (New York, N.Y.),* 324(5923), pp. 102-105.

Clark, I.E., Dodson, M.W., Jiang, C., Cao, J.H., Huh, J.R., Seol, J.H., Yoo, S.J., Hay, B.A. and Guo, M. (2006) 'Drosophila pink1 is required for mitochondrial function and interacts genetically with parkin', *Nature,* 441(7097), pp. 1162-1166.

Clemens, J.C., Worby, C.A., Simonson-Leff, N., Muda, M., Maehama, T., Hemmings, B.A. and Dixon, J.E. (2000) 'Use of double-stranded RNA interference in Drosophila cell lines to dissect signal transduction pathways', *Proceedings of the National Academy of Sciences of the United States of America,* 97(12), pp. 6499-6503.

Connor, T.J., Starr, N., O'Sullivan, J.B. and Harkin, A. (2008) 'Induction of indolamine 2,3-dioxygenase and kynurenine 3-monooxygenase in rat brain following a systemic inflammatory challenge: a role for IFN-gamma?', *Neuroscience letters,* 441(1), pp. 29-34.

Cornelissen, T., Vilain, S., Vints, K., Gounko, N., Verstreken, P. and Vandenberghe, W. (2018) 'Deficiency of parkin and PINK1 impairs age-dependent mitophagy in Drosophila', *eLife,* 7, pp. 10.7554/eLife.35878.

Costa, A.C., Loh, S.H. and Martins, L.M. (2013) 'Drosophila Trap1 protects against mitochondrial dysfunction in a PINK1/parkin model of Parkinson's disease', *Cell death & disease,* 4, pp. e467.

Cribbs, J.T. and Strack, S. (2007) 'Reversible phosphorylation of Drp1 by cyclic AMP-dependent protein kinase and calcineurin regulates mitochondrial fission and cell death', *EMBO reports,* 8(10), pp. 939-944.

Crozier-Reabe, K.R., Phillips, R.S. and Moran, G.R. (2008) 'Kynurenine 3-monooxygenase from Pseudomonas fluorescens: substrate-like inhibitors both stimulate flavin reduction and stabilize the flavin-peroxo intermediate yet

result in the production of hydrogen peroxide', *Biochemistry,* 47(47), pp. 12420-12433.

Cunningham, P.C., Waldeck, K., Ganetzky, B. and Babcock, D.T. (2018) 'Neurodegeneration and locomotor dysfunction in Drosophila scarlet mutants', *Journal of cell science,* 131(18), pp. 10.1242/jcs.216697.

Dacks, J.B., Field, M.C., Buick, R., Eme, L., Gribaldo, S., Roger, A.J., Brochier-Armanet, C. and Devos, D.P. (2016) 'The changing view of eukaryogenesis - fossils, cells, lineages and how they all come together', *Journal of cell science,* 129(20), pp. 3695-3703.

Dagda, R.K., Cherra, S.J.,3rd, Kulich, S.M., Tandon, A., Park, D. and Chu, C.T. (2009) 'Loss of PINK1 function promotes mitophagy through effects on oxidative stress and mitochondrial fission', *The Journal of biological chemistry,* 284(20), pp. 13843-13855.

de Brito, O.M. and Scorrano, L. (2008) 'Mitofusin 2 tethers endoplasmic reticulum to mitochondria', *Nature,* 456(7222), pp. 605-610.

De Castro, F., Price, J. and Brown, R., (1956) 'Reduced Triphosphopyridinenucleotide Requirement for the Enzymatic Formation of 3-Hydroxykynurenine from L-Kynurenine', *Journal of the American Chemical Society,* (78), pp. 2904-2905.

de Castro, I.P., Costa, A.C., Celardo, I., Tufi, R., Dinsdale, D., Loh, S.H. and Martins, L.M. (2013) 'Drosophila ref(2)P is required for the parkin-mediated suppression of mitochondrial dysfunction in pink1 mutants', *Cell death & disease,* 4, pp. e873.

Deas, E., Plun-Favreau, H., Gandhi, S., Desmond, H., Kjaer, S., Loh, S.H., Renton, A.E., Harvey, R.J., Whitworth, A.J., Martins, L.M., Abramov, A.Y. and Wood, N.W. (2011) 'PINK1 cleavage at position A103 by the mitochondrial protease PARL', *Human molecular genetics,* 20(5), pp. 867-879.

Decker, R.H., Kang, H.H., Leach, F.R. and Henderson, L.M. (1961) 'Purification and properties of 3-hydroxyanthranilic acid oxidase', *The Journal of biological chemistry,* 236, pp. 3076-3082.

Delettre, C., Lenaers, G., Griffoin, J.M., Gigarel, N., Lorenzo, C., Belenguer, P., Pelloquin, L., Grosgeorge, J., Turc-Carel, C., Perret, E., Astarie-Dequeker, C., Lasquellec, L., Arnaud, B., Ducommun, B., Kaplan, J. and Hamel, C.P. (2000) 'Nuclear gene OPA1, encoding a mitochondrial dynamin-related protein, is mutated in dominant optic atrophy', *Nature genetics,* 26(2), pp. 207-210.

Deng, H., Dodson, M.W., Huang, H. and Guo, M. (2008) 'The Parkinson's disease genes pink1 and parkin promote mitochondrial fission and/or inhibit fusion in Drosophila', *Proceedings of the National Academy of Sciences of the United States of America,* 105(38), pp. 14503-14508.

Dietzl, G., Chen, D., Schnorrer, F., Su, K.C., Barinova, Y., Fellner, M., Gasser, B., Kinsey, K., Oppel, S., Scheiblauer, S., Couto, A., Marra, V., Keleman, K. and Dickson, B.J. (2007) 'A genome-wide transgenic RNAi library for conditional gene inactivation in Drosophila', *Nature,* 448(7150), pp. 151-156.

DiMauro, S. and Schon, E.A. (2003) 'Mitochondrial respiratory-chain diseases', *The New England journal of medicine,* 348(26), pp. 2656-2668.

Du, F., Schmidt, W., Okuno, E., Kido, R., Kohler, C. and Schwarcz, R. (1992) 'Localization of kynurenine aminotransferase immunoreactivity in the rat hippocampus', *The Journal of comparative neurology,* 321(3), pp. 477-487.

DuBoff, B., Gotz, J. and Feany, M.B. (2012) 'Tau promotes neurodegeneration via DRP1 mislocalization in vivo', *Neuron,* 75(4), pp. 618-632.

Erhardt, S., Blennow, K., Nordin, C., Skogh, E., Lindstrom, L.H. and Engberg, G. (2001) 'Kynurenic acid levels are elevated in the cerebrospinal fluid of patients with schizophrenia', *Neuroscience letters,* 313(1-2), pp. 96-98.

Erhardt, S., Pocivavsek, A., Repici, M., Liu, X.C., Imbeault, S., Maddison, D.C., Thomas, M.A.R., Smalley, J.L., Larsson, M.K., Muchowski, P.J., Giorgini, F. and Schwarcz, R. (2017) 'Adaptive and Behavioral Changes in Kynurenine 3-Monooxygenase Knockout Mice: Relevance to Psychotic Disorders', *Biological psychiatry,* 82(10), pp. 756-765.

Erickson, J.B., Flanagan, E.M., Russo, S. and Reinhard, J.F.,Jr (1992) 'A radiometric assay for kynurenine 3-hydroxylase based on the release of 3H2O during hydroxylation of L-[3,5-3H]kynurenine', *Analytical Biochemistry,* 205(2), pp. 257-262.

Fedorowicz, M.A., de Vries-Schneider, R.L., Rub, C., Becker, D., Huang, Y., Zhou, C., Alessi Wolken, D.M., Voos, W., Liu, Y. and Przedborski, S. (2014) 'Cytosolic cleaved PINK1 represses Parkin translocation to mitochondria and mitophagy', *EMBO reports,* 15(1), pp. 86-93.

Fernandes, C. and Rao, Y. (2011) 'Genome-wide screen for modifiers of Parkinson's disease genes in Drosophila', *Molecular brain,* 4, pp. 17-6606-4-17.

Ferreiro, M.J., Perez, C., Marchesano, M., Ruiz, S., Caputi, A., Aguilera, P., Barrio, R. and Cantera, R. (2018) 'Drosophila melanogaster White Mutant w(1118) Undergo Retinal Degeneration', *Frontiers in neuroscience,* 11, pp. 732.

Forrest, C.M., Mackay, G.M., Stoy, N., Spiden, S.L., Taylor, R., Stone, T.W. and Darlington, L.G. (2010) 'Blood levels of kynurenines, interleukin-23 and soluble human leucocyte antigen-G at different stages of Huntington's disease', *Journal of neurochemistry,* 112(1), pp. 112-122.

Foster, A.C., Collins, J.F. and Schwarcz, R. (1983) 'On the excitotoxic properties of quinolinic acid, 2,3-piperidine dicarboxylic acids and structurally related compounds', *Neuropharmacology,* 22(12A), pp. 1331-1342.

Foster, A.C., Zinkand, W.C. and Schwarcz, R. (1985) 'Quinolinic acid phosphoribosyltransferase in rat brain', *Journal of neurochemistry,* 44(2), pp. 446-454.

Frezza, C., Cipolat, S., Martins de Brito, O., Micaroni, M., Beznoussenko, G.V., Rudka, T., Bartoli, D., Polishuck, R.S., Danial, N.N., De Strooper, B. and Scorrano, L. (2006) 'OPA1 controls apoptotic cristae remodeling independently from mitochondrial fusion', *Cell,* 126(1), pp. 177-189.

Fujigaki, H., Saito, K., Fujigaki, S., Takemura, M., Sudo, K., Ishiguro, H. and Seishima, M. (2006) 'The signal transducer and activator of transcription 1alpha and interferon regulatory factor 1 are not essential for the induction of indoleamine 2,3-dioxygenase by lipopolysaccharide: involvement of p38 mitogen-activated protein kinase and nuclear factor-kappaB pathways, and synergistic effect of several proinflammatory cytokines', *Journal of Biochemistry,* 139(4), pp. 655-662.

Fukushima, T., Sone, Y., Mitsuhashi, S., Tomiya, M. and Toyo'oka, T. (2009) 'Alteration of kynurenic acid concentration in rat plasma following optically pure kynurenine administration: a comparative study between enantiomers', *Chirality,* 21(4), pp. 468-472.

Fulop, L., Szanda, G., Enyedi, B., Varnai, P. and Spat, A. (2011) 'The effect of OPA1 on mitochondrial Ca(2)(+) signaling', *PloS one,* 6(9), pp. e25199.

Furmston, R.'Investigating the Role of LRRK2 in the Visual System in a Drosophila Model of Parkinson's Disease', *PhD Thesis (University of York),* .

Gargano, J.W., Martin, I., Bhandari, P. and Grotewiel, M.S. (2005) 'Rapid iterative negative geotaxis (RING): a new method for assessing age-related locomotor decline in Drosophila', *Experimental gerontology,* 40(5), pp. 386-395.

Garrison, A.M., Parrott, J.M., Tunon, A., Delgado, J., Redus, L. and O'Connor, J.C. (2018) 'Kynurenine pathway metabolic balance influences microglia activity: Targeting kynurenine monooxygenase to dampen neuroinflammation', *Psychoneuroendocrinology,* 94, pp. 1-10.

Geisler, S., Holmstrom, K.M., Skujat, D., Fiesel, F.C., Rothfuss, O.C., Kahle, P.J. and Springer, W. (2010) 'PINK1/Parkin-mediated mitophagy is dependent on VDAC1 and p62/SQSTM1', *Nature cell biology,* 12(2), pp. 119-131.

Gergalova, G., Lykhmus, O., Kalashnyk, O., Koval, L., Chernyshov, V., Kryukova, E., Tsetlin, V., Komisarenko, S. and Skok, M. (2012) 'Mitochondria express alpha7 nicotinic acetylcholine receptors to regulate Ca2+ accumulation and

cytochrome c release: study on isolated mitochondria', *PloS one,* 7(2), pp. e31361.

Ghosh, D. and Forrest, H.S. (1967) 'Enzymatic studies on the hydroxylation of kynurenine in Drosophila melanogaster', *Genetics,* 55(3), pp. 423-431.

Giles, G.I., Collins, C.A., Stone, T.W. and Jacob, C. (2003) 'Electrochemical and in vitro evaluation of the redox-properties of kynurenine species', *Biochemical and biophysical research communications,* 300(3), pp. 719-724.

Giorgini, F., Guidetti, P., Nguyen, Q., Bennett, S.C. and Muchowski, P.J. (2005) 'A genomic screen in yeast implicates kynurenine 3-monooxygenase as a therapeutic target for Huntington disease', *Nature genetics,* 37(5), pp. 526-531.

Giorgini, F., Huang, S.Y., Sathyasaikumar, K.V., Notarangelo, F.M., Thomas, M.A., Tararina, M., Wu, H.Q., Schwarcz, R. and Muchowski, P.J. (2013) 'Targeted deletion of kynurenine 3-monooxygenase in mice: a new tool for studying kynurenine pathway metabolism in periphery and brain', *The Journal of biological chemistry,* 288(51), pp. 36554-36566.

Giorgini, F., Moller, T., Kwan, W., Zwilling, D., Wacker, J.L., Hong, S., Tsai, L.C., Cheah, C.S., Schwarcz, R., Guidetti, P. and Muchowski, P.J. (2008) 'Histone deacetylase inhibition modulates kynurenine pathway activation in yeast, microglia, and mice expressing a mutant huntingtin fragment', *The Journal of biological chemistry,* 283(12), pp. 7390-7400.

Gnaiger, E. (2014) 'Mitochondrial Pathways and Respiratory Control', *OROBOROS MiPNet Publications,* (4).

Godoy, J.A., Valdivieso, A.G. and Inestrosa, N.C. (2018) 'Nicotine Modulates Mitochondrial Dynamics in Hippocampal Neurons', *Molecular neurobiology,* .

Goldstein, L.E., Leopold, M.C., Huang, X., Atwood, C.S., Saunders, A.J., Hartshorn, M., Lim, J.T., Faget, K.Y., Muffat, J.A., Scarpa, R.C., Chylack, L.T.,Jr, Bowden, E.F., Tanzi, R.E. and Bush, A.I. (2000) '3-Hydroxykynurenine and 3-hydroxyanthranilic acid generate hydrogen peroxide and promote alpha-crystallin cross-linking by metal ion reduction', *Biochemistry,* 39(24), pp. 7266-7275.

Gomes, L.C., Di Benedetto, G. and Scorrano, L. (2011) 'During autophagy mitochondria elongate, are spared from degradation and sustain cell viability', *Nature cell biology,* 13(5), pp. 589-598.

Green, E.W., Campesan, S., Breda, C., Sathyasaikumar, K.V., Muchowski, P.J., Schwarcz, R., Kyriacou, C.P. and Giorgini, F. (2012) 'Drosophila eye color mutants as therapeutic tools for Huntington disease', *Fly,* 6(2), pp. 117-120.

Greene, A.W., Grenier, K., Aguileta, M.A., Muise, S., Farazifard, R., Haque, M.E., McBride, H.M., Park, D.S. and Fon, E.A. (2012) 'Mitochondrial processing

peptidase regulates PINK1 processing, import and Parkin recruitment', *EMBO reports,* 13(4), pp. 378-385.

Greene, J.C., Whitworth, A.J., Kuo, I., Andrews, L.A., Feany, M.B. and Pallanck, L.J. (2003) 'Mitochondrial pathology and apoptotic muscle degeneration in Drosophila parkin mutants', *Proceedings of the National Academy of Sciences of the United States of America,* 100(7), pp. 4078-4083.

Greene, J.C., Whitworth, A.J., Andrews, L.A., Parker, T.J. and Pallanck, L.J. (2005) 'Genetic and genomic studies of Drosophila parkin mutants implicate oxidative stress and innate immune responses in pathogenesis', *Human molecular genetics,* 14(6), pp. 799-811.

Guardia-Laguarta, C., Area-Gomez, E., Rub, C., Liu, Y., Magrane, J., Becker, D., Voos, W., Schon, E.A. and Przedborski, S. (2014) 'alpha-Synuclein is localized to mitochondria-associated ER membranes', *The Journal of neuroscience : the official journal of the Society for Neuroscience,* 34(1), pp. 249-259.

Guidetti, P., Hoffman, G.E., Melendez-Ferro, M., Albuquerque, E.X. and Schwarcz, R. (2007) 'Astrocytic localization of kynurenine aminotransferase II in the rat brain visualized by immunocytochemistry', *Glia,* 55(1), pp. 78-92.

Guidetti, P., Amori, L., Sapko, M.T., Okuno, E. and Schwarcz, R. (2007) 'Mitochondrial aspartate aminotransferase: a third kynurenate-producing enzyme in the mammalian brain', *Journal of neurochemistry,* 102(1), pp. 103-111.

Guidetti, P., Bates, G.P., Graham, R.K., Hayden, M.R., Leavitt, B.R., MacDonald, M.E., Slow, E.J., Wheeler, V.C., Woodman, B. and Schwarcz, R. (2006) 'Elevated brain 3-hydroxykynurenine and quinolinate levels in Huntington disease mice', *Neurobiology of disease,* 23(1), pp. 190-197.

Guidetti, P., Luthi-Carter, R.E., Augood, S.J. and Schwarcz, R. (2004) 'Neostriatal and cortical quinolinate levels are increased in early grade Huntington's disease', *Neurobiology of disease,* 17(3), pp. 455-461.

Guidetti, P., Okuno, E. and Schwarcz, R. (1997) 'Characterization of rat brain kynurenine aminotransferases I and II', *Journal of neuroscience research,* 50(3), pp. 457-465.

Guillemin, G.J., Brew, B.J., Noonan, C.E., Takikawa, O. and Cullen, K.M. (2005) 'Indoleamine 2,3 dioxygenase and quinolinic acid immunoreactivity in Alzheimer's disease hippocampus', *Neuropathology and applied neurobiology,* 31(4), pp. 395-404.

Guillemin, G.J., Kerr, S.J., Smythe, G.A., Smith, D.G., Kapoor, V., Armati, P.J., Croitoru, J. and Brew, B.J. (2001) 'Kynurenine pathway metabolism in human astrocytes: a paradox for neuronal protection', *Journal of neurochemistry,* 78(4), pp. 842-853.

Guillemin, G.J., Smith, D.G., Smythe, G.A., Armati, P.J. and Brew, B.J. (2003a) 'Expression of the kynurenine pathway enzymes in human microglia and macrophages', *Advances in Experimental Medicine and Biology,* 527, pp. 105-112.

Guillemin, G.J., Williams, K.R., Smith, D.G., Smythe, G.A., Croitoru-Lamoury, J. and Brew, B.J. (2003b) 'Quinolinic acid in the pathogenesis of Alzheimer's disease', *Advances in Experimental Medicine and Biology,* 527, pp. 167-176.

Gulaj, E., Pawlak, K., Bien, B. and Pawlak, D. (2010) 'Kynurenine and its metabolites in Alzheimer's disease patients', *Advances in medical sciences,* 55(2), pp. 204-211.

Guo, X., Disatnik, M.H., Monbureau, M., Shamloo, M., Mochly-Rosen, D. and Qi, X. (2013) 'Inhibition of mitochondrial fragmentation diminishes Huntington's disease-associated neurodegeneration', *The Journal of clinical investigation,* 123(12), pp. 5371-5388.

Hamasaki, M., Furuta, N., Matsuda, A., Nezu, A., Yamamoto, A., Fujita, N., Oomori, H., Noda, T., Haraguchi, T., Hiraoka, Y., Amano, A. and Yoshimori, T. (2013) 'Autophagosomes form at ER-mitochondria contact sites', *Nature,* 495(7441), pp. 389-393.

Hampel, H., Blennow, K., Shaw, L.M., Hoessler, Y.C., Zetterberg, H. and Trojanowski, J.Q. (2010) 'Total and phosphorylated tau protein as biological markers of Alzheimer's disease', *Experimental gerontology,* 45(1), pp. 30-40.

Han, Q., Cai, T., Tagle, D.A. and Li, J. (2010) 'Structure, expression, and function of kynurenine aminotransferases in human and rodent brains', *Cellular and molecular life sciences : CMLS,* 67(3), pp. 353-368.

Han, Q., Cai, T., Tagle, D.A., Robinson, H. and Li, J. (2008) 'Substrate specificity and structure of human aminoadipate aminotransferase/kynurenine aminotransferase II', *Bioscience reports,* 28(4), pp. 205-215.

Han, Q., Calvo, E., Marinotti, O., Fang, J., Rizzi, M., James, A.A. and Li, J. (2003) 'Analysis of the wild-type and mutant genes encoding the enzyme kynurenine monooxygenase of the yellow fever mosquito, Aedes aegypti', *Insect molecular biology,* 12(5), pp. 483-490.

Han, X.J., Lu, Y.F., Li, S.A., Kaitsuka, T., Sato, Y., Tomizawa, K., Nairn, A.C., Takei, K., Matsui, H. and Matsushita, M. (2008) 'CaM kinase I alpha-induced phosphorylation of Drp1 regulates mitochondrial morphology', *The Journal of cell biology,* 182(3), pp. 573-585.

Hensman Moss, D.J., Pardinas, A.F., Langbehn, D., Lo, K., Leavitt, B.R., Roos, R., Durr, A., Mead, S., TRACK-HD investigators, REGISTRY investigators, Holmans, P., Jones, L. and Tabrizi, S.J. (2017) 'Identification of genetic variants associated

with Huntington's disease progression: a genome-wide association study', *The Lancet.Neurology,* 16(9), pp. 701-711.

Heyes, M.P., Chen, C.Y., Major, E.O. and Saito, K. (1997) 'Different kynurenine pathway enzymes limit quinolinic acid formation by various human cell types', *The Biochemical journal,* 326 (Pt 2)(Pt 2), pp. 351-356.

Heyes, M.P., Saito, K., Major, E.O., Milstien, S., Markey, S.P. and Vickers, J.H. (1993) 'A mechanism of quinolinic acid formation by brain in inflammatory neurological disease. Attenuation of synthesis from L-tryptophan by 6-chlorotryptophan and 4-chloro-3-hydroxyanthranilate', *Brain : a journal of neurology,* 116 (Pt 6)(Pt 6), pp. 1425-1450.

Hilmas, C., Pereira, E.F., Alkondon, M., Rassoulpour, A., Schwarcz, R. and Albuquerque, E.X. (2001) 'The brain metabolite kynurenic acid inhibits alpha7 nicotinic receptor activity and increases non-alpha7 nicotinic receptor expression: physiopathological implications', *The Journal of neuroscience : the official journal of the Society for Neuroscience,* 21(19), pp. 7463-7473.

Hirai, K., Aliev, G., Nunomura, A., Fujioka, H., Russell, R.L., Atwood, C.S., Johnson, A.B., Kress, Y., Vinters, H.V., Tabaton, M., Shimohama, S., Cash, A.D., Siedlak, S.L., Harris, P.L., Jones, P.K., Petersen, R.B., Perry, G. and Smith, M.A. (2001) 'Mitochondrial abnormalities in Alzheimer's disease', *The Journal of neuroscience : the official journal of the Society for Neuroscience,* 21(9), pp. 3017-3023.

Hirai, K., Kuroyanagi, H., Tatebayashi, Y., Hayashi, Y., Hirabayashi-Takahashi, K., Saito, K., Haga, S., Uemura, T. and Izumi, S. (2010) 'Dual role of the carboxyl-terminal region of pig liver L-kynurenine 3-monooxygenase: mitochondrial-targeting signal and enzymatic activity', *Journal of Biochemistry,* 148(6), pp. 639-650.

Hodgkins, P.S. and Schwarcz, R. (1998) 'Interference with cellular energy metabolism reduces kynurenic acid formation in rat brain slices: reversal by lactate and pyruvate', *The European journal of neuroscience,* 10(6), pp. 1986-1994.

Holtze, M., Saetre, P., Engberg, G., Schwieler, L., Werge, T., Andreassen, O.A., Hall, H., Terenius, L., Agartz, I., Jonsson, E.G., Schalling, M. and Erhardt, S. (2012) 'Kynurenine 3-monooxygenase polymorphisms: relevance for kynurenic acid synthesis in patients with schizophrenia and healthy controls', *Journal of psychiatry & neuroscience : JPN,* 37(1), pp. 53-57.

Howells, A.J., Summers, K.M. and Ryall, R.L. (1977) 'Developmental patterns of 3-hydroxykynurenine accumulation in white and various other eye color mutants of Drosophila melanogaster', *Biochemical genetics,* 15(11-12), pp. 1049-1059.

Hwa, J.J., Hiller, M.A., Fuller, M.T. and Santel, A. (2002) 'Differential expression of the Drosophila mitofusin genes fuzzy onions (fzo) and dmfn', *Mechanisms of development,* 116(1-2), pp. 213-216.

Ishii, K., Ogaya, T., Song, Z., Iizuka, H. and Fukushima, T. (2010) 'Changes in the plasma concentrations of D-kynurenine and kynurenic acid in rats after intraperitoneal administration of tryptophan enantiomers', *Chirality,* 22(10), pp. 901-906.

Ivatt, R.M., Sanchez-Martinez, A., Godena, V.K., Brown, S., Ziviani, E. and Whitworth, A.J. (2014) 'Genome-wide RNAi screen identifies the Parkinson disease GWAS risk locus SREBF1 as a regulator of mitophagy', *Proceedings of the National Academy of Sciences of the United States of America,* 111(23), pp. 8494-8499.

Iwahashi, H., Ishii, T., Sugata, R. and Kido, R. (1988) 'Superoxide dismutase enhances the formation of hydroxyl radicals in the reaction of 3-hydroxyanthranilic acid with molecular oxygen', *The Biochemical journal,* 251(3), pp. 893-899.

Jacobs, K.R., Castellano-Gonzalez, G., Guillemin, G.J. and Lovejoy, D.B. (2017) 'Major Developments in the Design of Inhibitors along the Kynurenine Pathway', *Current medicinal chemistry,* 24(23), pp. 2471-2495.

Janetzky, B., Hauck, S., Youdim, M.B., Riederer, P., Jellinger, K., Pantucek, F., Zochling, R., Boissl, K.W. and Reichmann, H. (1994) 'Unaltered aconitase activity, but decreased complex I activity in substantia nigra pars compacta of patients with Parkinson's disease', *Neuroscience letters,* 169(1-2), pp. 126-128.

Jansen, I.E., Ye, H., Heetveld, S., Lechler, M.C., Michels, H., Seinstra, R.I., Lubbe, S.J., Drouet, V., Lesage, S., Majounie, E., Gibbs, J.R., Nalls, M.A., Ryten, M., Botia, J.A., Vandrovcova, J., Simon-Sanchez, J., Castillo-Lizardo, M., Rizzu, P., Blauwendraat, C., Chouhan, A.K., Li, Y., Yogi, P., Amin, N., van Duijn, C.M., International Parkinson's Disease Genetics Consortium (IPGDC), Morris, H.R., Brice, A., Singleton, A.B., David, D.C., Nollen, E.A., Jain, S., Shulman, J.M. and Heutink, P. (2017) 'Discovery and functional prioritization of Parkinson's disease candidate genes from large-scale whole exome sequencing', *Genome biology,* 18(1), pp. 22-017-1147-9.

Jauch, D., Urbanska, E.M., Guidetti, P., Bird, E.D., Vonsattel, J.P., Whetsell, W.O.,Jr and Schwarcz, R. (1995) 'Dysfunction of brain kynurenic acid metabolism in Huntington's disease: focus on kynurenine aminotransferases', *Journal of the neurological sciences,* 130(1), pp. 39-47.

Javitch, J.A., D'Amato, R.J., Strittmatter, S.M. and Snyder, S.H. (1985) 'Parkinsonism-inducing neurotoxin, N-methyl-4-phenyl-1,2,3,6 -tetrahydropyridine: uptake of the metabolite N-methyl-4-phenylpyridine by dopamine neurons explains selective toxicity', *Proceedings of the National Academy of Sciences of the United States of America,* 82(7), pp. 2173-2177.

Jin, H., Zhang, Y., You, H., Tao, X., Wang, C., Jin, G., Wang, N., Ruan, H., Gu, D., Huo, X., Cong, W. and Qin, W. (2015) 'Prognostic significance of kynurenine 3-monooxygenase and effects on proliferation, migration, and invasion of human hepatocellular carcinoma', *Scientific reports,* 5, pp. 10466.

Jin, S.M. and Youle, R.J. (2013) 'The accumulation of misfolded proteins in the mitochondrial matrix is sensed by PINK1 to induce PARK2/Parkin-mediated mitophagy of polarized mitochondria', *Autophagy,* 9(11), pp. 1750-1757.

John Peter, A.T., Herrmann, B., Antunes, D., Rapaport, D., Dimmer, K.S. and Kornmann, B. (2017) 'Vps13-Mcp1 interact at vacuole-mitochondria interfaces and bypass ER-mitochondria contact sites', *The Journal of cell biology,* 216(10), pp. 3219-3229.

Jonckheere, A.I., Smeitink, J.A. and Rodenburg, R.J. (2012) 'Mitochondrial ATP synthase: architecture, function and pathology', *Journal of inherited metabolic disease,* 35(2), pp. 211-225.

Jones, S.P., Franco, N.F., Varney, B., Sundaram, G., Brown, D.A., de Bie, J., Lim, C.K., Guillemin, G.J. and Brew, B.J. (2015) 'Expression of the Kynurenine Pathway in Human Peripheral Blood Mononuclear Cells: Implications for Inflammatory and Neurodegenerative Disease', *PloS one,* 10(6), pp. e0131389.

Julienne, H., Buhl, E., Leslie, D.S. and Hodge, J.J.L. (2017) 'Drosophila PINK1 and parkin loss-of-function mutants display a range of non-motor Parkinson's disease phenotypes', *Neurobiology of disease,* 104, pp. 15-23.

Kane, L.A., Lazarou, M., Fogel, A.I., Li, Y., Yamano, K., Sarraf, S.A., Banerjee, S. and Youle, R.J. (2014) 'PINK1 phosphorylates ubiquitin to activate Parkin E3 ubiquitin ligase activity', *The Journal of cell biology,* 205(2), pp. 143-153.

Kang, P.J., Ostermann, J., Shilling, J., Neupert, W., Craig, E.A. and Pfanner, N. (1990) 'Requirement for hsp70 in the mitochondrial matrix for translocation and folding of precursor proteins', *Nature,* 348(6297), pp. 137-143.

Katayama, H., Kogure, T., Mizushima, N., Yoshimori, T. and Miyawaki, A. (2011) 'A sensitive and quantitative technique for detecting autophagic events based on lysosomal delivery', *Chemistry & biology,* 18(8), pp. 1042-1052.

Katoh, M., Wu, B., Nguyen, H.B., Thai, T.Q., Yamasaki, R., Lu, H., Rietsch, A.M., Zorlu, M.M., Shinozaki, Y., Saitoh, Y., Saitoh, S., Sakoh, T., Ikenaka, K., Koizumi, S., Ransohoff, R.M. and Ohno, N. (2017) 'Polymorphic regulation of mitochondrial fission and fusion modifies phenotypes of microglia in neuroinflammation', *Scientific reports,* 7(1), pp. 4942-017-05232-0.

Kawai, J., Okuno, E. and Kido, R. (1988) 'Organ distribution of rat kynureninase and changes of its activity during development', *Enzyme,* 39(4), pp. 181-189.

Kawajiri, S., Saiki, S., Sato, S., Sato, F., Hatano, T., Eguchi, H. and Hattori, N. (2010) 'PINK1 is recruited to mitochondria with parkin and associates with LC3 in mitophagy', *FEBS letters,* 584(6), pp. 1073-1079.

Kazlauskaite, A., Kondapalli, C., Gourlay, R., Campbell, D.G., Ritorto, M.S., Hofmann, K., Alessi, D.R., Knebel, A., Trost, M. and Muqit, M.M. (2014) 'Parkin is activated by PINK1-dependent phosphorylation of ubiquitin at Ser65', *The Biochemical journal,* 460(1), pp. 127-139.

Khalil, B., El Fissi, N., Aouane, A., Cabirol-Pol, M.J., Rival, T. and Lievens, J.C. (2015) 'PINK1-induced mitophagy promotes neuroprotection in Huntington's disease', *Cell death & disease,* 6, pp. e1617.

Kharazmi, J., Moshfegh, C. and Brody, T. (2012) 'Identification of cis-Regulatory Elements in the dmyc Gene of Drosophila Melanogaster', *Gene regulation and systems biology,* 6, pp. 15-42.

Kiebler, M., Pfaller, R., Sollner, T., Griffiths, G., Horstmann, H., Pfanner, N. and Neupert, W. (1990) 'Identification of a mitochondrial receptor complex required for recognition and membrane insertion of precursor proteins', *Nature,* 348(6302), pp. 610-616.

Kim, H.T., Na, B.K., Chung, J., Kim, S., Kwon, S.K., Cha, H., Son, J., Cho, J.M. and Hwang, K.Y. (2018) 'Structural Basis for Inhibitor-Induced Hydrogen Peroxide Production by Kynurenine 3-Monooxygenase', *Cell chemical biology,* 25(4), pp. 426-438.e4.

Kitada, T., Asakawa, S., Hattori, N., Matsumine, H., Yamamura, Y., Minoshima, S., Yokochi, M., Mizuno, Y. and Shimizu, N. (1998) 'Mutations in the parkin gene cause autosomal recessive juvenile parkinsonism', *Nature,* 392(6676), pp. 605-608.

Kondapalli, C., Kazlauskaite, A., Zhang, N., Woodroof, H.I., Campbell, D.G., Gourlay, R., Burchell, L., Walden, H., Macartney, T.J., Deak, M., Knebel, A., Alessi, D.R. and Muqit, M.M. (2012) 'PINK1 is activated by mitochondrial membrane potential depolarization and stimulates Parkin E3 ligase activity by phosphorylating Serine 65', *Open biology,* 2(5), pp. 120080.

Kotsen, C., Santorelli, M.L., Bloom, E.L., Goldstein, A.O., Ripley-Moffitt, C., Steinberg, M.B., Burke, M.V. and Foulds, J. (2018) 'A Narrative Review of Intensive Group Tobacco Treatment: Clinical, Research, and U.S. Policy Recommendations', *Nicotine & tobacco research : official journal of the Society for Research on Nicotine and Tobacco,* .

Koyano, F., Okatsu, K., Kosako, H., Tamura, Y., Go, E., Kimura, M., Kimura, Y., Tsuchiya, H., Yoshihara, H., Hirokawa, T., Endo, T., Fon, E.A., Trempe, J.F., Saeki, Y., Tanaka, K. and Matsuda, N. (2014) 'Ubiquitin is phosphorylated by PINK1 to activate parkin', *Nature,* 510(7503), pp. 162-166.

Kuhlbrandt, W. (2015) 'Structure and function of mitochondrial membrane protein complexes', *BMC biology,* 13, pp. 89-015-0201-x.

Kumar, J.P. (2012) 'Building an ommatidium one cell at a time', *Developmental dynamics : an official publication of the American Association of Anatomists,* 241(1), pp. 136-149.

Kurnasov, O., Jablonski, L., Polanuyer, B., Dorrestein, P., Begley, T. and Osterman, A. (2003) 'Aerobic tryptophan degradation pathway in bacteria: novel kynurenine formamidase', *FEMS microbiology letters,* 227(2), pp. 219-227.

Lam, H., Oh, D.C., Cava, F., Takacs, C.N., Clardy, J., de Pedro, M.A. and Waldor, M.K. (2009) 'D-amino acids govern stationary phase cell wall remodeling in bacteria', *Science (New York, N.Y.),* 325(5947), pp. 1552-1555.

Langston, J.W., Ballard, P., Tetrud, J.W. and Irwin, I. (1983) 'Chronic Parkinsonism in humans due to a product of meperidine-analog synthesis', *Science (New York, N.Y.),* 219(4587), pp. 979-980.

Lapin, I.P. (1978) 'Stimulant and convulsive effects of kynurenines injected into brain ventricles in mice', *Journal of neural transmission,* 42(1), pp. 37-43.

Larsen, S., Nielsen, J., Hansen, C.N., Nielsen, L.B., Wibrand, F., Stride, N., Schroder, H.D., Boushel, R., Helge, J.W., Dela, F. and Hey-Mogensen, M. (2012) 'Biomarkers of mitochondrial content in skeletal muscle of healthy young human subjects', *The Journal of physiology,* 590(14), pp. 3349-3360.

Lavebratt, C., Olsson, S., Backlund, L., Frisen, L., Sellgren, C., Priebe, L., Nikamo, P., Traskman-Bendz, L., Cichon, S., Vawter, M.P., Osby, U., Engberg, G., Landen, M., Erhardt, S. and Schalling, M. (2014) 'The KMO allele encoding Arg452 is associated with psychotic features in bipolar disorder type 1, and with increased CSF KYNA level and reduced KMO expression', *Molecular psychiatry,* 19(3), pp. 334-341.

Lazarou, M., Jin, S.M., Kane, L.A. and Youle, R.J. (2012) 'Role of PINK1 binding to the TOM complex and alternate intracellular membranes in recruitment and activation of the E3 ligase Parkin', *Developmental cell,* 22(2), pp. 320-333.

Lazarou, M., Sliter, D.A., Kane, L.A., Sarraf, S.A., Wang, C., Burman, J.L., Sideris, D.P., Fogel, A.I. and Youle, R.J. (2015) 'The ubiquitin kinase PINK1 recruits autophagy receptors to induce mitophagy', *Nature,* 524(7565), pp. 309-314.

Lee, K.S., Huh, S., Lee, S., Wu, Z., Kim, A.K., Kang, H.Y. and Lu, B. (2018a) 'Altered ER-mitochondria contact impacts mitochondria calcium homeostasis and contributes to neurodegeneration in vivo in disease models', *Proceedings of the National Academy of Sciences of the United States of America,* 115(38), pp. E8844-E8853.

Lee, J.J., Sanchez-Martinez, A., Zarate, A.M., Beninca, C., Mayor, U., Clague, M.J. and Whitworth, A.J. (2018b) 'Basal mitophagy is widespread in Drosophila but minimally affected by loss of Pink1 or parkin', *The Journal of cell biology,* 217(5), pp. 1613-1622.

Lehmann, S., Costa, A.C., Celardo, I., Loh, S.H. and Martins, L.M. (2016) 'Parp mutations protect against mitochondrial dysfunction and neurodegeneration in a PARKIN model of Parkinson's disease', *Cell death & disease,* 7, pp. e2166.

Lehmann, S., Loh, S.H. and Martins, L.M. (2017) 'Enhancing NAD+ salvage metabolism is neuroprotective in a PINK1 model of Parkinson's disease', *Biology open,* 6(2), pp. 141-147.

Lesage, S., Drouet, V., Majounie, E., Deramecourt, V., Jacoupy, M., Nicolas, A., Cormier-Dequaire, F., Hassoun, S.M., Pujol, C., Ciura, S., Erpapazoglou, Z., Usenko, T., Maurage, C.A., Sahbatou, M., Liebau, S., Ding, J., Bilgic, B., Emre, M., Erginel-Unaltuna, N., Guven, G., Tison, F., Tranchant, C., Vidailhet, M., Corvol, J.C., Krack, P., Leutenegger, A.L., Nalls, M.A., Hernandez, D.G., Heutink, P., Gibbs, J.R., Hardy, J., Wood, N.W., Gasser, T., Durr, A., Deleuze, J.F., Tazir, M., Destee, A., Lohmann, E., Kabashi, E., Singleton, A., Corti, O., Brice, A., French Parkinson's Disease Genetics Study (PDG) and International Parkinson's Disease Genomics Consortium (IPDGC) (2016) 'Loss of VPS13C Function in Autosomal-Recessive Parkinsonism Causes Mitochondrial Dysfunction and Increases PINK1/Parkin-Dependent Mitophagy', *American Journal of Human Genetics,* 98(3), pp. 500-513.

Lill, C.M., Roehr, J.T., McQueen, M.B., Kavvoura, F.K., Bagade, S., Schjeide, B.M., Schjeide, L.M., Meissner, E., Zauft, U., Allen, N.C., Liu, T., Schilling, M., Anderson, K.J., Beecham, G., Berg, D., Biernacka, J.M., Brice, A., DeStefano, A.L., Do, C.B., Eriksson, N., Factor, S.A., Farrer, M.J., Foroud, T., Gasser, T., Hamza, T., Hardy, J.A., Heutink, P., Hill-Burns, E.M., Klein, C., Latourelle, J.C., Maraganore, D.M., Martin, E.R., Martinez, M., Myers, R.H., Nalls, M.A., Pankratz, N., Payami, H., Satake, W., Scott, W.K., Sharma, M., Singleton, A.B., Stefansson, K., Toda, T., Tung, J.Y., Vance, J., Wood, N.W., Zabetian, C.P., 23andMe Genetic Epidemiology of Parkinson's Disease Consortium, International Parkinson's Disease Genomics Consortium, Parkinson's Disease GWAS Consortium, Wellcome Trust Case Control Consortium 2), Young, P., Tanzi, R.E., Khoury, M.J., Zipp, F., Lehrach, H., Ioannidis, J.P. and Bertram, L. (2012) 'Comprehensive research synopsis and systematic meta-analyses in Parkinson's disease genetics: The PDGene database', *PLoS genetics,* 8(3), pp. e1002548.

Linderholm, K.R., Skogh, E., Olsson, S.K., Dahl, M.L., Holtze, M., Engberg, G., Samuelsson, M. and Erhardt, S. (2012) 'Increased levels of kynurenine and kynurenic acid in the CSF of patients with schizophrenia', *Schizophrenia bulletin,* 38(3), pp. 426-432.

Liou, H.H., Tsai, M.C., Chen, C.J., Jeng, J.S., Chang, Y.C., Chen, S.Y. and Chen, R.C. (1997) 'Environmental risk factors and Parkinson's disease: a case-control study in Taiwan', *Neurology,* 48(6), pp. 1583-1588.

Littleton, J.T. and Bellen, H.J. (1994) 'Genetic and phenotypic analysis of thirteen essential genes in cytological interval 22F1-2; 23B1-2 reveals novel genes required for neural development in Drosophila', *Genetics,* 138(1), pp. 111-123.

Liu, H., Han, M., Li, Q., Zhang, X., Wang, W.A. and Huang, F.D. (2015) 'Automated rapid iterative negative geotaxis assay and its use in a genetic screen for modifiers of Abeta(42)-induced locomotor decline in Drosophila', *Neuroscience bulletin,* 31(5), pp. 541-549.

Liu, W., Acin-Perez, R., Geghman, K.D., Manfredi, G., Lu, B. and Li, C. (2011) 'Pink1 regulates the oxidative phosphorylation machinery via mitochondrial fission', *Proceedings of the National Academy of Sciences of the United States of America,* 108(31), pp. 12920-12924.

Loh, H.H. and Berg, C.P. (1971) 'Conversion of D-tryptophan to nicotinic acid in the rat', *The Journal of nutrition,* 101(12), pp. 1601-1606.

Lokireddy, S., Wijesoma, I.W., Teng, S., Bonala, S., Gluckman, P.D., McFarlane, C., Sharma, M. and Kambadur, R. (2012) 'The ubiquitin ligase Mul1 induces mitophagy in skeletal muscle in response to muscle-wasting stimuli', *Cell metabolism,* 16(5), pp. 613-624.

Loson, O.C., Song, Z., Chen, H. and Chan, D.C. (2013) 'Fis1, Mff, MiD49, and MiD51 mediate Drp1 recruitment in mitochondrial fission', *Molecular biology of the cell,* 24(5), pp. 659-667.

Luchowski, P., Luchowska, E., Turski, W.A. and Urbanska, E.M. (2002) '1-Methyl-4-phenylpyridinium and 3-nitropropionic acid diminish cortical synthesis of kynurenic acid via interference with kynurenine aminotransferases in rats', *Neuroscience letters,* 330(1), pp. 49-52.

Lucking, C.B., Durr, A., Bonifati, V., Vaughan, J., De Michele, G., Gasser, T., Harhangi, B.S., Meco, G., Denefle, P., Wood, N.W., Agid, Y., Brice, A., French Parkinson's Disease Genetics Study Group and European Consortium on Genetic Susceptibility in Parkinson's Disease (2000) 'Association between early-onset Parkinson's disease and mutations in the parkin gene', *The New England journal of medicine,* 342(21), pp. 1560-1567.

Lugo-Huitron, R., Blanco-Ayala, T., Ugalde-Muniz, P., Carrillo-Mora, P., Pedraza-Chaverri, J., Silva-Adaya, D., Maldonado, P.D., Torres, I., Pinzon, E., Ortiz-Islas, E., Lopez, T., Garcia, E., Pineda, B., Torres-Ramos, M., Santamaria, A. and La Cruz, V.P. (2011) 'On the antioxidant properties of kynurenic acid: free radical scavenging activity and inhibition of oxidative stress', *Neurotoxicology and teratology,* 33(5), pp. 538-547.

Lv, F., Yang, X., Cui, C. and Su, C. (2017) 'Exogenous expression of Drp1 plays neuroprotective roles in the Alzheimer's disease in the Abeta42 transgenic Drosophila model', *PloS one,* 12(5), pp. e0176183.

Maddison, D.C. and Giorgini, F. (2015) 'The kynurenine pathway and neurodegenerative disease', *Seminars in cell & developmental biology,* 40, pp. 134-141.

Malherbe, P., Alberati-Giani, D., Kohler, C. and Cesura, A.M. (1995) 'Identification of a mitochondrial form of kynurenine aminotransferase/glutamine transaminase K from rat brain', *FEBS letters,* 367(2), pp. 141-144.

Manczak, M., Calkins, M.J. and Reddy, P.H. (2011) 'Impaired mitochondrial dynamics and abnormal interaction of amyloid beta with mitochondrial protein Drp1 in neurons from patients with Alzheimer's disease: implications for neuronal damage', *Human molecular genetics,* 20(13), pp. 2495-2509.

Mann, V.M., Cooper, J.M., Daniel, S.E., Srai, K., Jenner, P., Marsden, C.D. and Schapira, A.H. (1994) 'Complex I, iron, and ferritin in Parkinson's disease substantia nigra', *Annals of Neurology,* 36(6), pp. 876-881.

Marti-Masso, J.F., Bergareche, A., Makarov, V., Ruiz-Martinez, J., Gorostidi, A., Lopez de Munain, A., Poza, J.J., Striano, P., Buxbaum, J.D. and Paisan-Ruiz, C. (2013) 'The ACMSD gene, involved in tryptophan metabolism, is mutated in a family with cortical myoclonus, epilepsy, and parkinsonism', *Journal of Molecular Medicine (Berlin, Germany),* 91(12), pp. 1399-1406.

Matsumine, H., Saito, M., Shimoda-Matsubayashi, S., Tanaka, H., Ishikawa, A., Nakagawa-Hattori, Y., Yokochi, M., Kobayashi, T., Igarashi, S., Takano, H., Sanpei, K., Koike, R., Mori, H., Kondo, T., Mizutani, Y., Schaffer, A.A., Yamamura, Y., Nakamura, S., Kuzuhara, S., Tsuji, S. and Mizuno, Y. (1997) 'Localization of a gene for an autosomal recessive form of juvenile Parkinsonism to chromosome 6q25.2-27', *American Journal of Human Genetics,* 60(3), pp. 588-596.

Mazarei, G., Neal, S.J., Becanovic, K., Luthi-Carter, R., Simpson, E.M. and Leavitt, B.R. (2010) 'Expression analysis of novel striatal-enriched genes in Huntington disease', *Human molecular genetics,* 19(4), pp. 609-622.

McCulloch, K.M., Mukherjee, T., Begley, T.P. and Ealick, S.E. (2009) 'Structure of the PLP degradative enzyme 2-methyl-3-hydroxypyridine-5-carboxylic acid oxygenase from Mesorhizobium loti MAFF303099 and its mechanistic implications', *Biochemistry,* 48(19), pp. 4139-4149.

McKenna, M.C., Stevenson, J.H., Huang, X. and Hopkins, I.B. (2000) 'Differential distribution of the enzymes glutamate dehydrogenase and aspartate aminotransferase in cortical synaptic mitochondria contributes to metabolic compartmentation in cortical synaptic terminals', *Neurochemistry international,* 37(2-3), pp. 229-241.

McManus, R.M. and Heneka, M.T. (2017) 'Role of neuroinflammation in neurodegeneration: new insights', *Alzheimer's research & therapy,* 9(1), pp. 14-017-0241-2.

Mears, J.A., Lackner, L.L., Fang, S., Ingerman, E., Nunnari, J. and Hinshaw, J.E. (2011) 'Conformational changes in Dnm1 support a contractile mechanism for mitochondrial fission', *Nature structural & molecular biology,* 18(1), pp. 20-26.

Mehler, A.H. and Knox, W.E. (1950) 'The conversion of tryptophan to kynurenine in liver. II. The enzymatic hydrolysis of formylkynurenine', *The Journal of biological chemistry,* 187(1), pp. 431-438.

Meissner, C., Lorenz, H., Weihofen, A., Selkoe, D.J. and Lemberg, M.K. (2011) 'The mitochondrial intramembrane protease PARL cleaves human Pink1 to regulate Pink1 trafficking', *Journal of neurochemistry,* 117(5), pp. 856-867.

Mendl, N., Occhipinti, A., Muller, M., Wild, P., Dikic, I. and Reichert, A.S. (2011) 'Mitophagy in yeast is independent of mitochondrial fission and requires the stress response gene WHI2', *Journal of cell science,* 124(Pt 8), pp. 1339-1350.

Meng, B., Wu, D., Gu, J., Ouyang, S., Ding, W. and Liu, Z.J. (2014) 'Structural and functional analyses of human tryptophan 2,3-dioxygenase', *Proteins,* 82(11), pp. 3210-3216.

Misko, A.L., Sasaki, Y., Tuck, E., Milbrandt, J. and Baloh, R.H. (2012) 'Mitofusin2 mutations disrupt axonal mitochondrial positioning and promote axon degeneration', *The Journal of neuroscience : the official journal of the Society for Neuroscience,* 32(12), pp. 4145-4155.

Mole, D.J., Webster, S.P., Uings, I., Zheng, X., Binnie, M., Wilson, K., Hutchinson, J.P., Mirguet, O., Walker, A., Beaufils, B., Ancellin, N., Trottet, L., Beneton, V., Mowat, C.G., Wilkinson, M., Rowland, P., Haslam, C., McBride, A., Homer, N.Z., Baily, J.E., Sharp, M.G., Garden, O.J., Hughes, J., Howie, S.E., Holmes, D.S., Liddle, J. and Iredale, J.P. (2016) 'Kynurenine-3-monooxygenase inhibition prevents multiple organ failure in rodent models of acute pancreatitis', *Nature medicine,* 22(2), pp. 202-209.

Morais, V.A., Haddad, D., Craessaerts, K., De Bock, P.J., Swerts, J., Vilain, S., Aerts, L., Overbergh, L., Grunewald, A., Seibler, P., Klein, C., Gevaert, K., Verstreken, P. and De Strooper, B. (2014) 'PINK1 loss-of-function mutations affect mitochondrial complex I activity via NdufA10 ubiquinone uncoupling', *Science (New York, N.Y.),* 344(6180), pp. 203-207.

Moroni, F., Cozzi, A., Sili, M. and Mannaioni, G. (2012) 'Kynurenic acid: a metabolite with multiple actions and multiple targets in brain and periphery', *Journal of neural transmission (Vienna, Austria : 1996),* 119(2), pp. 133-139.

Muchowski, P., Muchowski, J., Schwarcz, R. and Guidetti, P. (2008) ' Small molecule inhibitors of kynurenine-3-monooxygenase patent ', *World Patent WO2008022281,* (Feb 21).

Nakada, K., Inoue, K., Ono, T., Isobe, K., Ogura, A., Goto, Y.I., Nonaka, I. and Hayashi, J.I. (2001) 'Inter-mitochondrial complementation: Mitochondria-specific

system preventing mice from expression of disease phenotypes by mutant mtDNA', *Nature medicine,* 7(8), pp. 934-940.

Nakao, N., Grasbon-Frodl, E.M., Widner, H. and Brundin, P. (1996) 'Antioxidant treatment protects striatal neurons against excitotoxic insults', *Neuroscience,* 73(1), pp. 185-200.

Nalls, M.A., Pankratz, N., Lill, C.M., Do, C.B., Hernandez, D.G., Saad, M., DeStefano, A.L., Kara, E., Bras, J., Sharma, M., Schulte, C., Keller, M.F., Arepalli, S., Letson, C., Edsall, C., Stefansson, H., Liu, X., Pliner, H., Lee, J.H., Cheng, R., International Parkinson's Disease Genomics Consortium (IPDGC), Parkinson's Study Group (PSG) Parkinson's Research: The Organized GENetics Initiative (PROGENI), 23andMe, GenePD, NeuroGenetics Research Consortium (NGRC), Hussman Institute of Human Genomics (HIHG), Ashkenazi Jewish Dataset Investigator, Cohorts for Health and Aging Research in Genetic Epidemiology (CHARGE), North American Brain Expression Consortium (NABEC), United Kingdom Brain Expression Consortium (UKBEC), Greek Parkinson's Disease Consortium, Alzheimer Genetic Analysis Group, Ikram, M.A., Ioannidis, J.P., Hadjigeorgiou, G.M., Bis, J.C., Martinez, M., Perlmutter, J.S., Goate, A., Marder, K., Fiske, B., Sutherland, M., Xiromerisiou, G., Myers, R.H., Clark, L.N., Stefansson, K., Hardy, J.A., Heutink, P., Chen, H., Wood, N.W., Houlden, H., Payami, H., Brice, A., Scott, W.K., Gasser, T., Bertram, L., Eriksson, N., Foroud, T. and Singleton, A.B. (2014) 'Large-scale meta-analysis of genome-wide association data identifies six new risk loci for Parkinson's disease', *Nature genetics,* 46(9), pp. 989-993.

Naoe, M., Ohwa, Y., Ishikawa, D., Ohshima, C., Nishikawa, S., Yamamoto, H. and Endo, T. (2004) 'Identification of Tim40 that mediates protein sorting to the mitochondrial intermembrane space', *The Journal of biological chemistry,* 279(46), pp. 47815-47821.

Naon, D., Zaninello, M., Giacomello, M., Varanita, T., Grespi, F., Lakshminaranayan, S., Serafini, A., Semenzato, M., Herkenne, S., Hernandez-Alvarez, M.I., Zorzano, A., De Stefani, D., Dorn, G.W.,2nd and Scorrano, L. (2016) 'Critical reappraisal confirms that Mitofusin 2 is an endoplasmic reticulum-mitochondria tether', *Proceedings of the National Academy of Sciences of the United States of America,* 113(40), pp. 11249-11254.

Narendra, D.P., Jin, S.M., Tanaka, A., Suen, D.F., Gautier, C.A., Shen, J., Cookson, M.R. and Youle, R.J. (2010a) 'PINK1 is selectively stabilized on impaired mitochondria to activate Parkin', *PLoS biology,* 8(1), pp. e1000298.

Narendra, D., Kane, L.A., Hauser, D.N., Fearnley, I.M. and Youle, R.J. (2010b) 'p62/SQSTM1 is required for Parkin-induced mitochondrial clustering but not mitophagy; VDAC1 is dispensable for both', *Autophagy,* 6(8), pp. 1090-1106.

Narendra, D., Tanaka, A., Suen, D.F. and Youle, R.J. (2008) 'Parkin is recruited selectively to impaired mitochondria and promotes their autophagy', *The Journal of cell biology,* 183(5), pp. 795-803.

Neuspiel, M., Schauss, A.C., Braschi, E., Zunino, R., Rippstein, P., Rachubinski, R.A., Andrade-Navarro, M.A. and McBride, H.M. (2008) 'Cargo-selected transport from the mitochondria to peroxisomes is mediated by vesicular carriers', *Current biology : CB,* 18(2), pp. 102-108.

Nicklas, W.J., Vyas, I. and Heikkila, R.E. (1985) 'Inhibition of NADH-linked oxidation in brain mitochondria by 1-methyl-4-phenyl-pyridine, a metabolite of the neurotoxin, 1-methyl-4-phenyl-1,2,5,6-tetrahydropyridine', *Life Sciences,* 36(26), pp. 2503-2508.

Nilsson, L.K., Linderholm, K.R., Engberg, G., Paulson, L., Blennow, K., Lindstrom, L.H., Nordin, C., Karanti, A., Persson, P. and Erhardt, S. (2005) 'Elevated levels of kynurenic acid in the cerebrospinal fluid of male patients with schizophrenia', *Schizophrenia research,* 80(2-3), pp. 315-322.

Nisimoto, Y., Takeuchi, F. and Shibata, Y. (1977) 'Molecular properties of L-kynurenine 3-hydroxylase from rat liver mitochondria', *Journal of Biochemistry,* 81(5), pp. 1413-1425.

Niu, J., Yu, M., Wang, C. and Xu, Z. (2012) 'Leucine-rich repeat kinase 2 disturbs mitochondrial dynamics via Dynamin-like protein', *Journal of neurochemistry,* 122(3), pp. 650-658.

Nuytemans, K., Theuns, J., Cruts, M. and Van Broeckhoven, C. (2010) 'Genetic etiology of Parkinson disease associated with mutations in the SNCA, PARK2, PINK1, PARK7, and LRRK2 genes: a mutation update', *Human mutation,* 31(7), pp. 763-780.

Ogawa, T., Matson, W.R., Beal, M.F., Myers, R.H., Bird, E.D., Milbury, P. and Saso, S. (1992) 'Kynurenine pathway abnormalities in Parkinson's disease', *Neurology,* 42(9), pp. 1702-1706.

Ogaya, T., Song, Z., Ishii, K. and Fukushima, T. (2010) 'Changes in extracellular kynurenic acid concentrations in rat prefrontal cortex after D-kynurenine infusion: an in vivo microdialysis study', *Neurochemical research,* 35(4), pp. 559-563.

Okamoto, H. and Hayaishi, O. (1967) 'Flavin adenine dinucleotide requirement for kynurenine hydroxylase of rat liver mitochondria', *Biochemical and biophysical research communications,* 29(3), pp. 394-399.

Okamoto, H., Yamamoto, S., Nozaki, M. and Hayaishi, O. (1967) 'On the submitochondrial localization of l-kynurenine-3-hydroxylase', *Biochemical and biophysical research communications,* 26(3), pp. 309-314.

Okatsu, K., Saisho, K., Shimanuki, M., Nakada, K., Shitara, H., Sou, Y.S., Kimura, M., Sato, S., Hattori, N., Komatsu, M., Tanaka, K. and Matsuda, N. (2010) 'p62/SQSTM1 cooperates with Parkin for perinuclear clustering of depolarized

mitochondria', *Genes to cells : devoted to molecular & cellular mechanisms,* 15(8), pp. 887-900.

Okuda, S., Nishiyama, N., Saito, H. and Katsuki, H. (1996) 'Hydrogen peroxide-mediated neuronal cell death induced by an endogenous neurotoxin, 3-hydroxykynurenine', *Proceedings of the National Academy of Sciences of the United States of America,* 93(22), pp. 12553-12558.

Okuno, E., Nakamura, M. and Schwarcz, R. (1991) 'Two kynurenine aminotransferases in human brain', *Brain research,* 542(2), pp. 307-312.

Olsson, S.K., Samuelsson, M., Saetre, P., Lindstrom, L., Jonsson, E.G., Nordin, C., Engberg, G., Erhardt, S. and Landen, M. (2010) 'Elevated levels of kynurenic acid in the cerebrospinal fluid of patients with bipolar disorder', *Journal of psychiatry & neuroscience : JPN,* 35(3), pp. 195-199.

Olsson, S.K., Sellgren, C., Engberg, G., Landen, M. and Erhardt, S. (2012) 'Cerebrospinal fluid kynurenic acid is associated with manic and psychotic features in patients with bipolar I disorder', *Bipolar disorders,* 14(7), pp. 719-726.

Ordonez, D.G., Lee, M.K. and Feany, M.B. (2018) 'alpha-synuclein Induces Mitochondrial Dysfunction through Spectrin and the Actin Cytoskeleton', *Neuron,* 97(1), pp. 108-124.e6.

Osellame, L.D., Singh, A.P., Stroud, D.A., Palmer, C.S., Stojanovski, D., Ramachandran, R. and Ryan, M.T. (2016) 'Cooperative and independent roles of the Drp1 adaptors Mff, MiD49 and MiD51 in mitochondrial fission', *Journal of cell science,* 129(11), pp. 2170-2181.

Osterwalder, T., Yoon, K.S., White, B.H. and Keshishian, H. (2001) 'A conditional tissue-specific transgene expression system using inducible GAL4', *Proceedings of the National Academy of Sciences of the United States of America,* 98(22), pp. 12596-12601.

Otera, H., Wang, C., Cleland, M.M., Setoguchi, K., Yokota, S., Youle, R.J. and Mihara, K. (2010) 'Mff is an essential factor for mitochondrial recruitment of Drp1 during mitochondrial fission in mammalian cells', *The Journal of cell biology,* 191(6), pp. 1141-1158.

Otto, P.A. (2000) Drosophila viewer: a program on the formal genetics, anatomy and developmental biology of *Drosophila melanogaster* for students and specialists. Genet Mol Biol 23: 835-839.

Palacino, J.J., Sagi, D., Goldberg, M.S., Krauss, S., Motz, C., Wacker, M., Klose, J. and Shen, J. (2004) 'Mitochondrial dysfunction and oxidative damage in parkin-deficient mice', *The Journal of biological chemistry,* 279(18), pp. 18614-18622.

Palmer, C.S., Elgass, K.D., Parton, R.G., Osellame, L.D., Stojanovski, D. and Ryan, M.T. (2013) 'Adaptor proteins MiD49 and MiD51 can act independently of Mff and Fis1 in Drp1 recruitment and are specific for mitochondrial fission', *The Journal of biological chemistry,* 288(38), pp. 27584-27593.

Park, J., Lee, S.B., Lee, S., Kim, Y., Song, S., Kim, S., Bae, E., Kim, J., Shong, M., Kim, J.M. and Chung, J. (2006) 'Mitochondrial dysfunction in Drosophila PINK1 mutants is complemented by parkin', *Nature,* 441(7097), pp. 1157-1161.

Perez-de la Cruz, V., Amori, L., Sathyasaikumar, K.V., Wang, X.D., Notarangelo, F.M., Wu, H.Q. and Schwarcz, R. (2012a) 'Enzymatic transamination of D-kynurenine generates kynurenic acid in rat and human brain', *Journal of neurochemistry,* 120(6), pp. 1026-1035.

Perez-De La Cruz, V., Carrillo-Mora, P. and Santamaria, A. (2012b) 'Quinolinic Acid, an endogenous molecule combining excitotoxicity, oxidative stress and other toxic mechanisms', *International journal of tryptophan research : IJTR,* 5, pp. 1-8.

Perez-Severiano, F., Escalante, B. and Rios, C. (1998) 'Nitric oxide synthase inhibition prevents acute quinolinate-induced striatal neurotoxicity', *Neurochemical research,* 23(10), pp. 1297-1302.

Perkins, M.N. and Stone, T.W. (1982) 'An iontophoretic investigation of the actions of convulsant kynurenines and their interaction with the endogenous excitant quinolinic acid', *Brain research,* 247(1), pp. 184-187.

Pesah, Y., Pham, T., Burgess, H., Middlebrooks, B., Verstreken, P., Zhou, Y., Harding, M., Bellen, H. and Mardon, G. (2004) 'Drosophila parkin mutants have decreased mass and cell size and increased sensitivity to oxygen radical stress', *Development (Cambridge, England),* 131(9), pp. 2183-2194.

Pfaffl, M.W., Horgan, G.W. and Dempfle, L. (2002) 'Relative expression software tool (REST) for group-wise comparison and statistical analysis of relative expression results in real-time PCR', *Nucleic acids research,* 30(9), pp. e36.

Pickrell, A.M. and Youle, R.J. (2015) 'The roles of PINK1, parkin, and mitochondrial fidelity in Parkinson's disease', *Neuron,* 85(2), pp. 257-273.

Pihlstrom, L., Axelsson, G., Bjornara, K.A., Dizdar, N., Fardell, C., Forsgren, L., Holmberg, B., Larsen, J.P., Linder, J., Nissbrandt, H., Tysnes, O.B., Ohman, E., Dietrichs, E. and Toft, M. (2013) 'Supportive evidence for 11 loci from genome-wide association studies in Parkinson's disease', *Neurobiology of aging,* 34(6), pp. 1708.e7-1708.13.

Pogson, J.H., Ivatt, R.M., Sanchez-Martinez, A., Tufi, R., Wilson, E., Mortiboys, H. and Whitworth, A.J. (2014) 'The complex I subunit NDUFA10 selectively rescues Drosophila pink1 mutants through a mechanism independent of mitophagy', *PLoS genetics,* 10(11), pp. e1004815.

Poole, A.C., Thomas, R.E., Andrews, L.A., McBride, H.M., Whitworth, A.J. and Pallanck, L.J. (2008) 'The PINK1/Parkin pathway regulates mitochondrial morphology', *Proceedings of the National Academy of Sciences of the United States of America,* 105(5), pp. 1638-1643.

Poole, A.C., Thomas, R.E., Yu, S., Vincow, E.S. and Pallanck, L. (2010) 'The mitochondrial fusion-promoting factor mitofusin is a substrate of the PINK1/parkin pathway', *PloS one,* 5(4), pp. e10054.

Prendergast, G.C., Smith, C., Thomas, S., Mandik-Nayak, L., Laury-Kleintop, L., Metz, R. and Muller, A.J. (2014) 'Indoleamine 2,3-dioxygenase pathways of pathogenic inflammation and immune escape in cancer', *Cancer immunology, immunotherapy : CII,* 63(7), pp. 721-735.

Pryde, K.R., Smith, H.L., Chau, K.Y. and Schapira, A.H. (2016) 'PINK1 disables the anti-fission machinery to segregate damaged mitochondria for mitophagy', *The Journal of cell biology,* 213(2), pp. 163-171.

Pucci, L., Perozzi, S., Cimadamore, F., Orsomando, G. and Raffaelli, N. (2007) 'Tissue expression and biochemical characterization of human 2-amino 3-carboxymuconate 6-semialdehyde decarboxylase, a key enzyme in tryptophan catabolism', *The FEBS journal,* 274(3), pp. 827-840.

Puigserver, P., Wu, Z., Park, C.W., Graves, R., Wright, M. and Spiegelman, B.M. (1998) 'A cold-inducible coactivator of nuclear receptors linked to adaptive thermogenesis', *Cell,* 92(6), pp. 829-839.

Rafice, S.A., Chauhan, N., Efimov, I., Basran, J. and Raven, E.L. (2009) 'Oxidation of L-tryptophan in biology: a comparison between tryptophan 2,3-dioxygenase and indoleamine 2,3-dioxygenase', *Biochemical Society transactions,* 37(Pt 2), pp. 408-412.

Rahman, A., Ting, K., Cullen, K.M., Braidy, N., Brew, B.J. and Guillemin, G.J. (2009) 'The excitotoxin quinolinic acid induces tau phosphorylation in human neurons', *PloS one,* 4(7), pp. e6344.

Rambold, A.S., Kostelecky, B., Elia, N. and Lippincott-Schwartz, J. (2011) 'Tubular network formation protects mitochondria from autophagosomal degradation during nutrient starvation', *Proceedings of the National Academy of Sciences of the United States of America,* 108(25), pp. 10190-10195.

Ramsay, R.R. and Singer, T.P. (1986) 'Energy-dependent uptake of N-methyl-4-phenylpyridinium, the neurotoxic metabolite of 1-methyl-4-phenyl-1,2,3,6-tetrahydropyridine, by mitochondria', *The Journal of biological chemistry,* 261(17), pp. 7585-7587.

Rana, A., Oliveira, M.P., Khamoui, A.V., Aparicio, R., Rera, M., Rossiter, H.B. and Walker, D.W. (2017) 'Promoting Drp1-mediated mitochondrial fission in

midlife prolongs healthy lifespan of Drosophila melanogaster', *Nature communications,* 8(1), pp. 448-017-00525-4.

Rana, A., Rera, M. and Walker, D.W. (2013) 'Parkin overexpression during aging reduces proteotoxicity, alters mitochondrial dynamics, and extends lifespan', *Proceedings of the National Academy of Sciences of the United States of America,* 110(21), pp. 8638-8643.

Ravikumar, A., Deepadevi, K.V., Arun, P., Manojkumar, V. and Kurup, P.A. (2000) 'Tryptophan and tyrosine catabolic pattern in neuropsychiatric disorders', *Neurology India,* 48(3), pp. 231-238.

Ren, S. and Correia, M.A. (2000) 'Heme: a regulator of rat hepatic tryptophan 2,3-dioxygenase?', *Archives of Biochemistry and Biophysics,* 377(1), pp. 195-203.

Reyes-Ocampo, J., Ramirez-Ortega, D., Cervantes, G.I., Pineda, B., Balderas, P.M., Gonzalez-Esquivel, D., Sanchez-Chapul, L., Lugo-Huitron, R., Silva-Adaya, D., Rios, C., Jimenez-Anguiano, A. and Perez-de la Cruz, V. (2015) 'Mitochondrial dysfunction related to cell damage induced by 3-hydroxykynurenine and 3-hydroxyanthranilic acid: Non-dependent-effect of early reactive oxygen species production', *Neurotoxicology,* 50, pp. 81-91.

Rhodenizer, D., Martin, I., Bhandari, P., Pletcher, S.D. and Grotewiel, M. (2008) 'Genetic and environmental factors impact age-related impairment of negative geotaxis in Drosophila by altering age-dependent climbing speed', *Experimental gerontology,* 43(8), pp. 739-748.

Rios, C. and Santamaria, A. (1991) 'Quinolinic acid is a potent lipid peroxidant in rat brain homogenates', *Neurochemical research,* 16(10), pp. 1139-1143.

Ritz, C. and Spiess, A.N. (2008) 'qpcR: an R package for sigmoidal model selection in quantitative real-time polymerase chain reaction analysis', *Bioinformatics (Oxford, England),* 24(13), pp. 1549-1551.

Rizzuto, R., Pinton, P., Carrington, W., Fay, F.S., Fogarty, K.E., Lifshitz, L.M., Tuft, R.A. and Pozzan, T. (1998) 'Close contacts with the endoplasmic reticulum as determinants of mitochondrial Ca2+ responses', *Science (New York, N.Y.),* 280(5370), pp. 1763-1766.

Roberts, J.E. (2001) 'Ocular phototoxicity', *Journal of photochemistry and photobiology.B, Biology,* 64(2-3), pp. 136-143.

Roberts, R.C., Du, F., McCarthy, K.E., Okuno, E. and Schwarcz, R. (1992) 'Immunocytochemical localization of kynurenine aminotransferase in the rat striatum: a light and electron microscopic study', *The Journal of comparative neurology,* 326(1), pp. 82-90.

Rodgers, J., Stone, T.W., Barrett, M.P., Bradley, B. and Kennedy, P.G. (2009) 'Kynurenine pathway inhibition reduces central nervous system inflammation

in a model of human African trypanosomiasis', *Brain : a journal of neurology,* 132(Pt 5), pp. 1259-1267.

Rogers, S.L. and Rogers, G.C. (2008) 'Culture of Drosophila S2 cells and their use for RNAi-mediated loss-of-function studies and immunofluorescence microscopy', *Nature protocols,* 3(4), pp. 606-611.

Rojewska, E., Piotrowska, A., Makuch, W., Przewlocka, B. and Mika, J. (2016) 'Pharmacological kynurenine 3-monooxygenase enzyme inhibition significantly reduces neuropathic pain in a rat model', *Neuropharmacology,* 102, pp. 80-91.

Rojo, M., Legros, F., Chateau, D. and Lombes, A. (2002) 'Membrane topology and mitochondrial targeting of mitofusins, ubiquitous mammalian homologs of the transmembrane GTPase Fzo', *Journal of cell science,* 115(Pt 8), pp. 1663-1674.

Rongvaux, A., Andris, F., Van Gool, F. and Leo, O. (2003) 'Reconstructing eukaryotic NAD metabolism', *BioEssays : news and reviews in molecular, cellular and developmental biology,* 25(7), pp. 683-690.

Rosato, E. and Kyriacou, C.P. (2006) 'Analysis of locomotor activity rhythms in Drosophila', *Nature protocols,* 1(2), pp. 559-568.

Ruhoy, I.S. and Saneto, R.P. (2014) 'The genetics of Leigh syndrome and its implications for clinical practice and risk management', *The application of clinical genetics,* 7, pp. 221-234.

Sagan, L. (1967) 'On the origin of mitosing cells', *Journal of theoretical biology,* 14(3), pp. 255-274.

Saito, Y., Hayaishi, O. and Rothberg, S. (1957) 'Studies on oxygenases; enzymatic formation of 3-hydroxy-L-kynurenine from L-kynurenine', *The Journal of biological chemistry,* 229(2), pp. 921-934.

Santamaria, A. and Rios, C. (1993) 'MK-801, an N-methyl-D-aspartate receptor antagonist, blocks quinolinic acid-induced lipid peroxidation in rat corpus striatum', *Neuroscience letters,* 159(1-2), pp. 51-54.

Santel, A. and Fuller, M.T. (2001) 'Control of mitochondrial morphology by a human mitofusin', *Journal of cell science,* 114(Pt 5), pp. 867-874.

Sarraf, S.A., Raman, M., Guarani-Pereira, V., Sowa, M.E., Huttlin, E.L., Gygi, S.P. and Harper, J.W. (2013) 'Landscape of the PARKIN-dependent ubiquitylome in response to mitochondrial depolarization', *Nature,* 496(7445), pp. 372-376.

Sathyasaikumar, K.V., Stachowski, E.K., Wonodi, I., Roberts, R.C., Rassoulpour, A., McMahon, R.P. and Schwarcz, R. (2011) 'Impaired kynurenine pathway metabolism in the prefrontal cortex of individuals with schizophrenia', *Schizophrenia bulletin,* 37(6), pp. 1147-1156.

Schapira, A.H., Cooper, J.M., Dexter, D., Clark, J.B., Jenner, P. and Marsden, C.D. (1990) 'Mitochondrial complex I deficiency in Parkinson's disease', *Journal of neurochemistry,* 54(3), pp. 823-827.

Schlittler, M., Goiny, M., Agudelo, L.Z., Venckunas, T., Brazaitis, M., Skurvydas, A., Kamandulis, S., Ruas, J.L., Erhardt, S., Westerblad, H. and Andersson, D.C. (2016) 'Endurance exercise increases skeletal muscle kynurenine aminotransferases and plasma kynurenic acid in humans', *American journal of physiology.Cell physiology,* 310(10), pp. C836-40.

Schnorrer, F., Schonbauer, C., Langer, C.C., Dietzl, G., Novatchkova, M., Schernhuber, K., Fellner, M., Azaryan, A., Radolf, M., Stark, A., Keleman, K. and Dickson, B.J. (2010) 'Systematic genetic analysis of muscle morphogenesis and function in Drosophila', *Nature,* 464(7286), pp. 287-291.

Schon, E.A. and Gilkerson, R.W. (2010) 'Functional complementation of mitochondrial DNAs: mobilizing mitochondrial genetics against dysfunction', *Biochimica et biophysica acta,* 1800(3), pp. 245-249.

Schon, E.A. and Przedborski, S. (2011) 'Mitochondria: the next (neurode)generation', *Neuron,* 70(6), pp. 1033-1053.

Schousboe, A., Bachevalier, J., Braak, H., Heinemann, U., Nitsch, R., Schroder, H. and Wetmore, C. (1993) 'Structural correlates and cellular mechanisms in entorhinal-hippocampal dysfunction', *Hippocampus,* 3 Spec No, pp. 293-301.

Schwarcz, R., Bruno, J.P., Muchowski, P.J. and Wu, H.Q. (2012) 'Kynurenines in the mammalian brain: when physiology meets pathology', *Nature reviews.Neuroscience,* 13(7), pp. 465-477.

Schwarcz, R., Rassoulpour, A., Wu, H.Q., Medoff, D., Tamminga, C.A. and Roberts, R.C. (2001) 'Increased cortical kynurenate content in schizophrenia', *Biological psychiatry,* 50(7), pp. 521-530.

Schwarcz, R., Whetsell, W.O.,Jr and Mangano, R.M. (1983) 'Quinolinic acid: an endogenous metabolite that produces axon-sparing lesions in rat brain', *Science (New York, N.Y.),* 219(4582), pp. 316-318.

Schwartz, R.M. and Dayhoff, M.O. (1978) 'Origins of prokaryotes, eukaryotes, mitochondria, and chloroplasts', *Science (New York, N.Y.),* 199(4327), pp. 395-403.

Scialo, F., Sriram, A., Fernandez-Ayala, D., Gubina, N., Lohmus, M., Nelson, G., Logan, A., Cooper, H.M., Navas, P., Enriquez, J.A., Murphy, M.P. and Sanz, A. (2016) 'Mitochondrial ROS Produced via Reverse Electron Transport Extend Animal Lifespan', *Cell metabolism,* 23(4), pp. 725-734.

Searles, L.L. and Voelker, R.A. (1986) 'Molecular characterization of the Drosophila vermilion locus and its suppressible alleles', *Proceedings of the National Academy of Sciences of the United States of America,* 83(2), pp. 404-408.

Sellgren, C.M., Kegel, M.E., Bergen, S.E., Ekman, C.J., Olsson, S., Larsson, M., Vawter, M.P., Backlund, L., Sullivan, P.F., Sklar, P., Smoller, J.W., Magnusson, P.K., Hultman, C.M., Walther-Jallow, L., Svensson, C.I., Lichtenstein, P., Schalling, M., Engberg, G., Erhardt, S. and Landen, M. (2016) 'A genome-wide association study of kynurenic acid in cerebrospinal fluid: implications for psychosis and cognitive impairment in bipolar disorder', *Molecular psychiatry,* 21(10), pp. 1342-1350.

Sharma, M., Ioannidis, J.P., Aasly, J.O., Annesi, G., Brice, A., Van Broeckhoven, C., Bertram, L., Bozi, M., Crosiers, D., Clarke, C., Facheris, M., Farrer, M., Garraux, G., Gispert, S., Auburger, G., Vilarino-Guell, C., Hadjigeorgiou, G.M., Hicks, A.A., Hattori, N., Jeon, B., Lesage, S., Lill, C.M., Lin, J.J., Lynch, T., Lichtner, P., Lang, A.E., Mok, V., Jasinska-Myga, B., Mellick, G.D., Morrison, K.E., Opala, G., Pramstaller, P.P., Pichler, I., Park, S.S., Quattrone, A., Rogaeva, E., Ross, O.A., Stefanis, L., Stockton, J.D., Satake, W., Silburn, P.A., Theuns, J., Tan, E.K., Toda, T., Tomiyama, H., Uitti, R.J., Wirdefeldt, K., Wszolek, Z., Xiromerisiou, G., Yueh, K.C., Zhao, Y., Gasser, T., Maraganore, D., Kruger, R. and GEO-PD Consortium (2012) 'Large-scale replication and heterogeneity in Parkinson disease genetic loci', *Neurology,* 79(7), pp. 659-667.

Shiba-Fukushima, K., Imai, Y., Yoshida, S., Ishihama, Y., Kanao, T., Sato, S. and Hattori, N. (2012) 'PINK1-mediated phosphorylation of the Parkin ubiquitin-like domain primes mitochondrial translocation of Parkin and regulates mitophagy', *Scientific reports,* 2, pp. 1002.

Shirendeb, U.P., Calkins, M.J., Manczak, M., Anekonda, V., Dufour, B., McBride, J.L., Mao, P. and Reddy, P.H. (2012) 'Mutant huntingtin's interaction with mitochondrial protein Drp1 impairs mitochondrial biogenesis and causes defective axonal transport and synaptic degeneration in Huntington's disease', *Human molecular genetics,* 21(2), pp. 406-420.

Shirendeb, U.P., Calkins, M.J., Manczak, M., Anekonda, V., Dufour, B., McBride, J.L., Mao, P. and Reddy, P.H. (2012) 'Mutant huntingtin's interaction with mitochondrial protein Drp1 impairs mitochondrial biogenesis and causes defective axonal transport and synaptic degeneration in Huntington's disease', *Human molecular genetics,* 21(2), pp. 406-420.

Siddiqui, A., Hanson, I. and Andersen, J.K. (2012) 'Mao-B elevation decreases parkin's ability to efficiently clear damaged mitochondria: protective effects of rapamycin', *Free radical research,* 46(8), pp. 1011-1018.

Sirrenberg, C., Bauer, M.F., Guiard, B., Neupert, W. and Brunner, M. (1996) 'Import of carrier proteins into the mitochondrial inner membrane mediated by Tim22', *Nature,* 384(6609), pp. 582-585.

Smirnova, E., Griparic, L., Shurland, D.L. and van der Bliek, A.M. (2001) 'Dynamin-related protein Drp1 is required for mitochondrial division in mammalian cells', *Molecular biology of the cell,* 12(8), pp. 2245-2256.

Smith, A.J., Smith, R.A. and Stone, T.W. (2009) '5-Hydroxyanthranilic acid, a tryptophan metabolite, generates oxidative stress and neuronal death via p38 activation in cultured cerebellar granule neurones', *Neurotoxicity research,* 15(4), pp. 303-310.

Smith, F.D., Reichow, S.L., Esseltine, J.L., Shi, D., Langeberg, L.K., Scott, J.D. and Gonen, T. (2013) 'Intrinsic disorder within an AKAP-protein kinase A complex guides local substrate phosphorylation', *eLife,* 2, pp. e01319.

Soman, S., Keatinge, M., Moein, M., Da Costa, M., Mortiboys, H., Skupin, A., Sugunan, S., Bazala, M., Kuznicki, J. and Bandmann, O. (2017) 'Inhibition of the mitochondrial calcium uniporter rescues dopaminergic neurons in pink1(-/-) zebrafish', *The European journal of neuroscience,* 45(4), pp. 528-535.

Song, M., Gong, G., Burelle, Y., Gustafsson, A.B., Kitsis, R.N., Matkovich, S.J. and Dorn, G.W.,2nd (2015) 'Interdependence of Parkin-Mediated Mitophagy and Mitochondrial Fission in Adult Mouse Hearts', *Circulation research,* 117(4), pp. 346-351.

Song, W., Chen, J., Petrilli, A., Liot, G., Klinglmayr, E., Zhou, Y., Poquiz, P., Tjong, J., Pouladi, M.A., Hayden, M.R., Masliah, E., Ellisman, M., Rouiller, I., Schwarzenbacher, R., Bossy, B., Perkins, G. and Bossy-Wetzel, E. (2011) 'Mutant huntingtin binds the mitochondrial fission GTPase dynamin-related protein-1 and increases its enzymatic activity', *Nature medicine,* 17(3), pp. 377-382.

Sotillo, B., Bharadwaj, V., Hadden, J.P., Sakakura, M., Chiappini, A., Fernandez, T.T., Longhi, S., Jedrkiewicz, O., Shimotsuma, Y., Criante, L., Osellame, R., Galzerano, G., Ferrari, M., Miura, K., Ramponi, R., Barclay, P.E. and Eaton, S.M. (2016) 'Diamond photonics platform enabled by femtosecond laser writing', *Scientific reports,* 6, pp. 35566.

Stipek, S., Stastny, F., Platenik, J., Crkovska, J. and Zima, T. (1997) 'The effect of quinolinate on rat brain lipid peroxidation is dependent on iron', *Neurochemistry international,* 30(2), pp. 233-237.

Stone, T.W., Mackay, G.M., Forrest, C.M., Clark, C.J. and Darlington, L.G. (2003) 'Tryptophan metabolites and brain disorders', *Clinical chemistry and laboratory medicine,* 41(7), pp. 852-859.

Stone, T.W. and Perkins, M.N. (1981) 'Quinolinic acid: a potent endogenous excitant at amino acid receptors in CNS', *European journal of pharmacology,* 72(4), pp. 411-412.

Stoy, N., Mackay, G.M., Forrest, C.M., Christofides, J., Egerton, M., Stone, T.W. and Darlington, L.G. (2005) 'Tryptophan metabolism and oxidative stress in

patients with Huntington's disease', *Journal of neurochemistry,* 93(3), pp. 611-623.

Strausfeld, N.J. and Hirth, F. (2013) 'Deep homology of arthropod central complex and vertebrate basal ganglia', *Science (New York, N.Y.),* 340(6129), pp. 157-161.

Sullivan, D.T., Bell, L.A., Paton, D.R. and Sullivan, M.C. (1980) 'Genetic and functional analysis of tryptophan transport in Malpighian tubules of Drosophila', *Biochemical genetics,* 18(11-12), pp. 1109-1130.

Sullivan, D.T., Grillo, S.L. and Kitos, R.J. (1974) 'Subcellular localization of the first three enzymes of the ommochrome synthetic pathway in Drosophila melanogaster', *The Journal of experimental zoology,* 188(2), pp. 225-233.

Sullivan, D.T. and Sullivan, M.C. (1975) 'Transport defects as the physiological basis for eye color mutants of Drosophila melanogaster', *Biochemical genetics,* 13(9-10), pp. 603-613.

Swaih, A. (2016) 'Functional and localization studies of human knurenine 3-monooxygenase', *PhD Thesis (University of Leicester),* .

Szalai, G., Krishnamurthy, R. and Hajnoczky, G. (1999) 'Apoptosis driven by IP(3)-linked mitochondrial calcium signals', *The EMBO journal,* 18(22), pp. 6349-6361.

Taguchi, N., Ishihara, N., Jofuku, A., Oka, T. and Mihara, K. (2007) 'Mitotic phosphorylation of dynamin-related GTPase Drp1 participates in mitochondrial fission', *The Journal of biological chemistry,* 282(15), pp. 11521-11529.

Tanaka, A., Cleland, M.M., Xu, S., Narendra, D.P., Suen, D.F., Karbowski, M. and Youle, R.J. (2010) 'Proteasome and p97 mediate mitophagy and degradation of mitofusins induced by Parkin', *The Journal of cell biology,* 191(7), pp. 1367-1380.

Tanner, C.M., Kamel, F., Ross, G.W., Hoppin, J.A., Goldman, S.M., Korell, M., Marras, C., Bhudhikanok, G.S., Kasten, M., Chade, A.R., Comyns, K., Richards, M.B., Meng, C., Priestley, B., Fernandez, H.H., Cambi, F., Umbach, D.M., Blair, A., Sandler, D.P. and Langston, J.W. (2011) 'Rotenone, paraquat, and Parkinson's disease', *Environmental health perspectives,* 119(6), pp. 866-872.

Tavares, R.G., Tasca, C.I., Santos, C.E., Alves, L.B., Porciuncula, L.O., Emanuelli, T. and Souza, D.O. (2002) 'Quinolinic acid stimulates synaptosomal glutamate release and inhibits glutamate uptake into astrocytes', *Neurochemistry international,* 40(7), pp. 621-627.

Tearle, R. (1991) 'Tissue specific effects of ommochrome pathway mutations in Drosophila melanogaster', *Genetical research,* 57(3), pp. 257-266.

Teulier, L., Weber, J.M., Crevier, J. and Darveau, C.A. (2016) 'Proline as a fuel for insect flight: enhancing carbohydrate oxidation in hymenopterans', *Proceedings.Biological sciences,* 283(1834), pp. 10.1098/rspb.2016.0333.

Thevandavakkam, M. (2011) 'DECIPHERING THE KYNURENINE 3-MONOOXYGENASE INTERACTOME', *PhD Thesis (University of Leicester),* .

Thomas, R.E., Andrews, L.A., Burman, J.L., Lin, W.Y. and Pallanck, L.J. (2014) 'PINK1-Parkin pathway activity is regulated by degradation of PINK1 in the mitochondrial matrix', *PLoS genetics,* 10(5), pp. e1004279.

Thomas, S.R. and Stocker, R. (1999) 'Redox reactions related to indoleamine 2,3-dioxygenase and tryptophan metabolism along the kynurenine pathway', *Redox report : communications in free radical research,* 4(5), pp. 199-220.

Ting, K.K., Brew, B.J. and Guillemin, G.J. (2009) 'Effect of quinolinic acid on human astrocytes morphology and functions: implications in Alzheimer's disease', *Journal of neuroinflammation,* 6, pp. 36-2094-6-36.

Torok, N., Torok, R., Szolnoki, Z., Somogyvari, F., Klivenyi, P. and Vecsei, L. (2015) 'The Genetic Link between Parkinson's Disease and the Kynurenine Pathway Is Still Missing', *Parkinson's disease,* 2015, pp. 474135.

Trétiakoff, C. (1919) 'Contribution a l'étude de l'anatomie pathologique du Locus Niger de Soemmering avec quelques déductions relative à la pathogénie des troubles du tonus muscularaire et de la maladie de Parkinson. ', *These de Paris,* .

Trevisan, T., Pendin, D., Montagna, A., Bova, S., Ghelli, A.M. and Daga, A. (2018) 'Manipulation of Mitochondria Dynamics Reveals Separate Roles for Form and Function in Mitochondria Distribution', *Cell reports,* 23(6), pp. 1742-1753.

Twig, G., Elorza, A., Molina, A.J., Mohamed, H., Wikstrom, J.D., Walzer, G., Stiles, L., Haigh, S.E., Katz, S., Las, G., Alroy, J., Wu, M., Py, B.F., Yuan, J., Deeney, J.T., Corkey, B.E. and Shirihai, O.S. (2008) 'Fission and selective fusion govern mitochondrial segregation and elimination by autophagy', *The EMBO journal,* 27(2), pp. 433-446.

Uemura, T. and Hirai, K. (1998) 'L-kynurenine 3-monooxygenase from mitochondrial outer membrane of pig liver: purification, some properties, and monoclonal antibodies directed to the enzyme', *Journal of Biochemistry,* 123(2), pp. 253-262.

Uhlen, M., Fagerberg, L., Hallstrom, B.M., Lindskog, C., Oksvold, P., Mardinoglu, A., Sivertsson, A., Kampf, C., Sjostedt, E., Asplund, A., Olsson, I., Edlund, K., Lundberg, E., Navani, S., Szigyarto, C.A., Odeberg, J., Djureinovic, D., Takanen, J.O., Hober, S., Alm, T., Edqvist, P.H., Berling, H., Tegel, H., Mulder, J., Rockberg, J., Nilsson, P., Schwenk, J.M., Hamsten, M., von Feilitzen, K., Forsberg, M., Persson,

L., Johansson, F., Zwahlen, M., von Heijne, G., Nielsen, J. and Ponten, F. (2015) 'Proteomics. Tissue-based map of the human proteome', *Science (New York, N.Y.),* 347(6220), pp. 1260419.

Valadas, J.S., Esposito, G., Vandekerkhove, D., Miskiewicz, K., Deaulmerie, L., Raitano, S., Seibler, P., Klein, C. and Verstreken, P. (2018) 'ER Lipid Defects in Neuropeptidergic Neurons Impair Sleep Patterns in Parkinson's Disease', *Neuron,* 98(6), pp. 1155-1169.e6.

Valente, E.M., Abou-Sleiman, P.M., Caputo, V., Muqit, M.M., Harvey, K., Gispert, S., Ali, Z., Del Turco, D., Bentivoglio, A.R., Healy, D.G., Albanese, A., Nussbaum, R., Gonzalez-Maldonado, R., Deller, T., Salvi, S., Cortelli, P., Gilks, W.P., Latchman, D.S., Harvey, R.J., Dallapiccola, B., Auburger, G. and Wood, N.W. (2004) 'Hereditary early-onset Parkinson's disease caused by mutations in PINK1', *Science (New York, N.Y.),* 304(5674), pp. 1158-1160.

Valente, E.M., Bentivoglio, A.R., Dixon, P.H., Ferraris, A., Ialongo, T., Frontali, M., Albanese, A. and Wood, N.W. (2001) 'Localization of a novel locus for autosomal recessive early-onset parkinsonism, PARK6, on human chromosome 1p35-p36', *American Journal of Human Genetics,* 68(4), pp. 895-900.

van der Goot, A.T., Zhu, W., Vazquez-Manrique, R.P., Seinstra, R.I., Dettmer, K., Michels, H., Farina, F., Krijnen, J., Melki, R., Buijsman, R.C., Ruiz Silva, M., Thijssen, K.L., Kema, I.P., Neri, C., Oefner, P.J. and Nollen, E.A. (2012) 'Delaying aging and the aging-associated decline in protein homeostasis by inhibition of tryptophan degradation', *Proceedings of the National Academy of Sciences of the United States of America,* 109(37), pp. 14912-14917.

van der Goot, A.T. and Nollen, E.A. (2013) 'Tryptophan metabolism: entering the field of aging and age-related pathologies', *Trends in molecular medicine,* 19(6), pp. 336-344.

Vazquez, S., Garner, B., Sheil, M.M. and Truscott, R.J. (2000) 'Characterisation of the major autoxidation products of 3-hydroxykynurenine under physiological conditions', *Free radical research,* 32(1), pp. 11-23.

Verstreken, P., Ly, C.V., Venken, K.J., Koh, T.W., Zhou, Y. and Bellen, H.J. (2005) 'Synaptic mitochondria are critical for mobilization of reserve pool vesicles at Drosophila neuromuscular junctions', *Neuron,* 47(3), pp. 365-378.

Vilas, D., Fernandez-Santiago, R., Sanchez, E., Azcona, L.J., Santos-Montes, M., Casquero, P., Argandona, L., Tolosa, E. and Paisan-Ruiz, C. (2017) 'A Novel p.Glu298Lys Mutation in the ACMSD Gene in Sporadic Parkinson's Disease', *Journal of Parkinson's disease,* 7(3), pp. 459-463.

Vincow, E.S., Merrihew, G., Thomas, R.E., Shulman, N.J., Beyer, R.P., MacCoss, M.J. and Pallanck, L.J. (2013) 'The PINK1-Parkin pathway promotes both mitophagy and selective respiratory chain turnover in vivo', *Proceedings of the National Academy of Sciences of the United States of America,* 110(16), pp. 6400-6405.

Voss, C., Lahiri, S., Young, B.P., Loewen, C.J. and Prinz, W.A. (2012) 'ER-shaping proteins facilitate lipid exchange between the ER and mitochondria in S. cerevisiae', *Journal of cell science,* 125(Pt 20), pp. 4791-4799.

Walker, A.K., Kavelaars, A., Heijnen, C.J. and Dantzer, R. (2013) 'Neuroinflammation and comorbidity of pain and depression', *Pharmacological reviews,* 66(1), pp. 80-101.

Wallin, I. (1925) 'On the nature of mitochondria. IX. Demonstration of the bacterial nature of mitochondria', *Developmental Dynamics,* 36(1), pp. 131-149.

Wang, J., Simonavicius, N., Wu, X., Swaminath, G., Reagan, J., Tian, H. and Ling, L. (2006) 'Kynurenic acid as a ligand for orphan G protein-coupled receptor GPR35', *The Journal of biological chemistry,* 281(31), pp. 22021-22028.

Wang, X., Su, B., Fujioka, H. and Zhu, X. (2008) 'Dynamin-like protein 1 reduction underlies mitochondrial morphology and distribution abnormalities in fibroblasts from sporadic Alzheimer's disease patients', *The American journal of pathology,* 173(2), pp. 470-482.

Wang, X., Winter, D., Ashrafi, G., Schlehe, J., Wong, Y.L., Selkoe, D., Rice, S., Steen, J., LaVoie, M.J. and Schwarz, T.L. (2011) 'PINK1 and Parkin target Miro for phosphorylation and degradation to arrest mitochondrial motility', *Cell,* 147(4), pp. 893-906.

Wang, X., Yan, M.H., Fujioka, H., Liu, J., Wilson-Delfosse, A., Chen, S.G., Perry, G., Casadesus, G. and Zhu, X. (2012) 'LRRK2 regulates mitochondrial dynamics and function through direct interaction with DLP1', *Human molecular genetics,* 21(9), pp. 1931-1944.

Wang, X.D., Notarangelo, F.M., Wang, J.Z. and Schwarcz, R. (2012) 'Kynurenic acid and 3-hydroxykynurenine production from D-kynurenine in mice', *Brain research,* 1455, pp. 1-9.

Wang, Y., Lawson, M.A., Dantzer, R. and Kelley, K.W. (2010) 'LPS-induced indoleamine 2,3-dioxygenase is regulated in an interferon-gamma-independent manner by a JNK signaling pathway in primary murine microglia', *Brain, behavior, and immunity,* 24(2), pp. 201-209.

Warren, W.D., Palmer, S. and Howells, A.J. (1996) 'Molecular characterization of the cinnabar region of Drosophila melanogaster: identification of the cinnabar transcription unit', *Genetica,* 98(3), pp. 249-262.

Westergaard, N., Drejer, J., Schousboe, A. and Sonnewald, U. (1996) 'Evaluation of the importance of transamination versus deamination in astrocytic metabolism of [U-13C]glutamate', *Glia,* 17(2), pp. 160-168.

Whetsell, W.O.,Jr and Schwarcz, R. (1989) 'Prolonged exposure to submicromolar concentrations of quinolinic acid causes excitotoxic damage in organotypic cultures of rat corticostriatal system', *Neuroscience letters,* 97(3), pp. 271-275.

Whitworth, A.J., Theodore, D.A., Greene, J.C., Benes, H., Wes, P.D. and Pallanck, L.J. (2005) 'Increased glutathione S-transferase activity rescues dopaminergic neuron loss in a Drosophila model of Parkinson's disease', *Proceedings of the National Academy of Sciences of the United States of America,* 102(22), pp. 8024-8029.

Widner, B., Leblhuber, F. and Fuchs, D. (2002) 'Increased neopterin production and tryptophan degradation in advanced Parkinson's disease', *Journal of neural transmission (Vienna, Austria : 1996),* 109(2), pp. 181-189.

Wiedemann, N., Kozjak, V., Chacinska, A., Schonfisch, B., Rospert, S., Ryan, M.T., Pfanner, N. and Meisinger, C. (2003) 'Machinery for protein sorting and assembly in the mitochondrial outer membrane', *Nature,* 424(6948), pp. 565-571.

Wilson, K., Auer, M., Binnie, M., Zheng, X., Pham, N.T., Iredale, J.P., Webster, S.P. and Mole, D.J. (2016) 'Overexpression of human kynurenine-3-monooxygenase protects against 3-hydroxykynurenine-mediated apoptosis through bidirectional nonlinear feedback', *Cell death & disease,* 7, pp. e2197.

Wilson, K., Mole, D.J., Binnie, M., Homer, N.Z., Zheng, X., Yard, B.A., Iredale, J.P., Auer, M. and Webster, S.P. (2014) 'Bacterial expression of human kynurenine 3-monooxygenase: solubility, activity, purification', *Protein expression and purification,* 95, pp. 96-103.

Wong, Y.C. and Holzbaur, E.L. (2014) 'Optineurin is an autophagy receptor for damaged mitochondria in parkin-mediated mitophagy that is disrupted by an ALS-linked mutation', *Proceedings of the National Academy of Sciences of the United States of America,* 111(42), pp. E4439-48.

Wonodi, I., McMahon, R.P., Krishna, N., Mitchell, B.D., Liu, J., Glassman, M., Hong, L.E. and Gold, J.M. (2014) 'Influence of kynurenine 3-monooxygenase (KMO) gene polymorphism on cognitive function in schizophrenia', *Schizophrenia research,* 160(1-3), pp. 80-87.

Wonodi, I., Stine, O.C., Sathyasaikumar, K.V., Roberts, R.C., Mitchell, B.D., Hong, L.E., Kajii, Y., Thaker, G.K. and Schwarcz, R. (2011) 'Downregulated kynurenine 3-monooxygenase gene expression and enzyme activity in schizophrenia and genetic association with schizophrenia endophenotypes', *Archives of General Psychiatry,* 68(7), pp. 665-674.

Wu, W., Nicolazzo, J.A., Wen, L., Chung, R., Stankovic, R., Bao, S.S., Lim, C.K., Brew, B.J., Cullen, K.M. and Guillemin, G.J. (2013) 'Expression of tryptophan 2,3-dioxygenase and production of kynurenine pathway metabolites in triple

transgenic mice and human Alzheimer's disease brain', *PloS one,* 8(4), pp. e59749.

Wu, Z., Puigserver, P., Andersson, U., Zhang, C., Adelmant, G., Mootha, V., Troy, A., Cinti, S., Lowell, B., Scarpulla, R.C. and Spiegelman, B.M. (1999) 'Mechanisms controlling mitochondrial biogenesis and respiration through the thermogenic coactivator PGC-1', *Cell,* 98(1), pp. 115-124.

Yamano, K. and Youle, R.J. (2013) 'PINK1 is degraded through the N-end rule pathway', *Autophagy,* 9(11), pp. 1758-1769.

Yamashita, S.I., Jin, X., Furukawa, K., Hamasaki, M., Nezu, A., Otera, H., Saigusa, T., Yoshimori, T., Sakai, Y., Mihara, K. and Kanki, T. (2016) 'Mitochondrial division occurs concurrently with autophagosome formation but independently of Drp1 during mitophagy', *The Journal of cell biology,* 215(5), pp. 649-665.

Yanagawa, S., Lee, J.S. and Ishimoto, A. (1998) 'Identification and characterization of a novel line of Drosophila Schneider S2 cells that respond to wingless signaling', *The Journal of biological chemistry,* 273(48), pp. 32353-32359.

Yang, D., Oyaizu, Y., Oyaizu, H., Olsen, G.J. and Woese, C.R. (1985) 'Mitochondrial origins', *Proceedings of the National Academy of Sciences of the United States of America,* 82(13), pp. 4443-4447.

Yang, Y., Gehrke, S., Imai, Y., Huang, Z., Ouyang, Y., Wang, J.W., Yang, L., Beal, M.F., Vogel, H. and Lu, B. (2006) 'Mitochondrial pathology and muscle and dopaminergic neuron degeneration caused by inactivation of Drosophila Pink1 is rescued by Parkin', *Proceedings of the National Academy of Sciences of the United States of America,* 103(28), pp. 10793-10798.

Yang, Y., Ouyang, Y., Yang, L., Beal, M.F., McQuibban, A., Vogel, H. and Lu, B. (2008) 'Pink1 regulates mitochondrial dynamics through interaction with the fission/fusion machinery', *Proceedings of the National Academy of Sciences of the United States of America,* 105(19), pp. 7070-7075.

Yokochi, M. (1997) 'Familial juvenile parkinsonism', *European neurology,* 38 Suppl 1, pp. 29-33.

Yoneda, M., Miyatake, T. and Attardi, G. (1994) 'Complementation of mutant and wild-type human mitochondrial DNAs coexisting since the mutation event and lack of complementation of DNAs introduced separately into a cell within distinct organelles', *Molecular and cellular biology,* 14(4), pp. 2699-2712.

Yu, P., Li, Z., Zhang, L., Tagle, D.A. and Cai, T. (2006) 'Characterization of kynurenine aminotransferase III, a novel member of a phylogenetically conserved KAT family', *Gene,* 365, pp. 111-118.

Yun, J., Puri, R., Yang, H., Lizzio, M.A., Wu, C., Sheng, Z.H. and Guo, M. (2014) 'MUL1 acts in parallel to the PINK1/parkin pathway in regulating mitofusin and compensates for loss of PINK1/parkin', *eLife,* 3, pp. e01958.

Zakharov, G.A., Zhuravlev, A.V., Payalina, T.L., Kamyshov, N.G. and Savvateeva-Popova, E.V. (2012) 'The effect of mutations of the kynurenine pathway of tryptophan metabolism on locomotor behavior and gene expression in glutamatergic and cholinergic systems of D. melanogaster', 2(2), pp. 204.

Zhang, X., Koolhaas, W.H. and Schnorrer, F. (2014) 'A versatile two-step CRISPR- and RMCE-based strategy for efficient genome engineering in Drosophila', *G3 (Bethesda, Md.),* 4(12), pp. 2409-2418.

Zhang, Z., Liu, L., Wu, S. and Xing, D. (2016) 'Drp1, Mff, Fis1, and MiD51 are coordinated to mediate mitochondrial fission during UV irradiation-induced apoptosis', *FASEB journal : official publication of the Federation of American Societies for Experimental Biology,* 30(1), pp. 466-476.

Zhou, R., Mohr, S., Hannon, G.J. and Perrimon, N. (2014) 'Inducing RNAi in Drosophila cells by soaking with dsRNA', *Cold Spring Harbor protocols,* 2014(5), pp. 10.1101/pdb.prot080747.

Zhou, R., Mohr, S., Hannon, G.J. and Perrimon, N. (2013) 'Inducing RNAi in Drosophila cells by transfection with dsRNA', *Cold Spring Harbor protocols,* 2013(5), pp. 461-463.

Ziviani, E., Tao, R.N. and Whitworth, A.J. (2010) 'Drosophila parkin requires PINK1 for mitochondrial translocation and ubiquitinates mitofusin', *Proceedings of the National Academy of Sciences of the United States of America,* 107(11), pp. 5018-5023.

Zuchner, S., Mersiyanova, I.V., Muglia, M., Bissar-Tadmouri, N., Rochelle, J., Dadali, E.L., Zappia, M., Nelis, E., Patitucci, A., Senderek, J., Parman, Y., Evgrafov, O., Jonghe, P.D., Takahashi, Y., Tsuji, S., Pericak-Vance, M.A., Quattrone, A., Battaloglu, E., Polyakov, A.V., Timmerman, V., Schroder, J.M. and Vance, J.M. (2004) 'Mutations in the mitochondrial GTPase mitofusin 2 cause Charcot-Marie-Tooth neuropathy type 2A', *Nature genetics,* 36(5), pp. 449-451.

Zwilling, D., Huang, S.Y., Sathyasaikumar, K.V., Notarangelo, F.M., Guidetti, P., Wu, H.Q., Lee, J., Truong, J., Andrews-Zwilling, Y., Hsieh, E.W., Louie, J.Y., Wu, T., Scearce-Levie, K., Patrick, C., Adame, A., Giorgini, F., Moussaoui, S., Laue, G., Rassoulpour, A., Flik, G., Huang, Y., Muchowski, J.M., Masliah, E., Schwarcz, R. and Muchowski, P.J. (2011) 'Kynurenine 3-monooxygenase inhibition in blood ameliorates neurodegeneration', *Cell,* 145(6), pp. 863-874.